Design and operation of transparent adaptive façades from a visual comfort and energy use perspective

Doctoral Dissertation
Doctoral Program in Energetics (31st Cycle)

Design and operation of transparent adaptive façades from a visual comfort and energy use perspective

Luigi Giovannini
* * * * * *

Supervisors
Prof. Valentina Serra, Supervisor
Prof. Anna Pellegrino, Co-Supervisor
Prof. Valerio R. M. Lo Verso, Co-Supervisor

Doctoral Examination Committee:
Prof. Laura Bellia, Università degli studi di Napoli Federico II
Prof. Enrico Fabrizio, Politecnico di Torino
Prof. Jan Hensen, Referee, Eindhoven University of Technology
Prof. Marco Perino, Politecnico di Torino
Prof. Fabio Peron, Referee, Università Iuav Di Venezia

Politecnico di Torino
July 5th, 2019

I hereby declare that, the contents and organisation of this dissertation constitute my own original work and does not compromise in any way the rights of third parties, including those relating to the security of personal data.

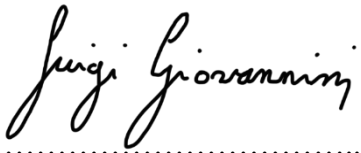

……

Luigi Giovannini

Turin, July 5th, 2019

Summary

Transparent adaptive façades are building envelope technologies able to dynamically adjust their thermo-optical properties according to environmental stimuli or to external custom-defined inputs. This ability can be exploited to respond to ever-changing performance requirements and boundary conditions, aiming at improving the overall energy performance of a building and/or the comfort condition of its occupants. Although transparent adaptive technologies show high potentialities in improving the overall building performance, both in terms of energy use and visual comfort for the occupants, their successful building integration currently results as a challenging task. This is mainly due to: (i) a low awareness in the possibilities and drawbacks relative to the integration of these components in the building envelope; (ii) intrinsic difficulties of the currently available Building Performance Simulation (BPS) tools to assess their performance on the different domains they affect in a reliable way. As regard the latter aspect, the BPS main limitations were identified in: (i) inability to simultaneously evaluate in an accurate and comprehensive way the effects of the behaviour of a transparent adaptive component on energy and visual comfort aspects; (ii) inability to model complex phenomena relative to the behaviour of some transparent adaptive technologies.

In this framework, the Ph.D. thesis proposes a novel integrated simulation methodology for a simultaneous and comprehensive evaluation, with a high degree of accuracy, of the effects of the behaviour of transparent adaptive façade technologies on the energy performance of a building and on the visual comfort condition of its occupants. As regard the latter, this is evaluated at a spatial level both as daylight availability on the visual task and as daylight glare condition of the occupants. This was enabled by the introduction of a simplified approach aimed at classifying a whole space according to daylight glare comfort classes, by means of solely the eye vertical illuminance. The main advantage of such simplified approach is that of allowing a spatial evaluation of the glare condition with a significantly lower computational effort compared to that necessary for evaluating Daylight Glare Probability (currently the most widespread and accurate metric for the assessment of daylight glare) for the whole space.

The proposed integrated methodology proved to be suitable for the evaluation of the performance related both to passive and active transparent adaptive façade components. In more detail, this one was applied to assess the effects of the behaviour over energy and visual comfort aspects of a passive transparent adaptive component, namely a thermochromic glazing, showing a complex hysteretic behaviour. In addition, the performance of different active transparent adaptive technologies, operated according to both mono-objective and advanced multi-objective rule-based control strategies, was assessed.

The application of such methodology enabled: (i) a simultaneous, accurate and comprehensive quantification of the effects of the behaviour of a transparent adaptive component over energy and visual comfort aspects; (ii) the simulation of complex phenomena relative to the behaviour typical of some transparent adaptive technologies (e.g. hysteretic behaviour of thermochromic and thermotropic glazing). Such methodology could effectively support with reliable outcomes the decision-making relative to the design and the operation of transparent adaptive components. A comprehensive evaluation of the energy and visual comfort performance of transparent adaptive technologies could in fact increase the understanding of possible risks and advantages related to their integration in the building envelope, helping thus exploiting their full technical potential. As a result, a more aware use of such technologies could make the expected improvements in the building energy use, as well as in the overall visual comfort condition of their occupants, really achievable.

Acknowledgments

My deepest and sincere gratitude goes, first and foremost, to my supervisors, for the enthusiastic attitude towards the Research that they were able to convey to me. This research would have never been possible without their insightful suggestions, encouraging support and clear guidance.

My gratitude goes also to all the people I had the opportunity to collaborate with, particularly to Dr. Fabio Favoino and to his challenging attitude, without which this thesis would never have seen the light.

A special thanks goes to Dr. Mauro Overend, for hosting me in his research group and for his constructive suggestions.

I would like to thank Eckersley O'Callaghan Ltd. for hosting me and for collaborating in the development of part of the work presented in this Ph.D. thesis.

I would like to acknowledge the European COST Action TU1403 – Adaptive façades Network, who supported part of the work carried out during the Ph.D. activity.

I would also like to acknowledge ENEA for providing support in the experimental characterisation of the transparent adaptive components considered within the present research.

A special thanks goes to all the TEBE Research Group colleagues, for being able to provide with the same lightness either constructive research inputs or cheerful fun, depending on the needs of the case.

I would also like to thank who every day, for two years, sat in front of me, for his unceasing challenging attitude, his "poetical" vision of the world and his scientific rigour allowed me to see my research under a whole new, extremely valuable, perspective.

My deepest gratitude goes to my family and friends, for their unconditional love and support, for constantly encouraging me, believing in me also when I did not and for always bearing with me, no matter what.

Finally, a special thanks goes to who stayed by my side in the long days and nights during which this work was carried out, for her presence and her unwavering support have been an endless source of encouragement and motivation.

Dedicated to all the people who made all this possible

Contents

List of Tables

List of Figures

 a

Chapter 1

Introduction

The building sector in the European Union (EU) is currently responsible for approximately 40% of energy consumption and 36% of greenhouse gas emissions [1]. For this reason, in the last decade the EU has pursued a policy aimed at the improvement of the overall energy efficiency in buildings by introducing new and progressively stringent targets for the decrease of the energy demand and CO_2 emissions, first in [2,3] and later in [1]. In this sense the building envelope, due to its function of interface between the outdoor and indoor environment, is responsible of heat, radiation and mass transfer and can therefore play a significant role in the fulfilling of the latest EU targets. As a result, over the last few years the research activity related to the building envelope has focused on exploring and developing new solutions aimed at reducing the overall building energy use.

In this framework, a promising solution is represented by the *adaptive*[1] *façades*, namely building envelope components able to manage heat, mass or radiation transfer (or a combination of these) by dynamically adjusting their features. This ability can be exploited with the purpose of responding to ever-changing performance requirements and boundary conditions with the aim of improving the overall energy performance of a building and/or indoor environmental comfort requirements. The adaptive behaviour of these components may be based on different working principles, including, but not limited to physical transformations (e.g. phase change, expansion/shrinking, physical adsorption, etc..), mechanical transformations (e.g. rotation or

[1] As far as the term adaptive is concerned, many synonyms can be found in literature including, but not limited to adjustable, controllable, dynamic, intelligent, reflexive, responsive, selective, smart, switchable and transient [5]. Multiple slightly different definitions may be associated to each of these terms, varying from author to author, meaning that a clear definition of these aspects is currently still lacking. Aiming at avoiding any ambiguity, within the present work only the term adaptive will be used, referred to the ability of a façade component to dynamically adjust its features according to dynamic boundary conditions with the aim of fulfilling pre-defined requirements.

displacement of parts of the component), and reversible chemical reactions and can take place at different component levels (micro or macro scale) [4]. Furthermore, the variation of their features can be automatically triggered by environmental stimuli (intrinsic or passive façade components) or activated by external inputs (active or extrinsic façade components) and can occur at different timescales, from short time intervals (few seconds or minutes) to seasonal adaptations [5].

Within the general concept of adaptive façades, a particular sub-category is represented by *transparent* adaptive façades, which are transparent building envelope technologies able to vary their thermo-optical properties, resulting in the possibility of modulating the solar radiation entering a building. These façade components are thus particularly complex to manage, design and operate, as their behaviour simultaneously affects different physical domains and different aspects, interdependent and often conflicting. For instance, the same operation may affect at the same time, but in an opposite way, the energy performance of a building and the visual and thermal comfort condition of its occupants.

Nowadays, a number of different transparent adaptive façade solutions is already available for the integration in the building envelope. Although these components show a large potential in improving the overall building performance, both in terms of energy use and comfort for the occupants, they have a low real-world uptake compared to traditional static façade solutions. This is due to the fact that successfully designing façades, and more in general buildings integrating these innovative technologies and materials results in a challenging task. Two main aspects are responsible for this, which were identified in: (i) a lack in the comprehension of the advantages and drawbacks deriving from the integration of transparent adaptive façades in the building envelope; (ii) intrinsic difficulties in evaluating the effects of the behaviour of these components on the different domains they affect in a reliable way. A dearth in the awareness relative to the effective benefits achievable through transparent adaptive technologies (also in terms of possible direct and indirect economic advantages) prevents most stakeholders from the adoption of such components.

Building Performance Simulation tools (BPS) could have a crucial role in this process, as they could theoretically provide to all the stakeholders involved the necessary information to foster the adoption of transparent adaptive façade components. However, a numerical assessment of the overall performance of transparent adaptive façade components is currently a difficult task, as the available BPS tools show some intrinsic limitations, which were identified in: (i) inability to simultaneously evaluate in an accurate and comprehensive way the effects of the behaviour of a transparent adaptive component on energy and visual comfort aspects; (ii) inability to model complex phenomena relative to the behaviour of some transparent adaptive technologies (e.g. hysteretic behaviour).

As a result, transparent adaptive components are mainly aimed at optimising the performance related to only one single domain (either energy or visual comfort performance) among those the variation of their thermo-optical properties

affects. However, focusing on a mono-domain optimisation may imply a series of drawbacks that can eventually negatively affect the overall building performance.

As far as visual comfort is concerned, this one is typically assessed through the availability of daylight on the visual task, and more rarely through the glare condition of the occupants, although this one plays an important role in the determination of their final visual comfort condition. Moreover, the presence of glare is proved to negatively affect the human performance, the human health and eventually the workplace productivity [6]. Since glare is a position- and view-dependant phenomenon, for which a spatial evaluation requires a high computation time, its assessment is generally limited to only one or few points in the room. However, such a punctual evaluation may not be representative of the visual comfort conditions occurring throughout the whole space, which may in turn negatively influence choices relative to the design or operation of a transparent adaptive component. These choices may eventually result in lower comfort conditions or in a higher energy demand than those estimated, depending on whether the occupant can or cannot interact with the transparent adaptive technology.

In this framework, with the aim of helping bridge the highlighted gaps, the present Ph.D. thesis proposes a novel integrated simulative methodology. This one enables to simultaneously and comprehensively quantify, with a high degree of accuracy, the effects of the modulation of the thermo-optical properties of transparent adaptive façade technologies on energy and visual comfort aspects. This methodology is meant to increase the awareness of the possible benefits and risks related to the integration of a transparent adaptive façade into a building, helping thus exploiting their full technical potential in order to reach the aforementioned EU targets. In this sense, it can play a key role by providing reliable outcomes to support the decision-making relative to both design and operation of these innovative components. As regard to the visual comfort evaluation, a simplified approach for a fast evaluation of the daylight glare comfort level of the occupants with a high spatial resolution is proposed as well, with the aim of allowing a more comprehensive assessment of the overall visual comfort condition occurring throughout the whole space considered. By providing a clear picture of the effects on energy and visual comfort performance of the integration of transparent adaptive façades, the present study may ultimately allow a multi-field optimisation of the overall building performance both through the design and the operation of the adaptive component. As far as the latter aspect is concerned, the application of the proposed methodology may support the conception, development and optimisation of advanced multi-objective and multi-domain control strategies for the operation of active transparent adaptive components with the aim of simultaneously improve both energy and visual comfort aspects.

Apart from the present chapter, aiming at introducing the background and motivations underlying the research work hereby presented, as well its objectives

and implications, the thesis is composed by the following chapters, which are interrelated according to the research methodology shown in Figure 1:

Chapter 2 provides an analysis of the state of the art which investigates the requirements relative to a comprehensive evaluation of the performance of transparent adaptive façades as far as energy and visual comfort aspects are concerned. This is done by reviewing the features of the different available typologies of transparent adaptive façades and the different solutions currently adopted for the operation of the active ones, as well as by analysing the different available methods for a numerical evaluation of the glare condition and the different approaches for a multi-domain numerical assessment of the performance related to adaptive components. For each of these the main advantages and limitations are highlighted.

Chapter 3 presents in detail the architecture, workflow and capabilities of the novel integrated simulation methodology proposed. In addition, two applications of such methodology, respectively relative to a passive and an active adaptive transparent façade component, are presented.

Chapter 4 provides a detailed explanation of the simplified approach for the spatial evaluation of the glare condition and provides an application example. Moreover, an example of the application of such methodology for the optimal operation of an active transparent façade component from the visual comfort point of view is presented.

Chapter 5 summarises the main conclusions from the present research work and recommends areas for future work.

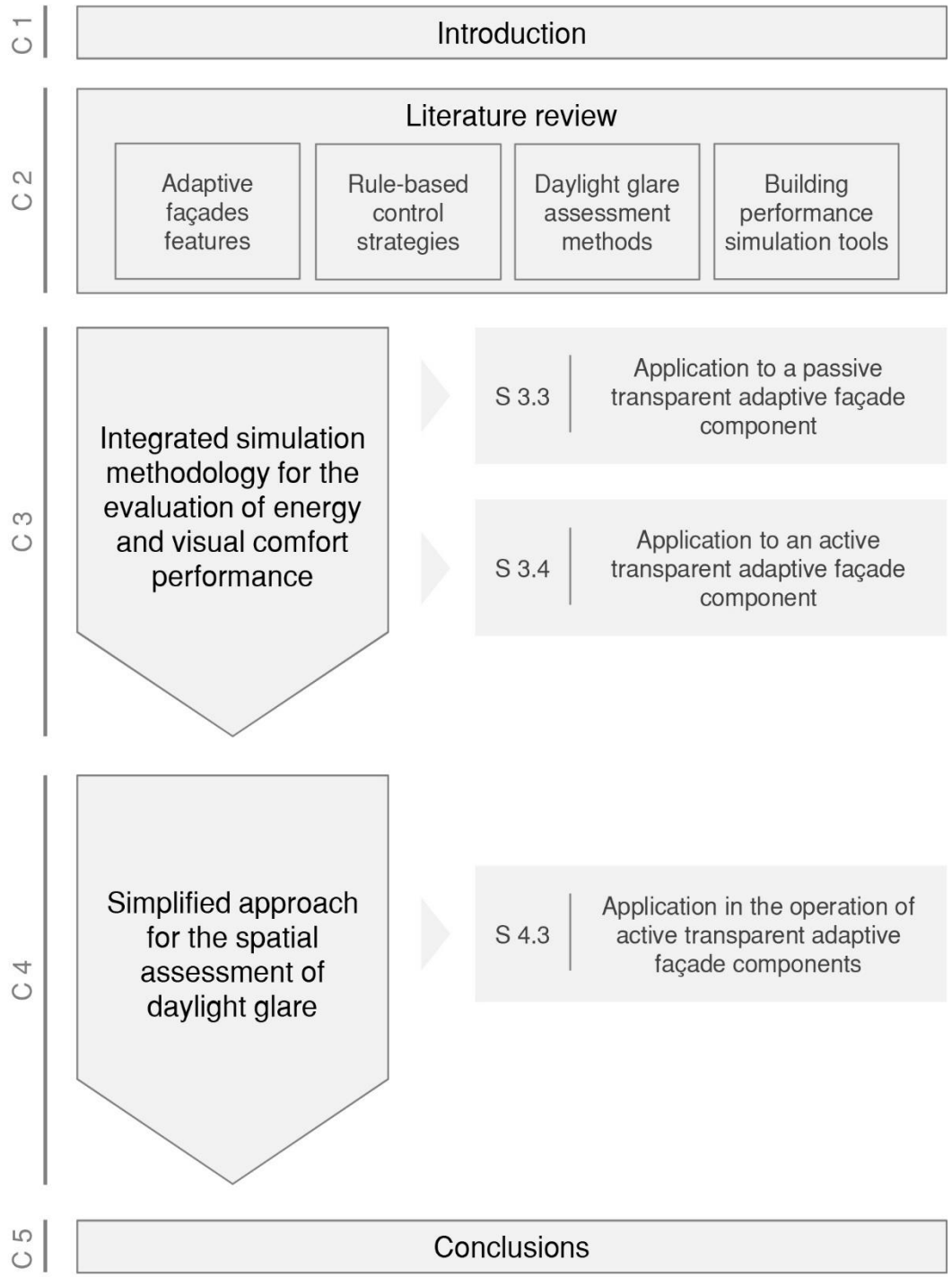

Figure 1. Graphical outline of the research methodology within the Ph.D. thesis (C=Chapter; S=Section).

Chapter 2

State of the art

2.1 Introduction

Part of the work described in this chapter has been previously published by the author and co-workers in international peer-reviewed journals [7,8].

This chapter provides a comprehensive literature review forming the basis from which the Ph.D. research work was developed. The state of the art was analysed with the aim of defining the current limitations and possibilities relative to an accurate and comprehensive evaluation of energy and visual comfort aspects relative to the behaviour of transparent adaptive façade components. Since this is a multidisciplinary task, dealing with aspects ranging from the adaptive component intrinsic features to building performance simulation tools and to visual comfort aspects, in this chapter different topics were addressed, which were then integrated in the overall research methodology. In section 2.2 a review of the different available typologies of transparent adaptive façade components is provided, along with an analysis of their working principles and of their general features. This is followed, in section 2.3, by a review of the different rule-based control strategies currently used for the operation of active transparent adaptive façade components. Section 2.4 provides an overview on the different methodologies and metrics available for a numerical assessment of the glare condition of the occupants. In section 2.5 an overview of the different tools and methodologies available for a multi-domain numerical assessment of the performance of transparent adaptive façade components is provided. Finally, section 2.6 summarises the main conclusion from this analysis of the state of the art.

2.2 Transparent adaptive façades

"*This next generation of facades (or building envelopes) consists of multifunctional and highly adaptive systems, where the physical separator*

between the interior and exterior environment (i.e. the building envelope) is able to change its functions, features or behaviour over time in response to transient performance requirements and boundary conditions, with the aim of improving the overall building performance" [9]

The above is a general definition of the concept of adaptive building envelope technology. Depending on the working principle of the adaptive façade component a first distinction can be drawn into passive (or intrinsic) and active (or extrinsic) building envelope technologies [4]. In passive technologies the ability to adapt is an inherent feature of the building envelope itself, meaning that it shows the capability to self-adjust, as its behaviour is automatically triggered by environmental stimuli comprising, but not limited to, temperature, humidity, solar radiation and CO_2 level. Active technologies instead require an external input to trigger their adaptive behaviour, meaning that their properties can be actively adjusted to meet one or more desired requirements.

A sub-category of the adaptive façades is represented by the *transparent adaptive façades*, which are transparent building envelope technologies able to vary their thermo-optical properties, resulting in the possibility of managing the solar radiation entering a building. As a consequence, these façade components are particularly complex, as their adaptiveness simultaneously affects different physical domains and different aspects, often highly interdependent and contrasting with each other. The same action by these components may in fact influence, but in opposite ways, the building energy performance and the comfort conditions of the occupants, the latter mainly in terms of visual and thermal comfort [10].

Transparent adaptive façades, also called *smart*, *intelligent* or *dynamic* glazing, are generally characterised by one or more transparent functional layers of different materials (inorganic and/or organic, including chromogenic materials) integrated between two or more layers of float glass and assembled into double-glazing. The basic principle of the dynamic glazing components consists in the possibility of controlling the transmitted solar radiation by means of the glazing component through the variation of the optical properties of the adopted chromogenic material.

The above subdivision of adaptive building envelopes between passive and active applies to the transparent adaptive façades as well. In more detail, the variation of the optical properties of the passive glazing occurs according to the stress acting on the component because of an intrinsic chromogenic mechanism of the material, while an external electrical signal (i.e. potential difference) causes the variation of the optical properties of the active glazing components. Depending on the variation mechanism of the chromogenic layer, the passive dynamic glazing can be further classified as: thermochromic [11,12], thermotropic [13,14], and photochromic [15].

In thermochromic (TC) and Thermotropic (TT) glazing the variation of the thermo-optical properties is triggered by an alteration of the temperature of their

chromogenic layer. Thermochromism in glazing is usually obtained by embedding vanadium dioxide (VO_2) in the glass pane [11,12]. At a critical temperature a reversible Semiconductor-Metal phase Transition (SMT) occurs, causing the compound to reflect the infrared solar radiation [16,17]. As the transition temperature of pure VO_2 is equal to 68.5 °C, which makes it unsuitable for architectural applications, different dopants are used to lower this temperature as well as enhance the switching range, among which the most effective ones showed to be W, Mg, Si and F [18,19]. However, the application of VO_2-based thermochromic glazing for daylight and solar control may be limited by the fact that they show a high transmittance variation in the near IR region, while the variation in the visible region of the solar spectrum (a highly energetic range) is in most cases negligible [20]. A promising alternative to VO_2-based is represented by Ligand-Exchange Thermochromic systems (LETC) [21], which, based on the addition of TC dopants to a transparent polymeric matrix, allow achieving a variation of the transmittance both in the visible and solar spectrum [22].

Thermotropic materials are based on the same working principle as TC materials, i.e. their thermo-optical properties vary according to the temperature of their chromogenic layer. However, while TCs exhibit a variation in the optical properties, TTs show a switching in the light scattering properties, meaning that the view through the window is progressively blocked as the component varies from specular to translucent [23]. This effect is obtained through the variation of the refractive index of different components within a transparent polymeric matrix. The more widespread techniques to obtain this result include phase separation (ionogels), change of particle size (hydrogel microparticles) and phase transition (polymer blends with phase transition and casting resins) [24]. Among these, hydrogel-based TTs have encountered the highest fortune, due to their wide variation both in visible and solar transmittance (equal approximatively to 80% for both τ_{vis} and τ_{sol}), and have also been demonstrated in smart glazing applications [25–27]. However, hydrogel-based TTs show cyclic stability issues due to freezing or evaporation of part of their water content. Ionogels instead, even if still under development, have shown a high stability at high and low limit temperatures. Although some promising results were obtained in improving the overall building energy performance [13,24], an architectural application of this technology seems unlikely, at least as far as a view to the outside is required.

Photochromic (PC) materials rely on a different working principle than TC and TT, as the variation of their thermo-optical properties varies according to the incident radiation on their chromogenic layer. In more detail, their adaptivity is due to a reversible transition of a single chemical species, usually a metal halide (chloride - Cl^-, or silver bromide, AgBr), between two different reticular structures, which determines a variation in the absorption spectrum of the PC. This transition is triggered by an alteration of the electromagnetic energy in the UV spectrum [28]. Depending on the incident energy on their chromogenic layers, PC materials linearly switch from highly transmissive (low UV radiation) to highly absorptive (high UV radiation) in respect to the visible spectrum [29,30].

Due to this feature, the main application of PC glazing would be that of controlling glare from sunlight. However, a scarce literature exists with regard to PC materials, and no application to smart glazing has been documented yet. This because since their conception, nearly 30 years ago, high difficulties have been encountered in the scaling of this materials from small samples to window-sized glass panes. For this reason, the idea of integrating this technology in smart windows was progressively abandoned, and nowadays PC materials main application is in glass for the optical and car industry [15]. However, in the last few years a renewed interest in this technology has been experienced, due to the technological improvements in the coating manufacturing field, leading to the study of new-generation photochromic coatings [31,32] and to the production of medium-scale PC prototypes [33].

An alternative to chromogenic materials is represented by Phase Changing Materials (PCM) integrated in the fenestration system. PCMs show a variation in the light scattering properties between their solid and liquid states: light is transmitted specularly in the liquid state, while in the solid state this one is completely scattered. Moreover, the Infrared part of the solar radiation is absorbed and stored by the PCM. Due to this feature, their integration in transparent components allows the visible region of solar radiation to enter the indoor environment for daylighting purposes, while the Infrared solar radiation is absorbed and stored within the glazing, with the purpose of reducing heating and cooling loads. In more detail, due to its thermal storing properties, a PCM-integrated glazing can allow decreasing and shifting in time the solar heat gains in summer days [34–36]. PCMs, depending on their composition, are subdivided between organic and inorganic. Organic PCMs, in respect to inorganic ones, show a higher durability and better cooling and freezing properties. Conversely, inorganic PCMs show a lower thermal conductivity and they are generally less expensive than organic ones [37]. Moreover, depending on the specific climate features, a PCM can be treated in order to modify its melting point, further enhancing the building energy performance. This PCMs category, which additions to the two highlighted above, is represented by Eutectic PCMs, which are composed by a mixture of different elements whose concentrations are studied in order to optimise (generally minimise) their melting point [38]. The effectiveness of this passive adaptive façade technology in improving the building energy performance has been proved in several studies, such as [36,39,40], but some drawbacks were observed in terms of visual comfort for the occupants. When in their solid state, PCMs show, other than a scattering behaviour, a lower visible transmittance in respect to that relative to the liquid state [41]. Due to its intrinsic working principle, the PCM is likely to be in a liquid state in the central (hottest) hours of the day, while in the early morning and late afternoon is usually in its solid state. These latter moments of the day are also characterised by a low daylight availability and, as a consequence, daylight penetration within the indoor space is further reduced. Moreover it showed not to be effective in glare

protection, as its light diffusing attitude is likely to cause a glare sensation from contrast to the occupants [42].

As far as active adaptive transparent glazing are concerned, these can be classified according to the chromogenic layer typology used to modulate their optical properties. According to this classification four main typologies of transparent adaptive active façade components exist: Electrochromic (EC) glazing, gasochromic (GC) glazing, Suspended Particle Devices (SPD) and Liquid Crystals (LC) glazing [43].

The electrochromic glazing consists in two transparent conductor films separated by a cathodic electroactive layer, an electrolyte layer and an anodic electroactive layer. The cathodic and anodic electroactive layers are generally referred to as the chromogenic layers. Under an external electric field, generated via a power difference, an oxidoreduction reaction is activated between the two electroactive layers, which is made possible by an ion migration through the electrolyte layer. In this reversible reaction the ions are inserted into or extracted from, depending on the voltage sign, the electroactive layers, which causes the variation of the component thermo-optical properties [44]. Two types of metal oxides exist, cathodic (Cr, Mn, Fe Co, Ni, Rh, Ir) and anodic (Nb, Mo, Ta, W, Ti), whose colouration is triggered when ions are inserted into and extracted from them respectively. Vanadium represents a peculiar case since, as seen for the thermochromic glazing, depending on its structure it can be both an anodic or cathodic metal oxide [45]. Among these, the most widely available and used transparent metal oxide is certainly tungsten oxide (WO_3), as it currently allows obtaining the largest modulation ranges for visible and solar transmittance [46]. The alteration of the ion concentration in the chromogenic layer causes the variation of the optical properties of the WO_3-based EC glazing [11,47]; the glass colour (in transmission) varies between a transparent/light blue (τ_{vis} = 0.5 – 0.6, g-value = 0.4 – 0.5) and dark prussian blue state (τ_{vis} = 0.05 – 0.01, g-value = 0.1 – 0.05) on a continuous basis [43]. The colouring speed varies according to the chromogenic layer size and it can range from few seconds up to several minutes [48]. An enhancement in the all-solid-state EC glazing is represented by the Photo-Electro-Chromic (PEC) devices. These components present an additional photovoltaic transparent layer that makes the electricity directly available to the EC element. As a consequence, the variation of the glazing thermo-optical properties is triggered by the photovoltaic electricity produced from the solar radiation conversion. The electrical separation of the photovoltaic layer from the electrochromic layer allows both a passive and an active control. However, due to the low transparency of the PV layer, these components show a narrow transmittance modulation range [49]. Another improvement to traditional all-solid-state EC glazing is represented by cutting-edge components able to independently vary their properties in the visible and Infrared Region. In all-solid-state EC components the application of a potential difference causes the simultaneous variation of visible and NIR transmittance. Recently, EC layers able to modulate NIR radiation without varying the visible transmittance were

produced [50,51]. Moreover, an EC component able to independently tune visible and NIR transmittance was realised [52,53]. This next-generation electrochromic technologies open new possibilities in the simultaneous improvement of the building energy performance and visual comfort for the occupants. These two aspects are in fact in some cases contrasting, and a priority to one of them must be given, with consequent drawbacks on the other one. With these new technologies it is theoretically possible in these cases to improve both aspects at a time.

As far as gasochromic glazing are concerned, in these the chromogenic behaviour is obtained exploiting the same oxidoreduction above described, activated here not by voltage application but through the exposition of the chromogenic layer to diluted hydrogen gas (H_2) [54]. The working principle of GC is thus similar to that underlying EC technology, but for the former a simpler equipment is necessary, consisting of a single chromogenic layer (transparent conducting films are no longer necessary as no electric field is applied). However, being gas exchange involved in the chromogenic process, a more sophisticated control equipment is required [55]. The highest transmittance modulation ranges have been obtained also in the case of GC glazing with WO_3 [56], coupled with a catalytic layer (PD or Pt) to turn H_2 molecules into H^+ ions [57]. The transmission modulation range obtainable for GC components showed to outperform that relative to most all-solid-state EC glazing [43].

Liquid Crystal (LC) glazing and Suspended Particle Devices (SPD), also called Electrophoretic glazing, are based on the same working principle: randomly scattered and oriented particles are suspended in an electrolytic solution. Whenever an electrically induced (by means of a voltage) magnetic field is applied to these components the particles are aligned, allowing the radiation to pass through the glazing. SPDs are composed by two transparent conductor films separated by a layer of organic fluid (or gel) in which dipolar particles are suspended [58,59]. As said, when a magnetic field is present these dipolar particles are aligned, allowing the transmission of light, otherwise light is absorbed, meaning that light is still transmitted specularly, but the visible transmittance is decreased. The transmittance modulation range of such components is dependent on the thickness of the fluid layer and on the concentration of the dipolar particles suspended [43]. The structure of LC glazing is similar to that of SPDs, but between the two transparent conductor films is here interposed a transparent polymeric matrix in which LC droplets are dispersed [60]. The absence of a magnetic field causes light to be scattered, due to the polymer matrix and the LC crystals having different refractive indexes, otherwise the LC droplets are aligned, allowing the light to be specularly transmitted [61]. Both LC and SPD materials show a rapid variation (high speed transition) of the optical properties and of the light scattering properties between two states, associated either to the presence or absence of an electrically induced magnetic field. As a result, the modulation of their optical properties is not continuous, but is instead of a *ON-OFF* type. Furthermore, for the transparent state to be maintained, a voltage has to be continuously applied, resulting in a higher energy

consumption for their operation in respect to that relative to EC components. As a consequence, they are more suitable for applications requiring the glazing to be opaque for most of the time. For the SPDs the visible transmittance typically ranges from approximatively 0.04-0.5 for the OFF state to about 0.5- 0.7 in the ON state [43,59,62], and their main architectural application is in skylights. As for the LC glazing, the high transparency of their darkest state (τ_{vis} = 0.15 – 0.20, g-value = 0.15 – 0.10) limits their architectural application mostly to internal separation elements for privacy purposes [63].

In Figure 2 [64] and Figure 3 [65] the variation of the thermo-optical properties of the adaptive glazing technologies (both active and passive) currently on the market (solid lines) and innovative (dotted lines) is compared with the properties of traditional double-glazing units (DGU, grey in Figure 2 and Figure 3). The thermo-optical properties of the DGUs reported in the figures are derived from the International Glazing Database [66] and each double-glazing unit is composed by two 10 mm thick glass panes and an air-filled 12 mm cavity, in which a low-emissive or selective coating is placed on the inner face of the external glass pane (face 2).

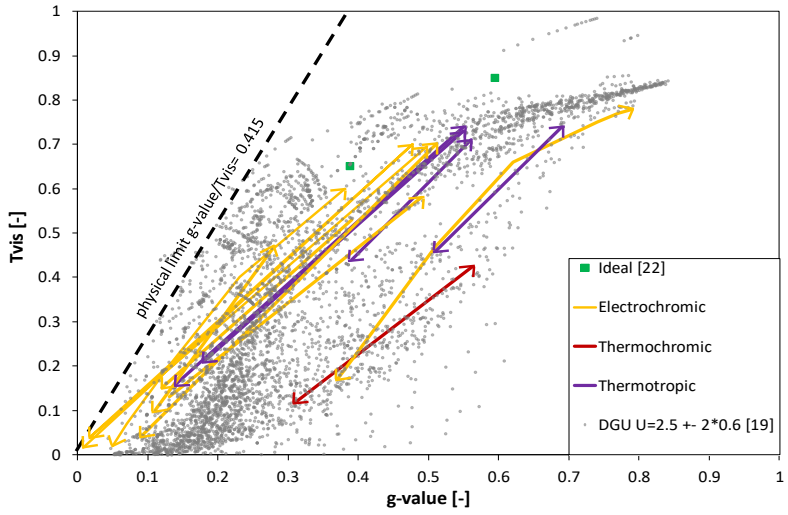

Figure 2. Comparison between τ_{vis} and g-value relative to active and passive dynamic glazing (currently on the market) and traditional double-glazing units [64].

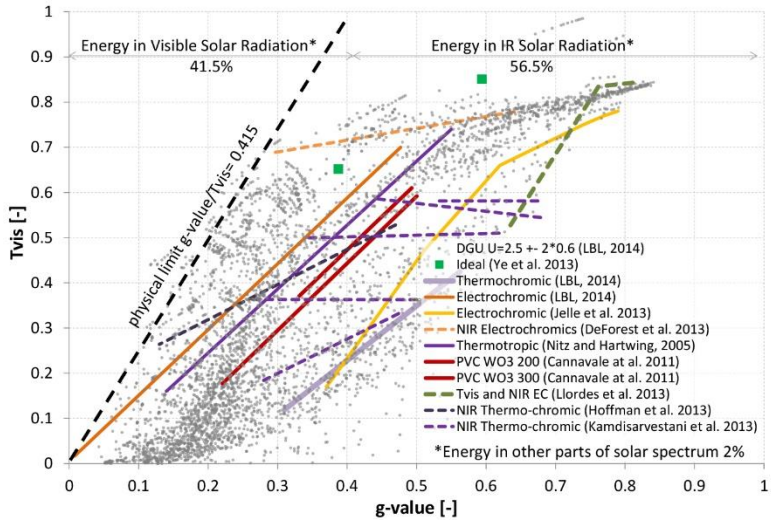

Figure 3. Comparison between τ_{vis} and g-value relative to innovative (dotted lines) and currently on the market (solid lines) active and passive dynamic glazing and to traditional double-glazing units [65].

Among the existing adaptive glazing technologies, the all-solid-state electrochromic glazing currently shows the widest construction market penetration. Moreover, this appears to be the most advantageous technology in terms of building performance improvements, by reducing the energy needs and electrical load peaks (for space cooling and lighting) while improving the visual and thermal comfort for the occupants. This is mainly due to: i) the robustness of the technology; ii) a large modulation range of its thermo-optical properties (see Figure 1 and Figure 2); iii) The higher versatility of an active control in respect to passive adaptive transparent façade technologies.

Current researches in the field of all-solid-state EC glazing are focused on the following aspects [12,43,67,68]:

- Scalability: increase the maximum size of production, sputtering and lamination of the functional transparent and chromogenic layers;
- Switch speed: increase the speed at which the component colouring transition occurs;
- Optical properties modulation range: increase the maximum and decrease the minimum achievable transparency;
- IR modulation: development and integration of electrochromic materials able to independently modulate visible and NIR solar radiation;
- Tint neutrality: improvement in the neutrality of the glass colouration (both in transmission and reflection);
- Substrate flexibility: Sputtering possibility for the functional and chromogenic layers on a flexible substrate for their integration into curved glazing;

- Control: maximisation of the building energy performance through the development and optimisation of the control strategies regulating the EC thermo-optical variations.

The integration of EC glazing technologies into the building envelope can potentially improve the overall building energy performance by affecting and lowering the primary energy needs, the heating, cooling and lighting loads and the summer overheating risk. Moreover, they may lead as well to an improvement in the daylight availability and to a reduction in the discomfort glare risk due to direct solar radiation and excessive contrast. The achievement of one or more of the aforementioned objectives especially depends on the control strategies adopted during the building operation and on the specific features of the adaptive glazing systems adopted as well [43,69].

2.3 Control strategies

The management of the transparent adaptive active façade technologies can be addressed to the compliance of different and often conflicting requirements, i.e. visual and thermal comfort, reduction in the heating and cooling loads, etc. For instance, the risk of discomfort glare occurrence in warm climates can be contrasting in winter with the maximisation of both the solar gains, for space heating and thermal comfort, and the daylight penetration in the space [70]. The design and implementation of control strategies for the adaptive glazing components is thus of paramount importance to ensure a beneficial management of the building indoor environment. Nonetheless, the conflicting requirements and the mutual influence of different aspects (i.e. variability of the indoor climatic conditions, the variation of the comfort requirements, the occupant preferences) make the design of control strategies for adaptive glazing particularly difficult [71].

Two different approaches exist in terms of working principle underlying a control strategy: Rule-Based Control (RBC) and Model Predictive Control (MPC), also called Receding Horizon Control (RHC) [72]. As far as MPC is concerned, this is a complex control approach based on the prediction of the response of a model of the *window-building* system over a finite-time horizon. Based on this feedback, a local optimisation of the sequence of states for the adaptive component to be assumed in this time horizon is carried out at each timestep [69]. This approach is very promising, as the optimal thermo-optical properties of an adaptive glazing are defined not relatively to a single moment, but considering also their effects over a prediction horizon, which theoretically allows further improvements in the optimisation of the overall energy performance of a building. So far MPC control strategies have been widely applied to heating, cooling and HVAC systems, showing to be able to effectively improve the energy efficiency of buildings beyond that obtainable with traditional methods [73–76]. However, the development and application of such control strategies to active adaptive transparent components is relatively recent, and although some

promising results have been obtained at a simulative level [69,72,77], its application to real cases, as well its real effectiveness are still to be proven.

Regarding Rule-Based Control strategies, this category of algorithms is by far the most adopted one in the control of active adaptive technologies in simulation studies, experimental analysis and real buildings. RBCs can be either based on a basic *if-then* logic or on the use of single/multiple pre-defined set-points, related to punctual measurement of internal and external environmental conditions [69]. RBCs control strategies can be applied both to innovative technologies, such as active adaptive glazing, and to dynamic shading systems, as their operation is meant for the same purposes and the environmental parameters accounted are the same. What changes instead are the actions correlated to the operation of the different technologies.

The RBCs with the most basic structure are those designed to meet only a single building performance requirement (mono-objective). These are also the most common ones, since their design is straightforward and their implementation in real buildings is relatively easy, as the monitoring of one, or at most very few environmental parameters is required. A great part of the mono-objective control strategies is designed to improve the overall building energy performance., typically in terms of decrease of the energy demand for space cooling, space heating and lighting considered separately. Since the primary feature of transparent adaptive façades is that of managing the incoming solar radiation, which is responsible for the overheating phenomena within a space, RBCs are often aimed at the minimisation of the energy demand for space cooling. In many cases this is done through a direct correlation between the incident radiation on the window plane and the operation of the adaptive glazing [78–83]. Different radiation values have been assumed as set-points for the operation of the adaptive glazing (either in *ON/OFF* control strategies - OCS or in linear switching control strategies - LCS), depending on the characteristics of the case study analysed, geographical location, orientation and Window-to-Wall Ration (WWR). As far as the WWR is concerned, Sullivan et al. [84] tested the effect of different set-point ranges for the linear switching of an EC glazing, concluding that for moderate WWR a large set-point range is preferable as it was proved to increase the daylight penetration within the room, resulting in a decrease in the energy demand for lighting, with no significant effect on the energy demand for space cooling. Conversely, for a high WWR, which already provides an adequate daylight level within the room, a smaller set-point range is more suitable, as it proved to prevent overheating phenomena and the consequent increase in the energy demand for space cooling. As for geographical location and orientation, Gugliermetti and Bisegna [70] analysed the effect of different radiation set-points on the four window orientations (N, S, E and W) in three different Italian cities, namely Bozen, Rome and Catania. They found out that a lower energy consumption, considering space cooling and lighting, is achievable through lower set-points for lower latitudes and, at the same latitude, decreasing set-points for south, west and east and north respectively. The typical radiation set-points adopted in the

literature range from 100 W/m^2 to 400 W/m^2, but also higher set-points can be found.

The energy demand for space cooling can also be reduced by correlating the operation of the adaptive glazing to the presence of a cooling load in the last timestep before the one considered [84,85]. Whenever a cooling load is detected the adaptive glazing is set to its darkest state with the purpose of minimising the solar heat gains. A similar solution can also be found relative to the minimisation of the energy demand for space heating, in which the glazing is brought to its clearest state whenever a heating load is detected, with the aim of maximising the solar gains [82,86]. In addition. these two solution are often combined, aiming at a simultaneous reduction of the energy demand for both space heating and space cooling [87,88]. An approach different from the ones seen so far consists in the minimisation of the energy demand for space cooling by controlling, through the operation of the glazing system, the indoor air temperature [86,89] or the indoor operative temperature [90]. RBCs correlating the adaptive glazing operation both to the presence of loads and to an indoor temperature (air or operative) often consider also the occupancy profile of the case study, so as to guarantee the comfort temperature, correlated to a higher energy consumption, only when the space is actually occupied [79,88]. A simpler alternative to all the aforementioned approaches is represented by the operation of the adaptive glazing according to a fixed schedule, determined according to the criticalities relative to climate and the features of the space [91]. The schedule might be referred to a daily time horizon, aimed at minimising the cooling loads in the hottest hours of the day in a hot climate [80], or can be referred to a whole season, with the purpose of maximising the winter solar heat gains and avoiding overheating phenomena in summer [92].

As far as the energy demand for lighting is concerned, this one fully depends on the amount of daylight entering the space. For this reason, in many RBCs it is considered as a consequence of how the glazing is operated in order to minimise the cooling loads, especially in those control strategies based on radiation set-point ranges. In fact, these two aspects are contrasting with each other, as the energy demand for lighting is minimised when the glazing is fully bleached, which in turn is the most unfavourable condition for the energy demand for space cooling in presence of solar heat gains in the hot season. In some control strategies the radiation set-points are determined so as to minimise the increment in the energy demand for lighting while minimising the energy demand for space cooling [70,84]. Apart from this, in the RBCs aiming at the minimisation of the energy demand for lighting the operation of the active adaptive transparent adaptive component is in most cases correlated to the horizontal illuminance within the space at the height of a workplane. In these control strategies the optical properties of the adaptive glazing are modulated in order to provide a daylight illuminance level just equal to a defined set-point, but not higher than that, in order to prevent summer overheating due to an excess in the solar radiation entering the room [81,84,85,89,93,94]. The illuminance set-point is defined so as to ensure an optimal visual comfort condition to the occupants, in

respect to the building typology and to the visual task that needs to be performed. Typical values for an office building range from 323 lx (30 fc) to 600 lx (56 fc), even if the most common set-point is equal to 500 lx, in compliance with [95].

Most Rule-Based Control strategies address only one of the aspects above analysed, nevertheless a small part of them deal with a combination of the approaches seen so far. Although these ones are more complex than the RBCs listed above, they still are mono-objective control strategies, as their purpose is that of optimising the building energy performance alone. The typical structure of these control strategies is that of nested *if,and-then* or *if,or-then* instances, in which the number of nested levels depends on the different aspects considered [81,86]. More advanced multi-criteria mono-objective RBCs show to have an even more complex structure, comparable to a decision tree [88]. As Multi-criteria mono-objective control strategies account for multiple aspects when operating the glazing, these are generally more effective than mono-criteria moo-objective control strategies in improving the overall building energy performance. The main aspects these RBCs consider in their algorithm include but are not limited to: the indoor air (or operative) temperature; the occupancy profile of the space; the presence of cooling or heating loads; the incident radiation on the window plane; the daylight level in the indoor space [79,82]. For a fine modulation of the thermo-optical properties of transparent adaptive components the most complex control strategies add to the aspects above listed also a seasonal schedule of the heating and cooling period and a sun tracking algorithm coupled with a cloud cover monitoring system [96,97].

Furthermore, a few studies investigated the use of either PI and PID control strategies based on internal illuminance or fuzzy logic based on both user preferences and measurements of internal illuminance, incident solar radiation on the window plane and internal air temperature [80,98]. Specifically, in the first control strategy the difference between the indoor average horizontal illuminance and a reference value is used as input for the PID controller, which in turn defines the operation strategy for the adaptive glazing. As for the strategy based on a fuzzy logic, this one, by means of a *backpropagation algorithm*, rather than having a predetermined rule structure, is able to automatically adjust the rules to the feedbacks deriving from the adaptive glazing operation. Although both types of control strategies showed to be very promising, their intrinsic complexity, as well as the high degree of expertise required for their development and implementation to real cases have acted as bias for their further development.

As regard visual comfort, Rule-Based Control strategies aimed at the optimisation of this aspect are less frequent than the ones conceived to reduce the building energy consumption. The visual comfort-related aspects considered in an RBC are in most cases two: daylight availability and glare condition.

As far as the daylight level within a room is concerned, this one is nearly always evaluated by means of the horizontal illuminance in one or few points on the workplane, so as to guarantee the minimum illuminance requirement to perform a visual task. This aspect is intrinsically linked to the energy demand for

lighting, and for this reason it is always considered in terms of the energy consumed to provide a given visual comfort level, this one ensured by the horizontal illuminance set-point. As a consequence, the same considerations made above relative to RBCs aimed at the minimisation of the energy demand for lighting apply here as well, as these two aspects are never considered separately. Generally the horizontal illuminance is assessed in one or few representative points on the workplane [80,81,94], which may not be suitable for applications in real buildings. Tzempelikos and Shen [99] proposed a different approach in which the horizontal illuminance on the workplane was experimentally correlated to the transmitted vertical illuminance, so as to reduce the points of measurement to only one point located far from the workplane. The authors concluded that for such a proxy the illuminance set-point correlated to a horizontal illuminance value of 500 lx is not fixed, but varies depending to the distance *window-workplane* and on the geometry of the space analysed. As a consequence, a correlation between the transmitted vertical illuminance and the horizontal illuminance on the workplane should be carried out for each space considered.

With regard to the glare condition, this one is considered in Rule-Based control strategies according the evaluation of different environmental parameters, the simplest and most widespread of which is the incident solar radiation on the window plane [81,94]. However, significant differences can be observed in the set-point or set-points determined in different studies for the operation of the adaptive glazing, ranging from 63 W/m^2 to 315 W/m^2, and in many cases a correlation to the actual glare sensation perceived by the occupants is not performed [87]. Gugliermetti and Bisegna [70] correlated the incident solar radiation on the window plane to the glare condition of the occupants, assessed by means of the Daylight Glare Index (DGI) [100–102] according to the procedure proposed in [103]. They found out that a set-point of 250 W/m^2 is adequate for preventing discomfort glare for a glazing with an overall visible transmittance equal to 0.211, while this value should be lowered to 100 W/m^2 in presence of a more transparent glazing system, with a visible transmittance of 0.455. A different but still simple approach consists in the evaluation of the vertical illuminance on the window plane, for which the typical set-point ranges from to 15000 lx to 30000 lx [89,94,104,105]. Other than the incident radiation or illuminance on the workplane, the glare condition is often correlated to the incident radiation on the workplane [92,106]. In this case a fixed set-point of 50 W/m^2 is adopted, in accordance to the specifications of the lightswitch model [107].

All the solutions analysed so far were all indirect approaches, i.e. the glare condition was indirectly assessed (and optimised) through the evaluation of a proxy based on an environmental parameter. As for the direct approaches, the most common one is that of assessing the glare sensation through the Daylight Glare Index [85,92,108]. This metric is quite old and some limitations relative to its applicability have been highlighted, among which the most critical one consists in the overestimation of the glare condition actually described by the users in presence of large-non uniform glare sources [109]. Nevertheless, the DGI is still

used to evaluate the glare condition of the occupants and the main reason for this lies in the fact that the calculation of this metric is implemented within EnergyPlus [110], currently one of the most widespread and used building performance simulation tools. Besides DGI, another metric can be used as glare predictor: the Daylight Glare Probability (DGP) [111]. Although this metric is more advanced and up-to-date in respect to DGI, its use is not very common, mainly due to the fact that its calculation has to be performed by means of a daylight simulation software and the required computational time is much higher than that necessary to calculate the DGI. Anyhow, some examples of RBCs aimed at a glare optimisation through the assessment of DGP can be found in literature [69,112].

RBC control strategies, as seen, are mainly designed to ensure only a single building performance requirement, i.e. only the reduction of the building energy use or the optimisation of the comfort condition of the occupants. Only a few studies assessed the effects of the control strategy in a comprehensive way by addressing at the same time both energy performance and visual comfort requirements [82,83]. Favoino et al. [69] compared the effects relative to mono-objective RBCs aimed either at reducing the overall building energy consumption or at optimising the glare condition for the occupants with multi-objective control strategies aimed firstly at a minimisation of the discomfort glare condition and then to the optimisation of the overall building energy performance. The study concluded that for cooling dominated climates the minimisation of the building energy use and the maximisation of visual comfort are overlapping aspects, while in cooling dominated climates multi-objective control strategies such as the ones proposed in the paper may negatively influence the final building energy consumption. In addition, also the variation of the control set-points for the operation of adaptive transparent components may significantly affect both the indoor environmental quality and the building energy performance: as an example, variations in the building heating and cooling needs (25% and 40%, respectively), and in the winter and summer electricity needs for lighting (20% and 65%, respectively), were reported in different studies [113,114]. Furthermore, Loonen et al. [86] also estimated the influence of the control parameters on the overall building energy use equal to approximatively 30%, while the influence of these on visual and thermal comfort aspects was quantified to be between 40% and 70%.

2.4 Daylight glare assessment

Daylight visual comfort is a complex phenomenon influenced by several lighting aspects, including the illuminance on task surfaces and the glare related to daylight sources. These are commonly taken into account with objective parameters, including: the horizontal illuminance on the workplane, which is the quantity most commonly used to assess the lighting performance in a space; the luminance distribution in the occupants' visual field; the colour of the light

perceived by the occupants. In spite of its importance for visual comfort, daylight discomfort glare is not so commonly addressed in the control and operation of active adaptive transparent façade components. Even when it is considered, glare from daylight is in most cases only indirectly evaluated through the incident radiation or illuminance on the window plane or the incident radiation on the workplane, all approaches that may result quite inaccurate in the estimation of such a complex matter. More advanced procedures and metrics for a more accurate estimation of the daylight glare condition exist, but they these are only seldom implemented in Rule-Based Control strategies aimed at operating the window to optimise the visual comfort level of the occupants. This is due to the intrinsic complexity of the glare phenomenon, which has both a *temporal* and a *spatial* variation: it is a function of the user's position and direction of view and it is influenced by the dynamically changing luminance of the sky dome. Moreover, it is influenced by material properties and geometrical aspects (i.e. window optical properties; presence, materials and geometry of moveable shading devices etc.), which makes the evaluation of annual daylight glare even more complex [115].

A number of different glare indices were proposed in the past to quantify the discomfort glare potentially perceived by building occupants. Most of them were developed and validated for glare conditions caused by artificial light sources only. The first attempt to quantify glare from daylight was the "Daylight Glare Index" (DGI) [100], which had the merit to introduce in its equation all the main factors potentially concurring in the determination of a glare condition from daylight: luminance and solid angle of the source, average luminance of the background, position of the light source relative to the observer's field of view. However, even if it was later implemented [116], DGI showed a low reliability as a glare predictor in the presence of windows (especially large windows, constituting most of the observer's field of view, or when the sun is in the occupant field of view), as in fact for most practical situations, the DGI showed to overestimate the glare condition actually described by the observers [109,117–119]. For a more general insight, a critical overview of the first glare indices is reported in [120]. As seen, despite the strong limitations highlighted, the DGI currently remains the most used glare predictor in the numerical assessment and development of Rule-Based Control strategies for adaptive glazing. This is mainly due to the fact that its calculation is implemented within EnergyPlus, i.e. one of the most widespread Building Performance Simulation tools. As a result, this metric can be calculated directly within an energy simulation software, without the need of coupling this one with a daylight simulation software, as it happens instead for most of the other glare metrics.

To simplify the calculation of the daylight glare, attempts were made to estimate it by using the vertical illuminance at the eye level of the occupant, in replacement of the background luminance [121]. Osterhaus [122] assessed experimentally the subjective glare rating expressed by a sample of observers in the presence of large surfaces of non-uniform luminance (produced with electric lighting) and compared them to objective measurements of several glare indices,

including DGI and eye vertical illuminance. In this study DGI showed the weakest correlation with subjective glare rating, while the vertical illuminance at the observer's eye showed the best correlation.

Following up an approach based on vertical illuminance, Wienold and Christoffersen [111] more recently introduced a new index, the Daylight Glare Probability (DGP), which expresses the percent of occupants disturbed by a daylighting glare situation. The index was validated by the same authors against a thorough set of experimental measures in real office rooms. Conceptually, the DGP accounts for luminance of daylight glare sources as well as for the vertical illuminance at eye level. This new method was implemented in the lighting calculation engine Radiance [123], through the purposely-developed tool Evalglare [124]. The calculation of DGP requires an HDR image (a photography or an image generated through a simulation) and a long computational time (especially for an annual glare analysis) to process luminances / illuminances in the scene with respect to one or more positions and directions of observations [125]. Moreover, a study by Pierson et al. [126] highlighted how a superficial understanding of the input data for Evalglare may lead to an inappropriate detection of glare sources, which in turn may determine an inaccurate estimation of glare indices. Since its introduction, the DGP has been adopted in several research studies to perform point-in-time or annual glare analyses, also in the presence of moveable shading or complex fenestrations systems [88,127–130].

At the same time, the evaluation of daylighting in buildings has moved toward the so-called climate based daylighting modelling (CBDM) [131,132], which considers annual dynamic daylight conditions (both sunlight and skylight), rather than limiting the analyses to single scenarios (i.e. overcast skies). The DGP is inherently a CBDM metric, as it depends on the sky luminance distribution, nevertheless, an annual DGP analysis is far time consuming, as it requires an HDR image to be generated for each time-step (typically an hour) considered during the course of a year. Furthermore, the DGP is dependent on the position and direction of view of the evaluation, which means that the calculation should be repeated for all relevant points in the space.

Different approaches to allow faster annual glare analyses were proposed in the past. Among the most relevant ones, two simplified methods were introduced by one of the authors of the DGP. The first one is the *enhanced simplified Daylight Glare Probability*, in which a simplified image is rendered for every considered time-step of the year, thus reducing the computational effort. This image accounts for the luminance of the main glare sources alone, without considering the exact luminance distribution within the room [133]. This solution allows a significant reduction in the computation time, as light inter-reflections are not accounted, but may present an underestimation problem in the presence of materials with a low visual transmission, translucent materials or materials that scatter the transmitted or reflected light. The enhanced simplified DGP proved to have a good correlation with DGP, therefore it was implemented in Radiance to allow faster annual glare simulations. The second simplified method introduced

by Wienold is the *DGPs* [134], which was conceived with the aim of excluding the luminance contrast component from the glare evaluation, hence further reducing the computational effort required. As a result, the DGPs is calculated from the eye vertical illuminance, which was correlated to DGP through a linear equation. Despite the DGPs allows faster annual evaluations (as it does not require an image to be generated for each time-step), it showed a good correlation with the DGP only for conditions when direct sunlight or highlight reflections are not present in the scene.

A further attempt to simplify the calculation of the daylight glare was carried out by Kleindeinst et al. and by Gagne et al. [135–137], who developed a simplified methodology (the *model-based DGP approximation method - DGPm*), that uses luminance sources only for contrast evaluations through low-render images for a limited but representative set of 56 time-steps throughout a year. When compared to the DGP, as calculated using the Evalglare program in Radiance, the DGPm showed a correspondence within a 10% error over 90% of the time [135]. Moreover, the DGPm also allows spatial glare assessments to be carried out for a grid of points inside a space. The algorithm to generate the DGPm was implemented in Lightsolve [138]. A more in-detail review of indexes to evaluate discomfort glare can be found in [139].

Besides the attempts to develop methods for simpler but reliable glare analyses, some metrics were introduced to assess the risk of discomfort due to over-lighting in the frame of the CBDM approach. They are based on the annual workplane illuminance, which gives several advantages in terms of computation time. Two metrics estimate the percentage of occupied time for which a potential glare condition, corresponding to global illuminance over a threshold value, occurs in a point (DA_{max} [132] and $UDI_{exceeded}$ [140,141]), while a third metric considers the percentage of space with a direct illuminance from the sun over a threshold value (1000 lux) for more than a certain amount of time (250 hours) over the year [142]. A review on the CBDM metrics that were proposed can be found in [143].

Following a different approach, Torres et al. [144] compared through a parametric study four illuminance-based metrics to the DGP: horizontal illuminance, vertical illuminance, vertical illuminance vector, and cylindrical illuminance. Through a fault-detection analysis, they found a correlation of each metric to the DGP in terms of capability of detecting or not a glare/non-glare condition. Based on the results, they proposed the use of the cylindrical illuminance as an accurate alternative metric to the DGP, with the advantage of retaining the vertical component of illuminance, while being view independent. A somewhat similar research, focused on studying a relation between the UDI and the DGP, was carried out by Mardaljevic et al. [145].

2.5 Building performance simulation tools

The performance of adaptive façade technologies can be assessed by means of numerical models and simulation software. However, due to their intrinsic complexity related to a dynamic variation of their features over time, this results in a difficult task. Moreover, due to their multi-domain influence, a comprehensive assessment of their performance should involve the evaluation of their effects both on energy-related and visual comfort-related aspects. In this sense, currently available dynamic simulation software show significant limitation in the evaluation of the performance of buildings embedding adaptive glazing systems.

As far as Building Energy Performance Simulation (BEPS) tools are concerned, an extensive review of the possibilities and limitations of the main currently available BEPSs in assessing the performance of adaptive façade components was carried out in [146]. This study shows that different BEPSs offer the possibility of numerically assessing the energy performance related to the most widespread transparent adaptive façade technologies (EC, LC, SPD, TC, TT, PC, PVC) by means of built-in models directly available within the program. For these components the thermo-optical properties are variated within the simulation run-time. The differences between the various BEPS lie in the different levels of expertise required to perform such evaluations and in different possibilities offered in the discretisation of the behaviour of the component into static states (ON/OFF or linear switching). However, for most innovative transparent adaptive façade components (near-infrared EC, independently visible-near infrared tunable EC, fluidglass, etc..) built-in models do not exist. In addition, the available built-in models are not able to take into account complex phenomena related to the behaviour of adaptive glazing, such as the hysteretic behaviour observed for different passive adaptive transparent components (TC, TT, PCM). In these cases, the performance of these adaptive façade components is assessed as sum of independent static states simulated separately and merged only afterwards according either to a control strategy (active components) or an intrinsic switching mechanism (passive components) [147] or a pre-defined schedule as well [148]. The authors conclude that on one hand such approach could be useful in the simulation of transparent adaptive façade technologies for which a model is not available, but on the other hand it is not able to consider the effect of a delayed thermal response due to the capacitance of building components. As a consequence, the use of approximate models may lead to significant errors in the results, as they are not able to handle the building thermal inertia.

Among the BEPSs the authors analysed [146], only three tools, namely EnergyPlus [110], IESVE [149] and IDA-ICE [150], showed the ability to perform, along with energy simulations, also daylight evaluations. These are performed by means of the radiosity method [151] in IDA-ICE and by means of the split-flux method [152] in IESVE, while EnergyPlus offers the possibility of choosing between these two approaches [153,154]. However, both these methods

show a lower degree of accuracy in respect to those implemented in daylight dedicated simulation tools, such as Radiance [123] or DAYSIM [155], for which an experimental validation was carried out [156,157]. Ramos and Ghisi [158] compared the indoor horizontal illuminance in two points with both the radiosity and the split-flux methods, assessed through EnergyPlus, to that calculated through the Daylight Coefficient method (DC method) [159,160], evaluated by means of DAYSIM. The comparison was performed for different room geometries and different orientations, highlighting differences between the EnergyPlus and DAYSIM results up to 20%. As far as transparent adaptive façade components are concerned, due to their strong influence on both energy and visual comfort aspects, a comprehensive and accurate evaluation of their effects on both these physical domains is preferable, in order to support design choices related to these innovative components with accurate and reliable data. Moreover, with regard to the operation of active transparent adaptive façade components, such a comprehensive multi-field evaluation implies also the possibility of developing, simulating and optimising advanced multi-objective rule-based control strategies, taking into account at the same time constraints relative to visual comfort and energy performance. To overcome the restricted (or absent) cross-domain capabilities shown by all the BEPS tools, the most effective solution is represented by the exchange of information between an energy dedicated simulation tool and a daylight dedicated simulation tool [146]. This solution allows exploiting the strength of the different software and evaluating with a high degree of accuracy the results relative to both domains. The information exchange between the two simulation tools can be managed either before the simulation (data integration) or during the simulation run-time (co-simulation). The former solution consists in a data exchange between two simulation tools, in which the simulation relative to one of them has to be performed and the results provided to the second tool before carrying out its simulation. Co-simulation instead refers to a simulation strategy in which two different simulation tools solve a system of coupled equations through a data-exchange directly within the simulation run-time [161]. Both approaches proved to be effective, and between them data integration is certainly easier, as a lower degree of expertise is required and the workflow is quite straightforward. However, attention should be paid in the data integration algorithm, as an incorrect exchange of information could cause inaccuracies or errors in the final outcomes. Co-simulation instead offers a more flexible approach, but at the same time requires a high level of expertise to be performed, as well as the use of middleware tools to manage together the different simulation software.

Different examples of application of the two simulation strategies can be found relative to moveable shading systems, specifically complex fenestration systems (CFS). Bustamante et al. [162] proposed an integrated energy-visual comfort approach for the determination of the optimal control of different CFSs. This approach makes use of EnergyPlus as energy simulation software and of Radiance as daylight simulation software, besides a dedicated tool, mkschedule

[163], used to determine at each timestep the optimal slat position in order to maximise visual comfort, evaluated through the sDA and ASE metrics [142], and contextually minimise the building energy use. Hoffmann et al. [164] proposed a similar approach to evaluate the effects of a control strategy aimed at the minimisation of the glare condition, assessed by means of both the DGI and the DGP, applied to different CFSs. Again, EnergyPlus was adopted as energy simulation software and Radiance as daylight simulation software. The glare calculations, performed by means of Radiance, were run prior to the actual simulation and an hourly scheduled based on the DGI or DGP results was used to control the shading system. Moreover, in this study the higher accuracy of Radiance, in respect to EnergyPlus, was exploited for a more precise evaluation of the radiation heat transfer through the façade, assessed by means of the absorbed solar radiation. De Michele et al. [165] proposed a different approach to evaluate the effects, both on energy and visual comfort aspects, of two control strategies for a CFS, one aimed at the minimisation of the energy use and the other aimed at the maximisation of the visual comfort condition for the occupants, assessed by means of horizontal illuminance levels on the workplane. This approach makes use of Radiance as daylight simulation software and TRNSYS (type 56) as energy simulation software. By means of a dedicated TRNSYS type (Type DLT), written on purpose by the authors, a co-simulation routine between the two software was enabled, allowing an optimisation of the CFS state according to the control strategy within each timestep. Examples concerning the integrated use of energy and a daylight simulation tools different from those analysed here can be found in the literature as well [166–168].

As far as transparent adaptive façade components are concerned, very few examples can be found of an integrated or coupled simulation strategy for a comprehensive evaluation of visual comfort related and energy related aspects.

Loonen [169] proposed a simulation approach in which a full coupling of the tools ESP-r (thermal domain) and Radiance (daylight domain) was performed through the use of BCVTB [170] as simulation manager. Such structure was used to carry out at each timestep an optimisation of the adaptive glazing state according to an MPC control strategy considering both daylight and thermal constraints at the same time. In more detail, at each timestep Radiance was used for the simulation of the daylight related aspects (illuminances, DGP and power fraction of the lighting system), whose outcomes were then fed, by means of BCVTB, to ESP-r for the thermal simulation. The results of both simulations were then evaluated through a pre-defined objective function implemented in an external MATLAB script, aimed at optimising the thermo-optical properties of the adaptive glazing in respect to a receding time horizon. Depending on the outcome of this phase, further simulations could be run within the same timestep, until the optimisation of the glazing state was carried out. The simulation process would then move a timestep forward, for which the same actions above described would be repeated until completion of the process. Although this approach is very promising, it requires a very high level of expertise to be carried out. Moreover,

the visual comfort aspects (including the horizontal illuminance on the wotkplane) were assessed only for one or few points in the room, which may not be representative for the whole space analysed. In addition, the proposed MPC control strategy makes use of a linear objective function to evaluate the different constraints and optimise the state of the adaptive glazing. In this one, the weighting factors assigned to visual comfort and energy performance were equal, although, as stated by the author itself, different weighting factors could lead to significant differences in the final outcomes.

Loonen et al. [89] assessed the effects of the operation of a switchable glazing according to different control strategies on both visual comfort condition of the occupants and building energy performance. The simulation approach proposed makes use of DAYSIM as daylight simulation software and TRNSYS (type 56) as energy simulation software. In more detail, annual daylight simulations relative to luminance, illuminance and DGP were carried out in a pre-processing phase. The outcomes are then provided to TRNSYS, in which during the simulation runtime the most adequate thermo-optical properties of the glazing are chosen according to the selected control strategy (based on either thermal or lighting considerations). Through the proposed approach it was possible to evaluate both the building energy performance and the visual comfort condition of the occupants, assessed in terms of Useful Daylight Illuminance and Daylight Glare Probability. However, all the control strategies considered were mono-objective rule-based control strategies referring either to the thermal physical domain or to the visual comfort one, but not to both at the same time.

Following a similar approach, Favoino et al. [69] proposed an integrated simulation strategy that, by managing together DAYSIM and EnergyPlus, allowed a simultaneous evaluation of the effects of the operation of a photovoltachromic glazing on energy performance and visual comfort, assessed by means of Useful Daylight Illuminance and Daylight Glare Probability. In more detail, annual illuminance and DGP simulations were performed for all the states the adaptive component could assume at a pre-processing stage. These outcomes were then supplied to EnergyPlus. through which, by means of the Energy Management System (EMS) module [171], the most adequate state of the adaptive glazing was chosen in accordance with the control strategy considered. The use of the EMS enabled: i) the variation of the thermo-optical properties of the component within the simulation runtime; ii) the computation of variables used for building services integration from both internal outputs (EnergyPlus) and external outputs (DAYSIM); iii) the control of building services and the artificial lighting system. Different rule-based control strategies were considered in this paper, including multi-objective multi-domain control strategies aiming at an optimisation of the glare condition for the occupants and consequently a minimisation of the building energy use. In this sense, the operation of the adaptive glazing was performed, within the EMS, by considering at the same time thermal and visual constraints. Furthermore, also model predictive control strategies were considered in this study, for which a custom-defined MATLAB [172] script and the tool GenOpt

[173] were used in the simulation strategy to perform a local optimisation directly within the simulation runtime to define the most suitable state the glazing should assume according to visual and thermal constraints in the prediction horizon defined. From the visual comfort point of view, the Useful Daylight Illuminance was calculated for two points only within the room, which may not be representative of the visual comfort conditions of the occupants occurring throughout the whole space considered.

2.6 Conclusions

From the analysis of the state of the art what emerges is that a number of different transparent adaptive façade solutions are available at present time, based on different working principles and each showing specific features in the way their thermo-optical properties are modulated. A numerical assessment of their performance is possible for only some technologies, which are the most widespread, but for most of them, including innovative components, this evaluation is not possible. Moreover, it is not currently possible to simulate complex phenomena relative to the behaviour of some transparent adaptive components, such as the hysteretic behaviour typical of some passive components (TC, TT, PCM). Some workarounds allow overcoming the above issues, but these are based on simplifications of the physical phenomena connected to the variation of the features of an adaptive material, implying a high degree of inaccuracy in the outcomes. Moreover, current BPS tools do not allow a comprehensive and simultaneous evaluation of the effects of the behaviour of transparent adaptive components on both visual comfort of the occupants and energy performance of a space. As a result, only a partial evaluation of these effects is possible, which may in turn negatively affect choices relative to the design or the operation of these components. As an example, transparent active adaptive façade components are mainly operated according to rule-based control strategies aiming at the optimisation of their performance relative to one single physical domain, either energy or visual comfort performance. Since a comprehensive evaluation is not possible, the effects of such operation on the other domain are neglected, although these may ultimately negatively influence the final overall building performance.

As regard the visual comfort condition of the occupants, this is assessed mainly in terms of horizontal illuminance on the visual task, and less often also in terms of glare condition of the occupant. Moreover, the daylight glare risk is mainly evaluated for one or few significant points in the space, as an analysis of this phenomenon for higher spatial resolutions (as already happens for the illuminance assessment) according to the most advanced and accurate metric (DGP) is far time consuming. This is true for both the daylight simulation tools and the available advanced methods for an assessment of the visual comfort performance of transparent adaptive façades. However, such punctual evaluation of this phenomenon may not be representative of the glare condition occurring throughout the whole space considered, which again may negatively affect

choices relative to the design and the operation of transparent adaptive façade components. These choices may ultimately result in a lower comfort condition or in a higher energy use than those estimated, depending on whether the occupant can or cannot interact with the transparent adaptive technology.

All the above issues prevent a full exploitation of the technical potential of transparent adaptive façade components, as it is currently possible to achieve only a partial picture of the performance of such technologies. The research activity was therefore aimed at overcoming the highlighted limitations, in order to make the expected energy savings and the high comfort level expectations related to these innovative components really achievable. In this framework, the Ph.D. thesis proposes a novel simulation methodology for a simultaneous, accurate and comprehensive assessment of the effects of the behaviour of transparent adaptive façade technology on visual comfort and energy aspects (Chapter 3). As for the latter, a simplified and fast approach is proposed for evaluating the glare condition of the occupants throughout a whole space (Chapter 4).

Chapter 3

Novel integrated simulation methodology for transparent adaptive façades

3.1 Introduction

Part of the work described in this chapter has been previously submitted by the author and co-workers to international peer-reviewed journals [7] or presented at international conferences [174].

The possibility of numerically assessing the performance of transparent adaptive façade components could play a crucial role in fostering their adoption in the building industry, as well as in supporting the development of innovative adaptive components. However, from the analysis of the state of the art presented in the previous chapter, it emerged how currently available BPS tools are inadequate to provide a comprehensive evaluation of the performance of transparent adaptive façade components. Two main limitation were identified: (i) inability to simultaneously evaluate in an accurate and comprehensive way the effects of the behaviour of a transparent adaptive component on energy and visual comfort aspects; (ii) inability to model complex phenomena relative to the behaviour of some transparent adaptive technologies (e.g. hysteretic behaviour).

Starting from these premises, a novel integrated simulation methodology was devised, aimed at overcoming the highlighted limitations of BPS tools in the evaluation of the performance of transparent adaptive façades.

Section 3.1 presents the architecture and workflow of the integrated simulation methodology proposed. The choice of the daylight and energy simulation tools selected for the data integration is detailed, as well as the methods used to overcome the limitations previously highlighted. Finally, an overview of the capabilities of the proposed simulation methodology is provided,

along with the advantages and possibilities deriving from its application for the evaluation of the performance of transparent adaptive façade components.

Sections 3.3 and 3.4 provides two applications of the above methodology to two case studies, with the aim to demonstrate the capabilities of the methodology proposed. In more detail, section 3.3 presents the application of the integrated simulation methodology for a comprehensive assessment of the performance of a passive adaptive transparent façade component, namely a thermochromic glazing characterised by a hysteretic behaviour. Section 3.4 presents the application of the proposed methodology for an accurate and comprehensive evaluation of the effects over both energy and visual comfort performance of an active transparent adaptive component, i.e. an electrochromic glazing, operated according to different mono-objective and mono-domain control strategies.

3.2 Simulation approach and workflow

In the present section the integrated simulation approach proposed in the framework of this thesis is described in detail.

This approach manages together an energy simulation tool and a daylight simulation tool by means of data-integration, within the methodology developed by Favoino et al. [69] to simulate adaptive glazing, which relies on the use of the Energy Management System (EMS) [171] module of EnergyPlus [110]. This approach was enhanced by custom-defined EMS and python [175] scripts to allow: i) a comprehensive evaluation of the visual comfort condition of the occupants, assessed both in terms of daylight availability within the whole space and glare condition for the occupants; ii) the assessment of the effects of advanced multi-objective multi-domain control strategies; iii) the evaluation of the effects due to complex phenomena relative to the behaviour of adaptive glazing, such as the hysteretic behaviour observed for some passive transparent adaptive components. In more detail, a bespoke BPS tool was developed within a parametric environment through Rhinoceros [176] parametric plugin Grasshopper [177]. Its add-on Ladybug/Honeybee [178] was used to manage together EnergyPlus and DAYSIM [155] and ensure a complete interoperability between the two software. Finally, a number of custom-defined Python [175] scripts was created for different purposes, including the parametric definition of the numerical model defining the adaptive components behaviour and modulation range and the post-processing of the daylight results to calculate the annual visual comfort metrics.

EnergyPlus was chosen as energy simulation software as its Energy Management System (EMS) tool [171] allows the definition of custom-defined numerical models for the behaviour of transparent adaptive components. In more detail, by means of its actuator *construction state* it is possible to vary the thermo-optical properties of the component within the simulation runtime [179]. The use of this EMS actuator to variate the thermo-optical properties of a transparent component was validated against both experimental data and numerical models

[180]. The error committed was found to be comparable to that relative to validated glazing numerical models [181]. Moreover, EnergyPlus software undergoes both analytical and comparative validation tests [182] and, as a consequence, the EnergyPlus model can be considered as validated.

DAYSIM 4.0 [155] was chosen as daylight simulation software. This is a Radiance-based daylight simulation tool allowing annual evaluation of daylight conditions within a space by means of the Daylight Coefficients (DC) method [159,160,183]. Not only DAYSIM is a validated software [157,184], but the higher accuracy of its daylight calculation engine, i.e. Radiance [123], in the simulation of the daylight conditions within a side-lit office space in respect to EnergyPlus was also numerically [158] and experimentally [179] demonstrated.

The simulation strategy workflow, graphically represented in Figure 4, is subdivided into 4 steps, explained in detail in the present section.

STEP 1 – Discretisation of the modulation range into static states

The thermo-optical range of variation of the adaptive glazing is discretised into a number of static states whose thermo-optical properties vary within those of the clearest and darkest states. Higher discretisation resolutions (a higher number of static states) allow a higher accuracy in the final results, but also imply a higher computational effort for the annual simulations to be carried out. The discretisation should be therefore performed in a number of static states offering the most viable trade-off between the accuracy of the outcomes and the computation time required, depending on the scope for which the integrated simulation methodology is applied.

STEP 2 - Daylight Simulation

For each static glazing, derived from the discretisation performed in the previous step, an annual daylight simulation is performed through the software DAYSIM. Horizontal illuminance and Daylight Glare Probability for one or more significant points within the room are calculated for every timestep of the year for each static state. Moreover, the power fraction relative to the lighting system, which depends on the horizontal illuminance values obtained and on the minimum illuminance requirement set, is calculated for every timestep of the year as well. Output of this step are, for each static state, a power fraction annual profile, a horizontal illuminance annual profile and a DGP annual profile. Relative to every timestep of the year, the first profile contains a power fraction while the second and the third one contain, for each point considered, a horizontal illuminance value and a DGP value respectively.

STEP 3 – Numerical model and Energy simulation

A numerical model describing the behaviour of the adaptive component is created within the EMS. This could be either the intrinsic behaviour of passive transparent adaptive façade technologies or a control strategy for the operation of

an active adaptive glazing. In this phase, inputs relative to thermal, energy and visual comfort aspects can be used, even at the same time, as drivers to control the adaptive component or to describe its behaviour. The power fraction profiles for the lighting system relative to each static state, evaluated in Step 1, are then supplied to EnergyPlus, to be used to calculate, with a high accuracy, the energy demand for lighting and the influence of the lighting system on the energy demands for heating and cooling. Afterwards, an annual simulation is performed to assess the energy performance of the space analysed equipped with the adaptive glazing. In more detail, within the EMS the thermo-optical properties of the transparent adaptive façade component are varied directly within the simulation run-time. At each timestep, the most suitable glazing state is selected, among the static states defined in Step 1, according to the constraints preliminarily defined. This state is then set as glazing through the EMS actuator *construction state* and the power fraction of the lighting system relative to that static state and the timestep considered is used. The thermal and energy balances are then solved, and the energy demands for heating, cooling and lighting are finally calculated. This operation is repeated for every timestep of the year. The simulation routine occurring at each timestep is illustrated in Figure 5. Output of this step are the annual energy demands for heating, cooling and lighting, as well as an annual profile indicating which static state, among those determined in Step 1, was used at every timestep of the year.

STEP 4 - Postprocessing

The different horizontal illuminance and DGP profiles created in Step 2 are merged together according to the annual profile created in Step 3, which indicates the static state assumed by the adaptive glazing at every timestep of the year. The resulting horizontal illuminance and DGP profiles, containing the horizontal illuminance and DGP value for every point considered at every timestep, describe the annual daylight and glare condition due to the adaptive behaviour of the transparent façade component. Starting from these profiles, annual visual comfort indicators are finally calculated. All the operations described in Step 4 are performed through a series of custom defined python scripts. Output of this step are annual Climate-Based Dynamic metrics relative to the visual comfort perceived by the occupants in the space analysed, assessed both in terms of daylight availability in the whole space and of glare condition for the occupants.

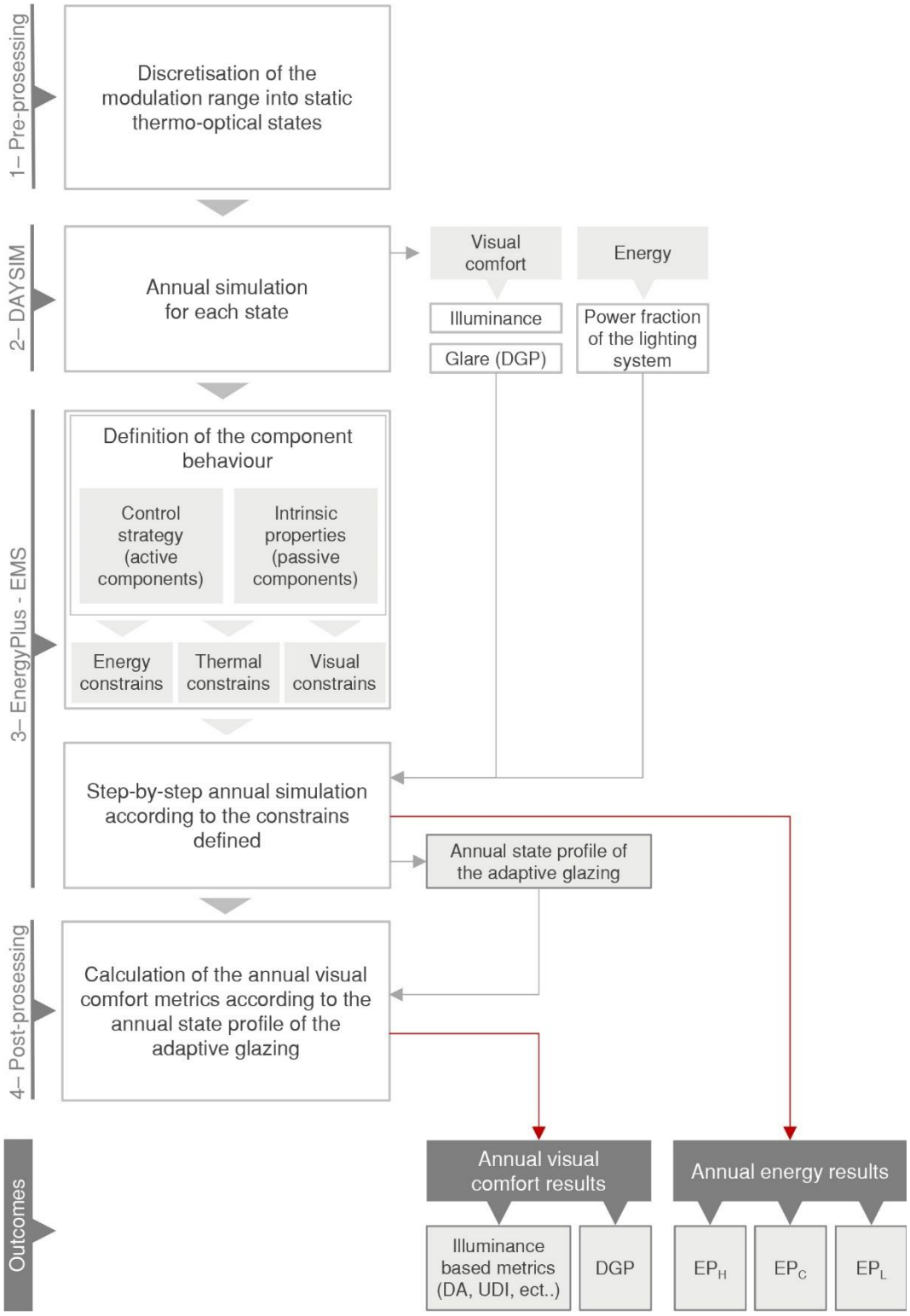

Figure 4. General workflow of the proposed simulation strategy.

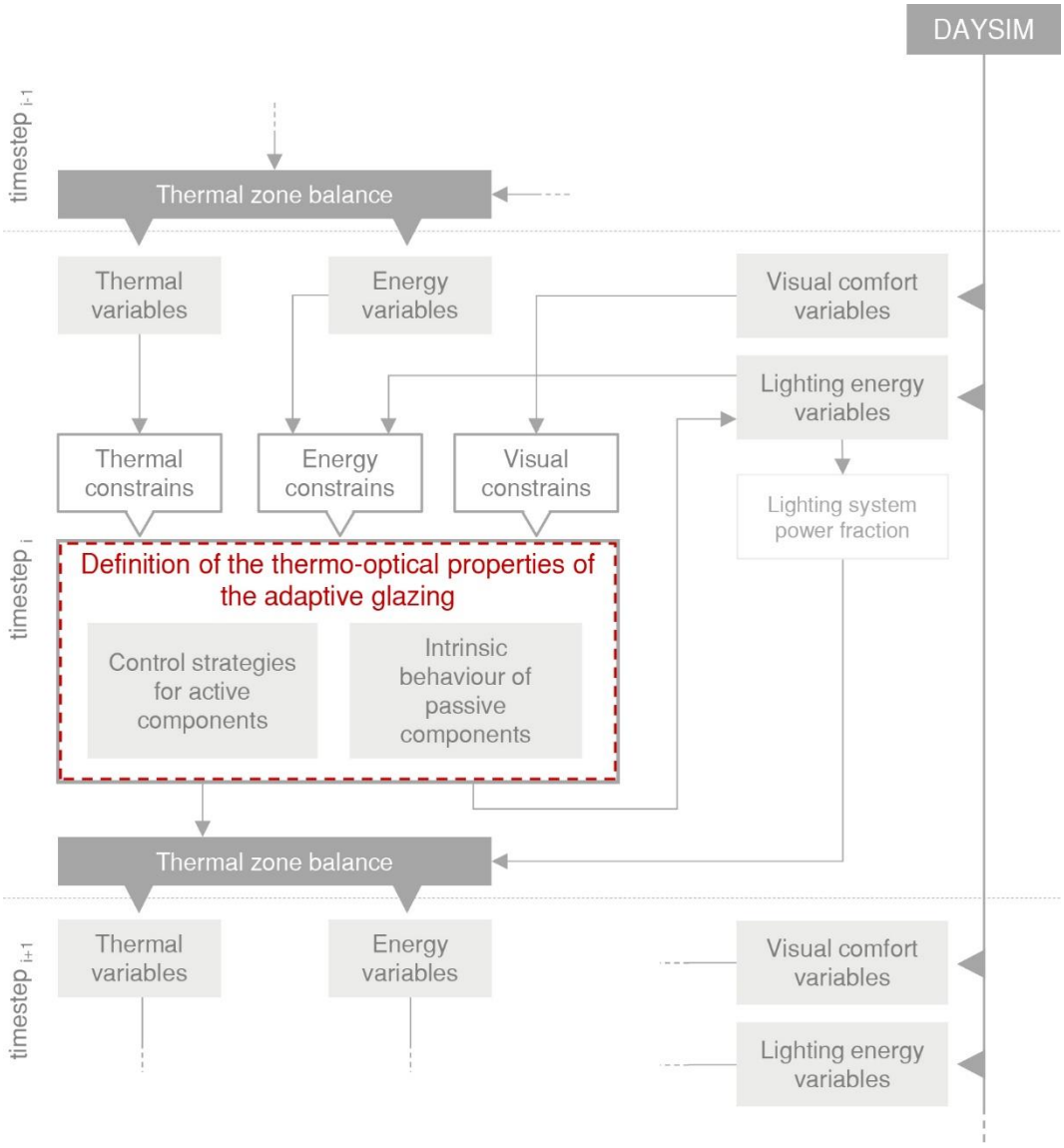

Figure 5. Simulation routine within each timestep.

The presented timestep-by-timestep simulation approach allows the variation of the thermo-optical properties of the adaptive component within the simulation runtime itself, which in turn implies to precisely consider the thermal inertia of the building and its effects on the energy demands for heating and cooling. Moreover, in such simulation approach, a full integration between the daylight simulation tool and the energy simulation tool is performed, allowing not only a simultaneous evaluation of the effects of the adaptive component behaviour on energy and visual comfort aspects, but also for daylight (visual comfort), thermal and energy constraints to be simultaneously used as drivers to operate an adaptive component or to describe its behaviour. This aspect is particularly valuable when dealing with advanced multi-domain control strategies, according to which the operation of the adaptive glazing is performed considering at the same time energy and comfort aspects. Moreover, in presence of adaptive components whose behaviour depends on constraints relative to a single physical domain, this approach allows an accurate assessment of the performance related to the other

interrelated physical domains (e.g. the energy performance relative to a photochromic glazing or the visual comfort provided by a thermochromic glazing). This last aspect represents a strength of the proposed integrated simulation approach, as a comprehensive evaluation of the performance of such adaptive transparent components, typically passive adaptive glazing, was not possible by means of currently available BPS tools, if not by introducing some simplifications in the analysis, with a consequent higher degree of inaccuracy in the final outcomes. Finally, the implementation in grasshopper of this simulation strategy allows a high flexibility for its application, as all the actions described in the previous four steps are performed in an automated way. The only requirement is that of specifying the numerical model describing the behaviour of the adaptive component, which allows simulating both control strategies for active components and the intrinsic behaviour of passive adaptive glazing.

3.3 Application to a passive component: thermochromic glazing

3.3.1 Introduction

In the present section the proposed novel integrated simulation methodology is applied to the case of a passive transparent adaptive façade component. Passive switchable glazing are gaining ever-increasing popularity and a widespread adoption in real buildings is therefore expectable in the next few years to compete with solar protection systems, particularly thermochromic (TC) and thermotropic (TT) transparent materials. These are transparent functional materials which exhibit a reversible change of optical properties as a response to a variation in temperature, most of the time concurrent with building performance requirements, i.e. the higher the incident solar radiation, the higher the functional material temperature, the lower the transparency and vice-versa. The building integration of such materials into glazing systems appears to be advantageous compared to other functional smart materials due to [24]: i) their intrinsic passive working principle allowing to reduce the amount of solar radiation passing through the transparent system as the incident solar radiation increases, which does not need any active control over their operations nor energy supply and wiring; ii) their possibility of integration into polymer based materials (which could enhance integration into curved glazing as well); iii) the potential overall lower costs compared to active smart glazing (i.e. electrochromics and liquid crystals); iv) a negligible influence of high temperatures on the switching mechanisms as compared to other technologies, such as photochromic materials [22].

In order to ensure effective building performance and building integration, the passive thermochromic switching mechanism feature shifts the challenge of designing and implementing effective operation strategies [89,185] to the need of optimising the switchable functional materials by design [65]. Research efforts have mainly focused at the material scale to improve different features of

thermochromic and thermochromic transparent functional materials with different techniques, particularly aimed at [24,67] maximising their range of variable solar and luminous transmittance (τ_{sol} and τ_{vis}), tuning the switching temperature range towards glazing applications, improving colour neutrality, ensuring material stability and durability, reducing overall costs of the functional material and of the processing for glazing integration. Nevertheless, understanding the effect of tuning functional material properties on overall building performance and the effectiveness of material design choices on building performance and integration aspects is not a trivial task. This requires in fact an evaluation and analysis of the transparent functional material behaviour at the building scale, which has to deal with the following aspects: different physical domains can be affected simultaneously by the transparent material adaptive behaviour (i.e. thermal and luminous), which are often highly interdependent to each other (as for thermochromic mechanisms); different performance aspects need to be considered, which may be conflicting with each other (i.e. energy efficiency, visual comfort requirements, thermal comfort requirements etc.); simulation models need to describe with enough accuracy material macroscale effects (i.e. optical properties variation over temperature) of microscale functional material behaviour and how this is influencing the interrelated building physical domains.

However, as seen in Chapter 2, currently available Building Performance Simulation (BPS) tools do not integrate simulation methodologies and models allowing a multi-physical, multi-performance and multi-scale evaluation, if not by introducing simplifications. As a result, most of the studies focused at evaluating the effect on building performance of thermochromic material features provides only a partial picture of its effectiveness as: influence of TC properties (mainly average switching temperature) is investigated by studying its effect only on heating and cooling energy uses [186]; influence of TC material properties on aspects related to comfort are carried out only for specific conditions during the whole year (i.e. design conditions) [187]; the temperature dependency of optical properties does not consider peculiar TC and TT features as temperature hysteresis [180,187,188], or it does so by introducing significant model simplifications [148,186]. The development of accurate analyses is of paramount importance for both material scientists, building performance researchers and building designers, enabling to optimise materials for effective building integration and building performance maximisation on one hand, informing decision making for material design at a smaller scale on the other, helping some of these technologies to go beyond the so-called “valley of death” [89,189].

The application of the proposed integrated simulation methodology to the case of a TC glazing is therefore aimed at showing its possibilities and advantages, compared to currently available BPS tools. Specifically, the use of such methodology enabled: i) a comprehensive whole building evaluation of TC glazing performance for office buildings application, considering both thermal related aspects (i.e. energy efficiency, in terms of energy demand for cooling, heating and lighting) and visual comfort aspects in an interrelated fashion; ii) the

correct modelling of peculiar material aspects, such as temperature dependency of optical properties and hysteresis.

In sub-section 3.3.2, a review of transparent thermochromic and thermotropic functional material features is presented. This is followed by the description and the optical experimental characterisation of the thermochromic material adopted as a case study, showing both large visual and solar transmittance variation range as well as temperature hysteretic dependency of optical properties. In sub-section 3.3.3 the simulation methodology is presented consisting of: i) a parametrical numerical model describing thermochromic material features (such as hysteresis phenomena and dependency of optical properties over material temperature), developed on the material optical characterisation; ii) the implementation of this model into the ad-hoc developed multi-physics simulation strategy for adaptive transparent materials. The developed transparent thermochromic material model, based on the experimental data, is thoroughly described and its validation is presented. Following, a virtual experiment is designed to study the influence of thermochromic hysteresis on building performance as related to energy use and visual comfort. The results and discussion sub-sections (3.3.4 and 3.3.5) present the performance of the characterised thermochromic material when building integrated and the influence of the hysteresis of this performance on multiple aspects.

3.3.2 Thermochromic and thermotropic materials and glazing

3.3.2.1 Literature review

In the present section, a more in-depth insight on thermochromic and thermotropic materials and glazing is provided, as integration to the more general review contained in section 2.2.

Thermochromism (TC) is the feature of a functional material to vary reversibly its optical properties as a response to a temperature variation. This mechanism is the optical effect of a change of material micro-structure, induced by the temperature variation, whose nature and effect on the transmitted solar radiation depends on the type of material adopted. The integration of such functional materials into a glazing system allows achieving a passive smart glazing with temperature dependent optical properties that can be used for different purposes such as controlling solar gains, daylight and view-out.

More specifically [24] distinguishes between thermochromic (TC) and thermotropic (TT) materials and glazing according to the interaction of the material with the solar radiation. In TC materials (and glazing) the temperature dependent solar transmittance is complementary to a temperature dependent absorption [24], such that the directionality of solar radiation is maintained when transmitted through the window and the material may vary its transparency and colour as a result of the temperature variation (it absorbs more as the temperature increase, so it may become darker if the luminous transmittance/absorption varies). Alternatively, in TT materials (and glazing), the temperature dependent

solar transmittance is a result of the variation of light scattering properties of the material (forward- and back-scattering) [24], so that the solar radiation and particularly the light is diffused (forward scattering) and reflected (back scattering) as the temperature exceeds a certain limit. Therefore, TT glazing usually ensure the view out only in their more transparent state, below the so called "Lower Critical Solution Temperature" (LCST), as due to an increase in light scattering they would assume a milky diffusive appearance.

To date, extensive research has been carried out on TC materials based on inorganic thin films on glass substrate [67], while fewer examples exist of thermochromic polymer systems.

TC thin films are based on Vanadium Oxide (VO_2) Semiconductor-Metal phase Transition (SMT), that is an automatic and reversible first-order transition happening at a certain critical temperature. In more detail, below the transition temperature VO_2 exhibits a monoclinic reticular structure, which determines the compound to have semiconductor properties, while above this temperature VO_2 shows a rutile structure, meaning that the material shows metallic properties. VO_2 as semiconductor (monoclinic) is transparent across a wide range of IR solar radiation, whereas in its rutile structure (metallic) it shows a reflective attitude towards the same IR solar radiation range [16,17]. Pure vanadium oxide shows a critical temperature for the SMT to occur equal to 68.5 °C, which makes this bare compound unsuitable for architectural use, as this temperature is seldom reached in architectural glazing. The possibility of enhancing VO_2 switching properties have been widely investigated [67], with the aim to: i) lower the transition temperature to room temperatures (i.e. 25 ÷ 35 °C); ii) widen the solar switching range; iii) increase the visual transmittance below the transition temperature; iv) improve the colour neutrality [190–192]. Different approaches are documented in literature to enhance VO_2-based TC layers. Cui et al. [193] provides an extensive review of these techniques and their effect on the optical properties, such as elemental doping the VO_2 layer (with tungsten, W, magnesium, Mg, and Silicon, Si [18,19]), embedding VO_2 nanoparticles into dielectric matrix (VO_2 nanocomposite) non thermo-responsive, increasing the porosity of the VO_2 layer, integrating anti-reflection coating and enhancing the nano- and micro-structure of VO_2 crystals (including bio-inspired and grid patterned nanostructures). The use of VO_2 based TC for solar and daylight control in buildings may be limited by the fact that a significant transmittance modulation is only achievable in the near IR region, while it is negligible in the visible part of the solar spectrum (accounting for 42% of the energy in the whole solar spectrum).

On the other hand, TC polymer systems, based on doping of a polymeric transparent matrix with TC additives, can achieve modulation of visible and solar spectrum, while maintaining their specular behaviour below and above the critical temperature. The temperature dependent optical properties in Ligand-Exchange Thermo-Chromic systems (LETC) [21,22] are based on the variation of the coordination environment around central metal ions (Ni, Co or Fe) into a transparent polymeric matrix (which is the common PVB, polyvinyl butyral,

interlayer used to laminate glass panes in glazing systems). Particularly the structure of the molecule and the nature of the chemical bonds around the central metal ion varies according to temperature: below a certain critical temperature the metal ion is coordinated with 6 low ε ligands (low molar extinction coefficient) assuming a lighter colouration (higher visible and solar transmittance), while above the critical temperature the metal ion coordinates with high ε ligands (high molar extinction coefficient ε assuming a darker colouration (lower visible and solar transmittance). The transition temperature (around 50 °C) is a function of the concentration of low and high ε ligands, while the nature of the counter ions (coordinating with the free high or low ε ligands, depending on the temperature) may reduce the thermochromic effect [21]. Leuco-dyes are weak acids varying their colour reversibly as a function of the pH of the dielectric they are embedded into. In order to achieve a Leuco-dye TC system, the weak acid dye and a dissociable salt are dispersed into a solid fatty alcohol matrix, around the transition temperature the matrix undergoes a phase change from solid to liquid and the salt dissociates, varying the pH of the solution, affecting the colour of the dye, hence of the whole TC system [194]. Successful integration of Leuco-dyes TC systems into PE films shows transition temperatures around 60-80 °C, with significant visible transmission modulation and high visible transmission in the non-coloured state ($\tau_{vis,h}$=61%, $\Delta\tau_{vis}$=27%), but negligible solar transmission modulation [24]. Although, the poor stability of the Leuco-dyes does not allow a reliable integration into smart glazing for building applications [22].

Thermotropic (TT) materials can achieve a very significant temperature dependent modulation of optical properties (both visible and solar), due to their light scattering properties above the LCST, which in contrast prevents view out. Temperature variation of optical properties is achieved by varying the ratio of the refractive index of different components of a polymer matrix, which is carried out mainly by means of phase separation (ionogels), change of particle size (hydrogel microparticles) and phase transition (polymer blends with phase transition and casting resins) [24]. Ionogels are a gel material containing ionic liquids (IL, salts with melting temperature below 100 °C), which are highly homogeneous and transparent at room temperature. When integrated into a PU matrix [195], by increasing the temperature above the LSCT (tunable, around 32 °C), molecular repulsion between IL and PU network increases, resulting in a temperature reversible phase separation which causes light scattering and reduces the solar and luminous transmittance. Hydrogels nanoparticles are crosslinked hydrophilic polymer network which undergo a hydrophilic-to-hydrophobic transition at LCST, this causes a change of nanoparticle sizes from a fully swollen gel state (hydrophilic below LCST) to a shrank hydrophobic state (above LCST), varying the refractive index between the nanoparticle and the surrounding matrix. Poly-N-isopropylacrymide (PNIPAm) is the most typical temperature responsive hydrogel (LCST ~32 °C) and has been demonstrated in smart glazing applications [25–27], with large modulation capability of both visible and solar radiation ($\Delta\tau_{vis}$ and $\Delta\tau_{sol}$

of nearly 80%, with $\tau_{vis,max}$ and $\tau_{sol,max}$ in the order of 80%). However, TT hydrogels have cyclic stability issues, as they inherently suffer (due to their water content and size variation) from water freezing or evaporation, severe shrinkage and poor mechanical strength. Ionogels instead retain high stability at high temperatures and no shrinkage issues. Polymer blends of polymers with different solid-liquid transition temperatures (alkanes or fatty acid esters as cores of casting resin shell matrix), can achieve a temperature dependent refractive index, resulting in light scattering as the temperature increases [24], so that reversible temperature dependent optical properties are achieved ($\Delta\tau_{vis}$ in the range of 9%-40%), although differently from other TT materials due to the phase transition optical modulation mechanism, this occurs over a wider range of temperatures (30-80 °C) rather than at a specific LCST.

Finally, hybrid approaches and materials are reported which mix TC VO_2 nanoparticles with TT hydrogels [196–198], in order to achieve improved luminous and solar modulation.

Table 1 summarises the ranges of optical properties achievable in the different TT and TC materials and systems reviewed, as reported by the reviewed literature in terms of $\Delta\tau_{vis}$ and $\tau_{vis,max}$, $\Delta\tau_{sol}$ and $\tau_{sol,max}$.

Table 1. Range of Temperature Modulation capabilities of optical properties for thermochromic and thermotropic smart glazing.

Thermochromic smart glazing (specular – specular)	**$\Delta\tau_{sol}$** [-]	**$\tau_{sol,max}$** [-]	**$\Delta\tau_{vis}$** [-]	**$\tau_{vis,max}$** [-]	**T_{crit} (SMT)** [°C]	**Reference** [-]
Thin films (VO_2-based)*	0.10÷0.40	0.20÷0.80	0..02÷0.09	0.10÷0.80	25÷70	[67] [193]
LETC	0.15÷0.25	0.40	0.57	0.62	25÷75	[25] [22] [25]
Leuco-Dyes	0.05÷0.06	0.50÷0.70	0.07÷0.30	0.30÷0.60	60÷80	[24]
Hybrids VO_2 LETC	0.10÷0.20	0.80	0.05÷0.10	0.60	40÷50	[199]
Thermotropic smart glazing (specular – scattering)	**$\Delta\tau_{sol}$** [-]	**$\tau_{sol,max}$** [-]	**$\Delta\tau_{vis}$** [-]	**$\tau_{vis,max}$** [-]	**LCST** [°C]	**Reference** [-]
Ionogel	0.55	0.70	0.70	0.85	32	[195]
Hydrogel microparticles	0.50÷0.80	0.85	0.66÷0.85	0.90	32	[25] [26] [27]
Casting Resin into PE films	0.09÷0.16	0.40÷0.50	0.09÷0.40	0.16÷0.64	30÷80	[24]
Hybrid VO_2 hydrogels	0.18÷0.35	0.79÷0.84	0.25÷0.39	0.82÷0.86	32÷68	[196] [197] [198]

Most of TT and TC materials presents a hysteretic behaviour between the heating and cooling phase, meaning that the relationship between the variable

optical properties and the temperature will follow a different path if the material is heated up or cooled down. This is due to the fact that a greater amount of energy (activation energy) may be required to reverse the thermochromic phenomenon allowing a homogenous nucleation of the thermochromic transition [17]. This additional thermal energy required determines the width of the hysteresis. This phenomenon is particularly documented for thermochromic and thermotropic materials whose optical properties variation is based on phase transition, i.e. VO_2 thin films and nanoparticles [18,200] and casting resins into PE films [24]. In VO_2 based thermochromics, hysteresis seems to be strongly influenced by the structure of the VO_2 film, as regular lattice structures proved to require a higher activation energy than irregular ones, meaning that the first ones present wider hysteresis than the second ones [18,200]. As a consequence, the hysteresis phenomenon can be controlled in the same way as the optical properties switching range, i.e. through a doping process or by controlling the microstructure [201,202].

Due to the negligible visual transmittance variation of thin film TC materials, BPS tools and simulation studies aimed at evaluating their performance and informing decision making at the material level, focused only on heating and cooling energy uses to date [148,186–188]. Nevertheless, according to this review, TC and TT materials can have a large visual transmittance modulation (see Table 1), therefore for these materials a more comprehensive evaluation should rely on multi-physical and multi-performance studies, taking into account the interrelation between physical aspects in the thermal and visual comfort domain and the effect of variable optical properties on total energy use (including lighting) and visual comfort.

3.3.2.2 Thermochromic sample description

In the present study a thermochomic glazing of dimensions 200 mm x 200 mm is optically characterised. The sample is a laminated glass composed by two clear glass panes connected to one another by a highly tear-resistant, thermochromic interlayer. The two glass panes have a thickness of 3 mm while the interlayer is 1 mm thick, for a total thickness of 7 mm. The thermochromic interlayer is a LETC system commercialised by Pleotint LCC (commercial name Suntuitive™ [21,22,203]), which exhibits modulation of solar and luminous transmittance and a specular behaviour below and above the transition temperature. The interlayer laminate is constituted by a three layers system to achieve colour neutrality, with a two Ni-based LETC systems tinting blue and orange divided by a clear separator. Figure 6 shows a thermochromic glazing with the same characteristics as the sample analysed, but bigger size, in its clear state and in an intermediate state, relative to a glass surface temperature equal to approximately 40 °C.

Figure 6. Views from outside (upper band) and inside (lower band) of a thermochromic glazing with the same characteristics as the sample analysed. The pictures are relative to the component in its clear state (left) and in an intermediate state, relative to a glass surface temperature equal to 39.2 °C (right).

3.3.2.3 Experimental apparatus and procedure

The optical measurements on the TC glazing sample were carried out by means of a customised optical bench, able to carry out tests on complex and large specimens, for which commercial spectrophotometers are not suitable. The experimental apparatus set-up for the experimental campaign hereby presented (see Figure 7) consists of the following components:

- 300 Watt xenon arc-lamp light source, whose radiant power covers the whole visible spectrum and 94% of the solar spectrum, as defined in the relevant standard [204]. The collimated beam can be modulated through a sequence of lenses and diaphragms, so as to adjust its size according to the measurement requirements and the geometric complexity of the sample. According to the incident radiation requirements and the characteristics of the thermochromic glass, the light beam diameter was set equal to 60 mm.
- The detection system is a diode-array spectrophotometer, equipped with two detectors to analyse different spectral bands: NMOS for the 250–1000 nm range (dispersion 1.4 nm/pixel) and InGaAs for the 900–1700 nm range (dispersion 3.125 nm/pixel). Spectral data are re-built in the data post-processing with a spectral resolution of 1 nm.

- The spectrophotometer is coupled with an integrating sphere whose internal diameter is equal to 75 cm, suitable for diffusing and complex glazing units. The sphere is constituted by an aluminum shell coated in its internal surface in Spectralon©, a highly diffusing material whose reflectivity is greater than 95% in the whole solar spectrum. The sphere is equipped with several ports to perform transmittance and reflectance measurements with the auxiliary port method, as required for single beam-type spectrophotometers. The sample port diameter can be varied according to the sample characteristics. A 200 mm port was used for this test. The signal (radiant power) collected inside the sphere is transmitted to the detection system via optic fibres.

The following optical measurements were performed:

- the transmission coefficient (τ), transmittance hereafter, was measured as the ratio between the radiation transmitted by the glass mounted on the sample port and the radiation entering the sphere by the same port without specimen. Measurements were carried out at normal incidence;
- the reflection coefficient (ρ), reflectance hereafter, was measured as the ratio between the radiation reflected by the specimen and that reflected by a calibrated white target. The two specimens were mounted in turn on the sample port. In reflection mode, the angle of incidence between the light beam entering the sphere and the specimen surface normal is equal to 8°.
- The absorption coefficient (α), absorptance hereafter, is calculated as the complement to 1 of the previous measurements.

The measurement procedure followed is explained in detail in [205]. The instrument error is estimated to be, in the 0-1 range, equal to 0.02 in both transmission and reflection mode.

Transmittance measurements were performed for different surface temperatures, with the aim of characterising the optical response of the sample in its cold and hot limit states, as well as in its intermediate states. The measurements were carried out in the following modes:

- Heating mode: the sample was measured from its cold limit state (fully bleached) to its hot limit state (fully tinted) at each 5 °C temperature increase. The sample was heated-up in an oven, next to the measurement apparatus, to the desired temperature and then the measurement was rapidly performed.
- Cooling mode: the sample was measured from its hot limit state (fully tinted) to its cold limit state (fully bleached) at each 5 °C temperature decrease. The sample was heated-up to maximum temperature in an

oven and then cooled-down by direct exposure to ambient temperature.

In the cooling mode, additional measurements were carried out at a surface temperature resolution smaller than 5 °C, with the aim of supporting the numerical analysis with a large experimental dataset. The surface temperature was monitored during each optical measurement, lasting between 15 and 20 seconds, by means of thermo-graphic images (previously calibrated with thermocouple measurement). Starting from the spectral measurements performed, broadband parameters were then calculated according to procedures defined in [206].

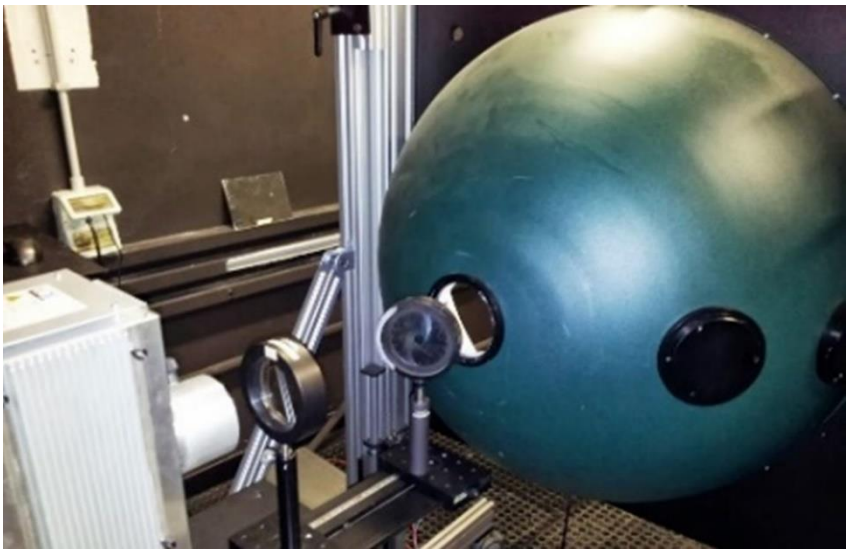

Figure 7. Close-up of the experimental apparatus, view of the light source, lens and diaphragm and integrating sphere.

3.3.2.4 Optical characterisation of the thermochromic material

Preliminary measurements were carried out on both faces of the sample, to detect eventual differences in the optical response of the glazing unit. As negligible differences were found, all the measurements were carried out to following the manufacturer specifications, i.e. with side 1 of the sample facing outwards. Spectral transmittance curves in cooling mode are presented in Figure 8. It can be observed that the material shows a relevant switching behaviour in the visible range (380-780 nm), while it significantly decreases in the near-infrared region (780-1700 nm).

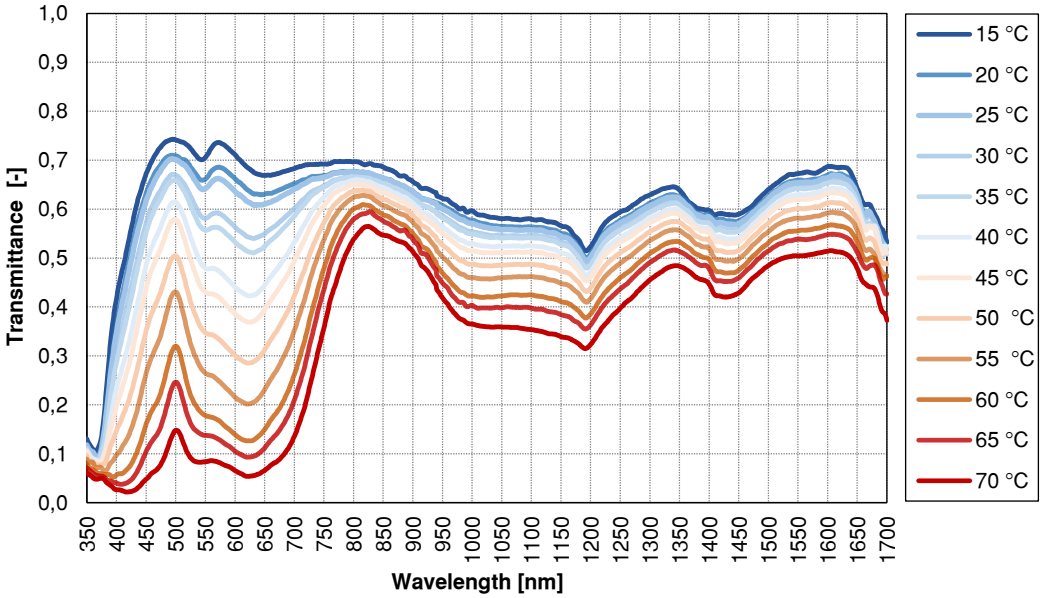

Figure 8. Spectral transmittance of the thermochromic sample for different surface temperature. Measures relative to the cooling mode.

This different response is better highlighted in Figure 10 and Figure 11, where the evolution of broad-band parameters is calculated with a resolution of 5 °C between the limit surface temperatures, equal to 15 °C and 75 °C. The visible transmittance switches between 0.71 in the clear state to 0.07 in the fully tinted (hot) state. The sample shows a switching factor approximatively of 10 between the extreme values, switching factor which remains higher than 2 between the cold state and 50 °C, a surface temperature rarely reached by vertical glazing systems. The solar transmittance shows a lower swathing factor (2.8) between the clear state (0.63) and the fully tinted state (0.23), switching factor which further decreases to 1.8 when 50 °C is considered as limit temperature in operation conditions. This trend is mainly due to the less significant switching factor observed in the near infrared region between the cold state and the solar transmittance value measured at 50 °C. The optical measurements are comparable with the range of optical characteristics of LETC system previously published [22].

Comparing the broad band transmittance relative to the heating and cooling mode, a hysteretic behaviour of the specimen can be observed between 25 °C and 55 °C. This was never previously documented for this kind of TC system (LETC) [21,22,203]. The hysteresis width varies depending on the glass surface temperature, reaching its peak at 45 °C. At this temperature the differences between the measurement in heating and cooling mode relative to visible and solar transmittance are equal to 0.16 and 0.09 (respectively 36% and 19% lower in respect to the visible and solar transmittance values in heating mode). It is worth highlighting that, despite a hysteresis between heating and cooling modes was observed, this is not considered as reliable by the Authors, due to uncertainty intrinsic in the cooling mode measurement procedure. The sample was in fact heated up to its limit hot state and then naturally cooled down by direct exposure

to ambient temperature. This procedure presents an intrinsic error due to the time elapsing between the glass surface temperature measurements and the spectral transmittance measurement through the integrating sphere. Although these steps were performed in rapid succession. The spectral transmittance measurements are referred to an average between temperature measurements before and after the optical measurement, which reached a maximum difference of 2 °C for higher glass surface temperatures, as the difference between the glass and the ambient temperature was higher. As a result, it was concluded that the specimen analysed certainly presents a hysteresis between the heating and cooling cycles, but it was not possible with the current procedure to ensure repeatability of the hysteresis width measurement, so that the measured width of the hysteresis (Figure 10 and Figure 11) of approximately 10 °C is affected by a maximum 2 °C error (including the IR camera accuracy).

Reflectance measurements were carried out for the hot and cold limit states of the sample. From the results obtained (Figure 9) it is possible to observe that this quantity is not significantly influenced by the temperature variation. Moreover, in both states the two spectral curves do not present any selectivity as function of the wavelength. Visible and solar reflectance were both found to be equal to 0.07 in the cold state, while these values decrease to respectively 0.06 and 0.05 for the hot state. The absorptance values were also calculated, according to the transmittance and reflectance results obtained. These were found to be equal to 0.22 and 0.31 respectively in the visible and solar ranges for the cold state, raising to 0.88 and 0.72 in the hot state.

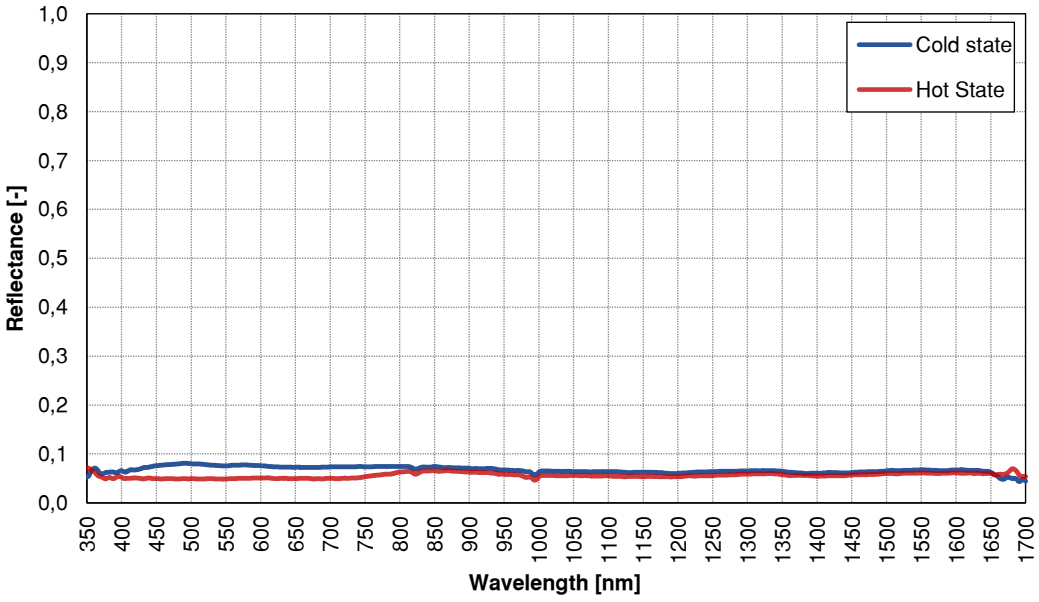

Figure 9. Spectral reflectance of the thermochromic sample in the clear and fully tinted state.

3.3.2.5 Experimental data fitting

A numerical model was derived from the experimental measurements, to be later used for the numerical analysis described in sub-section 3.3.3. A linear

regression model was applied to the experimental data representing the behaviour of the thermochromic glazing by a piecewise function formed by three different segments, whose typical equation is the following [148,186]:

$$\tau = \begin{cases} q_1, & if\ T < T_1 \\ m_2 \cdot T + q_2, & if\ T_1 \leq T \leq T_2 \\ q_3, & if\ T > T_2 \end{cases} \quad (1)$$

in which τ represents either the visible or solar transmittance; T is the glass surface temperature; T_1 and T_2 are limits, lower and upper respectively, of the temperature range in which the switching of the thermochromic glazing occurs. From equation (1) it is possible to observe that outside the transition temperature range, delimited by T_1 and T_2, the transmittance (either visible or solar) is constant, as the two lines are horizontal. For temperatures below the transition temperature range, τ is equal to the maximum transmittance value achievable, while temperatures above the transition temperature range correspond to a τ value equal to the minimum transmittance value achievable. Within the transition temperature range the function is a sloped line, with a linear variation of τ. The experimental data were fitted by means on an iterative process minimising the global variance of the least square differences between piece-wise linear regressions, as shown in Figure 10 and Figure 11. Table 2 summarises the coordinates of P_1 and P_2, the two knot-points of the segmented function, in a cartesian coordinate system OTτ, both for visible and solar transmittance, while Figure 10 and Figure 11 show the data fitting performed relative to visible and solar transmittance respectively.

Table 2. Coordinates of P_1 and P_2, in a Cartesian coordinate system OTτ, both for visible and solar transmittance.

	T [°C]	**τ_{vis} [-]**	**τ_{sol} [-]**
P_1	25.9	0.68	0.62
P_2	71.3	0.06	0.23

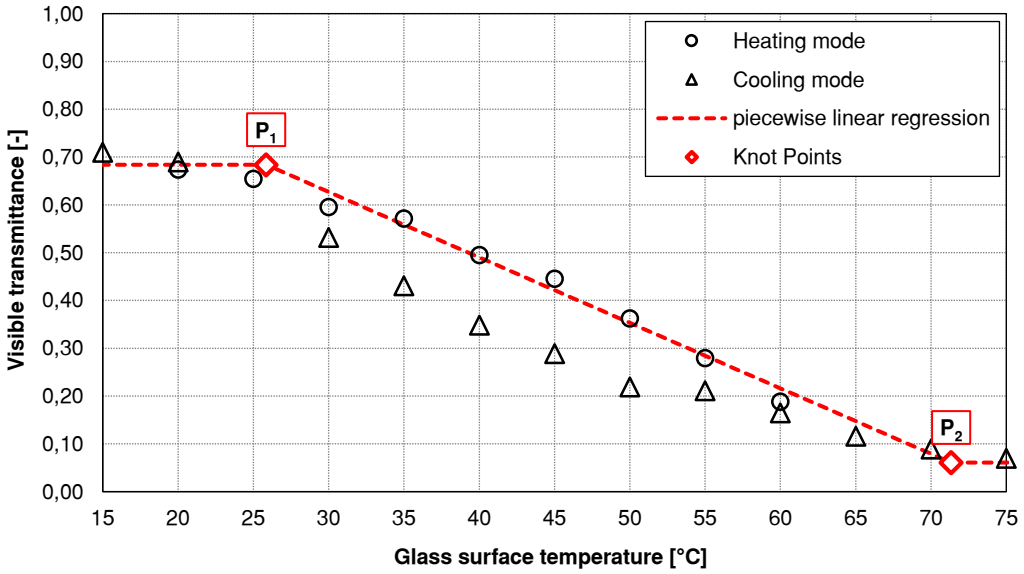

Figure 10. Piecewise linear interpolation relative to the visible transmittance.

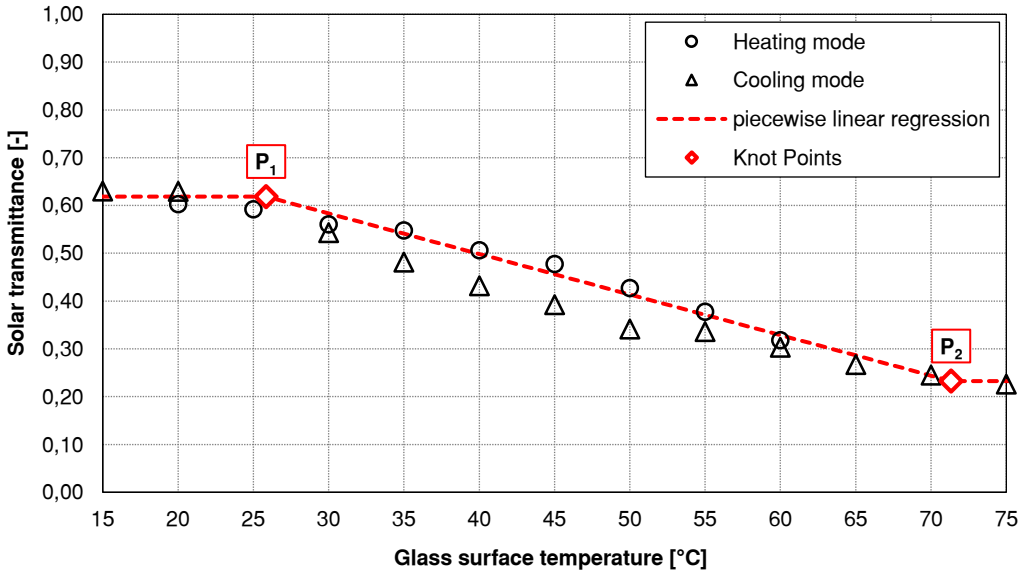

Figure 11. Piecewise linear interpolation relative to the solar transmittance.

3.3.3 Methodology for building performance evaluation

The performance of the characterised material and the influence of the hysteresis width on this performance are evaluated by means of a virtual experiment, simulating in different climatic locations a reference office room, in which the thermochromic glazing under investigation is integrated and by measuring the whole year performance relative to different domains of interest.

3.3.3.1 Simulation workflow

Current building performance simulation tools present the following limitations, which prevent an accurate and comprehensive evaluation of a

thermochromic glazing performance: (i) inability to model the thermochromic hysteresis phenomena; (ii) inability to simultaneously evaluate the effect over daylight domain of variation of thermo-optical properties and vice-versa. For these reasons an ad-hoc simulation tool was created, for which a detailed description is provided section 3.2. Relative to the present application, the simulation workflow is divided into four automated steps, which are herewith listed, while details relative to the hysteresis numerical model are provided in sub-section 3.3.3.2:

1) Discretisation of the thermochromic continuous modulation range into 10 discrete states, corresponding to 10 different static glazing whose thermo-optical properties vary within those of the clearest and darkest TCG states, named *State 0* and *State 9* respectively. Figure 12 shows the discretisation of the range of variation of the TCG relative to the visible transmittance.
2) Daylight Simulation of the different discrete thermochromic states with DAYSIM 4.0;
3) Energy simulation: the energy simulation is performed, including an accurate thermochromic model (based on the experimental data in sub-section 3.3.2.5) implemented within the EMS tool of EnergyPlus; additionally, by means of the EMS the data from step 2 are integrated within the thermal simulation model within this step depending on the results of the thermal simulation. The validation of the thermochromic model is provided in sub-section 3.3.3.2;
4) Postprocessing of the daylight simulation results into yearly performance metrics.

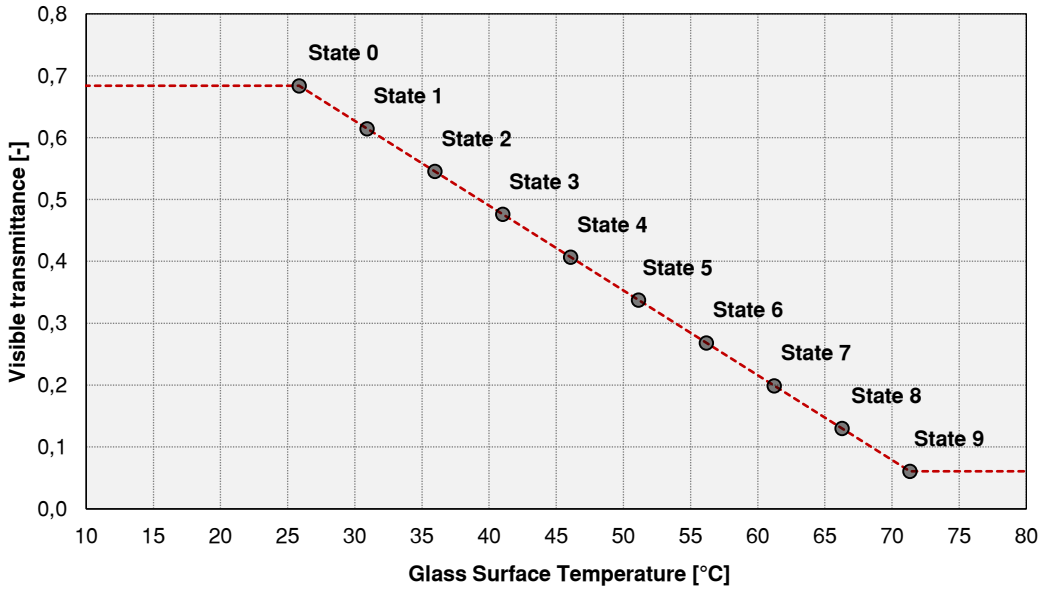

Figure 12. Discretisation of range of variation of the TCG into 10 static glazing, in terms of visible transmittance.

3.3.3.2 Numerical model of the hysteresis

The numerical model created within the EMS to describe the TCG behaviour is based on the step-wise linear regression performed on the experimental characterisation carried out on the TCG, as explained in detail in sub-section 3.3.2.5. The piecewise linear regression curve, based on the experimental characterisation, was adopted as heating curve. The curve defining the cooling cycle was instead defined by a displacement of the heating curve equal to a custom-defined hysteresis width. The working principle underlying the numerical model replicating the TCG behaviour is the following:

1) It is verified whether the TCG is in the heating or cooling cycle by evaluating the difference between the glass surface temperature at the present timestep and at the previous timestep. A positive result indicates that the glass is in the heating cycle, otherwise it is in the cooling cycle;
2) The visible transmittance is then calculated as function of the glass surface temperature according to the heating or cooling curve, depending on whether the TCG is in the heating or cooling cycle;
3) Whether a cycle, either heating or cooling, is interrupted before being completed, the visible transmittance is kept constant until an absolute variation of the glass surface temperature higher than the hysteresis width is observed. When this happens the curve of the inverse cycle - cooling cycle if the TCG originally was in the heating cycle and vice versa heating cycle whether the TCG originally was in the cooling cycle - is then used to calculate the visible transmittance depending on the glass surface temperature;
4) Depending on the visible transmittance calculated, the most suitable static state, among those in which the TCG behaviour was discretised, is then set as glazing through the EMS actuator *construction state*.

As an example, the numerical model is used to simulate a TCG with the following characteristics: τ_{vis} range between 0.68 and 0.06 (cold and hot state respectively); transition temperature range between 26 °C and 71 °C; hysteresis width equal to 5 °C. The behaviour of a TCG was analysed for two different days, one in which the hysteresis cycle was completed and the other one in which it was interrupted. Figure 13 shows the TCG surface temperature variation and the relative visible transmittance, as calculated through the numerical model created. It is possible to observe that when the hysteresis cycle is completed, minimum and maximum visible transmittance values are never exceeded, while when it is not completed the minimum visible transmittance is not reached. Moreover, in this last case, when the TCG surface temperature reaches its peak and starts decreasing (approximatively at 13:30) τ_{vis} remains constant until the surface temperature is decreased of 5 °C, i.e. the hysteresis width of the TCG analysed in

this example. Figure 14 shows instead the correlation between the TCG surface temperature and the calculated visible transmittance for the same two days. It is possible to observe that in both cases all the points are located on or within the grey dotted lines, representing the heating and cooling curve. In the case in which the hysteresis cycle is interrupted it is possible to observe that τ_{vis} remains constant until the cooling curve is met, after which it starts decreasing according to the cooling function.

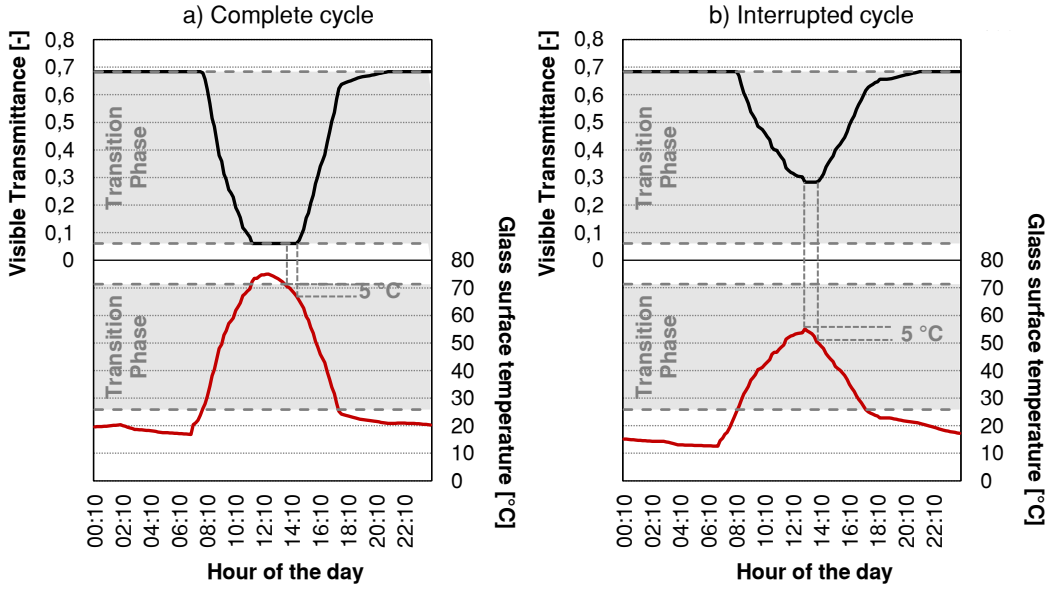

Figure 13. TCG surface temperature variation and the relative visible transmittance, as calculated through the numerical model created for: a) a day in which the hysteresis cycle is completed; b) a day in which in which it is interrupted.

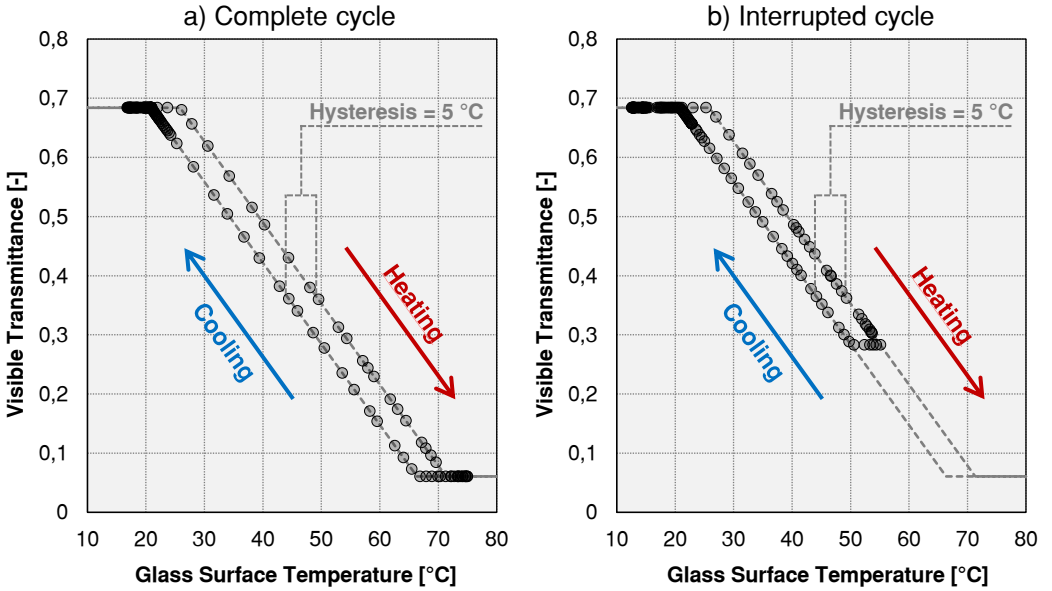

Figure 14. Correlation between the TCG surface temperature and the relative visible transmittance, as calculated through the numerical model created for: a) a day in which the hysteresis cycle is completed; b) a day in which in which it is interrupted.

From the above results, relative to two different conditions (hysteresis cycle completed and interrupted), it is possible to conclude that the numerical model created proved to be robust and suitable for describing the behaviour of a thermochromic glazing.

3.3.3.3 Performance evaluation parameters

In the present study both energy aspects and visual comfort aspects were analysed. This was done by means of the following performance metrics:

Energy Performance index (EP_{gl}): this metric is defined as total amount of primary energy consumed by a building, on annual basis, per unit area. It is expressed in kWh/(m^2·year) and is calculated according to the following equation:

$$EP_{gl} = EP_H + EP_C + EP_L \quad (2)$$

in which EP_H is the primary energy consumed per unit area, on annual basis, by the heating system [kWh/(m^2·year)]; EP_C is the primary energy consumed per unit area, on annual basis, by the cooling system [kWh/(m^2·year)]; EP_L is the primary energy consumed per unit area, on annual basis, by the lighting system [kWh/(m^2·year)]. The influence of the primary energy necessary for domestic hot water production (EP_{DHW}) on the EP_{gl} was considered negligible and was therefore not calculated in the present study.

Useful Daylight Illuminance (UDI): this metric, proposed by Mardaljevic and Nabil [140,207] identifies the percentage of occupied hours over a year in which the daylight horizontal illuminance on the workplane falls below, within or above the range 100 lx – 3000 lx. Daylight horizontal illuminance within the range 100-3000 lx ($UDI_{achieved}$) is considered *useful*, i.e. neither too poor not too strong to perform a visual task. Conversely, daylight horizontal illuminance below 100 lx ($UDI_{fell\text{-}short}$) is considered insufficient to significantly contribute to visual comfort while daylight horizontal illuminance greater than 3000 lx ($UDI_{exceeded}$) is correlated to visual discomfort due to a higher probability of occurrence of glare. The upper threshold was initially set equal to 2000 lx by the Authors [140] but after further studies a value of 3000 lx was found to correlate better with a potential glare condition [145,207]. Furthermore, this increased threshold was also confirmed by an independent study carried out by one of the Author [144]. UDI is calculated according the following equations:

$$UDI_{fell-short} = \left.\frac{\sum_{i=1}^{n} t_i(E_h < 100\ lx)}{n}\right|_{occupied} \quad (3)$$

$$UDI_{achieved} = \frac{\sum_{i=1}^{n} t_i(100\ lx \leq E_h < 3000\ lx)}{n}\Bigg|_{occupied} \quad (4)$$

$$UDI_{exceeded} = \frac{\sum_{i=1}^{n} t_i(E_h \geq 3000\ lx)}{n}\Bigg|_{occupied} \quad (5)$$

in which E_h is the horizontal illuminance on the workplane [lx]; t_i are the occupied hours in which daylight horizontal illuminance meets a given requirement, depending whether $UDI_{fell\text{-}short}$, $UDI_{achieved}$ or $UDI_{exceeded}$ is involved; n is the number of occupied hours over a year. The sum of $UDI_{fell\text{-}short}$, $UDI_{achieved}$ and $UDI_{exceeded}$ is always equal to 100%. In the present study, to characterise the daylight condition within the whole analysed space, UDI indexes are calculated as mean value of the UDI relative to all the sensor points considered within the space.

Daylight Glare Probability (DGP): introduced by Wienold and Cristoffersen [111], this metric accounts for the percentage of people that may experience a glare sensation due to a given daylight condition. Moreover, Wienold correlated different glare sensations (daylight glare comfort classes) to specific ranges of DGP values, in order to introduce a scale to rate the glare condition through DGP [133]. Table 3 summarises the daylight glare comfort classes with the relative DGP threshold values.

Table 3. Daylight glare comfort classes with the relative DGP threshold values.

Daylight glare comfort class	DGP Threshold
Imperceptible glare	DGP <35%
Perceptible glare	35% ≤ DGP < 40%
Disturbing glare	40% ≤ DGP < 45%
Intolerable glare	DGP ≥ 45%

In the present study the annual glare condition for the occupants is evaluated as percentage of occupied time for which each daylight glare comfort class is experienced.

3.3.3.4 Case study description

An enclosed office 3.6 m wide, 4.5 m deep and 2.7 m high was assumed as case study in the present work, which is shown in Figure 15. On one of the short walls, south oriented, is located a window 3.3 m wide and 1.5 m high, for a Window-to-Wall Ratio (WWR) of 50%. The office case study was assumed to be part of an office block, flanked by two identical offices on two sides on the same floor and on the floor immediately above and below and by a hallway with the same thermal conditions on the third side on the same floor. All the horizontal and vertical internal partitions were therefore considered as adiabatic.

The visible reflectance of all the internal surfaces is summarised in Table 4.

Table 4. Visible reflectance of the internal surfaces of the office case study.

Surface	ρ_{vis} [-]
Ceiling	0.80
Walls	0.65
Floor	0.20
External ground	0.10

The external opaque wall is a structural brick wall characterised by a thermal transmittance (U-value) of 0.25 W/m^2·K, internal and external areal heat capacity of 19.2 kJ/m^{2}K and 64.4 kJ/m^{2}K, respectively. Table 5 summarises the assembly and thermal properties of the opaque building envelope components. The thermal properties of the internal partitions are: i) horizontal partitions, U-value of 1.33 W/m^2·K, decrement factor of 0.4 and time lag of 7 hours (internal and external areal heat capacity of 28.2 kJ/m^{2}K and 82.8 kJ/m^{2}K); vertical partitions, U-value of 1.19 W/m^2·K, decrement factor of 0.62 and time lag of 5 hours (internal and external areal heat capacity of 48.3 kJ/m^{2}K and 67.0 kJ/m^{2}K). The thermal properties of the different materials were derived from [208–210].

Table 5. Assembly of the opaque building envelope with relative thermal properties for each layer. The layer numeration starts from the outermost one.

Layer	Material	Thickness [m]	Conductivity [W/m·K]	Specific heat [J/kg·K]	Density [kg/m^3]
1	Plaster	0.015	0.8	850	1900
2	Insulation	0.12	0.04	1500	18
3	Hollow clay bricks	0.18	0.22	1019	1394.6
4	Plaster	0.015	0.8	850	1900

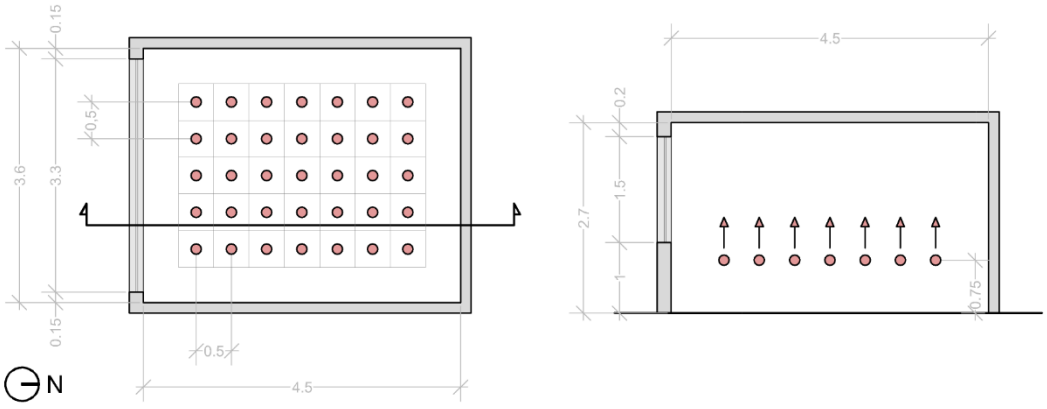

Figure 15. Enclosed office reference room and sensor points considered for lighting calculations: plan view and S-N section.

Schedules relative to occupation and equipment were adapted from [211] in order to suit the specific case study: 2 people occupation (0.12 people/m^2), equipment power density of 12 W/m^2; primary air ventilation rate of 1.56 l/s·m^2 when the office is occupied; infiltration rate per area of 0.15 l/s·m^2 [212]; heating and cooling systems were modelled as ideal systems, i.e. able to maintain under any circumstances the set-point and set-back temperatures, set equal to 20 °C and

12 °C for the heating system and to 26 °C and 40 °C for the cooling system, respectively. Heating and cooling set-point temperatures were to be maintained, in any moment of the year depending on the external boundary conditions, whenever the office was occupied.

The overall efficiency of the heating system was assumed equal to 0.85, while the cooling system SEER was set equal to 3.0. A dimmable lighting system controlled by a photosensor was considered for the office case study. A threshold of 500 lx was assumed as minimum illuminance requirement, in accordance with [95], to be maintained on the workplane by a combination of daylight and dimmable artificial lighting. The following characteristics were considered for the lighting system: installed power density of 10.76 W/m^2 [211] (this value is set as a reference by the ASHRAE with regard to a typical installation of ceiling-mounted luminaires equipped with traditional fluorescent sources, in order to guarantee at full power the target workplane illuminance of 500 lx); ballast absorption factor equal to 10%; photosensor standby power equal to 1 W, photosensor location at 0.75 m height in the middle of the room.

Table 6 summarises the building operations parameters considered for this study.

Table 6. Building operation parameters, lighting schedule is omitted as it is coincident with occupancy and dimmable according to daylight.

Working day building operations		**00÷08**	**08÷12**	**12÷13**	**13÷17**	**17÷18**	**18÷24**
Occupancy (2 people / room)	[-]	0.00	1.00	0.50	1.00	0.50	0.00
Equipment (Power Density 12 W/m^2)	[-]	0.00	1.00	0.50	1.00	0.50	0.00
Heating Set Point	[°C]	12	20	20	20	20	12
Cooling Set Point	[°C]	40	26	26	26	26	40

Horizontal illuminance on the workplane was assessed for a grid of sensors located 0.75 m above the floor and evenly distributed on the whole floor area, after deducing a stripe 0.5 m wide, as this peripheral portion of space is rarely occupied by desks. Spacing between the grid points was set equal to 0.5 m, for a total number of 35 sensor points (Figure 15). The DGP was assessed for a point located in the centre line of the room, 1.5 m away from the window and at a height above the floor of 1.2 m (eye of a seated person). The direction of observation was considered perpendicular to the window plane, which may not be consistent with the standard layout of an office, but allows accounting for the worst-case scenario in terms of glare risk.

As far as the transparent portion of the building envelope is concerned, a Double Glazing Unit (DGU) was adopted, equipped with a Low-E glazing on the internal side and with a 16 mm cavity filled with argon 90:10. As external glazing it was alternatively adopted the TCG and a set of static glazing, to be used as reference cases. The overall thermo-optical properties of all the different DGUs considered were calculated under CEN conditions [206,213] by means of the

software WINDOW 7.6 [66]. Table 7 summarises the thermo-optical properties of the DGU equipped with the TCG in its darkest and clearest state.

Table 7. Thermo-optical properties of the DGU equipped with the TCG in its limit states.

	τ_{vis} [-]	ρ_{vis} [-]	τ_{sol} [-]	ρ_{sol} [-]	g-value [-]	U-value [W/m²·K]
TCG - Clear	0.62	0.09	0.40	0.18	0.49	1.2
TCG - Dark	0.05	0.04	0.15	0.07	0.28	1.2

Starting from the numerical model describing the behaviour of the TCG derived from the experimental characterisation performed, as shown in sub-section 3.3.3.2, different hysteresis amplitudes were assumed for this component. In more detail, starting from the amplitude of the hysteresis observed, equal to 0 °C, 6 different hysteresis amplitudes between the heating and the cooling curves were defined, from 0 °C to 30 °C, with a resolution of 5 °C. The curve derived from the experimental characterisation was assumed as the heating curve; the cooling curve was obtained through a displacement of the heating curve equal to the aforementioned hysteresis amplitudes. As a result, seven different TCG glazing were obtained, with identical thermo-optical properties in their darkest and clearest state, identical heating curve, but different hysteresis amplitudes. These glazing were named after their hysteresis amplitude as *HST* and the hysteresis amplitude in Celsius degrees. As an example, the TCG with a 10 °C hysteresis will be named *HST 10* °C, the one presenting a 15 °C hysteresis width *HST 15* °C and so on. Figure 16 shows the different hysteresis amplitudes considered for the TCG in terms of visible transmittance.

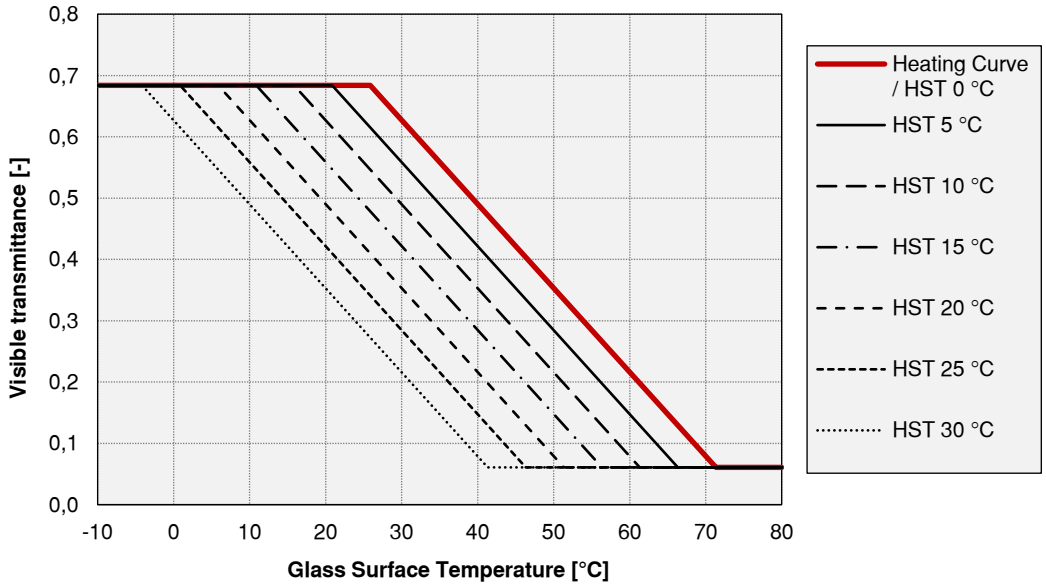

Figure 16. Hysteresis amplitudes considered for the TCG in terms of visible transmittance.

In addition to the TCG with different hysteresis widths, also different static glazing were alternatively equipped in the DGU as reference cases. From the

discretisation of the thermo-optical range of variation of the TCG (see the sub-section 3.3.3.1), 4 static states were selected: the darkest and clearest states, corresponding to State 0 and State 9 respectively, and two intermediate states, State 3 and State 6. In addition to these 4 glazing, a fifth glazing was also selected, that is a selective glazing with the same optical properties as the TCG in State 0, but with a higher selectivity index (τ_{vis}/g-value), corresponding to a lower g-value. Table 8 summarises the thermo-optical properties of the DGU equipped with the different static glazing considered in this study.

Table 8. Thermo-optical properties of the DGU equipped with the different static glazing considered.

	τ_{vis} [-]	ρ_{vis} [-]	τ_{sol} [-]	ρ_{sol} [-]	g-value [-]	U-value [W/m²·K]
State 0	0.62	0.09	0.40	0.18	0.49	1.2
State 3	0.43	0.07	0.32	0.13	0.42	1.2
State 6	0.24	0.06	0.23	0.09	0.35	1.2
State 9	0.05	0.04	0.15	0.07	0.28	1.2
Selective glazing (selective)	0.62	0.09	0.22	0.09	0.34	1.2

The enclosed office case study was alternatively located in three different climates, with the purpose of highlighting potential differences in the performance of the TCG due to the different climatic conditions. The geographical locations analysed are Abu Dhabi (ARE: 24.42°N, 54.65°E), Turin (ITA: 45.22°N, 7.65°E) and Östersund (SWE: 63.17°N, 14.50°E) characterised by a dry (arid), a temperate (mesothermal) and a continental (microthermal) climate respectively. Moreover, the latitudes of these three locations differ from one another of approximatively 20°. Figure 17 shows the Heating Degree Days (HDD) and Cooling Degree Days for the three locations considered, calculated according to a baseline of 12 °C and 18 °C respectively [214]. The Primary Energy Factor (PEF), i.e. the factor determining the efficiency of a country to produce electric energy from primary energy, was assumed equal to 3.26 for Abu Dhabi, as estimated from [215], 2.42 for Turin [216] and 1.5 for Östersund [217]. Table 9 summarises the geographical and climatic characteristics of the three locations selected.

Table 9. Geographical and climatic characteristics of the three locations analysed.

	Latitude [°]	Longitude [°]	HDD(12) [°C]	CDD(18) [°C]	Klöppen-Geiger Classification	PEF [-]
Abu Dhabi (ARE)	24.42°N	54.65°E	2	2627	BWh	0.31
Turin (ITA)	45.22°N	7.65°E	1192	452	Cfa	0.41
Östersund (SWE)	63.17°N	14.50°E	2763	34	Dfb	0.67

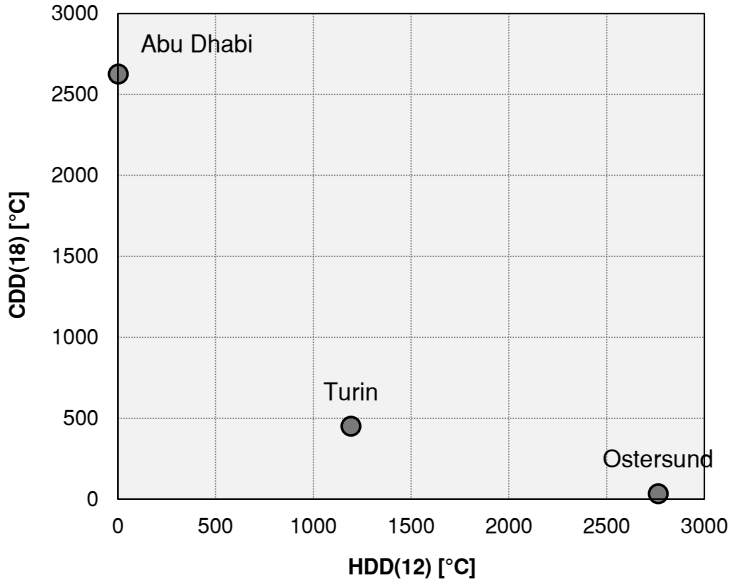

Figure 17. HDD(18) and CDD(12) for the three climates analysed, calculated according to [214].

3.3.4 Results

The performance of the office reference room integrating the different thermochromic glazing alternatives, with increasing hysteresis width, is measured in terms of both primary building energy use, EP [W/m^{2}K], and in terms of visual comfort, considering different Useful Daylight Autonomy ranges. The direct benchmark of the TCG performance is considered in this study as the performance of different static DGUs having static glass properties equal to the different TCG states (from the most transparent, State 0, to the darkest one, State 9). Moreover, an additional reference is considered, to take into account the highest performance achievable with static double glazing units, i.e. a selective glazing with the same visual properties of the clearest state of the TCG but a higher selectivity (ratio between τ_{vis} and g-value of 2) obtainable by integrating a double-silver coating on the outer surface of the DGU cavity.

Figure 18 shows the break up of specific primary building energy use for the typical office room in heating, cooling and lighting primary energy, integrating the different glazing (from static benchmarks to TGU with increasing hysteresis, from HST 0 to 30 °C). Figure 19 shows the relative energy use reduction of the TCG with increasing hysteresis, compared to the energy performance of the corresponding clearest static benchmark (State 0). In particular, for every climate, it is visible how the energy use of the thermochromic glazing with no hysteresis would always be less than the one of any static state of the TCG glazing (State 0 to 9). Compared to a static glazing having the same properties of the clearest state of the TCG (State 0), the thermochromic integrated glazing with no hysteresis use always less energy, with a magnitude varying from 3 to 12% of the total energy use depending on the climate (3% in Östersund, SWE, 12% in Turin, ITA, and 7% in Abu Dhabi, ARE).

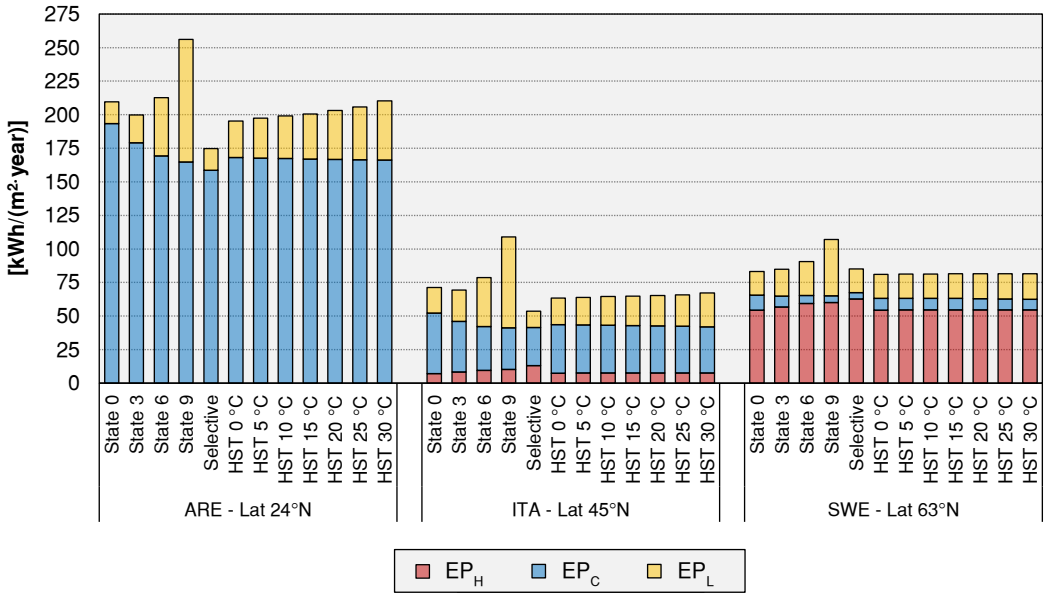

Figure 18. Specific building primary energy use break-up for the office reference room in the three climates of study.

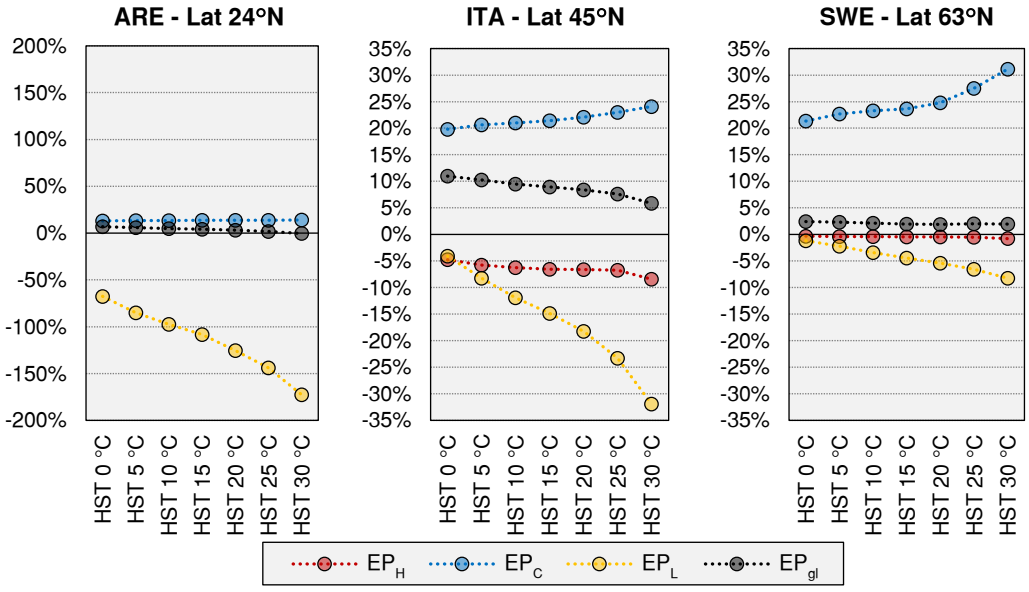

Figure 19. Improvement of specific building primary energy use break-up for the office reference room in the three climates of study.

In Abu Dhabi (ARE - Lat 24° N) the EP_{gl} (global specific primary energy use) of the office reference room integrating any of the static glazing ranges from 199 kWh/m^{2}y (State 3, the best performing one in this climate) to 256 kWh/m^{2}y (State 9, the poorest performing one), with the clearest glazing (State 0) using nearly 210 kWh/m^{2}y. The relative split between cooling and lighting energy uses varies according to the visible transmittance of the DGU, with the lighting energy use, which is the most sensitive to the variation of the visible transmission of the glazing, due to the high solar geometry corresponding to 24°N latitude (determining a low penetration of natural light within the room). A selective

glazing, instead, is able in this climate to minimise both lighting and cooling energy uses, resulting in an EP_{gl} of nearly 175 kWh/m^{2}y. As a comparison, a TCG, which has an intrinsic passive adaptive behaviour, outperforms any corresponding static glazing with properties within the TCG range of variation (State 0 to 9), with an Ep_{gl} of 195 kWh/m^{2}y, being able to dynamically balance lighting and cooling energy needs in a better way compared to a static glazing with similar or lower selectivity (ratio between τ_{vis} and g-value $\leq$ 1.26). Nevertheless, a TCG shows a higher energy use with respect to a static selective glazing (τ_{vis}/g-value $\approx$ 2), due to the higher selectivity of the latter. In this climate, enlarging the hysteresis width between the heating and cooling curve of the thermochromic glazing results in a worst energy performance, increasing the energy use from 195 to 210 kWh/m^{2}y (nearly 8%). In fact, as the hysteresis width increases from 5 to 30 °C (HST 5 °C to HST 30 °C in Figure 19) the cooling energy use is slightly decreased (2% compared to a TCG with no hysteresis), while the lighting energy use increases by nearly 70% compared to HST 0 °C (from 27 to 44 kWh/m^{2}y), and by almost 200% compared to the clearest glazing (State 0 or Selective glazing). In particular, hysteresis widths larger than 10 °C will decrease the energy performance of the TCG below the one of its direct static benchmarks (EP_{gl} of the hysteresis width larger than 10 °C is higher than the EP_{gl} of State 3).

In Turin (ITA - Lat 45° N) the EP_{gl} of the office reference room with the static glazing (properties corresponding to the TCG State 0 to 9) ranges from 69 kWh/m^{2}y (State 3, the best performing one in this climate as well) to 109 kWh/m^{2}y (State 9, the poorest performing one), with the clearest state (State 0) using 71 kWh/m^{2}y. In this climate the reference office room energy performance is highly sensitive on the glazing properties, whereas the highest energy uses are still cooling and lighting energy uses, heating can also play a significant role in the overall energy balance (between four and two times lower than cooling energy use). In fact, despite the high internal loads (equipment, people and lighting), the heat losses can be significant during the winter season, therefore an optimal choice of glazing properties would need to balance correctly the requirements for free or unwanted solar gains respectively in heating or cooling dominated seasons, with daylight requirements, to reduce lighting energy use. Given the prevalence of cooling and lighting energy requirements, a selective static glazing would be the best performing one, in terms of total energy uses, as shown in Figure 18 (with a total primary energy use of nearly 54 kWh/m^{2}y). Nevertheless, the integration of a thermochromic glazing (TCG), compared to static glazing with similar selectivity (State 0 to 9, and/or ratio between τ_{vis} and g-value $\leq$ 1.26), is able to mediate between heating, cooling and lighting energy requirements, resulting in an energy performance of the TCG of 63 kWh/m^{2}y (12% lower as compared to the static glazing State 0, and 9% lower as compared to the best performing static benchmark, State 3). In particular during the winter seasons, although the TCG assumes darker and darker states as the temperature of the material increases (hence the incident solar radiation increases), letting less and less solar radiation

in the internal space, the heating and lighting energy uses resulting by adopting a TCG are hardly affected. This can be due to two concurring reasons: i) the requirements for free solar gains to compensate heating and artificial lighting loads are lesser and lesser as the temperature of the glazing (incident solar radiation) increases; ii) a decrease in the visible transmission of the TCG results in an increase of the solar absorption of the thermochromic functional layer, hence transforming a significant part of the incident solar radiation into long-wave thermal radiation which will be transferred to the internal space (free solar gains) by means of convection (between the glazing and the internal air) and radiation (between the glazing and the internal surfaces, including building occupants). Analogously in the cooling season, due to its adaptive behaviour, the thermochromic glazing, will assume darker states (lower τ_{vis} and g-values) as the material temperature (hence the solar radiation) increases, in accordance with building energy use requirements (rejected unwanted solar gains and while having enough daylight level internally).

Where such a balance of heating, cooling and lighting energy uses is present (i.e. an office building in a temperate climate), although the hysteresis width between the heating and cooling curve of the thermochromic glazing still influences the overall energy use, this is always lower than that of static glazing with similar or lower selectivity (State 0 to 9). As shown in Figure 18 and Figure 19, a larger hysteresis width could result in an increase of 3% and up to 25% of the heating and lighting energy use respectively, as compared to a TCG without any hysteresis, although this is balanced by a decrease of up to 6% in the cooling energy use. Overall, not being able to reduce the hysteresis width, would result in these conditions, of a maximum performance loss of 6% (for HST 30 °C, 67 kWh/m^{2}y), as compared to HST 0 °C. This results anyway in an increased energy performance when compared with the clearest benchmark, State 0 (6% lower energy use), or with the optimal static benchmark, State 3 (3% lower energy use).

In Östersund (SWE - Lat 63° N) the EP_{gl} (global specific primary energy use) of the office reference room integrating any of the static glazing ranges between 82 kWh/m^{2}y (State 0) and 107 kWh/m^{2}y (State 9). Due to prevalent heating requirements, the best glazing properties choice in this climate, from an energy performance point of view is a high visible transmission and high g-value (low selectivity), corresponding in this case to a static glazing with properties similar to the clearest state of the TCG (State 0), instead of a selective one, conversely from other climates / building types in which heating energy requirements are the least important. In such conditions, the possibility to vary glazing optical properties according to the material temperature, as for the thermochromic glazing, does not present significant advantages in terms of reduction of building energy uses. In fact, adopting a thermochromic glazing, results in no more than 3% total primary energy use reduction, as compared to the best static glazing. Nevertheless, the energy performance of the TCG is the highest, compared to all the other static benchmarks and the selective reference. This is a result of the very low sensitivity of the heating and lighting energy use on the dynamic variation of glazing

properties (see Figure 18 and Figure 19), which also determines a very marginal influence (nearly none) of the hysteresis width on the energy performance of an office building.

The variation of optical properties of the thermochromic glazing can significantly affect the visual comfort in the space in which the TCG is integrated. In order to quantify the effect of the TCG and of its hysteresis on the visual comfort, different Useful Daylight Illuminance ranges are measured by means of the virtual experiments presented in this study. Particularly three ranges are shown in Figure 20 and Figure 21 showing the overall performance and the relative improvement compared to the best performing benchmark (glazing with highest τ_{vis}, equally State 0 and Selective glazing):

i. $UDI_{fell\text{-}short}$: representing the amount hours during one year in which the illuminance on the workplane is too low to perform an office task, as it is below 100 lux, and therefore ideally the full designed lighting power density would be required to lit the space when is occupied. Higher values of the $UDI_{fell\text{-}short}$ would imply a more poorly lit space and may result in higher energy needs for lighting;

ii. $UDI_{achieved}$: representing the amount of hours during one year in which the illuminance on the workplane is sufficient to perform an office task, as it is between 100 and 3000 lux, which is the sum of $UDI_{supplementary}$ (between 100 and 300 lux, in which the available daylight is compensated by artificial lighting) and $UDI_{autonomous}$ (between 300 and 3000 lux, no artificial lighting needed). Higher values of $UDI_{achieved}$ imply a good penetration of daylight and a well naturally lit environment, without potential glare discomfort issues and resulting in lower energy requirements for artificial lighting;

iii. $UDI_{exceeded}$: representing the amount of hours during one year in which the illuminance on the workplane is too high, so that glare visual discomfort due to an overlit space is highly likely to occur, illuminances higher than 3000 lux [207]. Higher values of $UDI_{exceeded}$ are characteristics of overlit spaces and may cause potential discomfort glare issues to the occupants.

Figure 20 shows the visual comfort performance of the investigated glazing in the three latitudes of interest, while Figure 21 measure the relative improvement of the same metric, compared to static benchmarks (State 0 and Selective glazing).

As visible from Figure 20 and Figure 21, in all the climates the integration of TCG always results in a better visual environment than its static benchmark. In fact, the $UDI_{achieved}$ for the TCG is always higher than the one of the clearest glazing. It is important to note that this results always from a reduction of overlit conditions which may cause glare issues, as the $UDI_{exceeded}$ is reduced. On the other hand, the $UDI_{fell\text{-}short}$ (underlit conditions) is kept to its minimum value when adopting a TCG with no hysteresis compared to its static benchmarks.

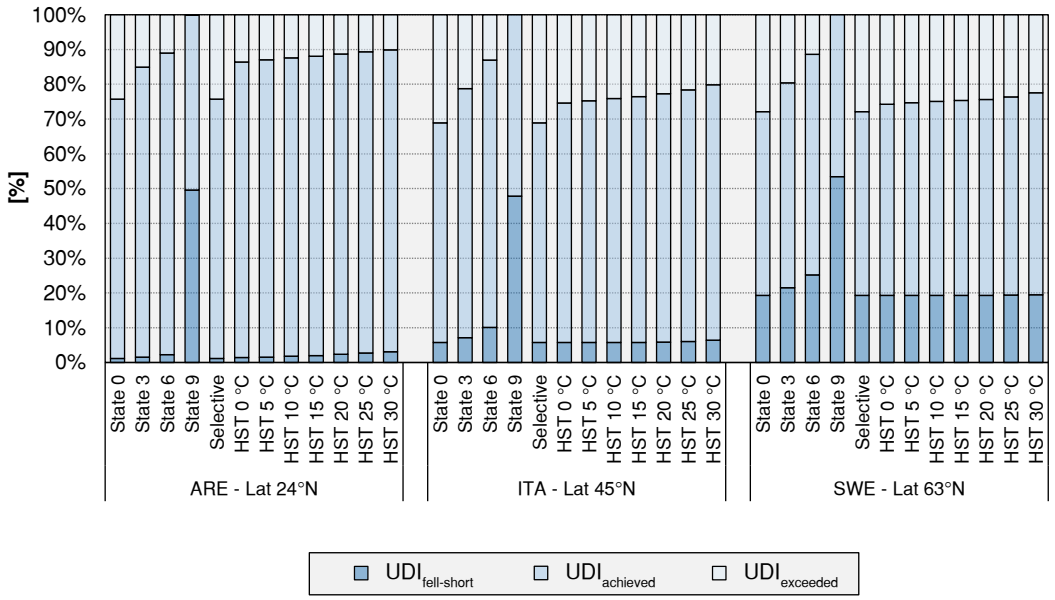

Figure 20. Useful Daylight Illuminance ranges for the office space integrating different DGU systems (from static to thermochromic with increasing hysteresis width).

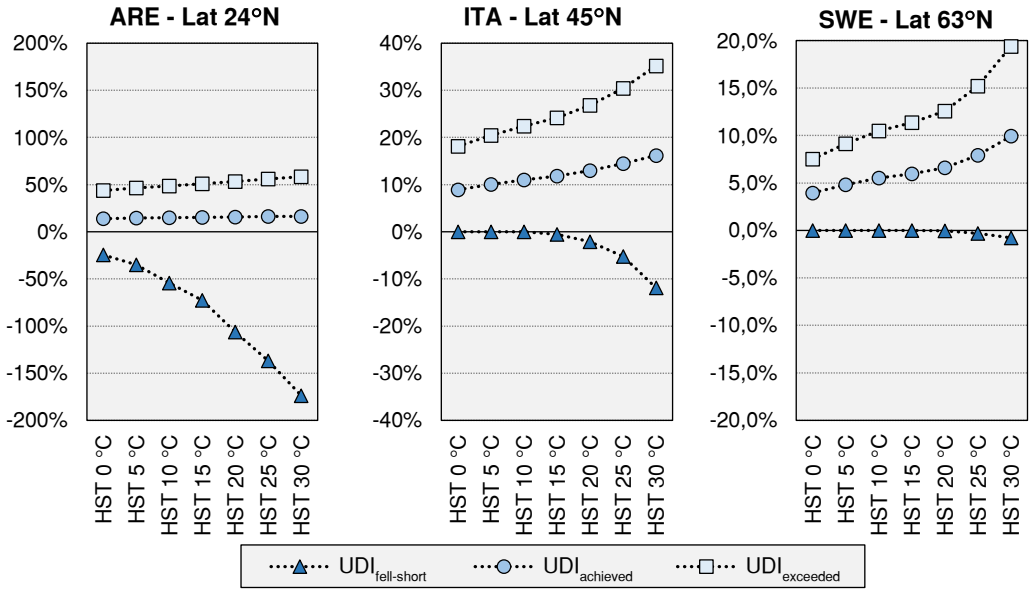

Figure 21. Variation of Useful Daylight Illuminance ranges for the office space integrating different DGU systems (from static to thermochromic with increasing hysteresis width).

In particular in Abu Dhabi (ARE – Lat 24° N), given the low latitude (implying higher number of daytime hours during occupation hours and higher solar geometry), the $UDI_{fell\text{-}short}$ is generally lower, but more sensitive to the variation of glazing visual properties; on the contrary the $UDI_{exceeded}$ is generally less compared to climates characterised by low solar angles. In such a climate the TCG provides the highest performance improvement as far as visual comfort is concerned compared to its static counterparts, with an overall improvement of more than 10% of the $UDI_{achieved}$ (HST 0 °C), which is only due to a reduction of hours in which workplane illuminances higher than 3000 lux are achieved

($UDI_{exceeded}$), potentially causing glare discomfort issues. It is noted that, counter-intuitively, a wider hysteresis results in a slight improvement of visual comfort (3% at 24°N), which is due to a significant decrease of the amount of hours with workplane illuminance higher than 3000 lux (6-7% reduction), which is counterbalanced by a slight increase of underlit hours ($UDI_{fell\text{-}short}$ increases steadily from HST 0 to 30 °C by 2-3%).

The results of Abu Dhabi have a similar trend to those of higher latitude climates (i.e. 45°N and 63°N), as thermochromic glazing would always results in a better visual comfort that the static glazing, and that an increase in the hysteresis width has a positive impact on the visual comfort (increase of $UDI_{achieved}$). In particular by increasing the latitude, improving the penetration of natural light in the room (due to lower solar geometry), the influence of the hysteresis width on the amount of underlit hours ($UDI_{fell\text{-}short}$) decreases. Similarly, wider ranges of hysteresis can prevent workplane illuminances to fall above 3000 lux threshold for a higher amount of time, reducing conditions of probable visual glare discomfort up to 15% (for HST 30 °C).

The trends observed for the Useful Daylight Illuminance are somehow confirmed by the results obtained for the Daylight Glare Probability. The effect of the TCG and of its hysteresis on the glare condition of the occupants was quantified by considering the percentage of occupied time for which each daylight glare comfort class (*imperceptible, perceptible, disturbing and intolerable glare*) was experienced. Figure 22 shows the annual glare condition, split in the four daylight glare comfort classes, relative to the investigated glazing in the three latitudes of interest, while Figure 23 measures the relative improvement for each class, compared to static benchmarks (State 0 and Selective glazing).

As observed for the UDI, also in terms of glare condition of the occupants the integration of the TCG results in all three climates in a better visual environment than its static benchmark. In fact, the percentage of hours for which an imperceptible glare condition is experienced for the TCG is always higher than the one of the clearest glazing. This is due to a reduction of the daylight levels within the indoor space, as confirmed by the simultaneous decrease of the hours in which intolerable glare is perceived by the occupants.

In more detail, in Abu Dhabi (ARE – Lat 24° N), given the low latitude and the related higher solar geometry (the sun is seldom in the observer's field of view), the percentage of hours in which discomfort glare is perceived are generally lower and little sensitive to the variation of the glazing optical properties. Conversely, an imperceptible glare condition is perceived for more hours in respect to higher latitudes, although the sensitivity of this parameter to the modulation of the glazing visible transmittance strongly depends on the latitude and the related solar geometry. In Abu Dhabi the integration of the TCG shows the highest performance improvements, in respect to its static counterparts, in terms of glare condition of the occupants, with an increase in the percentage of hours in which imperceptible glare is perceived of more than 40% (HST 0 °C) and a decrease of the occupied time in which intolerable glare is experienced equal to

28.14%. As already noted for the UDI, a wider hysteresis results in a further improvement of the imperceptible glare condition (+20.37% at 24°N), counterbalanced by a simultaneous reduction of the perceptible, disturbing and intolerable glare condition (-51.44%, -12.43% and -4.29% respectively).

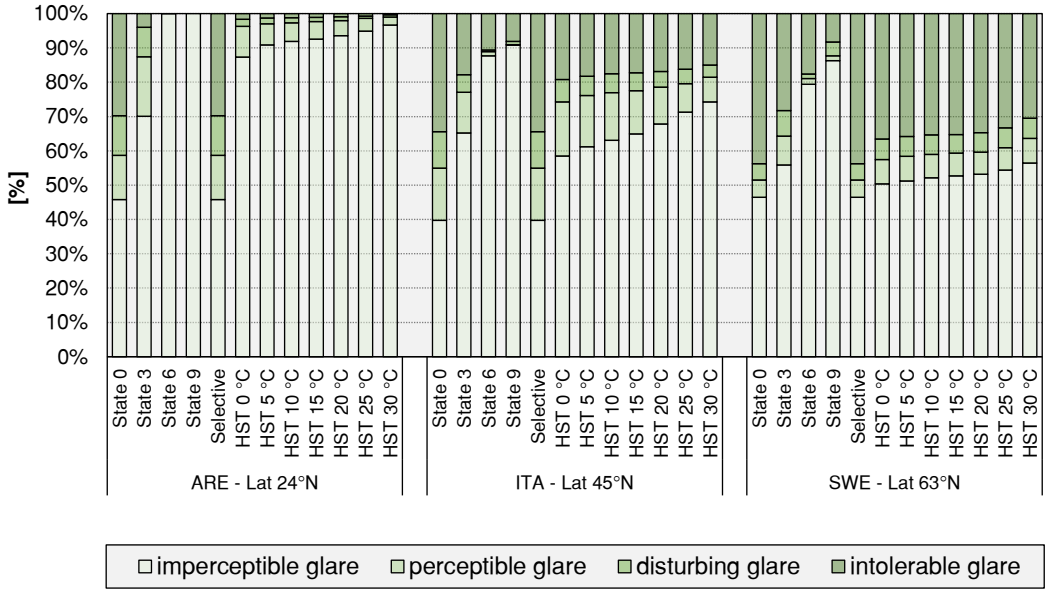

Figure 22. Annual percentage of the DGP in each daylight glare comfort class for the office space integrating different DGU systems (from static to thermochromic with increasing hysteresis width).

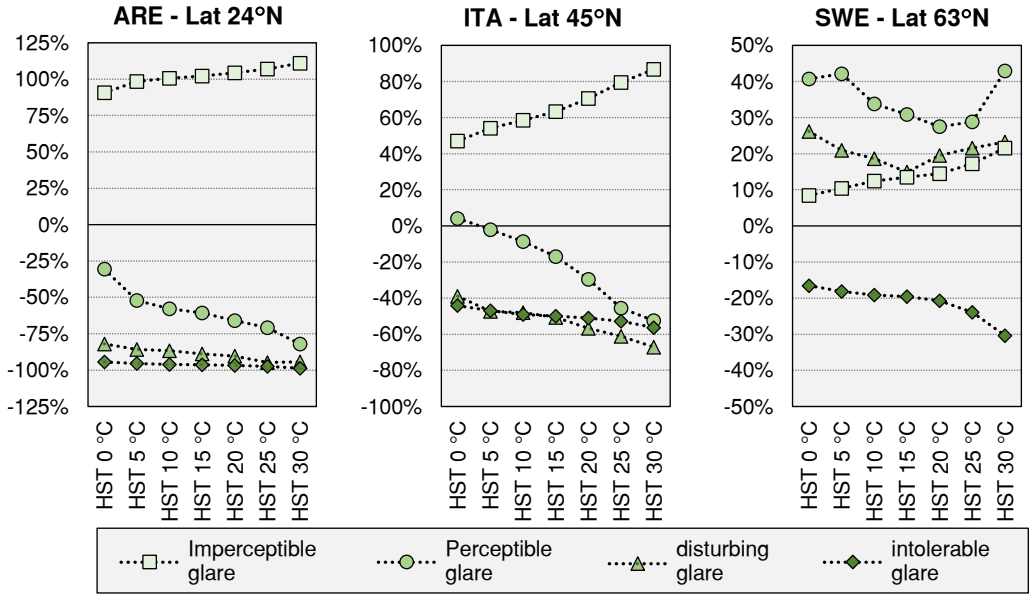

Figure 23. Variation of the annual percentage of the DGP in each daylight glare comfort class for the office space integrating different DGU systems (from static to thermochromic with increasing hysteresis width).

As far as the higher latitude climates (i.e. 45°N and 63°N) are concerned, the results obtained show a similar trend to those relative to Abu Dhabi, with the application of the TCG resulting in an improved glare condition for the occupant in respect to that provided by the static glazing. However, the extents of the above

improvement appear to decrease significantly for lower latitudes, with an increase of the hours in which the glare condition is imperceptible equal to 18.7% for Turin and only 3.92% for Östersund. Analogously, the percentage of hours in which intolerable glare is experienced shows smaller reduction for lower latitudes, and precisely of -15.21% for Turin and -7.23% for Östersund.

The increase of the hysteresis width shows to have a positive impact on the glare condition of the occupants for all three climates, as a further variation of the occupied time in which imperceptible and intolerable glare are perceived is observed, with an increase of the former and a decrease of the latter. In Turin a similar trend to that observed in Abu Dhabi was found, with an increase of the percentage of time in which intolerable glare was perceived and a decrease of the occupied hours in which perceptible, disturbing and intolerable glare are experienced. From HST 0 °C to HST 30 °C an increase of 39.71% of the hours in which intolerable glare is experienced by the occupants is observed, which is the highest improvement obtained in respect to all three climates considered. In Östersund instead a different trend was observed, with an increase and decrease respectively of the imperceptible and the intolerable glare condition from HST 0 °C to HST 30 °C, but a fluctuation of both perceptible and disturbing glare condition, for which the highest improvements are obtained for intermediate hysteresis width. Moreover, form HST 0 °C to HST 30 °C an improvement of +13.13% was observed in the time the glare sensation is imperceptible, which is the lowest improvement registered in respect to all three climates.

The differences highlighted in the three geographical locations depend mainly to their different latitudes and relative solar geometries. In Abu Dhabi, as the sun elevation is high for most of the year, most glare issues are caused by glare from contrast, so that the integration of a TCG in the window system results effective to solve these issues and improve the annual glare condition of the occupants. Conversely, a lower solar geometry characterises Östersund climate, with the sky low in the sky for most of the year. In this case most glare problems are caused by the presence of the sky within the observer's field of view, and the application of the TCG appear not to be able to solve these issues, possibly due to a too high visible transmittance exhibited in these situations. In Turin instead, due to its intermediate latitude, and consequent intermediate solar geometry, the highest improvements in the glare condition of the occupants were observed at the increase of the TCG hysteresis width.

3.3.5 Discussion

In the present study the performance of a thermochromic glazing and the effect of its transition hysteresis width on the energy and visual comfort performance is investigated. This may depend though on different factors, such as the thermochromic transition temperature, as well as on the specific boundary conditions in which the glazing is integrated (i.e. climate and building use), in the present section these two potential limitations are further discussed.

As far as the first issue is concerned, it appears from the present study that the largest impact of integrating a TCG on the performance, from an energy efficiency and visual comfort perspective, is in conditions where cooling and lighting energy uses are prevailing. In fact, on average, a significant reduction of cooling energy uses as compared to a less sensitive increase of energy uses for heating is measured as a result of an increasing hysteresis width. On the other hand, lighting energy uses is largely affected in cooling dominated climates, which also corresponds to lower latitudes (higher solar geometry). This is also reflected by the loss in performance due to the increase of the thermochormic hysteresis width, which is higher (up to 6-7% for 30 °C hysteresis width, corresponding to a steady performance decrement of only 0.2-0.25% per degree of temperature) for climates where cooling is the most significant energy use and in which solar geometry does not allow a sufficient penetration of natural light (i.e. lower latitudes).

The aforementioned interpretation, though, could be a partial result, which is specific to the characterised material, presenting a relatively high average thermochromic transition temperature. In fact, Figure 24 shows the cumulative frequency of the optical properties of the TCG for different hysteresis width, for the three climates investigated. It is possible to note that in cooling dominated conditions, there is a significant increase of the frequency of darker glazing properties, with an increase of hysteresis width. In fact in Abu Dhabi and Turin climate, the variation of the hysteresis width is affecting visible transmission of the TCG significantly: in Abu Dhabi from values below 0.42 for at least 50% of time for HST 0 °C, to values not higher than 0.27 for 50% of time for HST 30 °C; while in Turin from values below 0.62 for at least 50% of time for HST 0 °C, to values not higher than 0.43 for 50% of time for HST 30 °C. Conversely in heating dominated climates, as Östersund, given the relatively high switching transition temperature, much higher values of the visible transmission of the thermochromic glazing are measured (from values below 0.64 for at least 50% of time for HST 0 °C, to values not higher than 0.57 for 50% of time for HST 30 °C). This indicate that in cooling dominated climates / buildings, the boundary conditions (external temperature and solar radiation, as the internal set point air temperature is fixed to 26 °C) are such that the thermochromic material would experience the full range of temperature and optical properties characterised. Moreover, in these climates it is more likely that the glass would undertake complete heating and cooling cycles, which is demonstrated by the high influence of hysteresis width on the measured optical properties of the glass. While in a climate like Östersund, the glass optical properties are for most of the time in the clearer range (higher τ_{vis}), on the overall resulting from a lower temperature of the thermochromic material, which is due to the fact that external temperature and solar radiation are not sufficient for the thermochromic transparent functional layer to undertake the full heating and cooling cycles.

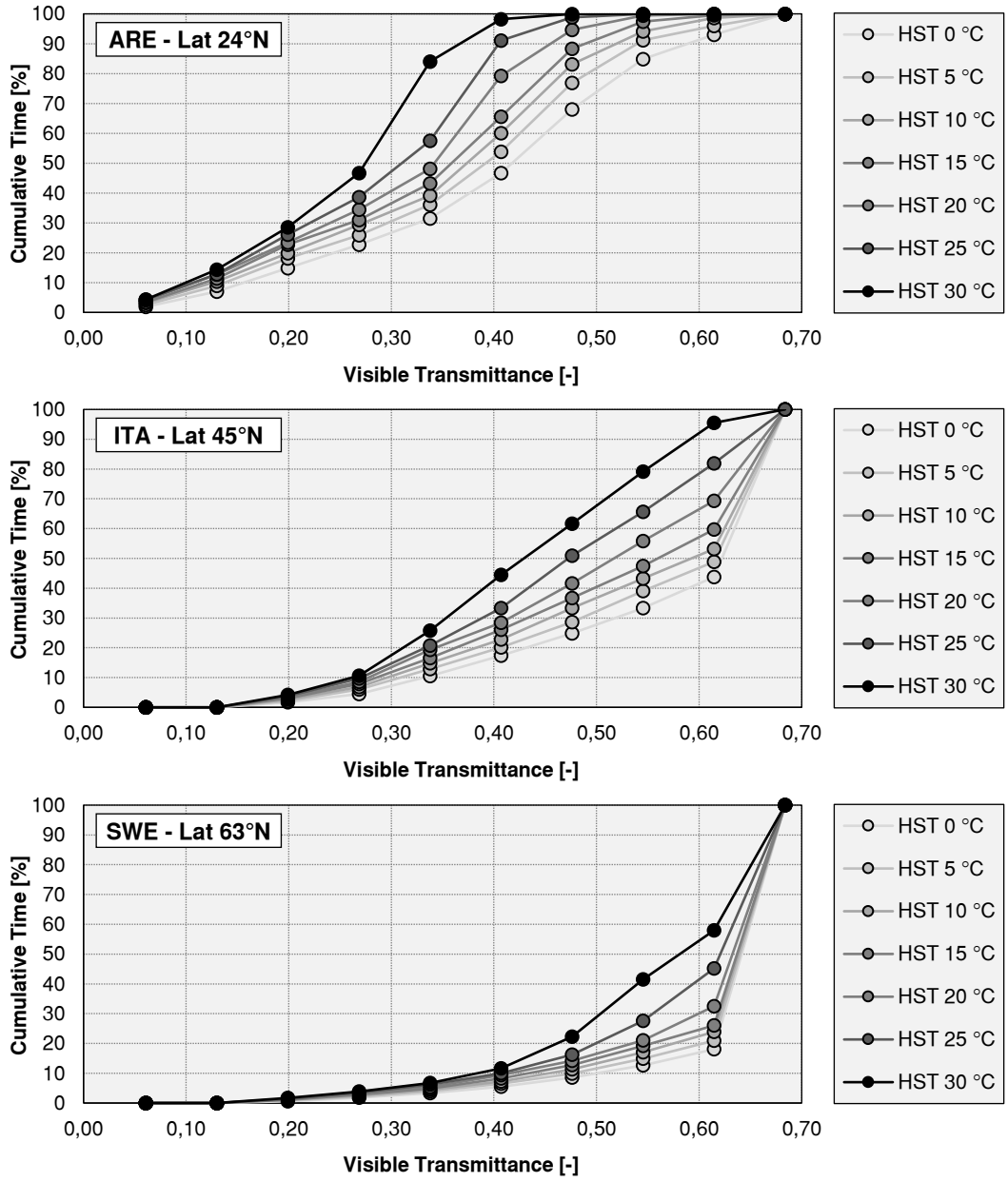

Figure 24. Cumulated time frequency of TCG optical properties according to the hysteresis width for the different climates tested: a) ARE – Lat 24°N; a) ITA – Lat 45°N; a) SWE – Lat 63°N.

As a comparison, in [186] and [187] it is shown as decreasing the transition temperature from 45 °C to 25 °C could reduce the energy use for total energy for heating and cooling of up to 15%, resulting in up to 25-30% less cooling energy uses [186,187], while up to 10% higher heating energy uses (10% more from 45 to 25 °C) [186,187]. On the other hand, lighting energy use appears not be significantly affected by the transition temperature [187]. This could result in even higher energy performance of thermochromic glazing achievable in cooling dominated climates, shall the thermochromic transition temperature be decreased to temperatures closer to 25 °C. On the contrary, it appears that a decrease of the thermochromic transition temperature does not result in lower heating energy demand in heating dominated seasons and/or climates. Moreover the influence of

the hysteresis width (6-7% maximum energy performance reduction) is found to be much lower than what previously documented in literature [186]: up to 15% for similar thermochromic transition temperatures, and with a higher difference between smaller and larger hysteresis width, nearly 10% for an hysteresis width passing from 0 °C to 5 °C, and only 5% if the hysteresis of the thermochromic transition is enlarged further. The difference can be explained by the simplified modelling approach adopted in [186], in which the variation of thermochromic glazing properties was defined as a simple linear regression depending on solar radiation alone, as well as by the fact that the lighting energy use was not considered.

On the other hand, the impact of the hysteresis on the TCG performance is also depending on the dynamicity of the phenomena as compared to the dynamicity of boundary conditions, and in particular on the concurrence of the effect of the hysteresis with specific local boundary conditions. In fact, it is noted how the hysteresis width of the thermochromic material has a certain influence on the speed at which the optical properties are going from a darker state to clearest ones (lower to higher visible and solar transmittance). By analysing the external boundary conditions, this would always occur when the incident solar radiation incident is decreasing (afternoon hours for the specific case study, south facing facade). On the other hand, if focusing on internal boundary conditions, the influence of the hysteresis on the variation of optical properties may or may not coincide with highest cooling or lighting energy use requirements (peak cooling and lighting energy uses in afternoon hours), or in conditions requiring a certain level of visual comfort (office occupation). As an explanatory example, in Figure 25 it is shown the effect of different hysteresis widths (0, 10 and 20 °C) on the hourly variation of thermochromic optical properties, on the energy uses (cooling and lighting), on the work-plane illuminances and on the DGP values for five specific week days, specifically for ITA - 45°N, between 30th Oct and 3rd Nov (the climate and the days are chosen in such a way to maximise the effects, with an explanatory aim).

Figure 25.b shows that a delay in recovering the clearest state (larger hysteresis of 10 °C and 20 °C), reduces the cooling and lighting loads during the central hours of the day (when the thermochromic material is cooling back to its clearer states). Although if this happened when cooling and lighting loads were at their peak (few hours later in the afternoon), the thermochromic hysteresis width could have a higher influence. Therefore, the influence of the hysteresis mechanisms may be slightly different if considering different orientations and/or different building uses or schedules. At the same time, from the point of view of the visual comfort, the contemporaneity of the delay in recovering clearer visual properties introduced by a wider hysteresis width, combined with a TCG integrated on a south facing facade, positively impacts on both the amount of hours below the threshold of 3000 lux (lower $UDI_{exceeded}$ values) and the discomfort glare condition (DGP above 45%), as visible in Figure 25.c and Figure 25.d, thus improving visual comfort.

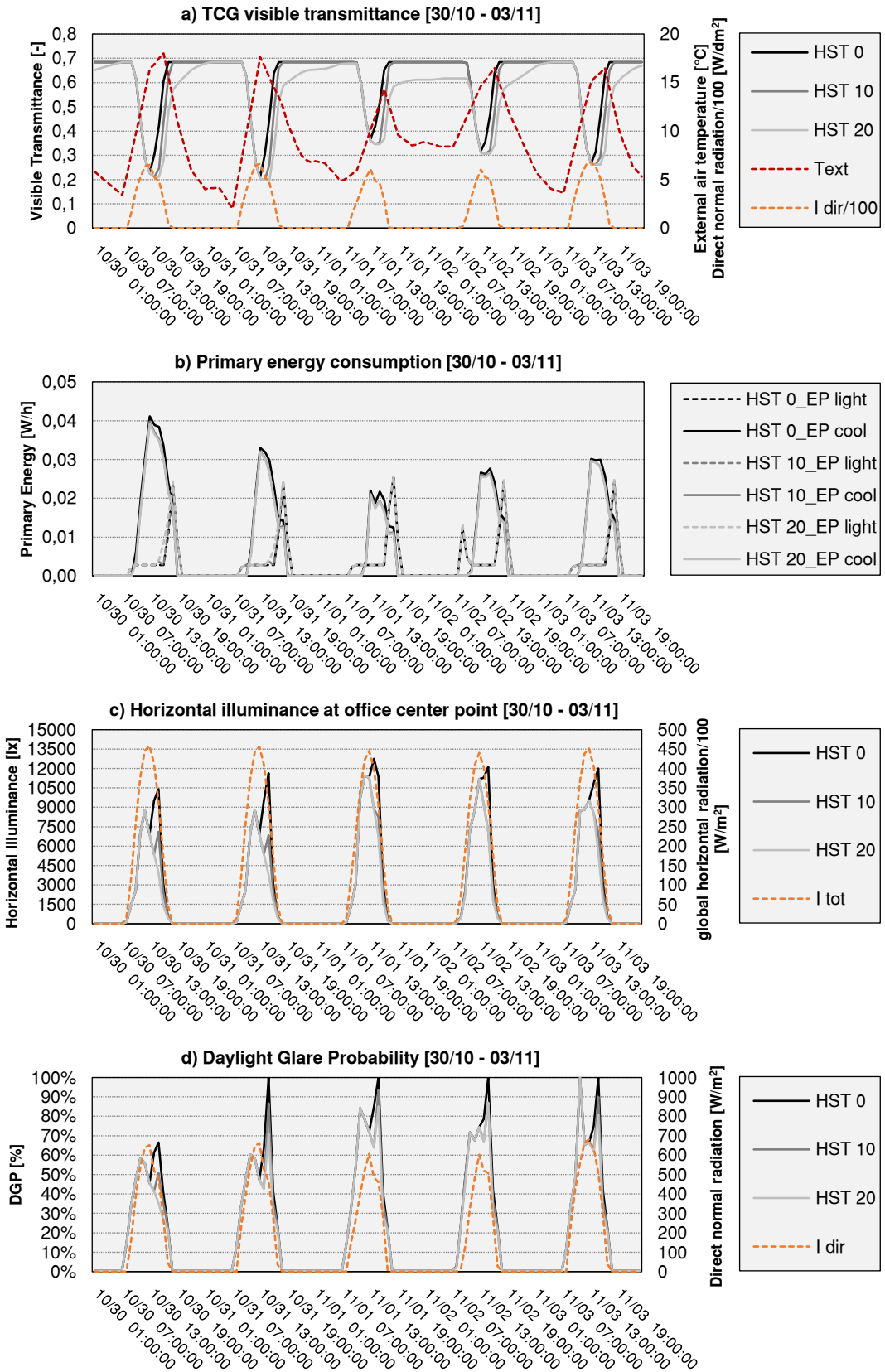

Figure 25. Profiles of a) TCG visible transmittance and external boundary conditions; b) cooling and lighting loads; c) workplane illuminances for centre of the office reference room; d) Daylight glare Probability for the point and view direction considered. The above profiles are represented for a cooling dominated week in ITA – Lat 45°N climate (between 30th Oct and 3rd Nov), for different TCG hysteresis widths (0 °C, 10 °C and 20 °C).

From a material point of view, large effort has been spent to evaluate the influence of hysteresis on heating and cooling energy use for VO_2 based TC systems and to reduce the hysteresis width [148,186,188,200]. The vast majority of transparent thermochromic functional layers in literature achieved hysteresis widths as low as 5 ˚C - 10 ˚C [148,186,188,200], similarly to the one of the LETC system characterised in this work. As a result, this could still give sufficient energy performance improvements compared to similar selective static glazing, although to outperform more selective static glazing from a performance point of view LETC systems should aim to: i) reduce the thermochromic transition temperature so that less transparent states could be maintained for a higher amount of time (see Figure 24) to reduce energy use and improve visual comfort; increase the range of solar transmission modulation beyond the current 40% range, in order to reduce energy use further. LETC systems, compared to other TC materials, are promising not only for the large modulation of luminous and solar optical properties, but also for their integration into flexible system (PVB interlayer) and potential cost reduction. In fact according to Queen [22], LETC systems cost roughly ten times standard double pane glazing, although they have great potential of cost reduction by reducing the amount of active ingredients to achieve similar or improved solar and visual modulation and colour neutral appearance (with reduced number of TC layers). The cost and performance objectives highlighted above could be obtained by designing active ingredients with higher molar extension coefficient, thus greater light and solar absorption [22].

3.3.6 Conclusions

The advantages deriving from the application of the proposed integrated simulation methodology were demonstrated through its application to a passive adaptive transparent component, namely a thermochromic glazing. This methodology enabled a comprehensive building performance evaluation of thermochromic glazing considering not only energy uses and visual comfort aspects, but also peculiar thermochromic material features, such as thermochromic hysteresis. As a result, the devised BPS tool showed to be able to effectively support the design of a thermochromic material, from the perspective of the building integration scale. In particular, an experimental campaign was undertaken to characterise a LETC thermochromic material, whose behaviour was parametrised, modelled and calibrated.

As far as the thermochromic glazing characterisation is concerned, it is observed that the LETC has a relevant switching capacity in the visible region of the spectrum, with a switching factor of 10 (relative to the minimum and maximum measured surface temperatures); this behaviour is a promising prerequisite for building applications aimed at optimising daylight control and solar gain management. Conversely, the low selectiveness (ratio between τ_{vis} and τ_{sol}) and the low switching factor in the near infrared range, limit the solar

management performance of the system (total solar transmittance can modulate in the 0.24-0.62 range) and its capability to reduce unwanted solar gains during cooling seasons.

As far as energy performance is concerned, thanks to the possibility of varying the glazing properties according to the temperature of the thermochromic functional layer, the TCG is always able to outperform any static glazing with properties within any of its possible states (absorbing glazing). Although in climates and building conditions in which cooling and lighting energy use are prevailing (cooling dominated climates and temperate climates within building with high endogenous loads, such as offices), selective static glazing (with double and triple silver coatings) may still be a better choice than thermochromic ones with similar transition temperature (average transition temperature 45 °C), from an energy saving stand point. The overall advantage of the thermochromic glazing is to reduce cooling energy uses, to the detriment of heating and lighting energy uses, despite its transition temperature. The thermochromic hysteresis has proved to have a positive impact on the reduction of cooling energy uses, which is though not counter balanced by the variation of lighting and heating energy uses. Therefore, on the overall the hysteresis width has a negative effect on the reduction of total energy uses, especially for high solar angles (lower latitudes).

As far as visual comfort is concerned thermochromic glazing always performs better than their static benchmark, in terms of possibility to exploit natural light, as well as reducing probable glare issues. Moreover the increase of the hysteresis width has shown to have a positive impact on reducing glare occurrence (reduction of work-plane illuminances higher than 3000 lux) especially for higher latitudes, but not on the improvement of the exploitation of natural light.

A wider thermochromic hysteresis is not always detrimental to the energy and visual comfort performance, differently from what has been published previously. Increasing the hysteresis width is always beneficial in reducing cooling energy uses (especially in higher latitudes), while it has a slight negative impact on heating and a significant negative impact on lighting energy uses (especially in lower latitudes). For the specific cases analysed this results in a negative impact on the total primary energy use. Although depending on the climate of interest, building type and specific configuration, building use and especially on the lighting power density, the impact of widening the thermochromic hysteresis on the total energy use may become positive instead. Moreover, from the point of view of the visual comfort, a wider thermochromic hysteresis is increasing the opportunity to exploit natural light, as it is decreasing (especially in higher latitudes) the occurrences of too high illuminances which may cause glare discomfort issues, without increasing the amount of time with lower illuminance values.

At a component level, the measurement of the hysteresis cycle is not a trivial task, and a proper test bench and methodology needs to be designed to improve the measurement accuracy. Although the accuracy needed for the thermochromic hysteresis measurement, as well as the accuracy in modelling it into building

simulation tools, is linked to its influence on the building performance. On average hysteresis width below 10 °C results in a performance variation generally lower than 5%.

3.4 Application to an active component: electrochromic glazing

3.4.1 Introduction

In the present section the proposed novel integrated simulation methodology is applied to the case of an active transparent adaptive façade component.

Active switchable glazing are currently the transparent adaptive technologies with the higher real-world uptake, due to their feature of adjusting their thermo-optical properties according to custom-defined constraints. Among these the all-solid-state electrochromic (EC) glazing currently shows the widest market penetration. In addition, it appears to be the transparent adaptive component with the highest potential in the improvement of the overall building performance, by reducing the energy use while improving the visual comfort condition of its occupants. This is mainly due to: (i) the robustness of the technology; (ii) a large modulation range of its thermo-optical properties; (iii) the higher flexibility of an active control in respect to passive adaptive transparent façade technologies.

In this sense, benefits and drawbacks deriving from the application of active smart glazing are not only related to the boundary conditions, but strictly depend also on the control logic used to manage these components [69]. Nonetheless, Energy performance and comfort requirements (visual and thermal) could be contradictory (for instance the need for winter solar gains and the risk of glare due to direct sunlight), although control strategies tend to be structured to meet a specific requirement (mono-objective) or to follow a hierarchy of objectives. The priority given to visual comfort could negatively influence the energy performance and vice versa, depending on the period of the year, the climatic context and the building use and characteristics.

Nevertheless, understanding the effectiveness of a control strategy on the overall building performance is not a trivial task. This requires in fact an evaluation of the effects of the operation of the active adaptive component which has to deal with the following aspects: different physical domains can be affected simultaneously by the transparent component adaptive behaviour (i.e. thermal and luminous), which are often highly interdependent to each other; different performance aspects need to be considered, which may be conflicting with each other (energy efficiency and visual comfort requirements). However, most of the currently available Building Simulation (BPS) tools do not integrate simulation methodologies allowing a multi-physical and multi-performance assessment, if not by introducing a series of simplifications (see Chapter 2). As a result, these tools provide only a partial picture of the effects of a control strategy on the overall building performance.

In this framework, the performance of an electrochromic glazing operated according to different mono-objective control strategies selected from literature was evaluated. The application of the integrated simulation methodology proposed enabled a comprehensive whole building evaluation of the performance of the EC component according to the different control strategies selected, considering both thermal related aspects (i.e. energy efficiency, in terms of cooling, heating and lighting demand) and visual comfort aspects in an interrelated fashion.

In sub-section 3.4.2 the office case study selected for the present analysis is presented, along with the description of the EC glazing considered in this study. This is followed by a detailed description of the different mono-objective control strategies selected from literature. Finally, the integrated simulation workflow followed in this study is thoroughly described. Sub-section 3.4.3 presents the results relative to the operation of the EC glazing according to the different typologies of control strategies selected, both in terms of energy and visual comfort performance. These are then compared to each other to highlight advantages and drawbacks relative to each mono-objective control strategy. Finally, sub-section 3.4.4 draws the main conclusions for the application of the proposed integrated simulation methodology for the evaluation the effect of different mono-objective control strategies over both energy performance and visual comfort.

3.4.2 Methodology

An extensive numerical analysis aimed at the evaluation of the influence of different control strategies on the overall building performance is presented in the following paragraphs. Specifically, the influence of control strategies aimed at the optimisation of different aspects (energy performance, visual comfort or both) was assessed on both the energy performance and the visual comfort condition of the occupants and compared.

3.4.2.1 Performance evaluation parameters

In the present study both energy aspects and visual comfort aspects were analysed. This was done by means of the following performance metrics:

Energy Performance Index (EP_{gl})*:* it is the amount of primary energy annually consumed by a building per unit area, expressed in kWh/(m^2·year). The EP_{gl} is calculated according to the following equation:

$$EP_{gl} = EP_H + EP_C + EP_L \quad (6)$$

in which EP_H is the amount of primary energy annually consumed by the heating system per unit area [kWh/(m^2·year)]; EP_C is the amount of primary energy annually consumed by the cooling system per unit area [kWh/(m^2·year)]; EP_L is the amount of primary energy annually consumed by the lighting system

per unit area [kWh/(m^2·year)]. The influence of the primary energy necessary for the production of domestic hot water (EP_{DHW}) on the EP_{gl} was considered negligible and was therefore not calculated in the present study.

***Daylight Glare Probability (DGP)**:* this metric quantifies the percentage of people that may experience a glare sensation due to a given daylight condition, and is calculated according to the following equation [111]:

$$DGP = 5.87 \times 10^{-5} E_v + 9.81 \times 10^{-2} \log\left(1 + \sum_i \frac{L_{s,i}^2 \omega_{s,i}}{E_v^{1.87} P_i^2}\right) + 0.16 \qquad (7)$$

in which E_v is vertical illuminance at eye level [lx]; L_s is the light source luminance [cd/m^2], ω_s is the light source solid angle [s_r]; P is the position index [-], which expresses the variation in glare sensation experienced relative to the angular displacement of the light source from the observer's line of sight. To be able to rate the glare condition through DGP, Wienold introduced a scale in which he correlated different glare sensations (daylight glare comfort classes) to specific ranges of DGP values [133]. Table 10 summarises the different daylight glare comfort classes, with relative upper and lower DGP threshold values.

Table 10. Daylight glare comfort classes, with relative DGP threshold values.

Daylight glare comfort class	Threshold
Imperceptible glare	DGP < 35%
Perceptible glare	35% ≤ DGP < 40%
Disturbing glare	40% ≤ DGP < 45%
Intolerable glare	DGP ≥ 45%

$DGP_{<40\%}$: this metric expresses the percentage of occupied hours over a year in which the glare condition of the occupants is below disturbing (DGP < 40%). $DGP_{<40\%}$ is calculated according to the following equation:

$$DGP_{<40\%} = \frac{\sum_{i=1}^{n_{occ}} (\alpha \cdot t_{i,occ})}{n_{occ}} \qquad with\ \alpha = \begin{cases} 1, & DGP < 40\% \\ 0, & DGP \geq 40\% \end{cases} \qquad (8)$$

in which $t_{i,occ}$ are the occupied timesteps (hours) in one year; n_{occ} is the number of occupied timesteps in one year; α is the weighting factor indicating if DGP is above or below the threshold determining a disturbing glare condition, equal to 40%.

***Daylight Autonomy (DA)**:* this metric is defined as the percentage of occupied hours over a year in which daylight alone satisfies a minimum illuminance requirement [132]. DA is calculated according to the following equation:

$$DA = \frac{\sum_{i=1}^{n_{occ}} (\alpha \cdot t_{i,occ})}{n_{occ}}$$
$$with\ \alpha = \begin{cases} 1, & E_h \geq 500 \\ 0, & E_h < 500 \end{cases} \quad (9)$$

in which E_h is the horizontal illuminance on the workplane [lx]; $t_{i,occ}$ are the occupied timesteps (hours) in one year; n_{occ} is the number of occupied timesteps in one year; α is the weighting factor indicating if daylight alone satisfies the minimum illuminance requirement. This one was set equal to 500 lx, to meet normative prescription for an office space [95].

3.4.2.2 Case study description

The considered case study is an enclosed office 3.6 m wide, 4.5 m deep, and 2.7 m high. A window 3.3 m wide and 1.5 m high (Window-to-Wall Ratio WWR equal to 0.5) is located on the south-oriented short wall.

The enclosed office was assumed to be part of an office building and surrounded by other identical offices with the same thermal conditions, thus all the horizontal and vertical internal constructions were modelled as adiabatic components. Table 11 reports the visible reflectance assumed for the different internal surfaces.

Table 11. Visible reflectance of the internal surfaces of the case study.

Surface	ρ_{vis}
Ceiling	0.7
Wall	0.5
Floor	0.3
Ground (albedo)	0.1

The external opaque wall is a structural brick wall characterised by a thermal transmittance (U-value) of 0.25 W/(m^{2}K), while the internal and external areal heat capacity are equal to 19.2 kJ/m^2·K and 64.4 kJ/m^2·K, respectively. Table 12 summarises the assembly and thermal properties of the opaque building envelope component.

Table 12. Assembly of the opaque building envelope with relative thermal properties for each layer. The layer numeration starts from the outermost one.

Layer	Material	Thickness [m]	Conductivity [W/m·K]	Specific heat [J/kg·K]	Density [kg/m^3]
1	Plaster	0.015	0.8	850	1900
2	Insulation	0.12	0.04	1500	18
3	Hollow clay bricks	0.18	0.22	1019	1394.6
4	Plaster	0.015	0.8	850	1900

The horizontal internal partitions have the following thermal properties: U-value of 1.33 W/m^2·K, decrement factor of 0.4 and time lag of 7 hours (internal and external areal heat capacity of 28.2 kJ/m^2·K and 82.8 kJ/m^2·K). The thermal

properties of the vertical internal partitions are as follows: U-value of 1.19 $W/m^2 \cdot K$, decrement factor of 0.62 and time lag of 5 hours (internal and external areal heat capacity of 48.3 $kJ/m^2 \cdot K$ and 67.0 $kJ/ m^2 \cdot K$). The thermal properties of the different materials were derived from [208–210].

Standardised schedules relative to occupancy and equipment were considered [211]. The office case study was assumed to be occupied by 2 people and the equipment power density was set equal to 12 W/m^2 [218]. The primary air ventilation rate was assumed equal to 1.56 $l/s \cdot m^2$ for the occupied hours, while the infiltration rate per area was set equal to 0.15 $l/s \cdot m^2$ [212].

The heating and cooling systems were modelled as ideal systems, able to guarantee under any condition set-point and set-back temperatures, set equal to 20 °C ad 12 °C for the heating system and 26 °C and 40 °C for the cooling system respectively. The mean seasonal efficiency of the heating system is equal to 0.85 while the cooling system SEER is equal to 3.00. The case study office was equipped with a dimmable lighting system controlled by means of a photosensor, which managed the power fraction of the lighting system in order to guarantee a minimum illuminance on the workplane, as a combination of daylight and dimmable artificial lighting, equal to 500 lx, in accordance with [95]. The considered lighting system has the following characteristics: installed power density equal to 10.76 W/m^2 [211]; ballast absorption factor equal to 10%, standby power of the photosensor equal to 1 W.

The horizontal illuminance on the workplane was assessed for a grid of sensors located 0.75 m above the floor and evenly distributed on the whole floor area, after deducing a stripe 0.5 m wide, as this peripheral portion of space is rarely occupied by desks. Spacing between the grid points was set equal to 0.5 m, for a total number of 35 sensor points. The Daylight Glare Probability was evaluated for a point positioned in the room centre line, 2.25 m away from the window and at a height of 1.2 m (height of the eye of a seated person). The direction of observation was considered perpendicular to the window plane, which may not be consistent with the standard layout of an office, but represents the worst-case scenario in terms of glare risk.

As far as the transparent portion of the building envelope is concerned, glazing with different optical properties were compared: an electrochromic glazing (EC) and two traditional selective glazing were alternatively used as external layer of a Double Glazing Unit (DGU) equipped with a Low-E glazing as inner glass pane and with a 16 mm cavity filled with argon 90:10.

As regard the electrochromic glazing, this is an active transparent façade component whose thermo-optical properties vary according to the application of an external voltage (see section 2.2). The EC component considered consists in a laminated glass composed by two glass panes connected one to another by a multi-ply electrochromic interlayer. This one is composed by two transparent conductor layers, one coated with tungsten oxide (for cathodic colouring) and the other coated with Prussian blue (for anodic colouring), separated by an electrolyte layer in PVB [219]. The EC glazing thermo-optical properties vary between 10

pre-defined states, from a maximum transparency state (bleached) and neutral colouring (EC_10) to a state of minimum transparency and intense Prussian blue colour (EC_1). The optical properties of the EC glazing in each state were experimentally characterised by means of an Ulbricht sphere and, starting from this data, the overall thermo-optical properties of the 10 resulting DGUs were calculated. This was done according to the CEN conditions [206,213] by means of the software WINDOW 7.6 [66]. In addition to the EC glazing, also two selective glazing were considered, to be used as static reference: these are a standard and a high-performance selective glazing, the latter characterised by a higher selectivity index (τ_{vis}/g-value), corresponding to a lower g-value. Table 13 summarises the thermo-optical properties of all the DGUs considered in the present study, i.e. equipped both with the two static glazing (Sel62, Sel72) and with the EC glazing in each of the 10 states it can assume (EC_1, EC_2, …, EC_10). Internal venetian blinds were considered as well for some of the control strategies presented in the next paragraph. These, adjustable on three slopes (0° - horizontal, 15° and 30°), were considered to have a slat depth of 2.5 cm and a visible reflectance (ρ_{vis}) equal to 0.44.

Table 13. Thermo-optical properties of the Double Glazing Unit considered equipped both with the two static glazing (Sel62, Sel72) and with the EC glazing in each of the 10 states it can assume.

Double Glazing Unit		τ_{vis} [-]	τ_{sol} [-]	g-value [-]	U [W/m^{2}K]
Reference glazing	Sel62	0.62	0.28	0.3	1.2
	Sel72	0.72	0.36	0.38	1.2
Electrochromic glazing states	EC_10	0.52	0.29	0.35	1.2
	EC_9	0.46	0.21	0.29	1.2
	EC_8	0.39	0.16	0.23	1.2
	EC_7	0.33	0.12	0.2	1.2
	EC_6	0.26	0.09	0.16	1.2
	EC_5	0.23	0.08	0.16	1.2
	EC_4	0.21	0.07	0.15	1.2
	EC_3	0.16	0.05	0.12	1.2
	EC_2	0.12	0.04	0.12	1.2
	EC_1	0.10	0.03	0.11	1.2

The office case study was located in the city of Turin (ITA: 45.22°N, 7.65°E), and energy performance and daylighting evaluations were carried out through annual climate-based simulations using the International Weather for Energy Calculations (IWEC) data file for this city [220]. The Primary Energy Factor (PEF), i.e. the factor determining the efficiency of a country to produce electric energy from primary energy, was assumed equal to 0.41 [216]. The Heating Degree Days (HDD) and the Cooling Degree Days (CDD) for the city of Turin are equal to 1192 °C and 542 °C respectively (calculated according to a baseline of 12 °C for HDD and 18 °C for CDD [214]), which means that its climate is mainly

heating-dominated, even though the summer cooling need is not negligible as well. This is particularly true in the case of office buildings, where the endogenous loads could have a significant impact on the heating and cooling needs. Moreover, at an intermediate latitude, such as the one of Turin, the solar geometry is characterised by low elevation angles in winter, which, depending on the orientation, may cause a discomfort glare condition to the occupants. In addition, the aim of reducing the energy demand for cooling could be contrasting with that of decreasing the energy use for artificial lighting. As a result, the control of a dynamic glazing aiming at optimising both energy-related and visual comfort-related aspects is not a trivial building operation task. In the present study the influence of energy and visual constraints in the control strategy of an adaptive glazing is analysed, relative to both the energy performance and the visual comfort condition of the occupants.

3.4.2.3 Control strategies description

Different mono-objective control strategies were selected from a literature review. The control strategies considered are aimed at the improvement of the building energy performance either by minimising the cooling energy needs, or by optimising the occupants' visual comfort through the minimisation of the discomfort glare risk. Depending on the aim of the strategy, the thermo-optical properties of the glass are managed based on monitored parameters: cooling loads, glare risk and occupant profile. As far as the strategies aimed at improving the visual comfort conditions are concerned, these are limited to the occupancy hours, while a static glass condition (or a strategy aimed at the optimisation of the energy performance) is considered in the unoccupied hours. In more detail, the following typologies of control strategies were analysed (the name of the control strategy is relative to the performance objective addressed):

1) **ML = minimising loads (ON/OFF switching)**: this type of strategy is aimed at minimising the building cooling needs, hence, to a certain extent, the final energy demand [84,87,88]. The EC glazing is totally bleached (EC_10) in presence of a heating load, so as to take full advantage of the solar heat gains. On the other hand, the adaptive component is totally tinted in presence of a cooling load, with the purpose of minimising the overheating phenomena;
2) **MG = minimising glare risk (linear switching)**: the EC glazing is operated to the clearest state ensuring to the occupants an acceptable glare condition, assessed by means of the Daylight Glare Probability. This type of control strategy is present in [85,92] and in [69], but in the former two the glare control is performed through the Daylight Glare Index (DGI), while in the latter it is performed through the DGP, for which a threshold of 35% is assumed. In the present study a laxer threshold is instead considered for the DGP, equal to 40%, meaning that a *perceptible glare* condition is still tolerated;

3) **VB_MG = minimising glare risk with blinds**: internal venetian blinds are coupled to a selective glazing to ensure a DGP lower than the threshold value, again assumed equal to 40%. When the DGP value exceeds this limit, the internal blinds are adjusted to the lowest slat angle (between 0°, 15°, 30°) able to ensure at least a *perceptible glare* condition. This solution, making use of a traditional moveable shading device coupled with a static glazing, represents an alternative to the active adaptive transparent component.

The aforementioned control strategies were analysed and modified according to considerations relative to the specific features of the climate considered, in order to further enhance their performance in respect to that of their basic version. Specific control strategies were thus defined by assuming different EC states (see Table 13) as minimum glass transparency limit, with the aim of maximising either the building energy performance or the visual comfort condition of the occupants. A detailed description of all the different control strategies considered in the present study is provided in the following section.

Enhanced control strategies for Turin climate

Minimising loads:

EC_ML1: control strategy aimed at minimising the cooling loads exploiting the whole modulation range of the EC thermo-optical properties, from EC_10 to EC_1. Whenever a cooling load is detected the EC glazing is operated to its darkest state (EC_1).

EC_ML6: control strategy aimed at minimising the cooling loads exploiting a reduced modulation range of the EC thermo-optical properties, from EC_10 to EC_6. Whenever a cooling load is detected the EC glazing is operated to its darkest state (EC_6).

EC_ML7: control strategy aimed at minimising the cooling loads exploiting a reduced modulation range of the EC thermo-optical properties, from EC_10 to EC_7. Whenever a cooling load is detected the EC glazing is operated to its darkest state (EC_7).

Minimising glare risk:

EC_MG_1: control strategy aimed at minimising the risk of glare exploiting the whole modulation range of the EC thermo-optical properties, from EC_10 to EC_1. The EC is operated to the most transparent state able to ensure a DGP lower than 40%.

EC_MG1_w: control strategy aimed at improving the winter energy performance and the daylight performance in respect to that obtained for MG_1. Figure 26 shows the annual glare condition relative to the states EC_10 (totally bleached) and EC_1 (totally tinted), considered static for the whole year. It is possible to observe that in winter even the most tinted EC state (EC_1) is not able to

eliminate an intolerable glare condition in the central hours of the day. In this period (from 15/12 to 15/01) the EC glazing is therefore set on its totally bleached state (EC_10), as for this one the same intolerable glare condition is observed, but with the advantage that daylight penetration and solar gains are maximised.

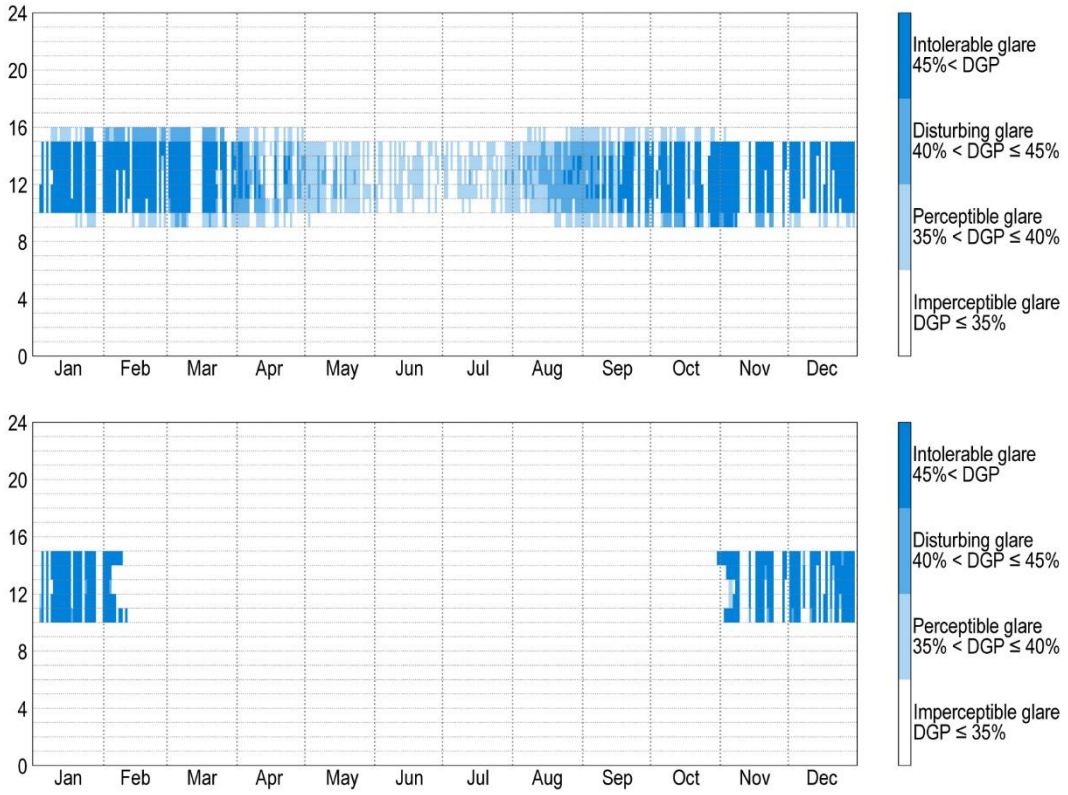

Figure 26. Annual profile of the Daylight Glare Probability relative to the EC_10 (upper chart) and the EC_1 (lower chart) states, considered static for the whole year.

EC_MG1_w-s: control strategy aimed at improving the summer energy performance relative to MG1_w. From 15/06 to 15/09, corresponding to the period in which the highest cooling needs are observed, EC_6 is used as minimum transparency limit state with the aim of minimising the cooling loads. With the same purpose EC_1 is used as minimum transparency state when the office is not occupied.

EC_MG_6: control strategy aimed at minimising the glare condition and maximising the daylight availability in the indoor space by exploiting a reduced modulation range of the EC thermo-optical properties, from EC_10 to EC_6. In this strategy, the EC_6 state was assumed as the minimum transparency limit after a preliminary analysis relative to the performance of the different EC states considered static for the whole year, which will be presented in detail in sub-section 3.4.3.1 (see Figure 27). The state EC_6 represents the most viable trade-off between the visual comfort and the energy performance aspects. the $DGP_{<40\%}$ value obtained for this state is

approximatively equal to those relative to all the darker EC states, including the fully tinted state EC_1, while, in respect to this one, the DA is significantly higher. The same trend is highlighted relative to the energy demand for cooling, which is almost constant for all the states between EC_1 and EC_6 and starts increasing for more transparent states than the EC_6. The present control strategy is thus aimed at simultaneously maximise the visual comfort performance and minimise the energy demands for cooling and lighting.

EC_MG6_w: control strategy aimed at improving the winter energy performance and the daylight performance relative to MG_6. In winter (from 15/12 to 15/01) the EC glazing is set to its most transparent state (EC_10) to maximise the solar gains.

EC_MG6_w-s: control strategy aimed at improving the summer energy performance in respect to that relative to MG6_w. From 15/06 to 15/09, corresponding to the period in which the highest cooling needs are observed, EC_6 is used as minimum transparency limit state to minimise the cooling loads, while EC_1 is used when the office is not occupied. This strategy is aimed at simultaneously minimising the energy use for space cooling and lighting.

Minimising glare risk with blinds:

Sel62+VB_MG: the basic control strategy VB_MG is applied to the internal venetian blinds coupled with the selective glazing Sel62.

Sel72+VB_MG: the basic control strategy VB_MG is applied to the internal venetian blinds coupled with the selective glazing Sel72.

3.4.2.4 Simulation workflow

The evaluation of the effects on visual comfort aspects of a control strategy for an adaptive glazing based on thermal or energy constraints is currently possible, by means of advanced simulation approaches [69,89], for only one or few points within the considered space. This is particularly limiting when dealing with the daylight availability within a space, which is usually assessed, by means of different dynamic metrics, for a grid of points evenly distributed in the whole space considered. In this case, such a punctual evaluation may not be representative of the daylight condition occurring within the whole space, which may lead to high inaccuracies in the results and eventually to wrong design choices. For these reasons an ad-hoc simulation tool was created, for which a detailed description is provided in section 3.2. Relative to the present application, the simulation workflow is divided into four automated steps, which are herewith listed:

1) Discretisation of the EC modulation range into 10 discrete states, corresponding to the 10 different pre-defined states available for the EC component considered. The optical properties of the DGU

equipped with the EC glazing in each static state are reported in Table 13.

2) Daylight Simulation of the different discrete electrochromic states with DAYSIM 4.0;
3) Energy simulation: the data from step 2 are supplied to EnergyPlus by means of its Energy Management System Module; then at each timestep the most suitable state of the EC glazing is selected, depending on the daylight and/or thermal constraints defined within the control strategy analysed.
4) Postprocessing of the daylight simulation results into yearly performance metrics.

3.4.3 Results

3.4.3.1 Performance of static glazing

This section analyses the performance of the two selective glazing considered as reference, compared to the 10 different states of the EC glazing, kept static for the whole year. Figure 27 shows the results relative to the primary building energy use, split in heating, cooling and lighting primary energy, as well as the visual comfort results, in terms of DA and $DGP_{<40\%}$, integrating the different glazing (from static benchmarks to the EC in each static state).

The selective glazing Sel72 shows the lowest overall energy consumption (–11% and –41% compared to the EC_10 and the EC_1 state respectively), and also the highest Daylight Availability. However, the related glare risk appears higher compared to that relative to the EC static states. Despite the selective glazing are characterised by a higher visible transmission, their use implies a higher EP_H compared to the electrochromic glazing with maximum transparency (EC_10). This is due to a different attitude between the two components towards the incident radiation: a selective glazing reflects most of the non-transmitted incident radiation, while the EC component, to reduce its transmittance, absorbs it. This is confirmed by the fact that the EC_10 static glazing shows a lower selectivity index (τ_{vis}/g-value), equal to 1.49, in respect to those relative to Sel72 and Sel62, equal to 1.89 and 2.07 respectively. Moreover, analysing the results relative to the Daylight Autonomy, it can be observed that the most transparent EC static state, EC_10 is outperformed by both the selective glazing, due to its lower τ_{vis} in respect to that of Sel72 and Sel62.

Since the climate of Turin is heating-dominated, the EC state leading to the lower energy consumption for space heating and artificial lighting results to be the bleached one (EC_10). The fully tinted EC state (EC_1) shows instead the minimum energy demand for space cooling, although this one is related to a significant increase in the energy demands for space heating and lighting (+99% and +185% compared to the EC_10 respectively). Generally speaking, it is

possible to observe that the overall building primary energy use increases for less transparent static EC states. In more detail, this increase appears more consistent for the energy demand for lighting compared to that relative to space heating. Due to the low U-value of the building envelope and to its boundary conditions (no heat transfer occurs between the case study and the surrounding offices), the office case study is characterised by a high energy performance for space heating. As a result, the energy use for space heating is significantly less sensible to the variation of the thermo-optical properties of the EC glazing compared to that relative to the artificial lighting. On the other hand, the low U-value of the building envelope does not allow to discharge the accumulated heat, thus leading to an increase of the cooling need, which is higher than the space heating decrease.

From Figure 27 it is possible to observe how, for the case study considered, there is a low incremental performance improvement between the states EC6 and EC1 in the energy demand for space heating (almost constant to approximatively 14 kWh/m^2·y for states darker than EC_6) and in terms of glare condition of the occupants (the $DGP_{<40\%}$ is almost constant, equal to approximatively 90%, for the states between EC_1 and EC_6). On the other hand, the primary energy use for lighting steadily increases, while the primary energy use for cooling decreases constantly for the states between EC10 and EC_6, state after which, no significant variation in the EP_C is observed. Moreover, a steady decrease in the Daylight Autonomy is observed between the EC states with a higher visible transmittance and darkest ones, with an absolute variation from EC10 to EC_1 equal to 59.16%. This means that the darkening of the glazing beyond the intermediate state EC_6 may not significantly improve the building performance as far as primary energy use and glare risk are concerned. As already highlighted in sub-section 3.4.2.3, these considerations underlie the modifications introduced in the basic control strategies when defining their enhanced climate-specific versions, particularly in respect to the EC_MG6 control strategy.

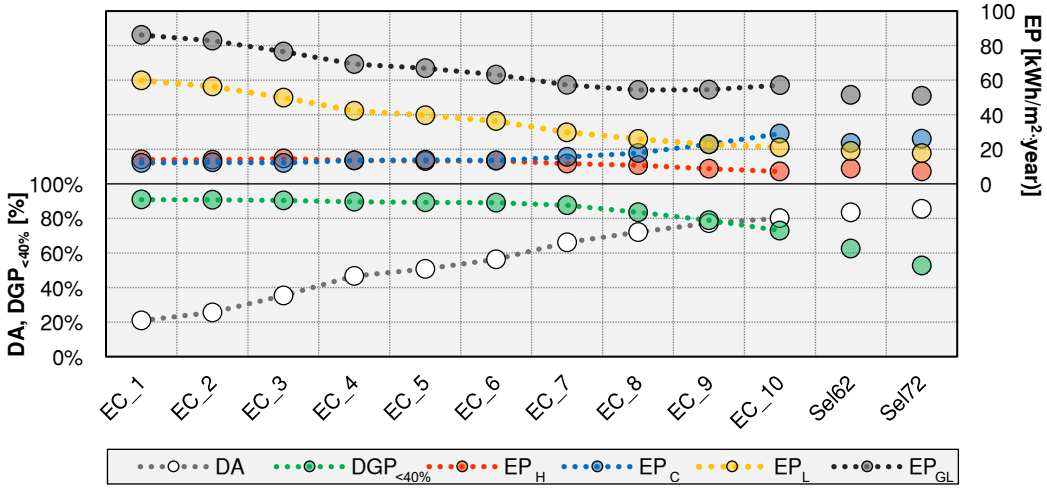

Figure 27. Annual results relative to energy performance (upper chart) and visual comfort (lower chart) for the two selective glazing and the 10 states of the Electrochromic glazing.

3.4.3.2 Performance of the controlled EC glazing

Minimising load strategies (ML)

Three control strategies are compared with the aim of minimising the cooling loads (see sub-section 3.4.2.3), namely EC_ML1, EC_ML6 and EC_ML7. Figure 28 shows the results relative to the primary building energy use (split in heating, cooling and lighting primary energy) and the visual comfort results (DA and $DGP_{<40\%}$) relative to the EC glazing operated according to the three control strategies considered. The results show how a narrower modulation range of the EC glazing (EC_ML6 and EC_ML7) positively affects the building primary energy use for space heating and cooling, as well as the visual comfort condition of the occupants, both in terms of glare condition and of daylight availability on the workplane. In more detail, the operation of the EC glazing according to both EC_ML6 and EC_ML7, in respect to EC_ML1, shows to reduce the overall primary energy need (-16.8% and -19.6%, respectively), as the primary energy use for space heating and space cooling does not significantly vary, while a reduction is observed in the primary energy consumption for artificial lighting (-28.4% and -36.8%, respectively). This is due to an increasingly higher transparency of the EC darker limit state in the control strategies EC_ML6 (EC_6 state) and EC_ML7 (EC_7 state), which shows to positively affect the visual comfort aspects, as no significant variation is observed for the $DGP_{<40\%}$, while the Daylight Autonomy is increased, in respect to EC_ML1, of 35.4% for EC_ML6 and 45.5% for EC_ML7.

It is possible to conclude, based on the outcomes obtained, that the purpose of minimising the cooling loads could be pursued with the same success by either exploiting the full EC modulation range or by using only a part of it, i.e. without taking advantage of EC the darkest states. In addition, this latter solution shows to improve both the overall primary energy use, as the energy demand for lighting is decreased, and the visual comfort for the occupants, as the daylight availability on the workplane is increased while the glare condition remains unchanged.

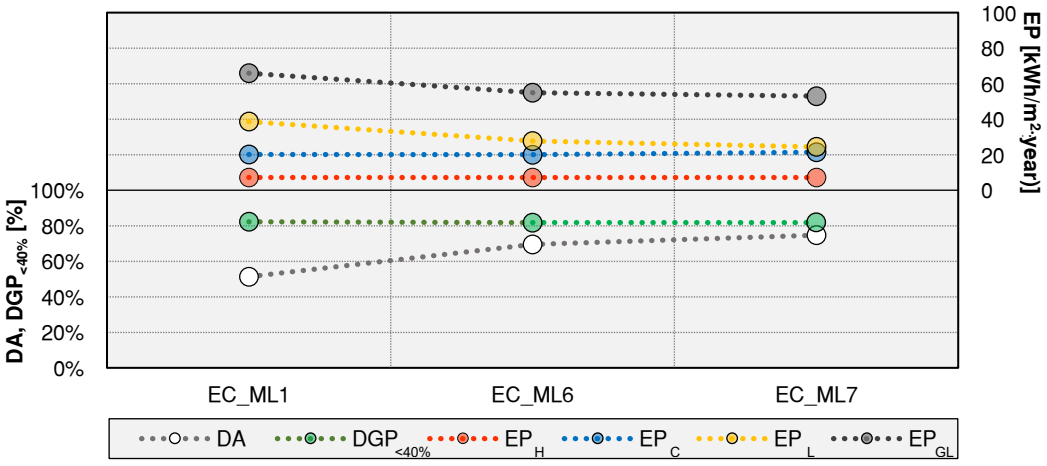

Figure 28. Annual results relative to energy performance (upper chart) and visual comfort (lower chart) for the Minimising Load (EC_ML) control strategies.

Minimising glare linear strategies (MG)

In this section the six control strategies aimed at the optimisation of the glare condition for the occupants (see sub-section 3.4.2.3) are compared. Different alternatives for this type of control strategies are considered, from a basic version aimed at the minimisation of the glare condition only (EC_MG1 and EC_MG6) to climate-specific enhanced versions modified with the purpose of improving also the overall building energy performance (EC_MG1_w, EC_MG1_w-s, EC_MG6_w and EC_MG6_W-s).

Figure 29 shows the results relative to the primary building energy use (split in heating, cooling and lighting primary energy) and the visual comfort results (DA and $DGP_{<40\%}$) relative to the EC glazing operated according to the six control strategies considered. From the results obtained it is possible to observe that the enhanced versions of this control strategy proved to be effective in improving the overall energy performance, in respect to their basic versions, but at the same time they negatively affect the daylight availability on the workplane. In more detail, the enhanced control strategies provide the same glare condition as the basic ones, as no significant variation in the $DGP_{<40\%}$ is observed, while a slight decrease in the overall building primary energy use is noted, equal to -3.7% for EC_MG1_w and to -8.1% for EC_MG1_w-s in respect to EC_MG1, and to -2.2% for EC_MG6_w and to -6.8% for EC_MG6_w-s in respect to EC_MG6. Specifically, as far as the two control strategies modified to improve both the winter and summer energy performance are concerned, i.e. EC_MG1_w-s and EC_MG6_w-s, these two show a consistent decrease in the primary energy need for space cooling in respect to their basic versions, equal to approximatively -34% for both strategies, while an increase on the energy demand for lighting is observed, equal to 20.9% and 27.2% respectively. On the other hand, along with an improvement in the overall energy performance, these two control strategies show a decrease in the DA, equal to -10.1% for EC_MG1_w-s (in respect to EC_MG1) and -8.5% for EC_MG6_w-s (in respect to EC_MG6).

The use of a narrower modulation range for the operation of the EC glazing (EC_MG6), in respect to the exploitation of the full switching range (EC_MG1), shows an improvement in the overall building energy performance, with a reduction of the total building primary energy use of -5.1%, while no significant variation is observed in the visual comfort condition provided to the occupants, both in terms of $DGP_{<40\%}$ and of DA. A more transparent dark limit state for the EC glazing allows a higher daylight penetration within the indoor space, which implies a reduction in the primary energy use for artificial lighting, equal to -10.6% for EC_MG6 in respect to EC_MG1. As far as the primary energy use for space heating is concerned, comparable values were obtained for all the EC_MG strategies.

The overall energy performance related to all the EC_MG strategies results worse than that relative to the two static benchmarks considered. The same is true also for the visual comfort, in terms of daylight availability on the workplane,

while as far as the glare condition is concerned, this one results improved for all the EC_MG strategies considered.

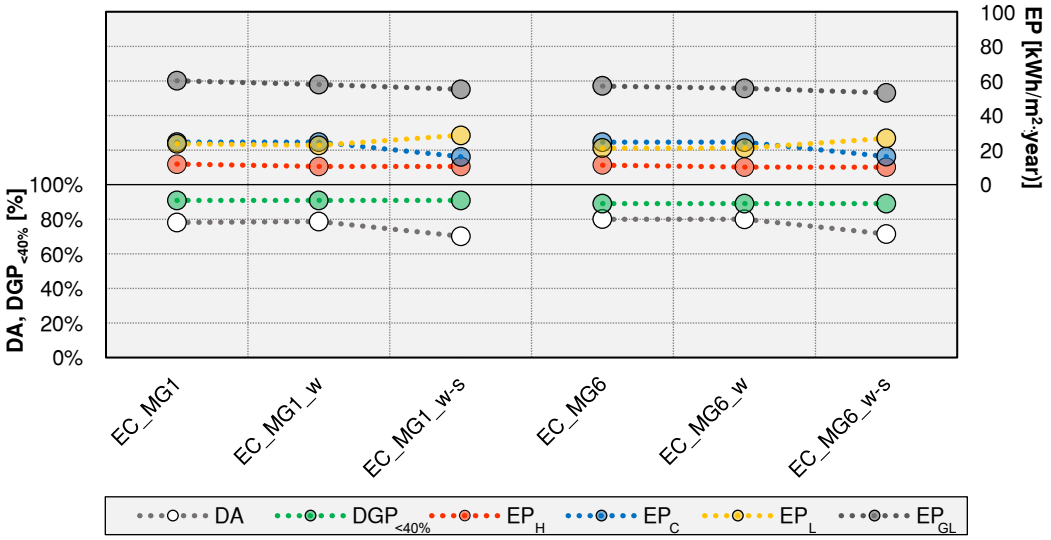

Figure 29. Annual results relative to energy performance (upper chart) and visual comfort (lower chart) for Minimising Glare by linear switching (EC_MG) control strategies.

To have a better understating of the way and extent at which the enhancements introduced to the basic MG control strategy affect the annual visual comfort condition of the occupants, a more in-depth insight of their related visual comfort performance is provided in Figure 30 and Figure 31. In more detail, Figure 30 shows the monthly variation of the Daylight Autonomy for EC_MG1, EC_MG1_w and EC_MG1_w-s. The operation of the EC glazing to its bleached state in the winter season (from 15/12 to 15/01), i.e. the EC_MG1_w control strategy, shows to slightly improve the daylight penetration within the office space in respect to the basic control strategy EC_MG1. Conversely, the use of EC_6 state as minimum transparency state in the summer season (from 15/06 to 15/09), i.e. the EC_MG1_w-s control strategy, shows to negatively affect the daylight availability on the workplane, as in this period the DA is reduced in respect to that relative both to EC_MG1 and EC_MG1_w. These considerations remain valid, even if the extents of the variations may slightly change, also with regard to the three control strategies considering the state EC_6 as the minimum transparency limit state (EC_MG 6, EC_MG6_w and EC_MG6_w-s).

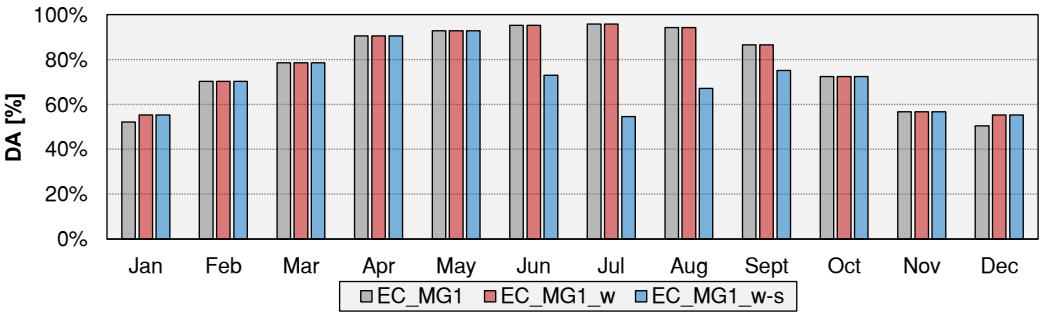

Figure 30. Monthly Daylight Autonomy for EC_MG strategies with EC_1 as darkest limit state.

Figure 31 shows the monthly variation of the glare condition of the occupants relative to the EC_MG1 and EC_MG6 control strategies, assessed by means of the $DGP_{<40\%}$ metric. The outcomes show how the use of different darkest EC, state as minimum transparency limit lead to similar monthly results. In more detail, from March to September both control strategies show to be able to ensure a glare condition below disturbing for 100% of the occupied time, while in December and January the use of either EC_1 or EC_6 as limit state does not significantly affect the resulting glare condition of the occupants, as the same results are obtained for both control strategies. In the remaining months, i.e. February, October and November, EC_MG1 always shows a slightly better performance in respect to that obtained for EC_MG6, with differences in the $DGP_{<40\%}$ ranging from 5% (November) to 12% (February). However, the differences highlighted are too small to affect the annual $DGP_{<40\%}$ value, which in fact is almost equal (differences below 1%) for the two strategies EC_MG1 and EC_MG6 (see Figure 29).

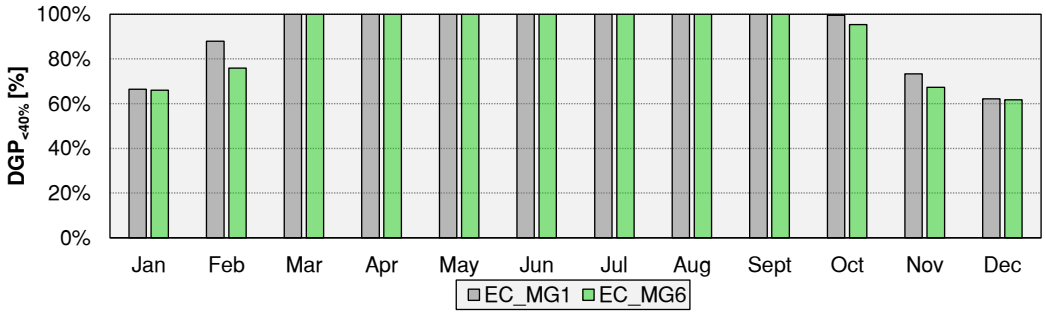

Figure 31. Monthly Daylight Glare Probability for Minimising Glare strategies EC_MG1 and EC_MG6.

Minimising glare risk with blinds (VB_MG)

In this section the results relative to the energy and visual comfort performance related to the two selective glazing coupled with internal venetian blinds are shown. The venetian blinds are operated according to a *minimising glare* control strategy, meaning that the slat are adjusted to the lowest angle (between 0°-horizontal, 15°, 30°) able to ensure a DGP value below 40% (see sub-section 3.4.2.3). Figure 32 shows the results relative to the primary building energy use (split in heating, cooling and lighting primary energy) and the visual comfort results (DA and $DGP_{<40\%}$) relative to the two selective glazing coupled with internal venetian blinds. The visual comfort results show that both these solutions are able to ensure an optimal glare condition (DGP < 40%) for the whole time in which the building is occupied, while in terms of DA they both show a slightly worse performance in respect to that of the EC operated according to the different *minimising glare* strategies. As far as the overall primary building energy use is concerned, the results relative to both solutions are comparable to those obtained for the EC operated according to EC_MG1, EC_MG6 and EC_MG1_w control strategies and below that relative to EC_ML1. Between the Sel62+VB_MG and Sel72+VB_MG a decrease in the primary energy need for

space cooling of -13.7%, and an increase in primary energy use for space heating equal to +19.9% are observed, resulting in increase of the global specific building primary energy use of +2.1%. This is due to the higher τ_{vis} and g-value of the Sel72 selective glazing, which imply higher solar gains, resulting in a lower energy demand for space heating and in a higher energy demand for space cooling.

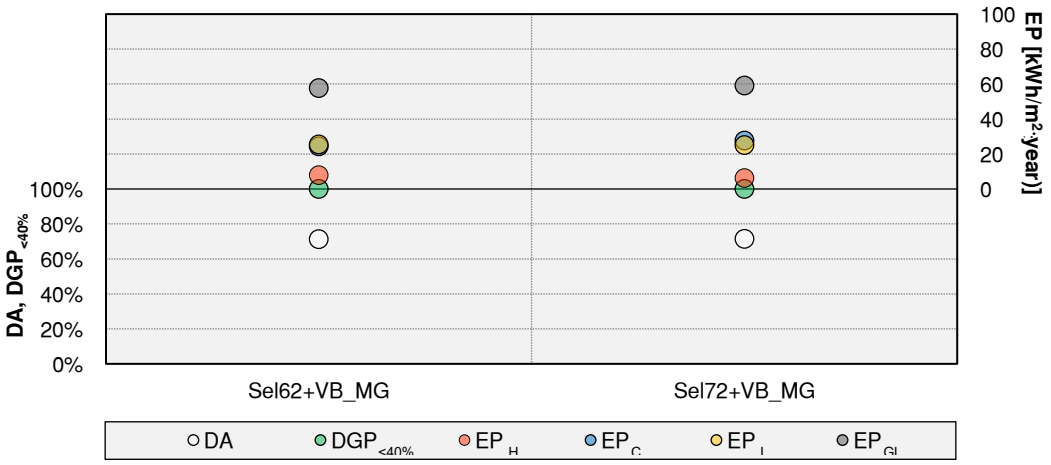

Figure 32. Annual results relative to energy performance (upper chart) and visual comfort (lower chart) for Minimising glare risk with blinds (VB_MG) control strategies.

Contrasting DA versus glare risk requirements

All the previous analyses were focused on comparing one single performance parameter at the time (only primary energy use, or single contributions of primary energy use, or only single aspects of visual comfort, i.e. glare risk or DA alternatively). Such approach does not allow a comprehensive evaluation of the mutual influence between energy and visual comfort aspects in the analysis of mono-objective and multi-objective control strategies for the operation of active adaptive façade components.

For this purpose, a different representation of the results obtained is proposed in Figure 33, which shows, for all the different static and adaptive glazing solutions considered, the visual comfort performance relative both to the daylight availability on the workplane and to the glare condition of the occupants. In addition, a qualitative indication of the specific building primary energy use relative to each case analysed is also provided. In more detail, the chart correlates the DA, reported on the x-axis, and the $DGP_{<40\%}$, reported on the y-axis, for all the façade solutions considered. As DA and $DGP_{<40\%}$ indicate the percentage of occupied hours in which daylight alone meets the minimum illuminance requirement of 500 lx and in which the glare sensation is below disturbing, a value of 100% represents for each of them the ideal condition. Therefore, in the chart proposed, the ideal optimal condition, or theoretical optimum, is represented by the top right-hand corner, point in which the two metrics show a value of 100% (the chart was clipped in order to best fit the outcomes obtained). The size of each

marker provides a qualitative indication of the overall primary energy use: the bigger the marker the higher the amount of primary energy consumed.

From Figure 33 it is possible to observe how the points representing the performance of the static glazing (selective and all the individual states of the electrochromic component, from EC_10 to EC_1) form a curve-shaped line with a well-defined trend. This curve represents the maximum performance achievable in terms of both glare risk and daylight autonomy by means of the adoption of static transparent components. As the visible transmittance (τ_{vis}) of the selected static glazing increases, both DA and glare increase. Conversely, a reduction in the transparency of the static glazing is associated with a lower risk of glare and a lower availability of daylight. The opposite trend is highlighted as regard the energy performance, as already highlighted in sub-section 3.4.3.1. The performance of any static glazing will always be below the curve defined above. On the contrary, the performance of a dynamic component, which is able to adapt its thermo-optical properties to external environmental conditions, can over-perform the static glazing as far as multiple performance objectives are concerned at the same time. The distance from this curve represents the effectiveness of a certain control of dynamic glazing as far as visual comfort is considered, globally.

Looking at the chart it is possible to observe that the control strategies closer to the optimal theoretical limit (top right corner), are those relative to the electrochromic glazing operated with the aim of minimising the glare phenomenon through a direct control of the DGP (EC_MG1, EC_MG1_w, EC_MG6, EC_MG6_w) and the control strategies for the Venetian blinds coupled with the two selective glazing (Sel62+VB_MG and Sel72+VB_MG). The two strategies implementing the internal venetian blinds show the highest values of $DGP_{<40\%}$, but with a poor value of DA. The strategies EC_ML1, EC_ML6 (those aimed at minimising thermal loads) are the only ones for which a visual comfort performance worse than that relative to static glazing was obtained. This means that, from the visual comfort point of view, it is more effective to use a static glazing with τ_{vis} included between that of EC_5 and EC_9 glazing rather than using the electrochromic component controlled by means of the aforementioned control strategies. Control strategies with EC_6 state limit show worse performances from the DGP point of view compared to those relative to control strategies exploiting the whole EC modulation range (EC_10 to EC_1), while a slightly improvement from the DA point of view is highlighted. Therefore, it is possible to conclude that by enlarging the variation of optical properties of the dynamic glazing, the real advantage relies on being able to respond to multiple performance requirements at the same time.

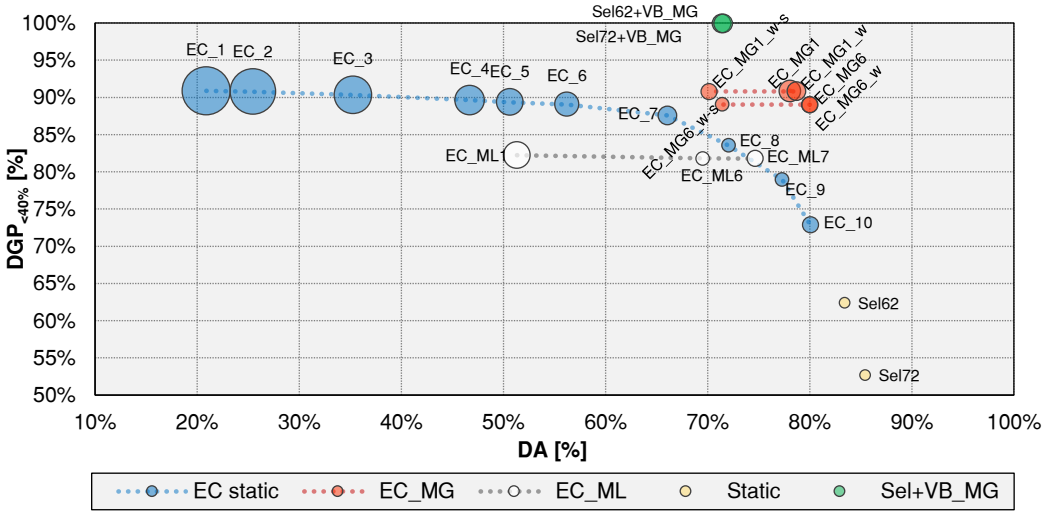

Figure 33. DA, $DGP_{<40\%}$ and EP_{gl} correlation for the control strategies examined.

Contrasting energy use versus glare risk requirements

As for Figure 33, also Figure 34 allows to represent the mutual influence between energy aspects and visual comfort. In more detail, Figure 34 correlates the reduction of disturbing glare, expressed as a percentage of occupied hours over the year in which it is imperceptible or perceptible ($DGP_{<40\%}$) and the global energy performance (EP_{gl}). In this case the ideal position is represented by the top left corner, for which both the energy performance index and the glare risk are equal to zero. Similarly to what happened contrasting Daylight Autonomy versus glare risk, the performances of the analysed static glazing (selective and all the individual states of the electrochromic component) form a curve-shaped line with a well-defined trend, defining the maximum performance achievable by means of the adoption of static glazing with similar selectivity (ratio between τ_{vis}/g-value). The difference between the two selective glazing and the EC states lies in the fact that the EC glazing is an absorbing glazing, modulating the transmitted energy by means of a variation in the absorptance, rather than in the reflectance (as for selective glazing). This results in an overall better performance of the static glazing, as the low infiltration and ventilation rate of the office case study, as well as the low thermal transmittance of its building envelope, do not allow the discharge of the additional heat gains derived from the EC higher absorption. The distance from this theoretical limit represents the effectiveness of controlling a dynamic glazing according to multiple performance objectives, compared to a static glazing.

Analysing the results of the EC static states, it is possible to observe that as the glazing gets darker the energy need increases (due to the reduction of the solar gains), while the glare risk decreases. The control strategies considered (excluding EC_ML1 and EC_ML6) show to be able to improve the visual performance by reducing the glare risk, while the related energy performance index results to be higher than that of the selective glazing, showing a value between those of EC_7

and EC_2. The control strategies for which the best performance was obtained, both in terms of energy and visual comfort performance, result to be Sel62+VB_MG, Sel72+VB_MG, EC_MG1_w-s and EC_MG6_w-s. The strategy ML_7 shows the best energy performance (slightly better than that related to EC_MG1_w-s), but with very poor DGP results. ML1 shows to be ineffective in reducing the overall energy demand compared to EC_10 and the two selective glazing, while from the visual comfort point of view significant improvements are observed. Similarly to what observed in the previous section, by enlarging the variation of optical properties, the performance is improved as far as the DGP is concerned. However, this seem to imply a little increase in the energy use, which could be due to the selectiveness of the electrochromic glazing. Nonetheless, enlarging the variation range shows to be effective in improving the performance as far as multiple performance objectives are concerned.

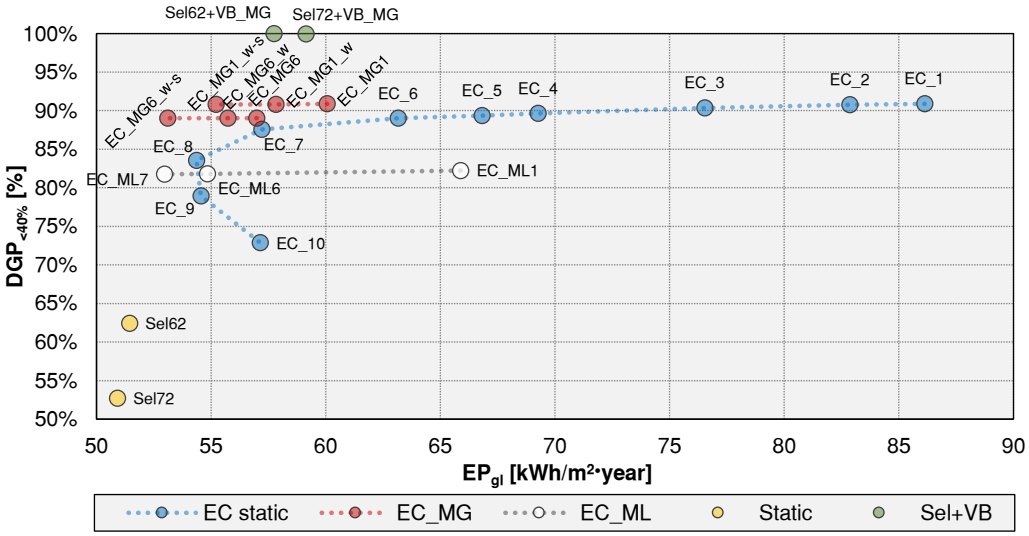

Figure 34. Energy performance and $DGP_{<40\%}$ correlation for the control strategies examined.

3.4.4 Discussion and conclusions

In this study the performance of an active adaptive transparent façade component, namely an electrochromic glazing, operated according to different control strategies, is compared to the one relative to different traditional static glazing, in terms of visual comfort condition of the occupant, as well as overall energy use. In more detail, as far as visual comfort is concerned, glare risk and daylight availability were analysed, while relatively to the energy aspects the primary energy indexes for heating, cooling and lighting were accounted. A south oriented enclosed office, located in a heating dominated climate (Turin), was used as a case study. The window was alternatively equipped with two different selective glazing (also coupled with internal venetian blinds), and with an electrochromic glazing, controlled according to different mono-objective control strategies. The outcomes of this study show how the use of a transparent adaptive façade component allows improving both energy and visual aspects at a time,

beyond what is theoretically achievable by means of a static glazing. Nonetheless a trade-off in the decision making between reduction of glare, decrease in energy use for heating and increase of daylight availability in a heating dominated climate will always exist.

The present study is limited to a single climate (which is heated dominated), as well as to one orientation and one building use, with only one Window-to-Wall Ratio. The choice of climate, building use, building characteristics and control strategies may have influenced the relative performance of the EC glazing compared to static glazing. Nonetheless, despite its limitations, this study highlights how the main potential of dynamic glazing, and more in general of the active modulation of solar radiation, is a way to achieve multiple performance requirements at the same time, beyond what is physically achievable by static glazing alone without modulating the entering solar radiation according to the boundary conditions.

This introduces further potential not only to reduce building energy uses, but to improve at the same time the comfort condition of the occupants. Moreover, this study highlights the dependency of the performance of dynamic glazing on their control strategy and on the aim of the control strategy itself. The development of optimised control strategies, as well as how they are implemented during operation of real buildings, thus becomes of foremost importance to ensure that a certain performance level is achieved, or, at worst, that integrating dynamic glazing does not introduce new issues compared to a static one.

3.5 Conclusions

The present chapter presented a novel integrated simulation methodology for a simultaneous and comprehensive evaluation of the effects of the behaviour of a transparent adaptive façade component on the overall energy performance of a space and on the visual comfort condition of its occupants. The capabilities of such integrated methodology were demonstrated through its application for assessing the performance relative both to a passive and an active transparent adaptive component. As for the former, the application of the simulation methodology proposed allowed the evaluation of the energy and visual comfort performance of a thermochromic glazing showing a complex behaviour, characterized by a thermal hysteresis. In the latter instead, the application of such simulative methodology allowed evaluating the drawbacks deriving from operating an electrochromic glazing according to mono-objective and mono-domain control strategies over both energy and visual comfort performance.

The novelty of the proposed methodology lies in the fact that, due to the data integration performed, coupling visual results to thermal simulations, a more comprehensive performance evaluation is possible, also taking into account complex phenomena at a material level, which determines an interdependence of the thermal domain with the variation of the optical one. The results presented highlight the importance of adopting an accurate simulation strategy to support

choices relative to the design and operation of transparent adaptive components, as mean to:

a) support the possibility of material design to optimise different material optical – thermal properties;

b) evaluate the interdependency between these properties and the component performance when building integrated;

c) evaluate the interdependency of multiple performance aspects, such as heating and cooling energy uses, artificial lighting energy use and daylight visual comfort.

As far as visual comfort is concerned, in the present chapter the relevant influence of this aspect on the final overall building energy use was shown. However, in the analyses performed only the horizontal illuminance on the visual task was assessed with a high spatial resolution, while the glare condition of the occupants was evaluated for only one significative point within the space considered. This may not be representative of the glare condition occurring throughout the whole space, which may also in turn negatively affect the overall building energy use. An evaluation of the glare condition with a high spatial resolution is therefore desirable for a more comprehensive and accurate understanding of the visual comfort levels occurring within a space. This aspect will be addressed in detail in the following chapter.

Chapter 4

Daylight glare spatial evaluation

4.1 Introduction

Part of the work described in this chapter has been previously published by the author and co-workers in international peer-reviewed journals [8].

The topic of daylighting has always been crucial in the design process of a building, both as far as the related energy demand for lighting is concerned and for its key role in determining the indoor environmental quality perceived by the occupants of a space. Daylighting shows to have a significant influence on the comfort level of the occupants, in terms both of visual comfort and non-visual effects [6,221–225].

Focusing on daylight visual comfort, this is a complex phenomenon influenced by several lighting aspects, including the illuminance on task surfaces and the glare related to daylight sources. These are commonly taken into account during the design phases with objective parameters, including: the horizontal illuminance on the workplane, which is the quantity most commonly used to assess the lighting performance in a space; the luminance distribution in the occupants' visual field; the colour of the light perceived by the occupants. In spite of its importance for visual comfort, daylight discomfort glare is not so commonly addressed in the evaluation of the overall visual comfort conditions of the occupants.

Moreover, the visual comfort condition is influenced by a series of external factors, including, but not limited to, the geometrical characteristics of the space considered, as well as the optical properties of its materials, presence of shading systems, position of the sun in the visual field, luminance of the sky, presence, geometry, and reflectance of external obstructions. All these aspects increase the complexity of this phenomenon, which may in fact significantly vary for different points within the same room. As a result, a spatial evaluation of the visual comfort condition of the occupants results more desirable in order to have a clear picture

of possible local situations of visual discomfort within the space analysed. This is also confirmed by the introduction, by the Illuminating Engineering Society, of two metrics aimed at assessing the annual availability of daylight and sunlight exposure at a spatial level, named spatial Daylight Autonomy (sDA) and Annual Sunlight Exposure (ASE) respectively [142]. As far as illuminance-based metrics are concerned, this is an easy task, as many daylight simulation software already allow the calculation of the illuminance for a grid of points within a room. Conversely, an accurate assessment of the glare condition of the occupants with a high spatial resolution results in a challenging task. This is mainly due to the fact that for daylight glare the complexity of the phenomenon is even increased, as it is both-position and view-dependant. Some simplified methodologies for an estimation of the glare condition through the horizontal illuminance on the visual task exist, but these ones result inaccurate in predicting the glare phenomenon due to luminance contrast (see section 2.4).

Currently, the most reliable metric to assess glare from daylight is the Daylight Glare Probability (DGP) [111], as it is able to assess both the influence of direct illuminance at the eye level and of the luminance contrast in the determination of the final glare condition. Moreover, this metric was validated against experimental data. However, the evaluation of the glare from contrast requires an HDR image to be rendered at each timestep, which results in a high computational time required to perform an annual analysis. As a consequence, this metric is only assessed for one or at most few significant points within the space considered. This, as seen, may inaccurately represent the different glare conditions occurring throughout the whole space analysed. As far as transparent adaptive components are concerned, such inaccuracies in the evaluation of the glare condition may eventually negatively affect choices relative to the design or the operation of these components, resulting in a lower visual comfort condition and/or in a higher building energy use than what numerically predicted.

In this framework, the present chapter presents a simplified and fast approach for the evaluation of the glare condition of the occupants with a high spatial resolution. This is based on the calculation of the sole eye vertical illuminance (E_v), which is compared to a threshold value for each daylight glare comfort class, as defined in [133]. These E_v threshold values are determined through a comparison with the DGP values on an annual basis through a fault-detection technique.

Section 4.2 provides a detailed description of the simplified approach proposed for a spatial assessment of the glare condition of the occupants. This approach was applied to a number of case studies and the error committed in respect to DGP was evaluated. Moreover, the advantages and drawbacks of this approach are discussed as well. Section 4.3 provides a demonstration of how such simplified approach could be effectively used in the operation of different active transparent adaptive components to spatially optimise the overall visual comfort condition of the occupants.

4.2 Simplified approach for the spatial evaluation of the daylight glare comfort classes

4.2.1 Introduction

The present section introduces a simplified approach aiming at the classification of an entire space in daylight glare comfort classes, for a whole year, in a computationally efficient way. To speed up the calculation, the evaluation of the daylight glare condition is based only on the vertical illuminance at the eye level. Furthermore, daylight glare is evaluated not through the exact DGP value, but in terms of daylight glare comfort classes, as defined by Wienold in [133]: imperceptible, perceptible, disturbing, intolerable glare. Similarly to the approach used by Torres et al. [144] a fault-detection analysis was used to correlate the vertical illuminances to the daylight glare comfort classes, which correspond to specific ranges of DGP values. The approach was tested for an indoor space with different orientations, to which different glazing types and shading systems are applied.

In sub-section 4.2.2 the idea underlying the proposed simplified approach is presented in detail, as well as its architecture and workflow. Moreover, the description of the case study for which the above simplified approach was tested is provided. Sub-section 4.2.3 presents the results obtained relative to each step in which the approach is subdivided. Finally, in sub-section 4.2.4 the main advantages and limitations of the proposed approach are presented and critically discussed.

4.2.2 Method and case study

The simplified approach presented in this section aims at a spatial annual evaluation of the glare classes within a space, with a reduced computation time compared to a comprehensive and accurate annual glare assessment through Daylight Glare Probability (DGP). The DGP [111], currently the most validated and widespread metric used to assess glare from daylight [143], is calculated according to the following equation:

$$DGP = 5.87 \cdot 10^{-5} E_v + 9.18 \cdot 10^{-2} log\left(1 + \sum_i \frac{L_{s,i}^2 \omega_{s,i}}{E_v^{1.87} P_i^2}\right) + 0.16 \qquad (10)$$

where E_v is vertical illuminance at eye level [lx]; L_s is the light source luminance [cd/m^2], ω_s is the light source solid angle [sr]; P is the position index [-], which expresses the variation in glare sensation experienced relative to the angular displacement of the light source from the observer's line of sight. The equation consists of two terms: the first one considers the vertical eye illuminance

(mainly due to direct solar radiation), while the second accounts for the contrast between the scene background luminance and the luminance of the light sources within one's visual field. The computation of the second term is the most time-consuming, as the luminance contrast assessment requires an image to be created for the evaluation. On the contrary, the E_v assessment is a much faster and easier calculation. For an annual evaluation of the DGP in a position of the space considered, the tool Radiance can be used or, alternatively, a set of Radiance-based software, such as *DAYSIM* [155] or *DIVA-for-Rhino* [226].

The DGP range of variation is subdivided in sub-ranges linked with different glare sensations. The idea of associating glare indices to classes of glare sensation comes from Hopkinson, who first defined four classes: *Just Perceptible*, *Just Acceptable*, *Just Uncomfortable* and *Just Intorelable* [101]. This approach was adopted by Wienold, in accordance to the methodology described in [227] for thermal comfort rating, when defining his daylight glare comfort classes by correlating different glare sensations to specific ranges of DGP values [133]. Wienold's objective was to introduce a scale to rate visual discomfort for daylighting, in which each category is defined according to the user's satisfaction to be within each DGP threshold for at least 95% of time during a whole year (a possible exceedance of DGP thresholds for 5% of time is still allowed). For each daylight glare comfort class, a DGP threshold value was therefore defined, based on the analysis of an extensive set of numerical case studies. Table 14 summarises all the daylight glare comfort classes with the relative DGP threshold values.

Table 14. Daylight glare comfort classes and relative DGP thresholds [133].

Daylight glare comfort class	DGP threshold
Imperceptible glare	DGP < 35%
Perceptible glare	35% ≤ DGP < 40%
Disturbing glare	40% ≤ DGP < 45%
Intolerable glare	DGP ≥ 45%

As outlined earlier, one of the drawbacks of the DGP is the computational effort needed to perform evaluations which are not limited to one point and one direction in space and to a single time-step, so that a spatial and multi-directional annual glare evaluation would be extremely computational expensive.

The present study presents a simplified approach which enables to classify a whole space in terms of glare comfort classes by means of the eye vertical luminance E_v alone, without considering the luminance of the light sources and the luminance contrast in one's field of view. This results in a significant reduction of the computation time required, although it could introduce some errors in the assessment of the daylight glare comfort classes, as the contribution of the luminance contrast to glare sensation is neglected. This reduction in computational time can support: i) a higher spatial and directional resolution of glare comfort assessment of the considered space; ii) the adoption of more cost-effective measurements and sensors for controlling the considered space to minimise glare discomfort. In order not to compromise the accuracy in the

estimation of the glare comfort class, the evaluation and minimisation of the errors introduced by the simplified approach presented hereby is of foremost importance. The simplified approach consists of the following steps, which will be discussed in detail in the following sub-sections:

Step 1: Calculation of E_v thresholds to classify each viewpoint / direction of observation of a custom-defined grid in a certain glare comfort class (corresponding to each DGP threshold value). This is done by means of a fault-detection technique;

Step 2: Quantification of errors from adopting E_v to classify a certain point in a daylight glare comfort class, compared to the exact DGP values, for each point of the custom-sized grid. The errors are expressed as underestimation and overestimation occurrences of the various glare conditions;

Step 3: Identification of the most suitable point (or points) in the space and direction of observation for the calculation of the E_v thresholds to be adopted to classify the whole space according to the glare comfort classes. This is done by identifying the point which minimises the maximum error committed for 95% of time and maximises the number of cases for which an $E_{v,thr}$ is calculated.

Unlike the DGPs method [134], the presented approach aims at classifying a certain space into glare comfort classes, rather than calculating the exact DGP for a certain point / direction of observation. Moreover it is worth noticing that the accuracy of this simplified approach also depends on factors such as shape, size and orientation of the space considered, direction of the viewpoint in respect to the daylight source (window), geometric and optical properties of windows and of solar shadings. The present study is a first evaluation of the suitability of the simplified approach, which was applied, as first exploration, to a case-study as described in the next sub-section.

Application of the simplified approach to a case study

The simplified approach was tested for an enclosed office 3.6 m large, 6 m deep and 2.7 m high, with a window of 3.3 m width by 1.5 m height within one of the short walls. The case-study office was located in Turin (45.06° N, 7.68° E) and was alternatively oriented so as to have the window facing south and west. Table 15 summarises the optical properties of the internal surfaces of the space.

Table 15. Optical properties of the materials used for the office selected as a case-study.

Surface	Visible reflectance (ρ_{vis})
Floor	0.35
Walls	0.65
Ceiling	0.80
External ground	0.10

The investigated window configurations consisted of glazing with different transmission properties (specular or scattering) and different visible transmittances (τ_{vis}), for a total number of 16 glazing types. The scattering glazing was considered to be perfectly diffusing, i.e. the entire incident transmitted light is scattered in a uniform way toward the interior of the space. Table 16 summarises all the glazing types and visible transmittances considered.

Table 16. Glazing types considered in the present study.

	Specular glazing	**Scattering glazing**
τ_{vis}	0.05	0.05
	0.15	0.15
	0.25	0.25
	0.35	0.35
	0.45	0.45
	0.55	0.55
	0.65	0.65
	0.75	0.75

Additionally, to glazing characterised by different properties, also shading devices were considered, specifically venetian blinds with different slat angles and roller blinds with different τ_{vis} values, as summarised in Table 17. Venetian blinds were considered to have a slat depth of 3.5 cm, modelled as a plastic material with a ρ_{vis} value of 0.44. Roller blinds were modelled as a perfectly diffusing translucent material. Two different roller blinds were considered, one aiming at glare control, with $\tau_{vis} = 0.04$, and one aiming at solar control, with $\tau_{vis} = 0.15$, according to the typical light transmission values of commercially available technologies. All the shading devices were applied to the clearest specular glazing investigated ($\tau_{vis} = 0.75$).

Table 17. Shading devices considered in the present study.

Venetian blinds (VB)					**Roller Blinds (RB)**	
Slat angle	0°	30°	60°	τ_{vis}	0.04	0.15

A 3x3 grid of points in the room was identified in order to consider all the different glare conditions occurring throughout the space analysed. The three rows of points parallel to the window (3 points in each row) are spaced of 1.5 m from one another. The row closest to the window is 1.5 m far from this one. In each row the central point is located in the room centre line and is 1.3 m distant from the two lateral points, which in turn are 0.5 far from the room lateral walls. All the points were located at a height of 1.2 m above the floor, i.e. the height of the eyes of a seated person. For all the points, five different directions of observation were considered, from -90° to 90° with a step of 45°, where 0° represents the direction of observation perpendicular to the window plane. These directions of observation were chosen so as to evaluate the different glare conditions occurring in each point for the possible view directions in which a glare condition may be

experienced. Figure 35 shows the location and direction of observation for all the points considered within the office space.

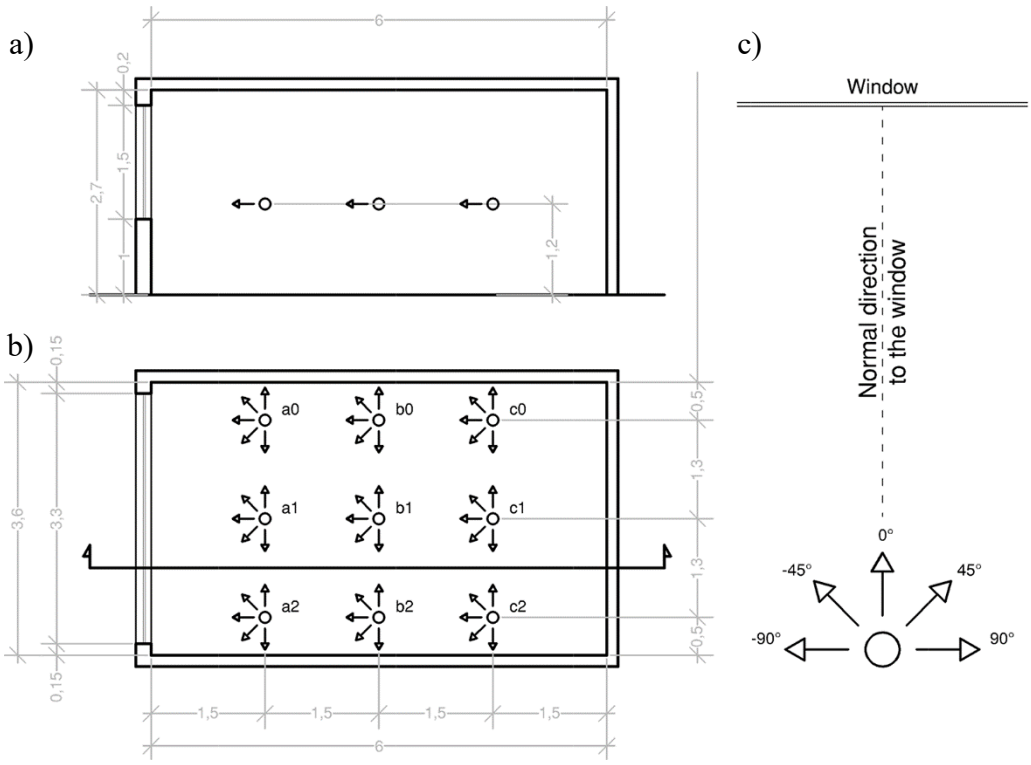

Figure 35. a) Office section view, b) office plan view, with the location and directions of observation for all the points considered; c) Detail of the directions of observation assumed, in respect to the normal to the window plane.

DGP and E_v values for each point and relative directions of observation were calculated, by means of DAYSIM software, for a whole year. To calculate annual DGP profiles DAYSIM uses the enhanced simplified DGP method described in [133], for which DGP is still evaluated through equation (10), but the second term of the equation, i.e. luminance contrast, is calculated analysing a simplified image (less time-consuming) in which the main scene luminance sources only are accounted. The following simulation parameters were chosen: ab=5, ad=1024, as=128, ar=300, aa=0.1. The simulations were performed with a time-step of 1 hour and only the moments in which daylight was present were considered, for a total amount of 4602 hours (the number of annual daylight hours in Turin). This operation was repeated for every glazing type and shading device considered (see Table 16 and Table 17) as well as for both orientations. The simulation outcome was an annual database for each glazing type and shading device, containing for each moment of the year a pair of values for every direction of observation relative to each of the 9 points: a DGP value and an E_v value.

These results were post-processed, according to the 3 steps of the simplified method, which are described in detail in the following sub-sections.

Step 1: E_v Determination of the E_v thresholds

The first step is aimed at defining the most suitable E_v values to be used as thresholds for each daylight glare comfort class (see Table 14). As four glare comfort classes are identified, three E_v thresholds need to be calculated, similarly to the DGP thresholds: the lower threshold (corresponding to DGP = 35%; the intermediate threshold, corresponding to DGP = 40%; the upper threshold, corresponding to DGP = 45%).

The two E_v - DGP values determined for each time-step were used to evaluate the occurrence of glare (glare/non glare condition), using the DGP thresholds (DGP_{thr}) for each daylight glare comfort class as a validation reference. The most suitable values of E_v to be used as thresholds ($E_{v,thr}$) for the daylight glare comfort classes were found through the application of a fault-detection technique. In principle, comparing E_v to DGP_{thr}, to determine the best $E_{v.thr}$ value, may yield either one of the following four different scenarios:

- True Positive (TP): when $E_v > E_{v,thr}$ and $DGP > DGP_{thr}$;
- True Negative (TN): when $E_v < E_{v,thr}$ and $DGP < DGP_{thr}$;
- False Positive (FP): when $E_v > E_{v,thr}$ and $DGP < DGP_{thr}$;
- False Negative (FN): when $E_v < E_{v,thr}$ and $DGP > DGP_{thr}$;

Figure 36 exemplifies the four scenarios that may occur when applying the fault-detection technique. The results that were obtained for the intermediate threshold DGP_{thr} = 40% are shown. Actually, Figure 36 shows the correlation of E_v with DGP values for a certain point. The threshold DGP_{thr} = 40%, shown as a horizontal line (disturbing glare as per [133]), identifies a corresponding E_v threshold (vertical line). These two lines divide the chart into four sectors containing a different number of data points. The error in the glare class estimation is represented by the percentage of data points within the FP and FN regions. The most suitable $E_{v,thr}$ value for each daylight glare comfort class can be therefore determined as the one minimising the sum FP+FN.

While a TP and TN results are “True” estimation conditions, i.e. they represent a correct estimation of the glare comfort class, the “False” estimations (errors) are represented by FP and FN scenarios, which show a discordance between the estimation of a glare/non glare condition made through E_v and by means of the DGP value. In more detail, for a False Positive scenario a glare condition is detected by means of the E_v threshold, which corresponds to an overestimation of glare (as no glare is actually detected through the DGP value). On the contrary, for a False Negative scenario an actual glare condition (measured by the DGP value) is not detected through the E_v, resulting in an underestimation of glare sensation. Therefore, between the two “fault” scenarios, FN appears to be the most problematic one, as visual comfort perceived by the occupant may be worse than the one estimated.

This fault-detection technique was applied to all the yearly simulated cases, i.e. different glazing types and properties and different shading devices, for each point and each window orientation. The outcome of such an analysis is a triplet of $E_{v,thr}$ (one $E_{v,thr}$ for each daylight glare comfort class threshold) for each glazing type and shading device, for each of the nine points in the space considered, for each direction of observation and for each window orientation. A total number of 1890 $E_{v,thr}$ triplets was obtained (21 façade technologies x 9 points x 5 directions of observation x 2 Orientations = 1890 $E_{v,thr}$ triplets).

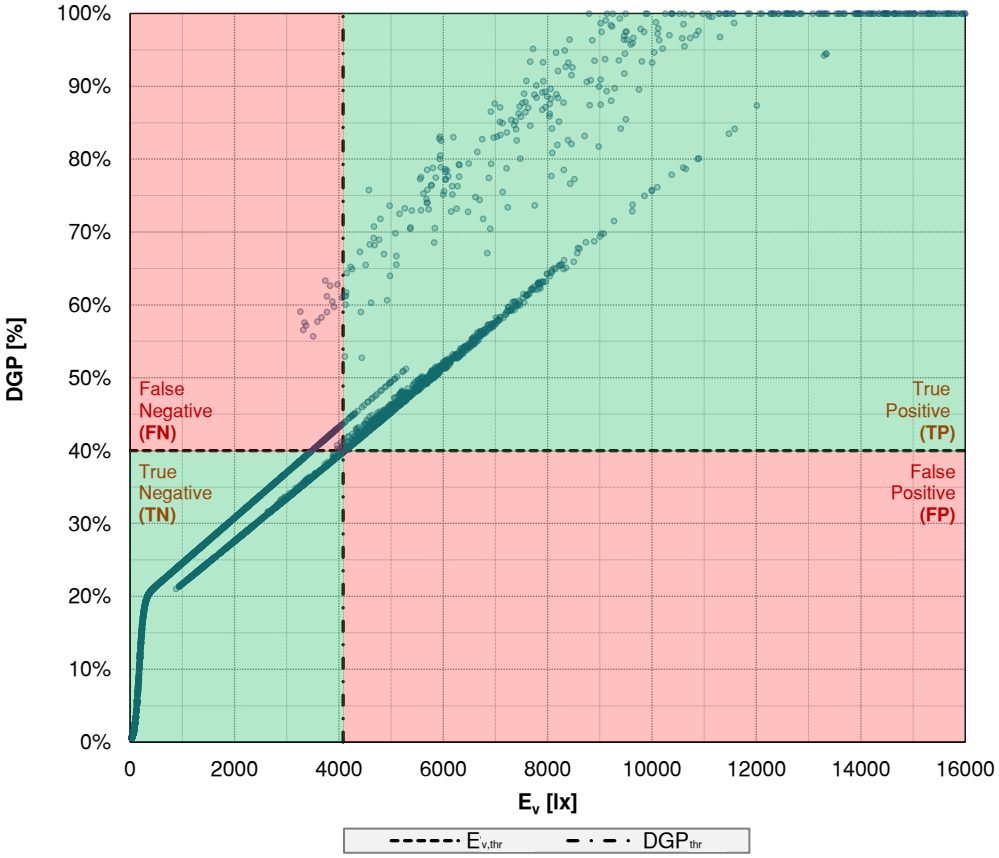

Figure 36. Example of the four scenarios occurring through a fault-detection technique to E_v and DGP values: green areas represent a correct estimation, while red areas represent an underestimation (FN) or overestimation (FP) of a glare comfort class by means of E_v.

Step 2: Error estimation

The second step of the approach consists in evaluating the magnitude of the error in the estimation of the glare comfort class by means of the E_v threshold triplets, as compared to the correct DGP values. This can enable the classification of the entire space, in terms of daylight glare comfort classes, by means of the calculation of only one E_v triplet, and therefore by means of only one DGP annual calculation.

Firstly, $E_{v,thr}$ triplets obtained from the previous phase for each specific point and direction of observation are used to estimate the daylight glare comfort class for all the points in the space, relatively to the direction of observation for which

the $E_{v,thr}$ triplets were calculated (for each window characteristics and orientation). Secondly the resulting error, expressed as the percentage of occurrences of FP and FN over a year, is quantified for each point, for every case.

The result is a triplet of errors for each point considered (one error value for each daylight glare comfort class threshold), for a total number of 1890 triplets of errors.

Step 3: Identification of most suitable points for an annual glare analysis

The aim of the last step is the identification, if possible, of the most suitable point in the space and direction of observation, among those considered, to be used to estimate the daylight glare comfort class for any point throughout the space considered. This could allow a certain space to be classified according to daylight glare comfort classes, by evaluating the annual DGP, and the relative $E_{v,thr}$ triplet, for one point only.

For each point and direction of observation the 95% percentile error was quantified. This one, expressed as percentages of FP+FN occurrences over a year, represents the maximum error committed for each point and direction of observation in 95% of cases. It was calculated considering every glazing type and shading device, as well as both south and west orientation. In addition, the number of cases relative to each point and direction of observation for which the calculation of an $E_{v,thr}$ value was possible were quantified for each point and direction of observation as well. Finally, the most suitable combination *point-direction of* observation was found as the one maximising the total number of cases for which it was possible to calculate the an $E_{v,thr}$ values while minimising the maximum error committed for 95% of time when estimating the specific daylight glare class by means of the $E_{v,thr}$ triplets calculated for that specific combination. It is possible that the maximisation of the first aspect and the maximisation of the second do not occur for the same combination, in this case, depending on the number of cases for which $E_{v,thr}$ values were calculated and on the 95° percentile maximum error value two different most convenient points for the calculation of the only DGP profile may be defined, depending also on the aim of the spatial daylight glare evaluation.

4.2.3 Results

The results are presented with regard to each step of the approach, with an additional preliminary step in which the results are screened. Finally, an explanatory example of this simplified approach is presented.

Results screening

The analysis was performed for 2 orientations of the office case study, for 9 points in the space and for 5 directions of observation for each point, resulting in 90 possible combinations *orientation–point–direction of observation*. However, only a part of these combinations could be considered for the scope of this study,

as all the other cases appeared not to be representative of the glare conditions occurring within the whole room.

In each combination *point-direction of observation* the window is seen under a different solid angle (ω), depending on the distance of the point of view from this one and from the angle between the direction of observation vector and the vector normal to the window plane. Moreover, for each combination, the window has a different position in the observer's field of view, resulting in a different value of the position index (P), as this one is determined by the angular displacement of the light source in one's field of view from both the direction of observation vector and the line of sight [228,229]. This parameter accounts for the sensibility of the eye to a light flux coming from a light source in a given position within the field of view and grows as the eye sensibility decreases. Table 18 contains P and ω values for each combination *point-direction of observation*.

Table 18. Solid angle [sr] and Position index [-] relative to the window for each point and direction of observation considered.

		-90°	**-45°**	**0°**	**45°**	**90°**
a0	**ω [sr]**	0.74	0.92	0.92	0.75	0.18
	P [-]	5.7	2.0	1.9	5.6	12.7
a1	**ω [sr]**	0.60	1.18	1.21	1.18	0.60
	P [-]	7.1	3.4	1.9	3.4	7.2
a2	**ω [sr]**	0.18	0.75	0.92	0.92	0.74
	P [-]	12.7	5.6	1.9	2.0	5.7
b0	**ω [sr]**	0.33	0.38	0.38	0.39	0.05
	P [-]	6.5	1.8	1.5	5.3	11.8
b1	**ω [sr]**	0.22	0.45	0.45	0.45	0.22
	P [-]	8.4	2.9	1.4	2.9	8.4
b2	**ω [sr]**	0.05	0.39	0.38	0.38	0.33
	P [-]	11.8	5.3	1.5	1.8	6.5
c0	**ω [sr]**	0.18	0.20	0.20	0.20	0.02
	P [-]	7.2	1.8	1.3	4.3	11.3
c1	**ω [sr]**	0.11	0.22	0.22	0.22	0.11
	P [-]	8.9	2.7	1.3	2.7	8.9
c2	**ω [sr]**	0.02	0.20	0.20	0.20	0.18
	P [-]	11.3	4.3	1.3	1.8	7.2

Both P and ω are present in the DGP equation (10), and specifically they influence the part of the equation evaluating the glare from contrast. Both lower solid angles and higher position index values decrease in fact the glare sensation from contrast. In these cases, for a glare condition to be experienced, a higher eye vertical illuminance or a higher luminance of the light source are required. From Table 18 it is possible to observe that for some points and some directions of observations the window is either seen under small solid angles or its position in the observer's field of view is peripheral (high P values), or even both. In more

detail, from point c0, c1 and c2, the three points farthest from the window, this one is seen in any direction of observation under a solid angle lower than 0.25 sr. This is also true for the points a2 and b2 in the direction of observation -90° and for the points a0 and b0 for a direction of observation equal to 90°, as in these cases the observer is located at 0.5 m from the wall and is looking perpendicularly to this one. The same condition occurs for point b1 in the directions of observation 90° and -90° as well. In addition, for points a0, b0, b1, c0 and c1 in the direction of observation 90° and for points a2, b1, b2, c1, c2 in the direction of observation -90°, the position index of the window results higher than 7.5. For these cases, as said, a glare sensation could be perceived only in presence of a high eye vertical illuminance or if the window showed a high luminance value, condition with could occur in presence of a very bright sky. In addition, both conditions occur when the sun is directly within the observer's field of view. An analysis of the sun path for the city of Turin (Figure 37) showed that, for the south-oriented room, direct sunlight only hits the analysis points in winter, and among these, only the points in the two rows closest to the window (points c0, c1, c2 are never hit by direct sunlight). In the west orientation, the sensor points in row b and c are reached by sunlight only in autumn (and spring) and only for a short time in the late afternoon, with the exception of points c0 and b2, which are hit by sunlight also in the latest moments of the afternoon in summer.

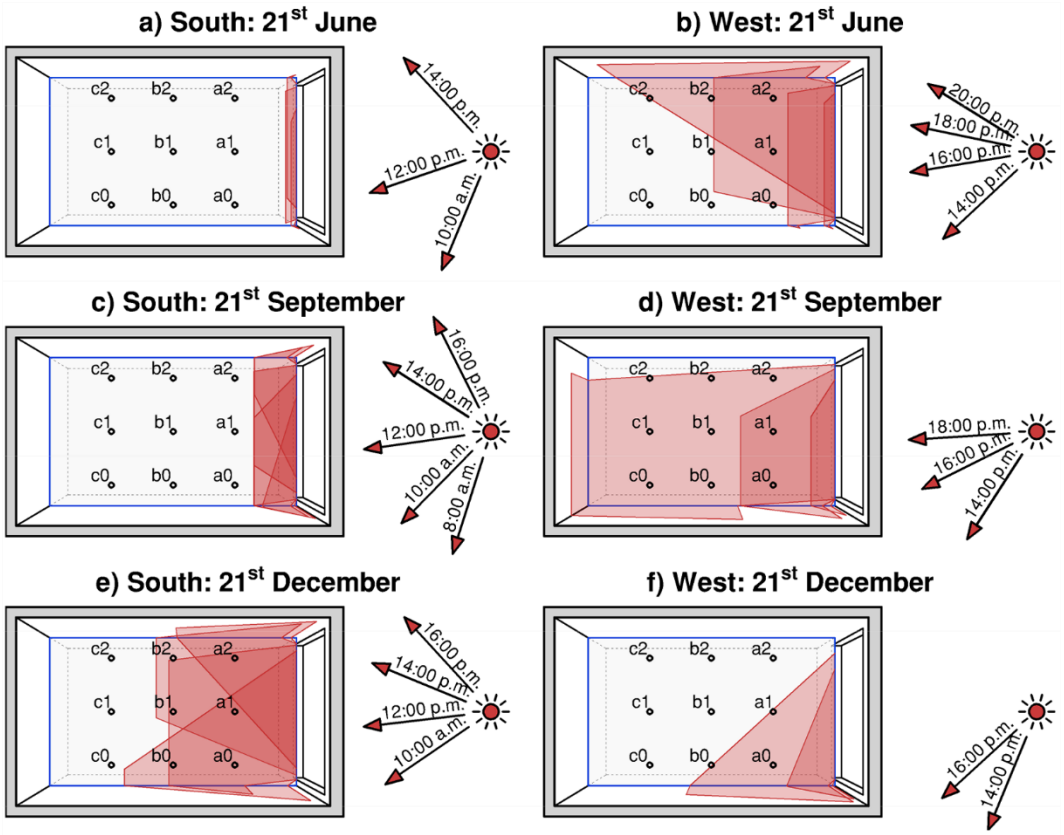

Figure 37. Sunlight penetration in the office case study (for both south and west orientations) on a plane located 1.2 m above the floor for different significant moments of the day and of the year.

It is possible to conclude that for all the combinations *point-direction of observation* highlighted above, a glare sensation is rarely or even never perceived throughout the whole year. In fact, direct sunlight reaches these points at most for a few moments in the year (at least it never reaches them), and for such solid angles and position indices a too high luminance would be necessary in respect to the one the sky could provide. Figure 38 shows the DGP values, for a whole year, relative to 4 combinations *point-direction of observation* among the ones above highlighted as potentially problematic.

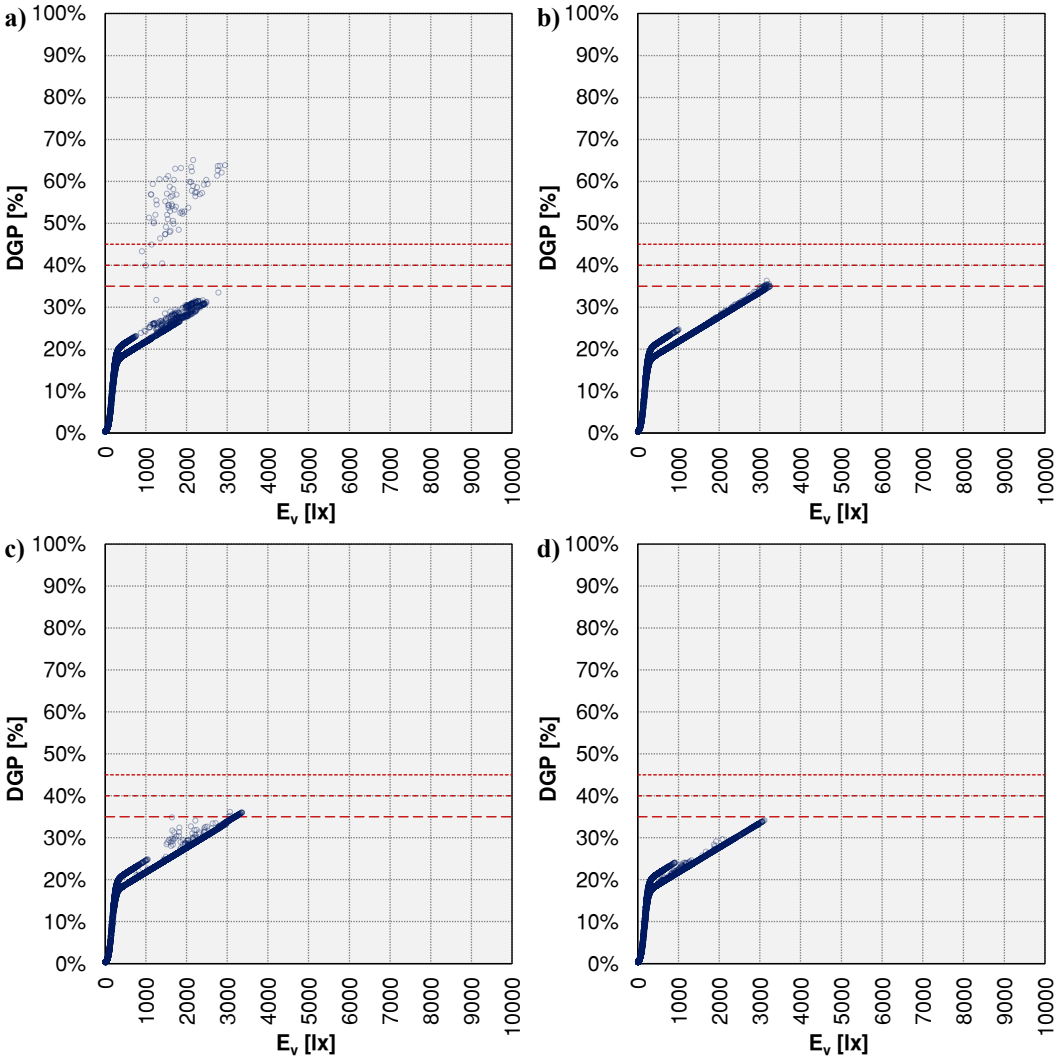

Figure 38. Correlation between eye vertical illuminance and DGP relative to four cases: a) west orientation, point c1, direction of observation 45°, scattering glazing with τ_{vis} 0.35; b) south orientation, point a0, direction of observation 90°, scattering glazing with τ_{vis} 0.65; c) south orientation, point b1, direction of observation -90°, scattering glazing with τ_{vis} 0.55; d) west orientation, point b2, direction of observation 90°, scattering glazing with τ_{vis} 0.55.

The figure shows that, for each case, values of DGP higher than 35% are very rarely experienced, even though the glazing technologies considered in charts b), c) and d) have a relatively high τ_{vis}. As higher daylight glare comfort classes for such combinations are seldom or never reached, the estimated E_v thresholds may

not be suitable to rate the glare condition for the whole space, as this may result in a high degree of inaccuracy. As an example, if the *disturbing glare* daylight glare comfort class is not reached in a particular point in the space, but it is experienced in the remaining portion, by rating the glare condition of the space through the E_v thresholds calculated for that point it won't be possible to detect the disturbing glare condition for the whole space, as the E_v threshold relative to this daylight glare comfort class won't be calculated.

From the above considerations it was decided not to consider in the analysis of the results all the combinations *points-directions of observation* for which direct sunlight is almost never present in one's field of view and either the window is seen under a solid angle smaller than 0.25 sr or the position index is higher than 7.5. In addition to these cases, summarised in Table 19, it was decided for the same reasons not to consider also the direction of observation of 90° for all the points in the west orientation. In this case the direction of observation vector is pointing towards north, hence sunlight never hits the observer's eye, with the exception of the late afternoon in summer. In addition, the portion of sky vault seen through the window, as it is far from the sun, is characterised by a lower luminance than the sky portion closer to the sun. As a result, for all these cases a glare condition is never perceived throughout the whole year, as also shown in Figure 38.c.

Table 19. Points and relative directions of observation considered (✗) and not considered (✓) in the analysis of the results.

	Direction of observation				
Point	**-90°**	**-45°**	**0°**	**45°**	**90°**
a0	✓	✓	✓	✓	✗
a1	✓	✓	✓	✓	✓
a2	✗	✓	✓	✓	✓
b0	✓	✓	✓	✓	✗
b1	✗	✓	✓	✓	✗
b2	✗	✓	✓	✓	✓
c0	✗	✗	✗	✗	✗
c1	✗	✗	✗	✗	✗
c2	✗	✗	✗	✗	✗

For all the points and directions of observation highlighted as problematic in terms of estimation of E_v thresholds, these, as well as the relative errors committed when rating the whole space through them, won't be analysed. However, all these combinations are still considered for evaluating the errors committed when rating the whole space through E_v thresholds relative to other points and directions of observation.

The data screening performed according to the considerations above explained allowed eliminating a series of combinations for which the E_v thresholds calculated were not suitable to estimate the glare condition for a whole space. As a consequence, the errors obtained related to these estimations were

significantly higher than those relative to E_v thresholds more representative of the glare condition throughout all the space. Figure 39 shows an example of the effect of the data screening performed. It is possible to observe that all the cases showing significant higher errors than the greatest part of the population were successfully excluded. The same result was obtained also for the other thresholds and for the south orientation.

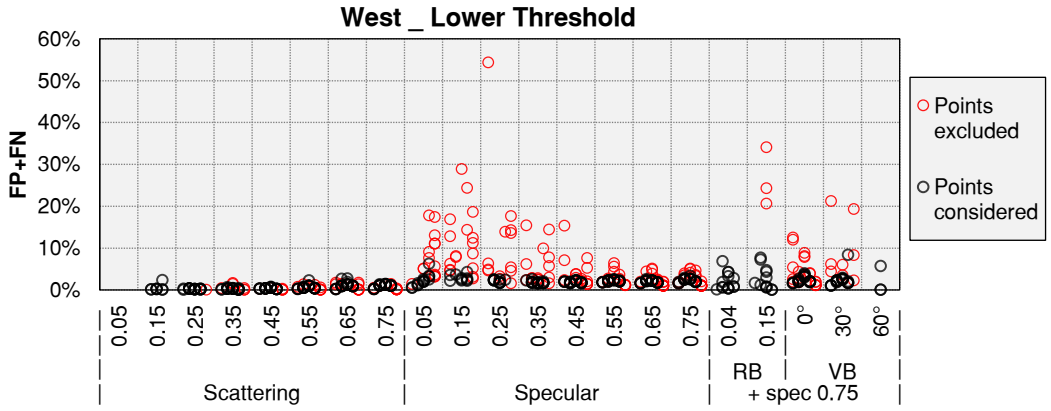

Figure 39. Errors after the data screening relative to the estimation of the daylight glare comfort classes using the E_v lower threshold in the west orientation. Red markers represent the points not considered.

Step 1: Determination of E_v thresholds

The $E_{v,thr}$ values for each daylight glare comfort class threshold relative to the south and west orientation are shown in Figure 40 and Figure 41 respectively. These are relative to all the points and directions of observation considered for all the different glazing types and shading devices. As one would expect, for both window orientations $E_{v,thr}$ values relative to the lower daylight glare comfort class threshold are lower than those relative to the intermediate threshold, which are in turn lower than $E_{v,thr}$ values obtained for the upper threshold.

It is possible to observe that, for both south and west orientation, $E_{v,thr}$ values relative to some combinations *point-direction of observation* for some glazing types or shading devices are missing. This is true for all the three daylight glare comfort class thresholds, but especially for the upper one. The reason is that for these glazing types or shading devices the comfort class for which the threshold value is missing is never reached throughout the whole year. In fact, the technologies for which threshold values are missing are either glazing types or roller blinds with low τ_{vis} or venetian blinds with a high slat angle, i.e. technologies that allow a low amount of light inside the space. In these cases, higher daylight glare comfort classes, corresponding to worse glare conditions, are never experienced by the users, as these façade technologies prevent glare by blocking a high rate of the window incident light.

A common trend between the different daylight glare comfort class thresholds can be observed: $E_{v,thr}$ values tend to increase as the glazing or the shading devices allow a higher amount of light inside the room (glazing, both specular and scattering; roller blinds with higher τ_{vis}; venetian blinds with low slat angles).

From another viewpoint, the lower the visible transmission of the glazing (whether with specular or scattering properties), the more likely to perceive glare for lower eye illuminance levels.

For both specular and scattering glazing, beyond a certain τ_{vis} of the window, which varies depending on the daylight glare comfort class threshold, $E_{v,thr}$ values reach a plateau value (i.e. they fluctuate around an almost flat value). However, specular and scattering glazing show a different dispersion of the $E_{v,thr}$ values around this plateau value (only on the lower side), with a higher dispersion for the specular glazing and nearly no dispersion at all for the scattering ones. This dispersion is due to the glare from contrast phenomenon, for which worse glare conditions are experienced with lower eye E_v values. For the specular glazing this can occur if within one's field of view the sun is not directly but are present sunlight patches on the walls or on the floor, which is not likely to take place for the scattering glazing, as all the incident radiation is completely scattered. Due to this feature, glare from contrast with scattering glazing could be experienced only when the glazing is intercepted by the eye-sun vector, as in this case the glazing is comparable to a luminous panel whose luminance can be considerably higher than the eye adaptation luminance. However, this phenomenon can occur only for high transmissive scattering glazing, and in any case with a lower intensity than the previous case. This is confirmed by the fact that this kind of dispersion of data around the E_v plateau value is observed only for scattering glazing with τ_{vis} higher than 0.45 and only for the lower daylight glare comfort class thresholds. The $E_{v,thr}$ values relative to the venetian blinds with a 0° and 30° slat angle showed to be somehow close to the E_v plateau value reached for specular and scattering glazing, but the dispersion around this one is greater than that observed relative to the two glazing. The $E_{v,thr}$ maximum value is instead never reached for the roller blinds and the venetian blinds with a slat angle equal to 60°. The E_v plateau value reached for each daylight glare comfort class threshold show to be orientation-independent, as the same value is reached both for south and west orientation.

Comparing the outcomes relative to each point and direction of observation considered, it appears that higher differences in the $E_{v,thr}$ values can be observed for glazing and shading devices that allow a low amount of light within the room. As the quantity of light admitted to the internal space increases (higher τ_{vis} for specular and scattering glazing and for the roller blinds, lower slat angles for the venetian blinds) these differences tend to decrease. When the above mentioned $E_{v,thr}$ maximum value is reached, the differences between $E_{v,thr}$ relative to the three points are minimal, even though, as said, a certain dispersion is observed for the specular glazing.

Generally speaking, it can be observed that for the less transparent specular glazing the lowest $E_{v,thr}$ values are found relative to 90° and -90° directions of observation, when it was possible to calculate them. The only exception is represented by the specular glazing with τ_{vis} of 0.05, for which, due to the very low amount of light, similar values to the ones relative to these directions of observations can be observed also for the 45° view direction in the south

orientation and for the 45° and 0° view directions for the west orientation. Regarding the scattering glazing instead, the lowest $E_{v,thr}$ values appear to be relative to 45° and -45° directions of observation, with the exception of the scattering glazing with τ_{vis} of 0.15, for which for the lower daylight glare comfort class threshold the lowest $E_{v,thr}$ values are observed for the 0° direction of observation in the south orientation and for the 45° direction of observation in the west orientation. Relative to the venetian blinds and roller blinds instead, a common trend cannot be observed.

Within the same direction of observation, lower $E_{v,thr}$ values are in most cases relative to the viewpoints further from the window (row b), and among these, the lateral points b0 and b2. Although this does not occur in all the cases analysed, this was observed for the majority of them, with the exception of the scattering glazing of τ_{vis} equal to 0.55 for the lower daylight glare comfort class threshold and the scattering glazing of τ_{vis} equal to 0.65 and 0.75 for the intermediate threshold. In these cases, for both west and south orientation, the lower $E_{v,thr}$ values are relative to the point a1 in the 0° direction. The same consideration applies to the scattering glazing with τ_{vis} equal or greater than 0.65 as well. The only difference lies in the fact that here the view direction relative to the lower $E_{v,thr}$ values can be equal to 45° or -45°, and this occurs in the south orientation relative to the lower and intermediate thresholds, for the specular glazing with τ_{vis} of 0.65 and 0.75 respectively.

Table 20 summarises the minimum and maximum errors, for each orientation and daylight glare comfort class threshold, committed when estimating a certain glare class by means of the different $E_{v,thr}$ (lower, intermediate and upper threshold). The errors are expressed in terms of FP+FN percentage, i.e. the percentage of time over the year in which each daylight glare comfort class was overestimated (FP) or underestimated (FN) by using the $E_{v,thr}$ values calculated.

Table 20. Minimum and maximum error, for each orientation and every daylight glare comfort class threshold, committed when calculating all the $E_{v,thr}$. The errors are expressed as yearly percentage of occurrence of FP+FN.

		Lower Threshold		**Intermediate Threshold**		**Upper Threshold**	
		Min	**Max**	**Min**	**Max**	**Min**	**Max**
a0	**South**	0.02%	17.54%	0.00%	3.20%	0.00%	2.93%
	West	0.13%	11.54%	0.00%	4.62%	0.04%	4.47%
a1	**South**	0.06%	6.04%	0.00%	4.11%	0.08%	5.07%
	West	0.00%	3.92%	0.00%	3.76%	0.00%	3.53%
a2	**South**	0.02%	19.74%	0.00%	3.87%	0.00%	3.47%
	West	0.00%	3.22%	0.00%	3.13%	0.00%	4.64%
b0	**South**	0.02%	9.62%	0.00%	1.89%	0.00%	2.06%
	West	0.00%	8.65%	0.00%	3.05%	0.00%	3.54%
b1	**South**	0.04%	4.47%	0.00%	2.51%	0.02%	2.44%
	West	0.02%	8.31%	0.00%	2.67%	0.00%	16.00%
b2	**South**	0.02%	16.00%	0.00%	1.93%	0.00%	2.18%
	West	0.02%	2.91%	0.00%	2.11%	0.00%	1.49%

It is possible to observe how, for each orientation, lower maximum errors are in most cases committed for higher daylight glare comfort class thresholds, meaning that the higher maximum errors are relative to the lower threshold. Exceptions to this trend are represented in the west orientation by the points a1, b0 and b2 and by the points a2 and b1 in the south orientation. Most of the maximum FP+FN values appear to be lower than 10%, with 5 exceptions: a0, a2 and b2 for the lower threshold in the south orientation, a0 for the lower threshold in the west orientation and b1 for the upper threshold in the west orientation. These are the only errors higher than 10% committed for all the points considered and most likely represent outliers in respect to the average error committed for these points and these thresholds. In next section this subject will be analysed in detail.

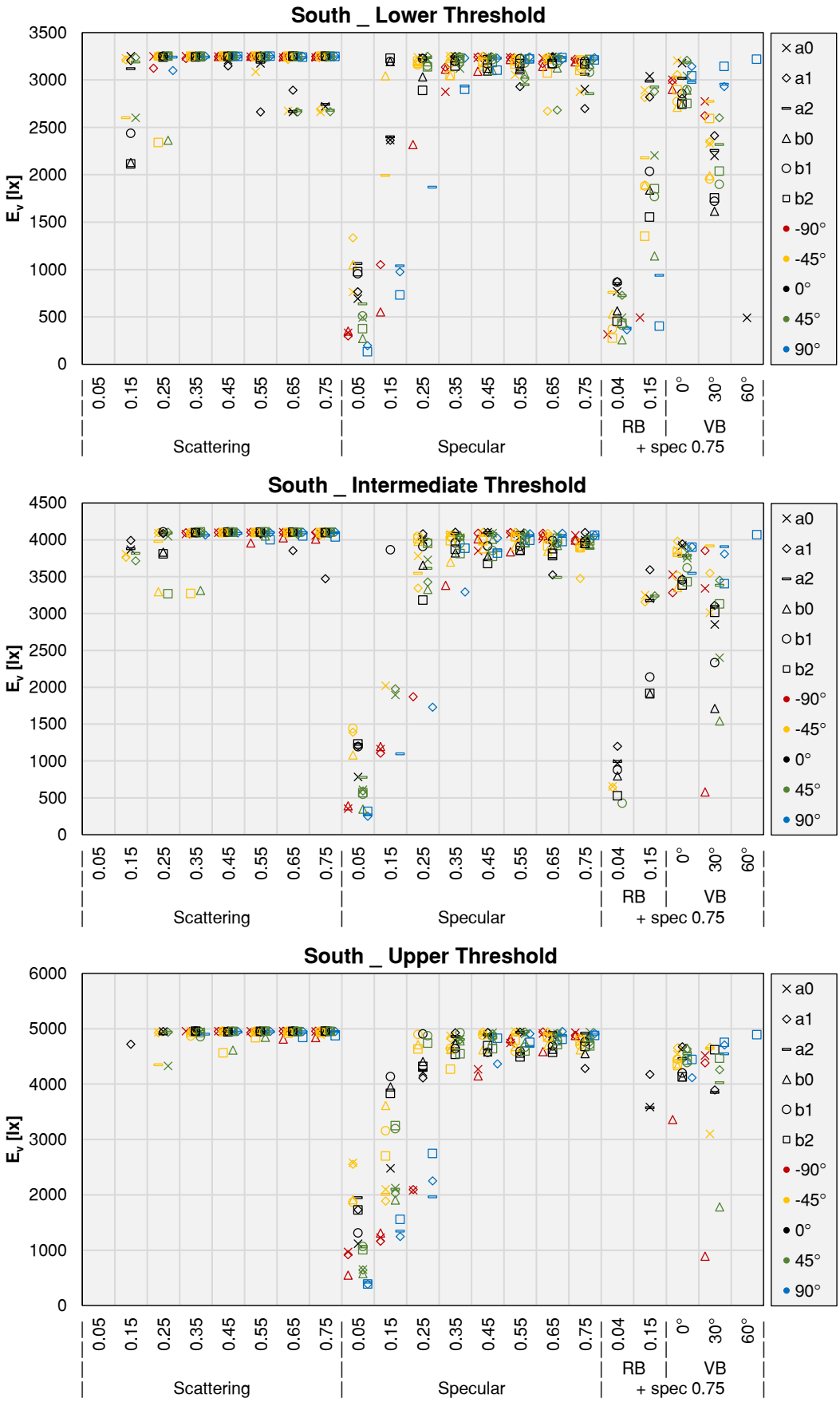

Figure 40. $E_{v,thr}$ values, for each daylight glare comfort class threshold, relative to every glazing type and shading device. Results relative to the south orientation.

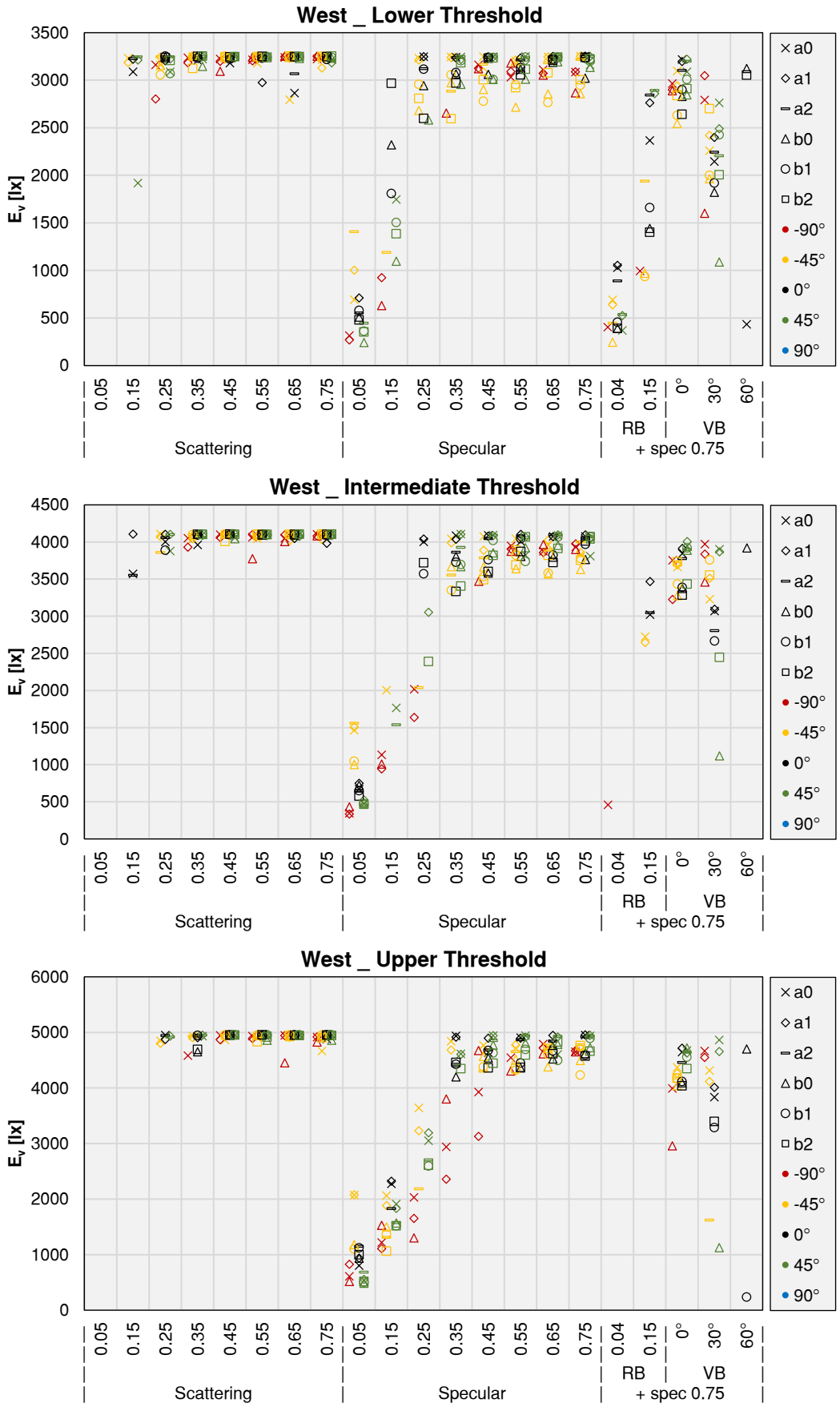

Figure 41. $E_{v,thr}$ values, for each daylight glare comfort class threshold, relative to every glazing type and shading device. Results relative to the west orientation.

Step 2: Error estimation

This section provides an overview of the results relative to the step two of the approach, i.e. the calculation of the error committed when spatially evaluating the daylight glare comfort classes. This was done by applying the triplet of $E_{v,thr}$ values calculated for each point and direction of observation to all the other points considered for the glare analysis, relatively to the same direction of observation for which each $E_{v,thr}$ triplet was calculated. The error committed is expressed in terms of percentage of occurrences over a whole year when each daylight glare comfort class was overestimated (FP) or underestimated (FN). The outcomes of this phase are summarised in Figure 42 and Figure 43, containing the results relative to the south and west orientation respectively.

It is possible to observe that for some glazing types or shading devices, the errors relative to some points and directions of observation are missing, for both orientations. This happens as in the first step of the simplified approach it was not possible to calculate some $E_{v,thr}$ values, due to the fact that for some technologies a given daylight glare comfort class was never experienced by the user throughout the whole year. As a consequence, the errors relative to the cases with missing $E_{v,thr}$ values could not be calculated as well.

The results show how, generally speaking, to higher daylight glare comfort class thresholds correspond lower errors. In addition, for each daylight glare comfort class threshold, for the scattering glazing are found lower errors compared to those relative to the specular glazing, this in both orientations. In addition, a different trend can be observed for the two glazing technologies. For the scattering glazing lower errors are associated to lower τ_{vis} values, and for most cases the errors found are below 2%, for every daylight glare comfort class in both orientations. However, the presence of outliers can be observed for the lowest and highest τ_{vis} values, below 0.35 and above 0.55 respectively. This is true for each daylight glare comfort class threshold in the south orientation and for the lower threshold in the west one. For the specular glazing instead, the lower errors are associated to intermediate τ_{vis} values, i.e. 0.35 and 0.45. In more detail, as τ_{vis} grows from lower to intermediate values, a decrease in FP+FN values can be observed, while an increase in these ones is observed when moving from intermediate to high τ_{vis} values. However, a higher dispersion is associated to the errors relative to high τ_{vis}, while for low τ_{vis} values similar errors are found for all the combinations *point-direction of observation* analysed, with the exception of the lower daylight glare comfort class threshold, where this is not true. In addition, smaller differences in FP+FN relative high, intermediate and low τ_{vis} are observed for higher daylight glare comfort class thresholds. Some differences can be highlighted for the two orientations, as the above trend appears less pronounced in the west one. In more detail, the differences between FP+FN values relative to lower, intermediate and higher τ_{vis} appear smaller than those observed in the south orientation, to the extent that for the upper daylight glare comfort class threshold the trend appears almost flat. Moreover, a smaller

dispersion of values than what observed in the south orientation is associated to higher τ_{vis} values. For the scattering glazing outliers are present as well, mainly for τ_{vis} equal to or lower than 0.25 or equal to or higher than 0.65, and mainly in the west orientation. The presence of outliers appears to decrease for higher daylight glare comfort class thresholds. For the shading devices considered it is possible to observe a very high dispersion of the error values, dispersion which decreases for higher daylight glare comfort class thresholds and which appears to be smaller for the west orientation. Moreover, smaller error seems to be associated to venetian blinds with higher slat angles. Apart from these considerations, a common trend for these technologies is difficult to be defined.

Both a higher dispersion of results and the presence of outliers can be observed, for all the technologies considered, mainly for those cases for which a high dispersion in $E_{v,thr}$ values was found. This is due to the fact that a high dispersion in $E_{v,thr}$ results means that high differences between $E_{v,thr}$ values were found, which in turn implies that some of these E_v threshold values are not suitable for rating the whole space, which is confirmed by the high FP+FN values obtained.

Analysing then the single points and directions of observations considered, it is possible to observe how very similar results are obtained for all the viewpoints relative to each direction of observation. Apart from the 0° direction of observation, for which small differences can still be observed, and apart from the outliers as well, the differences relative to each point for the same direction of observation appear in most cases negligible. In the south orientation, the lower errors are found relative to the 90° and -90° directions of observation, with the exception of the scattering glazing of intermediate τ_{vis} values, for which the 45° and -45° directions of observation show the minimum FP+FN values. The highest errors appear to be relative to the 0° direction of observation, particularly in the specular glazing with intermediate and high τ_{vis} values, while for the other technologies smaller differences are observed between the 0° direction of observation and the 45° and -45° ones. In the west orientation instead, for the scattering glazing the lowest errors are obtained relative the 90° direction of observation. For the specular glazing instead, depending on τ_{vis} and daylight glare comfort class threshold the lower error can be observed relative to 90° (lower τ_{vis} and for the lower threshold higher τ_{vis} as well), 0° (intermediate τ_{vis} values) and 45° and -45° (higher τ_{vis} for the intermediate and upper threshold).

Table 21 summarises the minimum and maximum error committed when evaluating each daylight glare comfort class by applying the $E_{v,thr}$ values calculated for each point in the space on all the three points considered. Again, the errors are expressed in terms of FP+FN percentage. It is possible to observe how, for each orientation, lower maximum errors are in most cases committed for higher daylight glare comfort class thresholds, meaning that the higher maximum errors are relative to the lower threshold. Exceptions to this trend are represented in the west orientation by the points a2, b1 and b2 and by the point a2 in the south orientation. Most of the maximum FP+FN values appear to be approximatively of

5%, with two kind of exceptions: i) values slightly higher than 5%, represented by points b1 (south and west for the lower threshold) and b0 (west in all thresholds); ii) values significantly higher than 5%, obtained in the south orientation for points a0 (lower threshold), b0 (lower and intermediate threshold) and b2 (lower threshold) and in the west one for point b1 (upper thresholds). These last values, from the trends highlighted relative to the FP+FN errors, as well as from the observation of the results, can be considered as outliers.

Table 21. Minimum and maximum error committed when evaluating each daylight glare comfort class by applying the $E_{v,thr}$ values calculated for each point on all the other points considered, relatively to the same direction of observation for which the $E_{v,thr}$ values were calculated. The errors are expressed as FP+FN percentage.

		Lower Threshold		**Intermediate Threshold**		**Upper Threshold**	
		Min	**Max**	**Min**	**Max**	**Min**	**Max**
a0	**South**	0.03%	15.42%	0.00%	3.29%	0.03%	2.48%
	West	0.02%	5.65%	0.01%	2.53%	0.02%	2.39%
a1	**South**	0.10%	5.47%	0.02%	4.43%	0.02%	2.54%
	West	0.01%	3.51%	0.03%	2.54%	0.03%	2.34%
a2	**South**	0.02%	5.37%	0.00%	2.97%	0.01%	2.46%
	West	0.00%	3.62%	0.04%	3.71%	0.03%	5.12%
b0	**South**	0.16%	12.73%	0.21%	15.06%	0.19%	4.09%
	West	0.05%	8.38%	0.04%	8.27%	0.04%	8.15%
b1	**South**	0.30%	6.13%	0.23%	4.40%	0.17%	2.23%
	West	0.06%	7.68%	0.05%	2.23%	0.03%	21.09%
b2	**South**	0.03%	20.48%	0.03%	5.57%	0.03%	2.30%
	West	0.04%	4.70%	0.05%	2.84%	0.03%	4.19%

The errors presented so far are expressed as the percentage of FP and FN scenarios occurring over a year when estimating the daylight glare comfort class for the three points considered by means of the $E_{v,thr}$ calculated. But, as earlier outlined, between a False Positive and a False Negative estimation, the latter is certainly the most dangerous one, as this scenario negatively affects the evaluation of visual comfort of the occupants. In fact, for a yearly percentage of time comparable to the error committed a possible glare risk is not detected by means of this approach. For this reason it is worth analysing also the maximum and minimum errors committed, in terms of percentage of FN alone, when evaluating each daylight glare comfort class by applying the $E_{v,thr}$ values calculated for each point in the space on all the three points considered. The results of this analysis are summarised in Table 22.

Table 22. Minimum and maximum percentage of False Negative (FN) occurrences obtained when evaluating each daylight glare comfort class by applying the $E_{v,thr}$ values calculated for each point on all the other points considered, relatively to the same direction of observation for which the $E_{v,thr}$ values were calculated.

		Lower Threshold		**Intermediate Threshold**		**Upper Threshold**	
		Min	**Max**	**Min**	**Max**	**Min**	**Max**
a0	**South**	0.00%	4.65%	0.00%	3.10%	0.00%	2.36%
	West	0.00%	3.53%	0.00%	2.49%	0.02%	2.29%
a1	**South**	0.00%	3.66%	0.00%	3.25%	0.02%	2.45%
	West	0.00%	3.42%	0.00%	2.49%	0.02%	2.30%
a2	**South**	0.00%	3.40%	0.00%	2.45%	0.00%	2.43%
	West	0.00%	2.92%	0.00%	2.57%	0.02%	2.21%
b0	**South**	0.01%	2.68%	0.00%	1.93%	0.05%	2.12%
	West	0.00%	2.03%	0.04%	1.97%	0.01%	2.01%
b1	**South**	0.01%	2.74%	0.00%	2.17%	0.08%	2.10%
	West	0.00%	2.49%	0.04%	1.96%	0.01%	1.50%
b2	**South**	0.00%	2.59%	0.00%	2.16%	0.03%	1.86%
	West	0.00%	2.74%	0.05%	1.86%	0.01%	1.72%

The results show how the trend highlighted for FP+FN errors is present when analysing FN errors alone as well. In fact, in both orientations, lower maximum errors are in most cases committed for higher daylight glare comfort class thresholds. The cases which showed high FP+FN values (close to 5%), show in most cases a significant reduction when considering the FP alone. Moreover, no outlier is present relative to FN errors alone, meaning that for all the cases with high errors (in terms of FP+FN), a great part of the incorrect estimations of the daylight glare comfort class is represented by a glare overestimation (FP), i.e. a less dangerous condition than the glare underestimation.

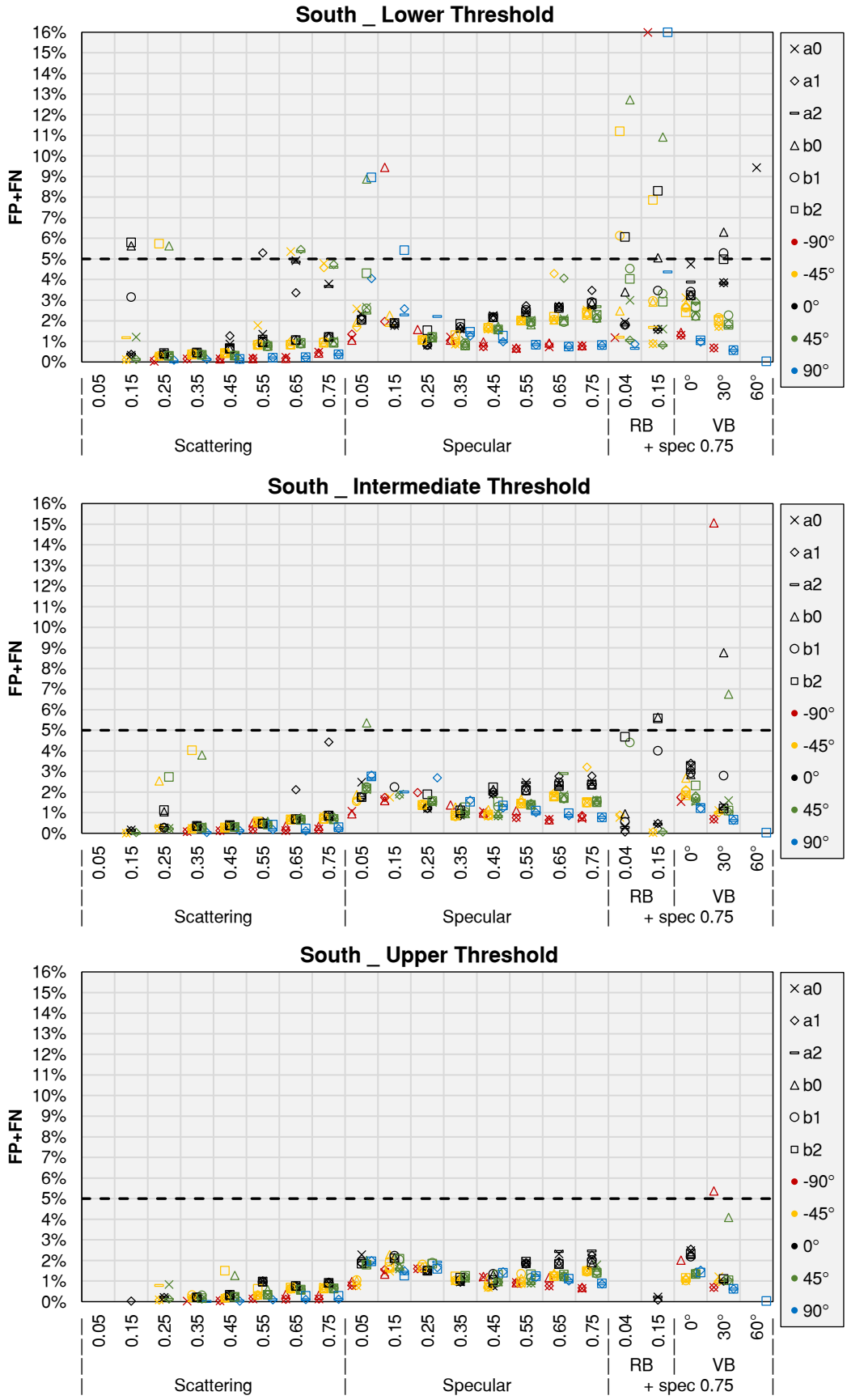

Figure 42. Error committed (in terms of percent occurrence of FP and FN over a year), for each daylight glare comfort class, relative to every glazing type and shading device considered. Results relative to the south orientation.

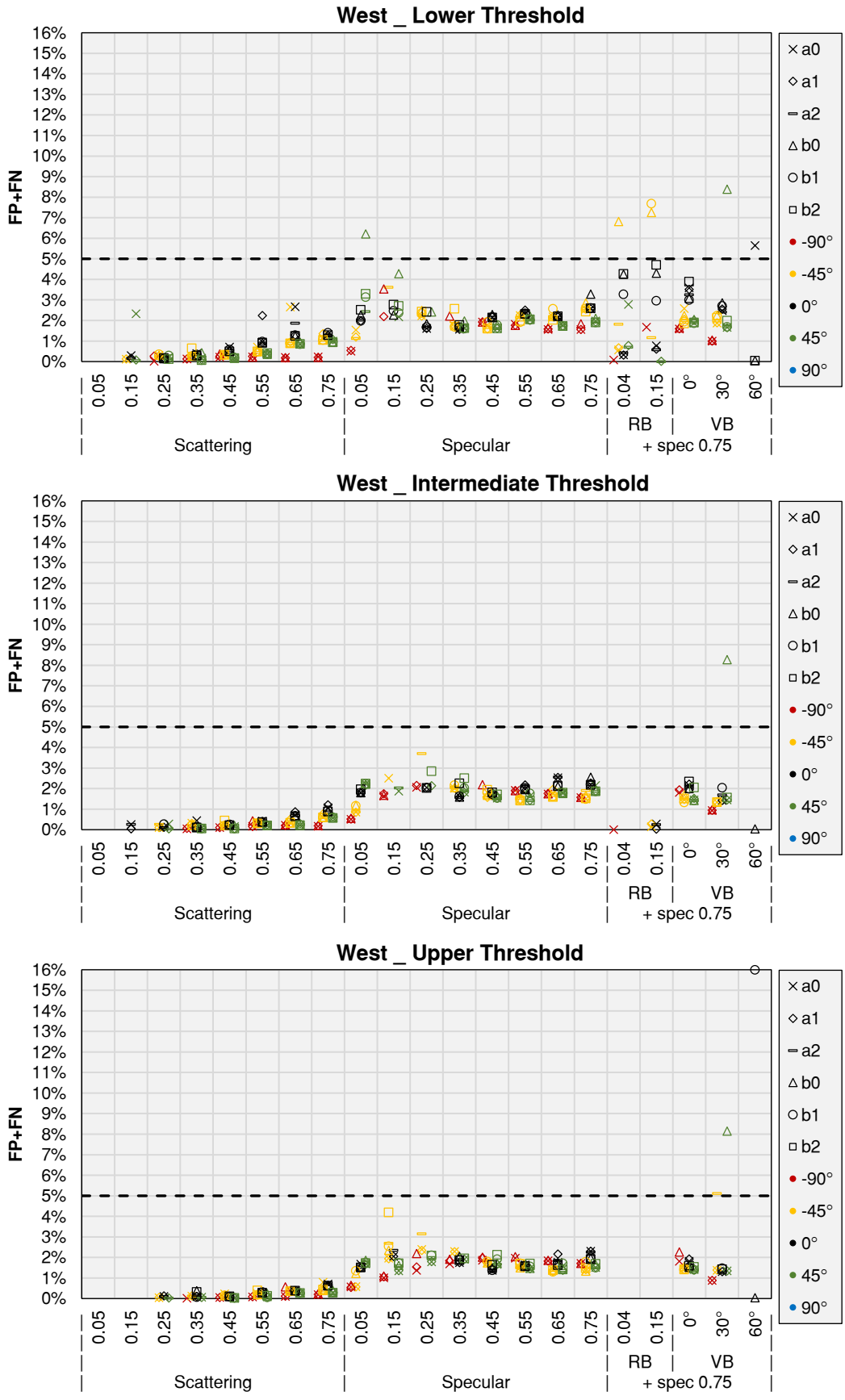

Figure 43. Error committed (in terms of percent occurrence of FP and FN over a year), for each daylight glare comfort class, relative to every glazing type and shading device considered. Results relative to the west orientation.

Step 3: Identification of most suitable points for annual glare analyses

The aim of the last step of the simplified approach was that of identifying the most suitable point and direction of observation, among the ones considered, for the calculation of the only annual DGP profile. From this, an $E_{v,thr}$ value for each daylight glare comfort class should be defined, to be then used to estimate the daylight glare comfort class for every point in the space considered. This was done by evaluating the maximum error committed relative to each point and direction of observation. Following the same approach used in [133] to define the DGP thresholds for each daylight glare comfort class, a 95% confidence interval was assumed as benchmark, meaning that a possible exceedance for 5% of time is still allowed. For each point and direction of observation the maximum error 95° percentile was hence calculated, relative to the error committed in each daylight glare comfort class threshold considering each technology and both orientations. The error committed is expressed in terms of mean percentage of times over the year for which FP and FN scenarios occur for each point. Figure 44 shows the boxplots relative to the distribution of the errors for each viewpoint and direction of observation. The 95° percentile relative to the maximum error distribution for each combination is displayed as well.

From an overview of the results it is possible to observe that the error distribution is in most cases not symmetrical, with the first and second quartile comprised in a narrower range than the third and fourth ones. As the first two quartiles represent the lower side of the distribution, and as the physical limit of the errors is equal to 0%, half of the population results comprised in a narrow interval close to 0%, meaning that for 50% of the time the error committed is very small. It is then possible to observe in most cases the presence of outliers, whose amount and extent depend on the viewpoint and direction of observation considered. For the directions of observation relative to the points in row b it is possible to observe a higher number of outliers in respect to the same directions of observation for the points in the same position in row a (a0 and b0, b1 and a1, b2 and a2). This means that the higher the distance from the window, the higher the dispersion of errors around the median. Specifically, points b0 and b2 show several outliers for all the directions of observation, and in most cases their distance from the median is high. For this reason these two points, for every direction of observation, are not suitable for the calculation of the $E_{v,thr}$ values for to estimate the daylight glare comfort class for every point in the space.

Analysing then the 95° percentiles relative to the maximum errors committed for each combination *point-direction of observation*, it is possible to observe how values lower than approximatively 3.5% are obtained for each combination. This means that a wrong estimation of the daylight glare comfort classes, either false positive or false negative, occurs more than 3.5% of time only for 5% of the cases considered. The lowest 95° percentiles are obtained for point a0 in the -90° direction of observation and for the point a1 in the -90° and 45° directions of observation; for these combination 95° percentiles lower than 2% are observed.

Values close, but not lower than 2% are observed for the points a0 in the 45° direction of observation, a1 in the –45° direction of observation and b1, again for a direction of observation of 45°. The lowest 95° percentile value, equal to 1.86%, was found for the point a0 in the -90° direction of observation.

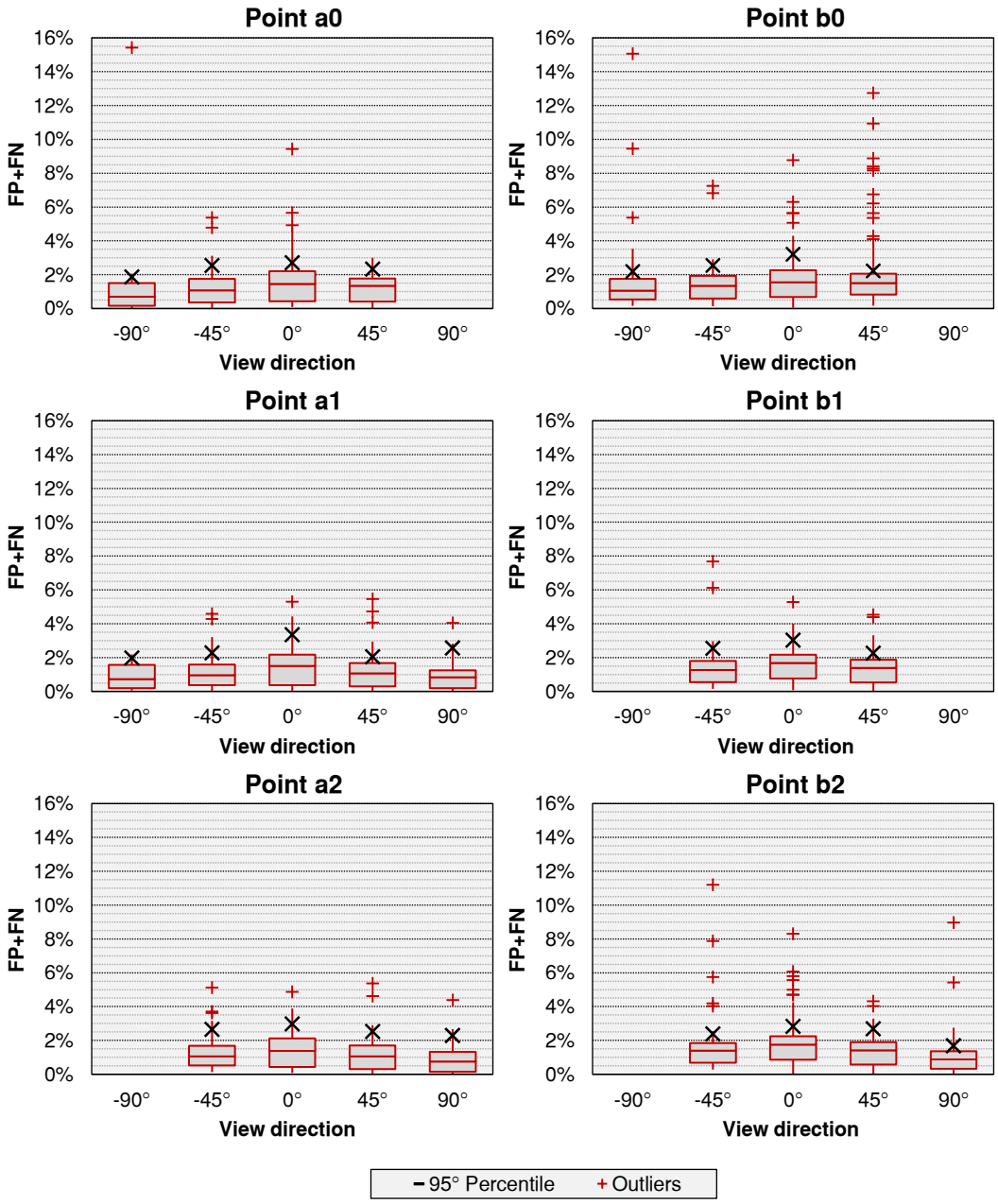

Figure 44. Boxplots and 95° percentile values relative to the distribution of the errors, expressed as FP + FN, for each viewpoint and direction of observation.

However, to define the most suitable point for which the only DGP profile should be calculated, other than the distribution and 95° percentile of the maximum FP+FN errors, another aspect should be considered. In fact, for the different points and directions of observation analysed, it was possible to calculate the $E_{v,thr}$ values for a different number of glazing and shading devices applied to the window. As seen, this is due to the different position of the window in the

observer's field of view, and strongly depends also on the transparency of the technology considered. Less transparent glazing technologies are less likely to cause glare for the occupants, resulting in the impossibility of calculating the relative $E_{v,thr}$ values for one or even all the daylight glare comfort classes.

A higher number of cases for which it was possible to calculate a $E_{v,thr}$ values results in a higher capability of rating the daylight glare condition of a space, with an error higher than the maximum FP+FN error 95° percentile for 5% of time. Figure 45 summarises the number of different glazing types and shading devices (for both west and south orientations and for each daylight glare comfort class threshold) for which it was possible to calculate an $E_{v,thr}$ value, relative to all the points and directions of observation considered. It is possible to observe that, for every point, the highest number of cases for which the calculation of the $E_{v,thr}$ value was possible is relative to the 0° direction of observation, then the directions of observation of 45° and -45°, and finally the 90° and -90° ones. Moreover, relative to the same position in the room, points in row a show a higher number of cases for which it was possible to calculate the $E_{v,thr}$ value than those obtained for points in row b. The highest number of cases for which the $E_{v,thr}$ values were calculated is relative to point a0 and a1, both for the 0° direction of observation.

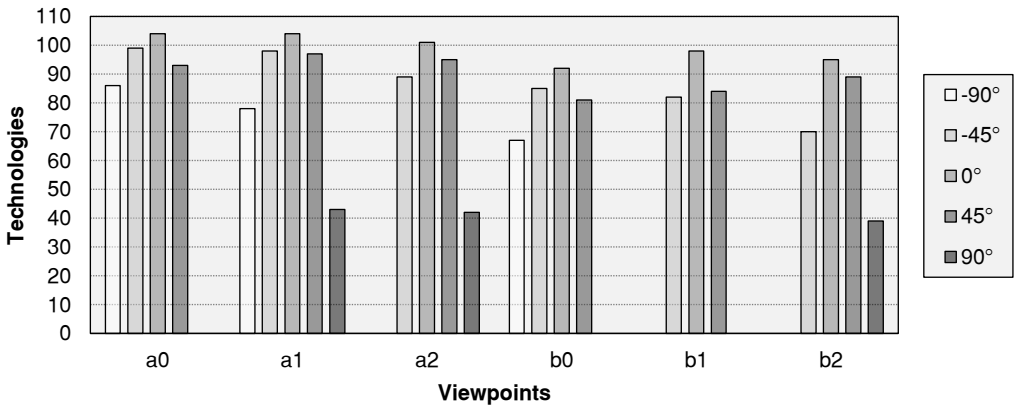

Figure 45. Number of different glazing types and shading devices for which it was possible to calculate an $E_{v,thr}$ value, relative to all the points and directions of observation considered.

From what said so far it is possible to conclude that it is not possible to define a single most suitable point in the space for which calculating the only DGP profile, to be used to calculate the $E_{v,thr}$ values to rate the glare condition for the whole space. In fact, depending on the purpose for which the evaluation of the daylight glare comfort classes is carried out, a point and a direction of observation could be more appropriate than another. In more detail, if this approach is used for *standard* evaluations, i.e. analyses relative to static glazing with relatively high τ_{vis} values, then the most adequate point results to be that minimising the maximum FP+FN error 95° percentile. In this case in fact the $E_{v,thr}$ values are likely to be calculated for glazing technologies with an average or high transparency for all the points and directions of observation. As a consequence, the combination *point-direction of* observation minimising the 95° percentile error should be

chosen for the calculation of the annual DGP profile. Therefore, the most suitable point and direction of observation result to be the point a0 and the -90° direction of observation. Conversely, when the evaluation is relative also to glazing with low τ_{vis} values, the combination *point-direction of observation* maximising the number of cases for which the calculation of the $E_{v,thr}$ values is possible should be preferred. In this case the most suitable point and direction of observation result to be the point a1 and the 0° direction of observation. Moreover, also the direction of observation represents an important aspect to be considered, depending again on the object and aim of the glare evaluation. In fact, in real spaces the 0° direction of observation is often avoided, as it is the most problematic one for the occupants from the glare point of view. Therefore, for a spatial evaluation of glare for real spaces or rooms whose layout is known, the point a0 and the -90° direction of observation should be preferred, as more representative of a real-case scenario. On the other hand, for spatial glare analysis aiming at characterising theoretical spaces, or whose purpose is that of taking into account the worst-case scenario, the calculation of the $E_{v,thr}$ values should be based on point a1 and 0° direction of observation. This distinction is possible since on one side the 95° percentile error for this combination, equal to 3.36%, is still quite low compared to the minimum value obtained (1.86%), relative to the point a0 and the -90° direction of observation. On the other hand, the number of cases for which it is possible to calculate the $E_{v,thr}$ values for this combination (86) is significantly lower than the maximum value (104), obtained for be the point a1 and the 0° direction of observation.

Example of application

In this section an example of the application of the presented simplified approach is provided. The case study used refers to the enclosed office considered in this study, south oriented, and with the window with specular properties with a τ_{vis} equal to 0.55. The eye vertical illuminance was calculated for a 5x10 grid of points, with a grid spacing of 0.5 m x 0.5 m, for a total number of 50 points across the room (deducting a peripheral stripe of 0.5 m). The points were located 1.2 m above the floor, with a direction of observation of -90° in respect to the vector perpendicular to the window plane. A single annual DGP profile was calculated, relative to the same direction of observation, for the point a0, which is shown in Figure 46. For this point, $E_{v,thr}$ values for each daylight glare comfort class were calculated by means of the fault-detection technique presented as the first step of the simplified approach. The following $E_{v,thr}$ values were estimated:

- Lower threshold: 3239 lx
- Intermediate threshold: 4077 lx
- Higher threshold: 4744 lx

By means of the above $E_{v,thr}$ values, the daylight glare comfort class for each of the 35 points in the room was estimated. Figure 46 shows the E_v values and

relative daylight glare comfort class for the 50 points in the office for the 25th of January at 14:00. This specific moment of the year was chosen as all the four daylight glare comfort classes appear to be experienced by the user for at least one point in the grid considered.

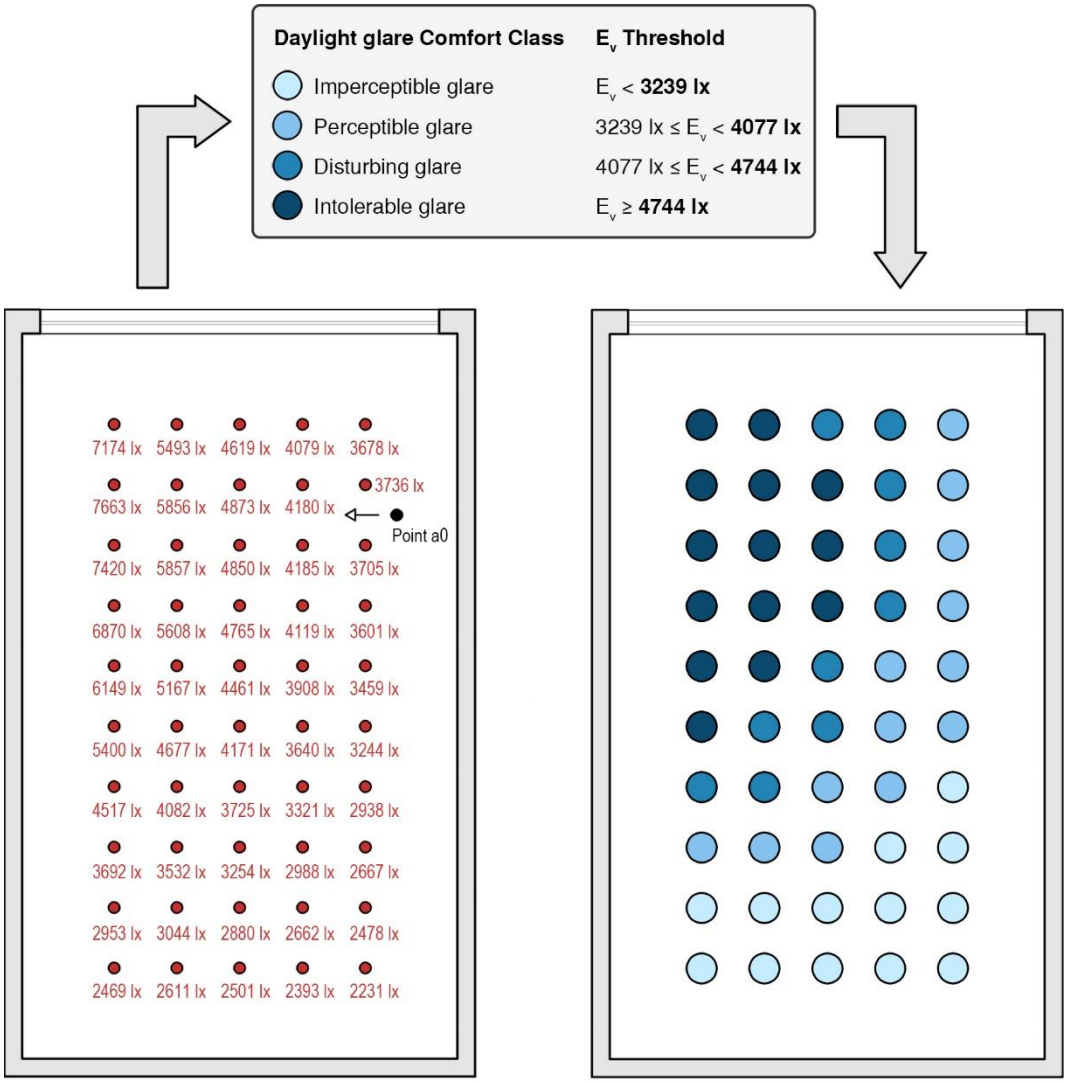

Figure 46. a) Eye vertical illuminance values and b) relative daylight glare comfort classes for the enclosed office case study with a south facing window equipped with a specular glazing with τ_{vis} = 0.55. Results relative to January 25th at 14:00.

Analysing the outcomes obtained, the following considerations can be drawn:

- For 26% of the space (13 points) an *imperceptible glare* condition is experienced;
- For 26% of the space (13 points) a *perceptible glare* condition is experienced;
- For 20% of the space (10 points) a *disturbing glare* condition is experienced;

- For 28% of the space (14 points) an *intolerable glare* condition is experienced.

The spatial distribution of the daylight glare comfort classes shows, as one would expect, that a worse glare condition is perceived for the points closer to the window, while it improves as their distance from the window increases. The perception of the different daylight glare comfort classes appears to vary in the room according to a diagonal direction, from the upper left corner, in which the glare perceived is *intolerable*, to the lower right corner, where the glare condition is *imperceptible*. This can be explained considering that in the specific moment considered the sun is low in the sky in the direction SSW (azimuth = 200.2°, elevation 23.4°). The variation of the glare condition throughout the room appears hence to occur for stripes parallel to the solar vector. The analysis presented is performed for a single hour during the year, nonetheless it could be easily extended to evaluate the percentage of the space in a certain daylight glare comfort class throughout the whole year.

4.2.4 Discussion

The possibility of estimating daylight glare comfort classes by means of solely the eye vertical illuminance was explored. The most suitable $E_{v,thr}$ values (correlated to DGP values of 35%, 40%, and 45%) to classify a certain space according to daylight glare comfort classes were calculated for different glazing types and shading devices and for nine different points and five directions of observation within a sample enclosed office for a certain climate. This was done by means of the minimisation of the error committed when estimating each daylight glare comfort class for all the points in each view direction considered through the $E_{v,thr}$ calculated for each point, as compared to DGP values. This error, calculated as the maximum sum of underestimation (FP) and overestimation (FN) of the glare comfort class, was found for all the cases analysed to be below 3.5% for 95% of time. The 95% benchmark is in line with the maximum error threshold defined in [227] and adopted by Wienold [133] for the definition of the DGP ranges for the daylight glare comfort classes. In fact, in both works comfort categories are defined according to the user satisfaction and within each category a 5% exceedance is allowed. In general, it is worth noticing that all the cases for which the maximum error 95° percentile value of 3.5% is exceeded are relative to technologies with a low τ_{vis}. This means that the fault-detection technique used to determine the $E_{v,thr}$ values can be less reliable for technologies with low luminous transmittance values.

By a closer look at the results, it can be easily understood that this is due to intrinsic simplifications of the presented approach, which only accounts for vertical illuminance at the observer eye, neglecting the contrast contribution to daylight glare comfort. In presence of diffusing window (or blind) materials (scattering technologies), the eye vertical illuminance is reduced while the area of the window with a higher luminance is enlarged, compared to the background

luminance. For diffusing materials with a low τ_{vis} this effect is even amplified, as the ratio of the luminance of the source (the whole window) compared to light transmitted to the room is high. In the case of specular glazing with low light transmission the background luminance of the room is quite low, as well as the luminance of the window, except for the very high luminance either of the light source within the window area (sun disk) or, when the sun is not directly within the observer's field of view, of the sunlight patches on the floor and on the walls. In all these cases a high luminance contrast between the light source luminance and the scene background luminance is perceived by the observer. As the luminance contrast is neglected in the simplified method higher errors are found for glazing with a low τ_{vis}, both specular or scattering, compared to the errors relative to glazing with a higher τ_{vis} (for which the luminance contrast plays a negligible role). An example of such conditions is presented in Figure 47, where the luminance map of the scene is shown, as seen from point a0 in the -90° direction of observation, for the same time-step of the year (February 21th at 12:30), for three different glazing.

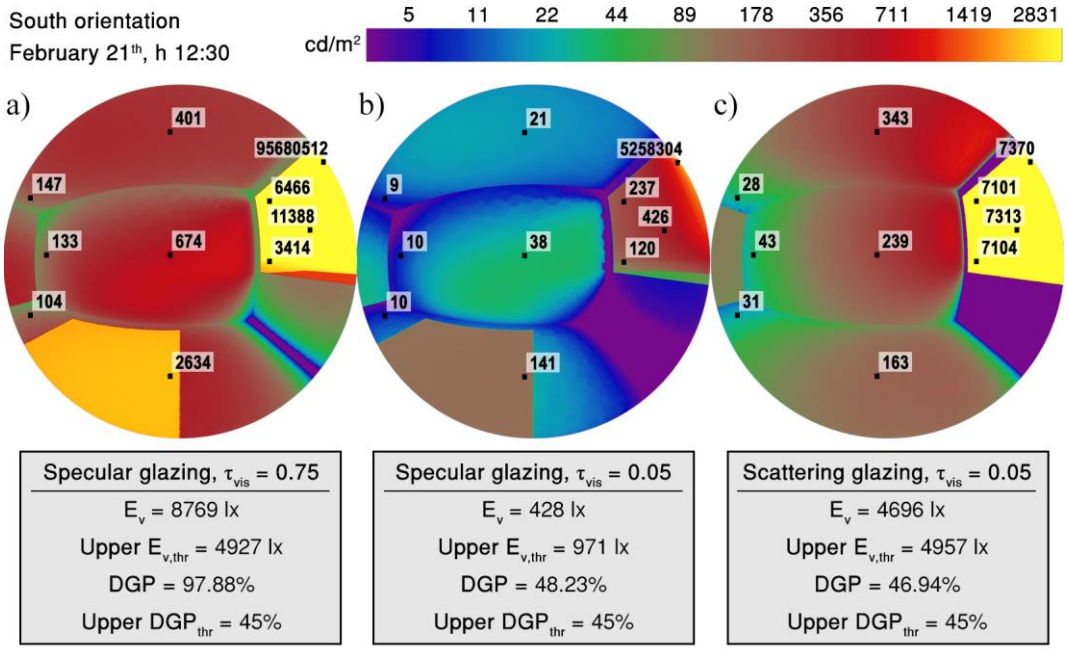

Figure 47. Luminance map of the observer's view field from point a0 in the -90° direction of observation, for: a) specular glazing with τ_{vis}=0.75; b) Specular glazing with τ_{vis}=0.05; c) scattering glazing with τ_{vis}=0.35. All the luminance maps are relative to the 21th February at 12:30 and to south orientation.

For Figure 47.a, i.e. specular glazing with τ_{vis} = 0.75, the estimation of the daylight glare comfort class by means of E_v is correct, as an eye E_v value higher than $E_{v,thr}$ and a corresponding DGP value higher than the DGP_{thr} are measured ($E_v > E_{v,thr}$ and analogously DGP > DGP_{thr}). For Figure 47.b and Figure 47.c (same daylight conditions but considering a specular glazing with τ_{vis} = 0.05 and the scattering glazing with τ_{vis} = 0.35 respectively), the eye E_v fails at classifying the condition into the correct daylight glare comfort class. For both the specular

glazing (Figure 47.b) and the scattering glazing (Figure 47.c) the E_v is lower than $E_{v,thr}$ (corresponding to a DGP_{thr} of 45%), while the real DGP value is higher than 45%. In more detail, in Figure 47.b the background luminance of the window is extremely low compared to the solar disk in the field of view of the observer (top right of the window), while in Figure 47.c the window has a relatively high uniform luminance on its entire area (solar radiation diffused by the window), compared to the room background luminance.

In light of the above, the application of the simplified approach presented for glazing with low light transmission properties, either specular or scattering, may result in errors in classifying a space according to the daylight glare comfort classes. This can occur for a significant number of time-steps throughout the year, during building operations. Nevertheless, as calculated for the presented case studies, this error results in a wrong estimation of the glare risk for a percentage of time lower than 3.5% in 95% of cases. In more detail, for all points and directions of observation and all the daylight glare comfort class thresholds analysed, the glare risk underestimation (i.e., FN) occurs for a percentage of time always lower than 5% (Table 22). Therefore, for the cases for which a total error (FP+FN) higher than 5% was found, a significant part of this is due to FP occurrences (overestimation of glare condition). Between these two classification errors, the underestimation of glare risk is certainly the most problematic, as it can lead to visual comfort conditions potentially worse than those estimated through this simplified approach. An overestimation of glare risk instead could actually result in lower glare risk than what estimated, even though this may lead to design or control choices towards a lower overall visible transmission of the window, potentially resulting in higher energy uses (higher artificial lighting and heating energy use, but potentially lower cooling energy use).

Among the points and directions of observation considered, point a0 in a -90° direction of observation and point a1 in a 0° direction of observation resulted as the most suitable to be used as a reference to define the $E_{v,thr}$ values to classify the whole space according to daylight glare comfort classes. In fact, for the former combination *point-direction of observation* the lowest maximum error (1,86%) is committed in 95% of cases when estimating the daylight glare comfort classes, while for the latter one the calculation of the maximum number of $E_{v,thr}$ values was possible, committing an error lower than 3.36% for 95% of time, value still considered as acceptable. Nonetheless the impact of these errors on annual glare estimation may not be negligible, as they correspond to a significant number of time-steps (number of hours during an annual analysis). Considering that in Turin the number of daylight hours per year is equal to 4602, these errors translate into the following amount of time in which glare is not correctly estimated:

- point a0 for the -90° direction of observation: maximum error committed for 95% of cases: 1.86% = 86 h;
- point a1 for the 0° direction of observation: maximum error committed for 95% of cases: 3.36% = 155 h

Despite the occurrence of these errors, as well as of their magnitude, it is important to highlight that this approach is aimed at providing a simplified and computationally efficient method to classify an entire space according to daylight glare comfort classes. As an example, considering the demonstration of application of the method provided in sub-section 4.2.3, to calculate the annual DGP profile for all the 50 points of the grid defined one would require a computation time 50 times higher compared to the presented approach: assuming to use an i7 processor (8 CPUs, 3.40 GHz), the evaluation of annual DGP for all the 50 points would require a time-machine of 25 hours, against the 45 minutes needed for the whole space with this simplified approach. Furthermore, the application of this method becomes even more convenient as the size of the space increases. Nevertheless, in the presence of larger spaces, such as open-plan offices, a set of $E_{v,thr}$ triplets (instead of only one) may be necessary to classify the entire space in terms of daylight glare comfort classes, as the glare condition may substantially diverge in different areas within the same space. Although the determination of the minimum number of significant points (and their position) for which an $E_{v,thr}$ triplet should be calculated, is an open research point.

The present work investigated the potential of the simplified approach proposed on a limited data set (in terms of office geometry / size, orientation and latitude). Moreover the daylight comfort classes are evaluated by minimising the total error in the estimation of the $E_{v,thr}$, although the False Positive (overestimation) or the False Negative (underestimations) may have a different influence on the visual comfort provided to the occupants or on the global energy performance of a space. Future study will explore the possibility of using $E_{v,thr}$ values defined minimising different objective functions (FP, FN or FP+FN), depending on the aim of the analysis. Finally, it has to be noted that a spatial glare evaluation is currently possible only if the same direction of observation is considered for all the points on the custom-defined grid (this is the direction assumed for the DGP annual profile). Therefore, if the layout of the space is not known, the approach proposed should most suitably be applied for a direction of observation representing the worst-case scenario within the space considered, so that for all the other directions of observation equal or better glare conditions are highly likely.

The presented approach can be used to support decision making at an early design stage (when a large number of solutions needs to be compared) and/or to support the design and implementation of real time control of façades with dynamic properties, aimed at reducing daylight glare discomfort risk. The main disadvantage of the approach lies in the fact that an estimation of the exact value of DGP is not possible, but the performance of the space (and of the selected façade technology and/or façade operation) is evaluated only in terms of daylight glare comfort classes.

4.2.5 Conclusions

The present section presented a simplified approach to classify a space according to daylight glare comfort classes, by means of vertical illuminances at eye level. DGP for a whole year is calculated for one point only and is then used as a valid reference to define the most suitable vertical illuminance threshold values for each daylight glare comfort class for that point. These thresholds are then used for all the other custom-defined points across the room (for which, calculating the annual DGP is not necessary).

This simplified approach proved to be sufficiently accurate for the case study investigated, with a maximum error committed, for all the cases analysed, lower than 3.5% for 95% of time. The main advantages of this simplified approach are that (i) a spatial evaluation of the daylight glare comfort classes within a room is possible and that (ii) the computation time required for its application is significantly lower than that necessary for calculating DGP for the whole space. The main disadvantage is instead represented by its inability to estimate the exact DGP value, as only the daylight glare comfort class can be estimated for each point. However, this information could be useful enough to support decision making at an early design stage and building operation in a perspective of improving the control of glare conditions for the occupants.

The analysed case study showed a good correlation between the daylight glare comfort classes estimated by means of the proposed approach and those deriving from the DGP evaluation. This is particularly true in the presence of glazing with a high value of τ_{vis}, for which the error committed was always below 5%, while for less transparent technologies, i.e. glazing with a lower value of τ_{vis} and shading devices, an error higher than 5% was found in few cases.

The simplified approach was tested on a limited number of cases (i.e. in terms of room geometry and façade options), therefore future work will be aimed at: i) evaluating the accuracy of the approach on larger spaces, different grid resolution, façade options; ii) testing the implication of adopting the presented approach on the design evaluation of alternative façade technologies and on the operations of dynamic facades.

4.3 Application in the operation of active components

4.3.1 Introduction

The present section demonstrates the advantages of the simplified approach for a spatial evaluation of the daylight glare comfort classes when applied to the operation of active transparent adaptive components. The integrated simulation methodology presented in Chapter 3 was enhanced by implementing the simplified approach for a spatial evaluation of the glare condition presented in section 4.2. This resulted in the possibility of simultaneously evaluating the effects of the variation of the thermo-optical properties of a transparent adaptive

component on the energy performance of a building and on the overall visual comfort condition of its occupant at a spatial level. In more detail, this enhanced version of the integrated simulation methodology allows evaluating visual comfort with a high spatial resolution both in terms of daylight availability on the visual task and glare condition of the occupants. As for the former, a spatial evaluation was already possible (see sections 3.3 and 3.4), while for the latter, assessed in terms of daylight glare comfort classes, this was enabled by the simplified approach presented in the previous section.

The ability to perform an evaluation of the glare condition at a spatial level was also implemented in a control strategy for the operation of active transparent adaptive components aimed at a spatial optimisation of the overall visual comfort conditions of the occupants. This was tested, through a virtual experiment, for different transparent adaptive active façade technologies, as well as different traditional moveable shading systems. The effects over the energy and visual comfort performance deriving from the operation of these technologies according to the proposed control strategy were evaluated in a comprehensive and accurate way by means of the above enhanced integrated simulation methodology.

In sub-section 4.3.2 the logic underlying the proposed control strategy, as well as its architecture and the possible advantages deriving from its application are described in detail. Moreover, a description of the different active transparent adaptive technologies selected, along with their modulation features is provided. Sub-section 4.3.3 presents the results obtained while in sub-section 4.3.4 the main advantages and drawbacks relative to the proposed control strategy are presented and critically discussed.

4.3.2 Methodology

This section contains an overview of all the performance metrics considered for this study, relative both to visual comfort and energy performance. A detailed explanation of the control strategy devised to optimise visual comfort at a spatial level is then provided. Finally, a description of the case study adopted, as well as of the different transparent adaptive active façade technologies and dynamic shading devices considered is reported.

4.3.2.1 Performance metrics

In the present analysis both visual comfort and energy aspects were considered. This was done by means of a series of performance metrics either currently used in literature or developed on purpose for this work.

Visual comfort

The two main factors determining the visual comfort condition of the occupants were assessed, i.e. daylight availability on the workplane and their glare condition. The daylight availability was analysed by means of the following metric:

Daylight Autonomy (DA): introduced by Cristoph Reinhart [132,184], this metric identifies the percentage of occupied hours over a year in which the daylight illuminance on the workplane meets the minimum horizontal illuminance threshold required to perform a given visual task. DA is calculated according to the following equation:

$$DA = \frac{\sum_{i=1}^{n} t_i(E_h \geq E_{h,threshold})}{n} \Bigg|_{occupied} \quad (11)$$

in which E_h is the horizontal illuminance on the workplane [lx]; $E_{h,threshold}$ is the minimum horizontal illuminance threshold required to perform a given visual task [lx]; t_i is the number of occupied hours over a year in which horizontal illuminance meets the minimum horizontal illuminance requirement; n is the number of occupied hours over a year. In this study the final DA is calculated as mean value of the DA relative to all the sensor points considered within the space.

The glare condition of the occupants was assessed by means of the following metrics:

Daylight Glare Probability (DGP): introduced by Wienold and Cristoffersen [111], this metric indicates the percentage of people that may experience a glare sensation due to a given daylight condition. Moreover, Wienold correlated different glare sensations (daylight glare comfort classes) to specific ranges of DGP values, in order to introduce a scale to rate the glare condition through DGP. For each of these daylight glare comfort classes a DGP threshold was therefore defined, based on the analysis of an extensive dataset. Table 23 summarises the daylight glare comfort classes with the relative DGP threshold values.

Table 23. Daylight glare comfort classes with the relative DGP threshold values.

Daylight glare comfort class	DGP Threshold
Imperceptible glare	DGP <35%
Perceptible glare	35% ≤ DGP < 40%
Disturbing glare	40% ≤ DGP < 45%
Intolerable glare	DGP ≥ 45%

The assessment of the annual DGP for different points in the space requires a high computational effort and is much time consuming. For this reason DGP was evaluated not through the algorithm defined by Wienold [105,111], but by means of the simplified approach presented in section 4.2. This one relies on the calculation, for each point in the space, of the vertical illuminance (E_v), which is compared to an E_v threshold value for each daylight glare comfort class. This simplified approach allows the evaluation of the daylight glare comfort classes only, and not of the DGP exact values, but is less time consuming.

DGP<35%: this metric, developed on purpose for this study, expresses the percentage of occupied hours over a year in which the glare condition is

imperceptible (DGP < 35%). $DGP_{<35\%}$ is calculated according to the following equation:

$$DGP_{<35\%} = \frac{\sum_{i=1}^{n} t_i(DGP < 35\%)}{n} \Bigg|_{occupied} \quad (12)$$

in which t_i are the occupied hours in which the DGP value is below 35%; n is the number of occupied hours over a year. $DGP_{<35\%}$ is calculated as mean value of the $DGP_{<35\%}$ relative to all the points considered within the space.

Energy Performance

The energy performance of the case study was assessed through the following metric:

Energy Performance index (EP_{gl}): this metric is defined as the total amount of primary energy consumed by a building or a space, on annual basis, per unit area. It is expressed in kWh/(m^2·year) and is calculated according to the following equation:

$$EP_{gl} = EP_H + EP_C + EP_L \quad (13)$$

in which EP_H is the primary energy consumed per unit area, on annual basis, by the heating system [kWh/(m^2·year)]; EP_C is the primary energy consumed per unit area, on annual basis, by the cooling system [kWh/(m^2·year)]; EP_L is the primary energy consumed per unit area, on annual basis, by the lighting system [kWh/(m2·year)]. The influence on the EP_{gl} of the primary energy necessary for domestic hot water production (EP_{DHW}) was considered negligible in the present work and was therefore not calculated.

4.3.2.2 Control strategy description

A control strategy was devised with the aim of optimising the visual comfort at a spatial level. This one was therefore assessed in the space in exam with a high spatial resolution. The transparent adaptive façade components or dynamic shading devices considered were then controlled in order to optimise the visual comfort condition for the occupants relative to an area, within the space considered, as large as possible.

Visual comfort was considered in terms of both daylight availability on the workplane and glare condition of the occupants. These two aspects are often contrasting with each other, as a too high daylight level on the workplane was proved to cause also discomfort glare to the occupants [140,145]. Moreover, relatively low daylight levels on the workplane may still be linked to a glare sensation for the occupants if the sun elevation angle is very low, as in this case

the sun may be directly within the occupants' field of view. A simultaneous optimisation of both these aspects is therefore not always possible, so a priority must be given to one of them on the other.

Starting from this consideration, a control strategy for transparent adaptive active façade components and dynamic shading devices was developed and tested for different technologies. As seen, a multi-objective optimisation of visual comfort aspects is not always possible, therefore a multi-criteria Rule-Based control strategy was devised, each criterium representing a different aspect influencing visual comfort. In presence of an adaptive façade technology able to modulate the amount of radiation entering the room, among daylight availability on the workplane and glare sensation for the occupants, the latter was identified as the most influencing factor in determining the overall visual comfort condition, especially if the user cannot actively interact with the control strategy of the adaptive technology. This because in presence of low daylight levels on the workplane the minimum illuminance requirement can still be reached by means of the artificial lighting system, allowing thus the user to perform its visual task. Conversely, a glare condition cannot be improved if not by modifying the state of the adaptive component in order to decrease the amount of radiation entering the room; if this is not possible a glare condition may reduce or at worst inhibit the ability of a user to carry out a visual task. Furthermore, also the view to the outside was considered in the multi-criteria control strategy as a factor influencing the visual comfort. This was considered in a simplified way in relation only to the attitude of the adaptive façade component to allow a view towards the exterior, not accounting, as suggested by some building protocols [230,231], for other factors like size and position of the window, view factor of the window from a given point in the space or presence and distance of external obstructions.

The working principle on which the proposed control strategy relies is based on the considerations made above relative to the priority given to the different aspects determining visual comfort. According to this working principle the state of a transparent adaptive façade technology or a dynamic shading device is chosen, among the different states it can assume, in accordance with the following rules:

1. The state is chosen as the one minimising the space in which glare is intolerable. In more detail:
    - 1.1. The state is chosen as the one maximising the space in which glare is imperceptible;
    - 1.2. If condition 1.1 is met by two or more states, the state is chosen among them as the one maximising also the portion of remaining space in which glare is perceptible;
    - 1.3. If two or more states meet both conditions 1.1 and 1.2, the state is chosen among them as the one maximising also the portion of remaining space in which glare is disturbing;

2. If two or more states meet condition 1 (i.e. conditions 1.1, 1.2 and 1.3), the state is chosen among these ones as the one maximising also the space in which the horizontal illuminance on the workplane meets the minimum horizontal illuminance threshold required to perform a given visual task;

3. If conditions 1 and 2 are met by two or more states, the state is chosen among these ones as the one allowing also a higher view towards the outside to the user. In more detail:

   3.1. The state is chosen as the one with the higher specular visible transmittance, that is the state allowing the lower distortion in the perception of the external ambient;

   3.2. If two or more states meet condition 3.1 the state is chosen among these ones as the state with the highest overall visible transmittance, that is the state allowing both a better and clearer perception of the external ambient and more daylight inside the space analysed.

A multi-criteria objective function was created based on the above algorithm, considering as criteria the different factors determining the final visual comfort condition of the occupants. For every timestep in which the analysis period is subdivided the state of the transparent adaptive façade technology or dynamic shading device is chosen as the one maximising the objective function created. What follows is the equation of the objective function developed for the control strategy proposed:

$$State = \max[\, c_0(k_0 \cdot S_{DGP<35\%} + k_1 \cdot S_{35\%\leq DGP<40\%} + k_2 \cdot S_{40\%\leq DGP<45\%}) + c_1\left(S_{E_h \geq E_h, threshold}\right) + c_2(s) + c_3(\tau_v)\,] \quad (14)$$

in which c_0, c_1, c_2, c_3 are the priority coefficients for the different criteria considered in the equation; k_0, k_1, k_2 are the priority coefficients for the different daylight glare comfort classes; $S_{DGP<35\%}$ is the percentage of space in which glare is imperceptible (DGP<35%); $S_{40\%\leq DGP<45\%}$ is the percentage of space in which glare is perceptible (35%≤DGP<40%); $S_{35\%\leq DGP<40\%}$ is the percentage of space in which glare is disturbing (40%≤DGP<45%); $S_{Eh\geq Eh,threshold}$ is the percentage of space in which the daylight horizontal illuminance on the workplane (E_h) meets the minimum horizontal illuminance threshold ($E_{h,threshold}$); s is the *specularity index*, that is the ratio of light specularly transmitted by a component ($\tau_{vis,spec}$) to the amount of light it globally transmits (τ_{vis}), and is calculated as $\tau_{vis,spec}/\ \tau_{vis}$; τ_{vis} is the overall visible transmittance of a component.

The above equation is composed by four members, each multiplied by a priority coefficient c_x. It is possible to observe that the first member considers the glare condition at a spatial level, the second member is relative to the daylight

availability on the workplane while the third and fourth members refer to the view towards the outside. To set the order of priority of these members it is necessary to define the priority coefficients c_0, c_1, c_2, c_3. Since all the variables in the equation are expressed as percentages, the priority coefficients can be expressed as different powers of 10. This is true also for the priority coefficients k_0, k_1, k_2 relative to the percentage of surface in which glare is in the different daylight glare comfort classes. Table 24 summarises all the priority coefficients as set in the present study to comply with the order of priorities above described.

Table 24. Priority coefficients used in the present study.

Coefficient	Value
c_0	10^2
c_1	10^{-1}
c_2	10^{-3}
c_3	10^{-5}
k_0	10^2
k_1	10^0
k_2	10^{-2}

4.3.2.3 Case study description

An enclosed office located in Turin (ITA: 45.22°N, 7.65°E) was assumed as case study in the present work. This geographical site is characterised by a temperate (mesothermal) climate with Heating Degree Days (HDD) and Cooling Degree Days (CDD) equal to 1192 °C and 452 °C respectively (calculated according a baseline of 12 °C for the HDD and 18 °C for the CDD [214]).

The enclosed office case study was considered to be 3.6 m large, 4.5 m deep and 2.7 m. A window 3.3 m large and 1.5 m high was located on one of the short walls, south oriented, for a Window-to-Wall Ratio (WWR) of 50%. The office case study was considered to be part of an office building, so as to be adjacent to identical offices on two sides on the same floor and on the floors immediately above and below it, while on the third side of the same floor it was considered to be flanked by a hallway with its identical thermal conditions. As a result, all the horizontal and vertical internal partitions were considered to be adiabatic. Table 25 summarises the visible reflectance assumed for all the internal surfaces of the case study.

Table 25. Visible reflectance of the internal surfaces of the office case study considered.

Surface	ρ_{vis} [-]
Ceiling	0.80
Walls	0.65
Floor	0.20
External ground	0.10

The external opaque wall was assumed to be a structural brick wall with a thermal transmittance (U-value) equal to 0.25 W/m^2·K and internal and external areal heat capacity equal to 19.2 kJ/ m^2·K and 64.4 kJ/ m^2·K, respectively. Its assembly, as well as the thermal properties of each layer are summarised in Table 26. The thermal properties of the horizontal internal partitions were assumed to be as follows: U-value of 1.33 W/m^2·K, decrement factor of 0.4 and time lag of 7 hours (internal and external areal heat capacity of 28.2 kJ/ m^2·K and 82.8 kJ/ m^2·K). The vertical internal partitions were assumed to have the following thermal properties: U-value of 1.19 W/ m^2·K, decrement factor of 0.62 and time lag of 5 hours (internal and external areal heat capacity of 48.3 kJ/ m^2·K and 67.0 kJ/ m^2·K). The thermal properties of the different materials were derived from [208–210].

Table 26. Stratigraphy and thermal properties of each layer of the external opaque wall.

Layer	Material	Thickness [m]	Conductivity [W/m·K]	Specific heat [J/kg·K]	Density [kg/m^3]
1	Plaster	0.015	0.8	850	1900
2	Insulation	0.12	0.04	1500	18
3	Hollow clay bricks	0.18	0.22	1019	1394.6
4	Plaster	0.015	0.8	850	1900

The schedules relative to occupancy and equipment were set in accordance with [211]. The office was assumed to be occupied by two people and the equipment load per area was assumed equal to 12 W/m^2 [218]. The primary air ventilation rate in presence of the occupants was set equal to 1.56 l/s·m^2, while the infiltration rate per area was assumed equal to 0.15 l/s·m^2 [212]. The heating and cooling systems were assumed to be ideal systems, that is to say that they were considered to be able to maintain the set-point or set-back temperature under any circumstances. The set-point and set-back temperatures were set equal to 20 °C and 12 °C for the heating system and to 26 °C and 40 °C for the cooling system. The heating and cooling set-point temperatures were to be maintained whenever the office was occupied, depending on the external boundary conditions. The heating system was assumed to have an overall efficiency of 0.85, while the cooling system SEER was set equal to 3.00. The lighting system was considered to be dimmable and controlled by a photosensor. A value of 500 lx was assumed as minimum illuminance requirement ($E_{h,threshold}$), in accordance with [95]. This illuminance threshold was to be maintained on the workplane by a combination of daylight and dimmable artificial lighting whenever the office was occupied. The lighting system was considered to have the following characteristics: installed power density of 10.76 W/m^2 [211]; ballast absorption factor of 10%; photosensor standby power of 1 W.

The horizontal illuminance on the warplane was assessed for a grid of points located at a height of 0.75 above the floor and evenly distributed throughout the whole floor area, excluding a peripheral stripe 0.5 m wide, as this portion of space

is seldom occupied by desks. The spacing between the grid points was set equal to 0.5 m, for a total number of 35 sensors.

The glare condition was evaluated for grid of points equal to the one just described, but with a height above the floor of 1.2 m (the height of a seated person). For all the points, the direction of observation was assumed to be perpendicular to the window, in order to evaluate the glare for an unfavourable scenario. As the calculation of an annual DGP profile for each of the 35 points would be much time-consuming, DGP was estimated by means of the simplified approach presented in section 4.2, which requires a far lower computation time. As a result, for each grid point only the annual profile of the daylight glare comfort classes was assessed. This was done by assessing the vertical illuminance for each point of the grid, while the annual DGP profile was calculated for one representative point only within the space considered. The vertical illuminance thresholds for each daylight glare comfort class were then calculated and the daylight glare comfort class profile for each point of the grid was finally estimated. These operations were repeated for any state assumed by the different transparent adaptive façade technologies and dynamic shading devices considered. The only DGP profile, for each of these states, was calculated for a point located in the room centre line, 1.5 m away from the window and with the same height above the floor and direction of observation as all the other grid points. This point and direction of orientation were chosen as, dealing with adaptive components potentially able to switch into states with a very low τ_{vis}, the number of cases for which the daylight glare comfort class estimation is possible should be maximised. From the outcomes of the previous section (4.2) such point and direction of observation result as the most suitable to fulfil this requirement.

A Double Glazing Unit (DGU) was adopted for the transparent building envelope, equipped with a Low-E on the internal side and with a 16 mm cavity filled with argon 90:10. As external glazing different transparent adaptive façade technologies were adopted, as well as a set of static glazing, to be used as reference cases. The transparent adaptive active façade technologies considered in the present study are represented by an electrochromic glazing (EC) and two new-generation liquid crystal glazing (LC and LC+). The EC glazing can linearly switch from a clear specular state (EC clear) to a tinted specular state (EC tinted). The first new-generation liquid crystal glazing, as all the components of this category, can switch from a clear specular state (LC sp_clear) to a clear scattering state (LC sc_clear). In addition, it is also able to modulate its visible transmission in order to linearly switch from the above clear specular state to a tinted specular state (LC sp_tinted). The second new-generation liquid crystal glazing represents an implementation of the liquid crystal component above described and can linearly switch from a clear to a tinted state both in a specular and in a scattering mode. It can therefore linearly switch from a clear specular state (LC+_sp_clear) to a tinted specular state (LC+_sp_tinted) and from a clear scattering state (LC+_sc_clear) to a tinted scattering state (LC+_sc_tinted). All the transparent adaptive active façade components presented are commercially available products

or prototypes under development, therefore their overall thermo-optical properties were measured directly by the manufacturers. Table 27 contains the overall thermo-optical properties of the DGU equipped with the different transparent adaptive active technologies in their limit states.

Table 27. Thermo-optical properties of the DGU equipped with the different transparent adaptive façade technologies in their limit states.

		Specular glazing			Scattering glazing			
Technology	Limit state	τ_{vis} [-]	g-Value [-]	U-Value [W/m²·K]	τ_{vis} [-]	g-Value [-]	U-Value [W/m²·K]	Diffusivity [-]
EC	Clear	0.66	0.46	1.22	x	x	x	x
	Tinted	0.03	0.05	1.22	x	x	x	x
LC	Clear	0.55	0.43	1.22	0.45	0.40	1.22	0.9
	Tinted	0.15	0.22	1.22	x	x	x	x
LC+	Clear	0.55	0.43	1.22	0.45	0.40	1.22	0.9
	Tinted	0.15	0.22	1.22	0.12	0.20	1.22	0.9

In addition to the different transparent adaptive technologies considered, the DGU was also equipped with different static glazing, as reference cases. These are represented by glazing with the same thermo-optical properties as the different limit states of EC, LC and LC+, summarised in Table 27.

Moreover, the performance of different traditional dynamic shading devices was evaluated. These are an external venetian blind (VB) with adjustable angle of the slats and two different internal roller blinds (RB). All the dynamic shading technologies were applied to the DGU equipped with the EC_clear static glazing. The venetian blinds were considered to be composed by dark-coated anodised aluminium slats (ρ_{vis} = 0.44) 40 mm wide and 2.5 mm thick. They were considered to be either fully up or fully down, and in this case 4 different slat angles were considered: 0° (VB_0 - horizontal slats), 30° (VB_30), 60° (VB_60), 90° (VB_90 - vertical slats). Two different roller blinds were considered, one aimed at glare control (RB_glr), of τ_{vis} = 0.04, and one aimed at solar control (RB_slr), of τ_{vis} = 0.15. Both roller blinds were considered to be perfectly diffusing materials. In addition to the dynamic shading devices above described, also some static shading devices were considered, to be used as a reference cases. These are represented by the limit states of the dynamic shading technologies presented, applied to the DGU equipped with EC clear and kept fully closed and static for the whole year. (RB glr, RB slr, VB_60 and VB_90).

The annual simulations were carried out according to the integrated simulation strategy presented in Chapter 3. In more detail, the simulation workflow was divided into four automated steps:

1. Discretisation of the continuous switching ranges of the different transparent adaptive active technologies considered into discrete

states. The visible transmittance modulation range for the different components was discretised with a resolution of 0.1;

2. Daylight Simulation of all the different discrete states with DAYSIM 4.0 [155]. This include both horizontal and vertical illuminance for the two grids of points defined, as well as the DGP profile for the only point in the space selected. For the DGP calculation DAYSIM actually makes use of the software Evalglare [124] in background;
3. Thermal simulation: the thermal simulation is performed by means of EnergyPlus [110] and its Energy Management System (EMS) module [171]; an accurate model for each adaptive façade technology and dynamic shading considered is implemented within the EMS. Additionally, by means of the EMS, the results from step 2 are integrated within the thermal simulation model, and are post-processed in an automated way, within this step, according to the control strategy created;
4. Postprocessing of the daylight simulation results and calculation of yearly performance metrics.

4.3.3 Results

This section contains the annual performance results obtained for the office case study equipped with the transparent adaptive active façade technologies, the dynamic shading devices and the static solutions considered. The Performance is measured in terms both of primary building energy use, EP [W/m^{2}K], and visual comfort provided to the occupant. For this one both the daylight availability on the workplane, by means of the Daylight Autonomy, DA, and the glare condition of the occupants, through the $DGP_{<35\%}$ were evaluated. For each transparent façade solution analysed, the performances of the limit states of their range(s) of variability, kept static for the whole year, were considered as the direct benchmarks.

4.3.3.1 Visual comfort results

Figure 48 shows, for each façade solution considered, either static or dynamic, the visual comfort performance relative both to the daylight availability on the workplane and to the glare condition of the occupants. In more detail, the chart correlates these two metrics for each façade solution considered. As DA and $DGP_{<35\%}$ indicate the percentage of occupied hours in which daylight alone meets the minimum illuminance requirement of 500 lx and in which the glare sensation is imperceptible, a value of 100% represents for each of them the ideal condition. Therefore, in the chart proposed, the ideal optimal condition, or theoretical optimum, is represented by the top right corner, point in which the two metrics show a value of 100% (the chart was clipped in order to best fit the outcomes obtained). The red edged markers represent the adaptive solutions controlled

through the control strategy proposed in this study, while the black edged markers are relative to the static limit states. The size of the markers provides a qualitative indication of the annual electric energy use for the lighting system: the bigger the marker the higher the amount of electric energy consumed by the lighting system.

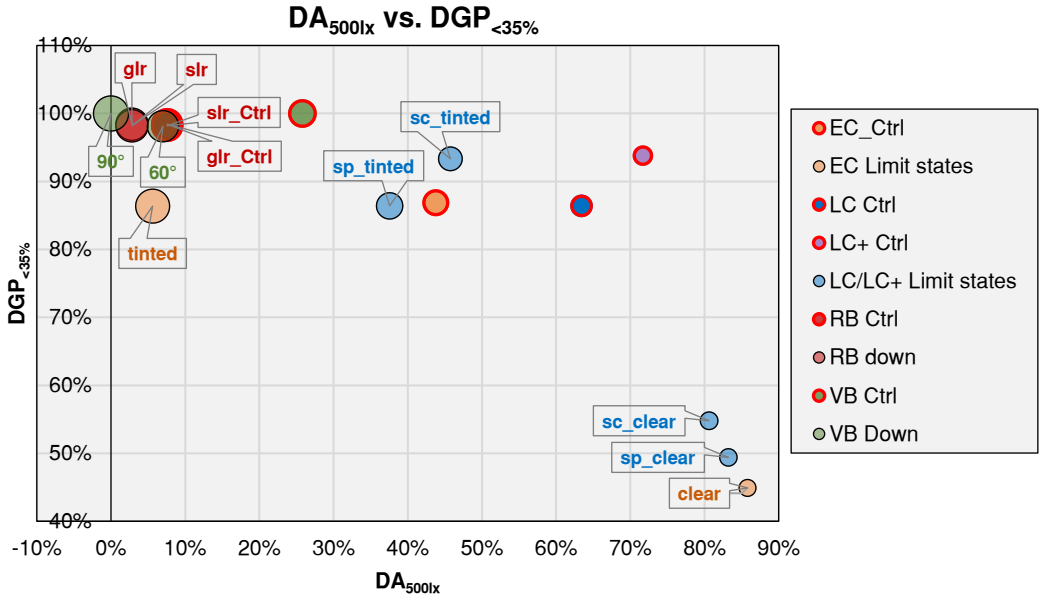

Figure 48. Visual comfort annual results relative to all the static and dynamic solutions considered.

The results obtained allow a better understanding of the effects that the control strategy proposed has on the two main aspects of visual comfort. It is in fact possible to observe that, for each controlled façade solution, the $DGP_{<35\%}$ is equal to that of its most performing static limit state, while the DA shows an intermediate value between those relative to its static limit states. This means that the control strategy allows achieving the highest possible glare performance, i.e. that relative to the most performing static limit state, while the daylight availability is reduced from that of the best performing static limit state, but is never equal to that of the least performing one. The extent of this reduction depends on the range of variability of the façade solution considered. This behaviour is in accordance with the order of priorities set for the different aspects of visual comfort when defining the control strategy to adopt.

In more detail, all the dynamic shading devices considered (VB, RB_glr and RB_slr) show a high gap between the results relative to their static limit states. When the shading device is fully up, solution represented by EC clear limit state, the highest value of DA is obtained, but also the lowest value of $DGP_{<35\%}$. Conversely, all the static limit states in which the shading device is fully down show a $DGP_{<35\%}$ close to 100%, but also values of DA always below 10%. When controlled, these solutions show a high drop in the amount of daylight entering the room. For the VB a decrease of the DA of 60.0% was observed, while for both RB_glr and RB_slr this decrease was even higher, equal to 78.2%. These shading devices can only switch between a very transparent state (EC_clear) to states which block the greatest part of the incoming solar radiation and, as a

consequence, whenever glare is detected and their state is switched, a high rate of solar radiation is blocked as well.

A different trend can instead be observed for the transparent adaptive façade technologies considered (EC, LC, LC+). In this case, as their switching ranges are continuous, they can more efficiently modulate the light entering the room with the purpose of minimising the glare condition for the whole the space while still admitting a good amount of daylight in the interior space. The electrochromic glazing shows a high variation in terms of both DA and $DGP_{<35\%}$ for its limit states, with a DA value of 85.8% and a $DGP_{<35\%value}$ of 45% for the clear state and a DA close to 0 and a $DGP_{<35\%}$ equal to 86.4% for the tinted state. Through the control strategy proposed it was possible to optimise the glare condition while reducing the extent of the decrease of the DA, in respect to what observed relative to VB and RB. The reduction of the DA observed for the EC, equal to 45%, even if still significant is in fact sensibly lower than the decrease found for the dynamic shading devices. The decrease in the DA value found when controlling the liquid crystal glazing was lower than that relative to the EC component, due to the fact that its tinted limit states, either specular or scattering, are characterised by a visible transmittance higher than the EC tinted limit state. As far as the $DGP_{<35\%}$ is concerned, similar values were found for the LC and EC when controlled. A higher value was instead obtained for the LC+ component. The overall best visual comfort performance was obtained when controlling the two liquid crystal glazing, as for both, in respect to the controlled electrochromic glazing, an equal or higher $DGP_{<35\%}$ and a higher DA were obtained. Between LC and LC+, the overall best visual comfort performance was found relative to the LC+ component, for which the highest DA and $DGP_{<35\%}$were obtained. With regard to the DA, the lowest reduction in respect to the most performant static state, equal to only 11.5%, was observed.

Summing up, it is possible to affirm that the transparent adaptive façade technologies proved to be much more effective than the dynamic shading devices in controlling both the glare condition and the daylight availability for a whole space. Among these, the liquid crystal glazing showed a better performance than the electrochromic glazing. Furthermore, between the two liquid crystal glazing technologies, the LC+ showed to be the most effective one in the optimisation of visual comfort at a spatial level. This trend depends on two different factors influencing the final performance of the different adaptive façade components: i) the amplitude of their switching range; ii) their *attitude* in transmitting daylight. The amplitude of the switching range of an adaptive façade component refers to the thermo-optical properties of its limit states, while for *attitude* it is intended the way an adaptive component interacts with and transmits the incoming daylight, i.e. if it is able to modulate only the visible transmittance or also the way light is transmitted (scattered or specularly transmitted). The combination of these two factors results in the total number of different possibilities among which the control strategy can choose for the spatial optimisation of visual comfort. The higher this number is and potentially the higher is the related visual comfort

performance. As an example, the component for which the highest DA and $DGP_{<35\%}$ values were obtained is the LC+ component, i.e. the only adaptive façade technology, among the ones considered, able to modulate its visible transmittance both in a specular and in a scattering mode.

4.3.3.2 Energy performance results

Figure 49 shows the break-up of specific primary building energy use for space heating, space cooling and lighting for all the adaptive and static solutions considered. The energy performance of the controlled adaptive façade technologies fully depends on the control strategy developed, which is aimed only at the spatial optimisation of visual comfort aspects. Energy aspects are in fact not controlled when operating the adaptive technologies adopted and are therefore hereby only evaluated as a consequence of choices relative to a different physical domain.

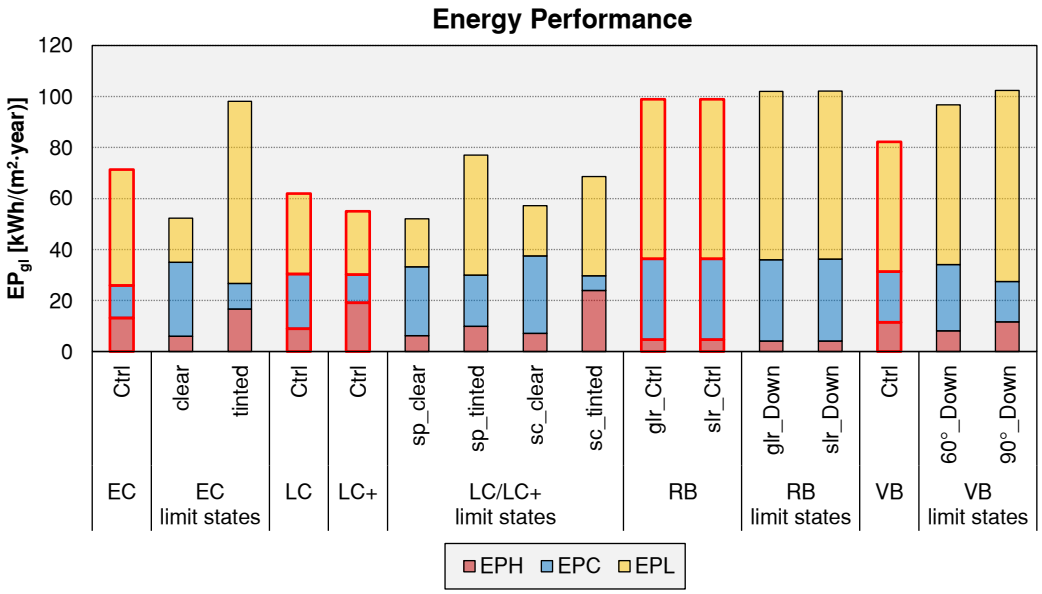

Figure 49. Annual energy performance results relative to all the static and dynamic solutions considered.

The results show that the overall energy performance of every controlled solution falls between those of its most and least efficient static limit states. Similarly to the trend observed for the results relative to the DA, also in this case the increase of the EP_{gl} relative to the technologies controlled, in respect to their most performant static limit state, show to be strongly dependant on the adaptive technology switching range. The growth of the EP_{gl} observed for the dynamic shading devices is higher than that relative to the transparent adaptive active façade technologies. In more detail, the two internal roller blinds, when operated according to the control strategy proposed, show an overall energy performance equal to that obtained for the same roller blinds kept fully closed for the whole year. This can be explained considering that the roller blinds are positioned on the inner side of the window, therefore their operation has no effect on the thermal energy performance of the building. For the external venetian blinds an increase

in the EP_{gl} equal to 30 kWh/(m^2·year), in respect to that relative to the EC clear static limit state, is observed. Nonetheless, an improvement in respect to VB kept closed for the whole year is present. The energy performance relative to the controlled dynamic shading devices is not comparable to that obtained when controlling the transparent adaptive active façade components, which can again be explained considering that these shading devices can only switch between a very transparent state (EC_clear) to states which block the greatest part of the incoming solar radiation. For this reason, both the controlled dynamic shading devices and the static limit states in which they are fully closed show the highest EP_L values among all the cases analysed, comparable only with the EC in its tinted state.

As far as the transparent adaptive façade technologies are concerned, lower increases in the overall energy performance were obtained when controlling the technologies with the control strategy proposed, in respect to their most performant static limit state. This is due to their intrinsic capability, higher than that of the dynamic shading devices, to manage the incoming solar radiation, which in turn affects, at different extents, EP_H, EP_C and EP_L. An increase in the EP_{gl} of 9.9 kWh/(m^2·year) was observed for the electrochromic glazing, while LC and LC+ components showed an increment equal to 12.1 kWh/(m^2·year) and 2.9 kWh/(m^2·year) respectively. Liquid crystal glazing show the lowest distance between the energy performance of the component controlled according to the proposed control strategy and that relative to their best performance achievable and, among these two, the LC+ component proved to be the most efficient one. Analysing then the break-up of the Energy Performance index into heating, cooling and lighting, a common trend to the transparent adaptive façade technologies considered can be observed. In fact, when the technology is controlled, in respect to its most efficient static limit state, EP_H and EP_L are increased, while EP_C is decreased, though the extents of these increment and decrement depend on the technology considered. This common trend is due to the working principle on which the control strategy proposed is based. It is in fact firstly aimed at eliminating a glare condition to the occupants from the space analysed. In a location such as Turin and in an orientation such as that of the case study considered, the glare phenomenon mainly occurs in winter, as the sun elevation angle is low throughout the whole day and the sun often falls within one's visual field. When this happens, the adaptive glazing are then switched to their darker states, in order to prevent, if possible, discomfort glare for the occupants. Operating an adaptive component in such way implies that the solar radiation is mostly blocked, resulting in two main drawbacks on the energy performance: i) the solar heat gains are reduced, with a consequent increase of EP_H; ii) the artificial lighting system needs to be switched on for a higher number of hours to provide the minimum illuminance on the workplane, with a consequent increase of EP_L. Conversely, the EP_C is reduced as often in summer, to control the glare condition within the space, only intermediate states of the adaptive façade technologies are necessary, resulting in a reduction of the solar gains, and in a consequent decrease of EP_C.

Summing up, the onclusions drawn for the visual comfort performance remain valid also for the energy performance of the façade solutions considered. Transparent adaptive façade technologies proved to be more effective than dynamic shading devices also in terms of how they affect the specific primary building energy use. Among these, the liquid crystal glazing showed a better performance than the electrochromic glazing. Finally, between the two liquid crystal façade components, the LC+ showed to be the most effective one also as far the energy aspects are concerned, as its energy performance is very close to that of its most performing static limit state.

4.3.4 Discussion and conclusions

In the present study the performance of different transparent adaptive façade technologies and dynamic shading systems, when controlled according to a control strategy aimed at optimising the visual comfort at a spatial level, was assessed. The energy performance related to each technology, as well as the visual comfort performance were evaluated, the latter assessed both as glare condition of the occupants and daylight availability on the workplane. All the façade solutions analysed showed to be able to provide the same protection from glare as their most efficient static limit state. In terms of ability to allow daylight within the room, as well as in terms of energy performance, the technologies analysed showed a performance between those of their most and least efficient static limit states. The transparent adaptive active façade technologies showed to be more efficient than the dynamic shading devices, as lower reductions in these two aspects were achieved. Among these, the liquid crystal glazing able to modulate its visible transmittance both in a specular and scattering way (LC+) proved to be the most efficient technology analysed, as its performance, both in terms of daylight availability and energy performance, showed to be the closest to that of its most efficient static limit state. This is due to the fact that the adaptive façade technologies considered can continuously vary their thermo-optical properties, resulting in a fine modulation of the incoming solar radiation. A wider range of possibilities is thus possible when the technology is controlled. Among these, the state of the adaptive component is chosen as the one *just* minimising the glare condition at a spatial level, but still allowing the highest possible amount of daylight within the room. As a result, the adaptive technologies with a wider switching range, as well as with the ability of changing the way they transmit daylight (specular or scattering mode) showed results closer to those of their most efficient static limit states.

Although the control strategy devised was aimed at a spatial optimisation of visual comfort only, for some technologies (LC and LC+) the specific primary building energy use was found to be close to that of their most performant static limit state. Nevertheless, results below this limit were never obtained for any of the technologies analysed, and actually all the other technologies analysed showed a specific primary building energy use significantly higher than that of their most

performant static limit state. This is mainly due to the fact that, in order to optimise the glare sensation at a spatial level, when discomfort glare is present the glazing is often kept at its darkest state. This reduces in turn the daylight penetration within the room, resulting in a higher energy consumption of the lighting system (EP_L) to provide the minimum horizontal illuminance requirement on the workplane. Lower daylight levels in the space considered may in turn positively or negatively affect also the energy consumption of the heating and cooling system, depending on the season and on the external boundary conditions. For a case study such as the one considered in this work, located at an intermediate latitude and south-oriented, the control strategy shows to be able to reduce the energy demand for space cooling, while that relative to space heating is increased. In winter a higher daylight penetration within the room is connected to lower energy consumption for the heating system (higher solar heat gains), but also to a higher probability for the occupants to perceive discomfort glare. According to the control strategy created, the adaptive glazing is switched to a dark state in order to prevent a glare condition, resulting thus in a higher energy use for the heating system. Conversely in summer, whenever the adaptive façade technology is switched to a darker state the energy demand for the cooling system is decreased, as the solar heat gains are reduced, and with them the overheating problems.

According to the control strategy proposed, the operation of the adaptive façade solutions results in some cases contrasting with the optimisation of the energy performance (mainly in winter), while in other cases these two aspects show a good agreement (mainly in summer). As a result, the specific primary building energy use is reduced in respect to that of the least efficient static limit states, but results higher than that of the most efficient ones. Nonetheless, the energy performance is in this study only evaluated, and not controlled. By implementing the energy aspects in the proposed control strategy the achievement of a building energy use closer, or even higher than that relative to their most performant static limit states would be theoretically possible. However, this is not a trivial task, since energy and visual comfort aspects, as highlighted above, are often contrasting with each other. In these cases, setting the adaptive component to a state assuring a trade-off between the two aspects may be counterproductive, as, if the occupants are not in comfort, they tend to override the control strategy to increase their visual comfort condition, resulting in a higher energy consumption than that theoretically achievable. Conversely, if they cannot override the control strategy, the human performance is negatively affected, in terms healthiness and ultimately of productivity. An order of priority between comfort and energy must therefore be defined, even if this is not a trivial task either, since the optimisation of one aspect may negatively affect the other, resulting in a lower final performance. An extensive investigation is necessary since this field has not been fully explored yet. A first solution could be that of optimising the visual comfort only in presence of occupants, while optimising the energy aspects when the

space is not occupied. This solution could yield a further reduction of the energy consumption without affecting the visual comfort aspects.

The control strategy proposed was devised and optimised at a theoretical level, but it is unlikely to be applied to real case-scenarios in its current form for two reasons: a) it accounts for variables which are difficult to measure in real spaces, such as horizontal and vertical illuminance for a grid of sensors throughout the whole space; b) it makes a choice by already knowing the effects any single state would have on the aforementioned variables. Future work should therefore focus on the reduction of the spatial variables to significant physical quantities measured in one or at most in few points in the room. Correlating a single quantity to its distribution across the space is not an easy task and needs to be thoroughly investigated. Moreover, the possibility of predicting the effects of the different states a transparent adaptive component can assume on the physical quantities measured (and their spatial distribution) should be deeply explored as well. Nonetheless, the approach proposed in this work proved to be effective in all the cases analysed and promising also for real-case applications.

4.4 Conclusions

The present chapter presented a simplified approach for the annual evaluation of the glare condition of the occupants with a high spatial resolution. This approach relies on the classification of a space according to daylight glare comfort classes, by means of solely the eye vertical illuminance. This one is compared to a threshold value for each daylight glare comfort class (imperceptible, perceptible, disturbing and intolerable glare sensation), which is determined through a comparison to DGP values, on annual basis, through a fault-detection analysis.

The main advantages related to such simplified approach are that: (i) it enables a spatial assessment of the daylight glare comfort classes throughout a whole space; (ii) the computation time required for its application is significantly lower compared to that necessary for evaluating DGP for the whole space. The main disadvantage related to this approach was identified in its inability to evaluate the exact value of Daylight Glare Probability, as only the daylight glare comfort classes can be estimated at a spatial level.

When implemented in the integrated simulation methodology presented in Chapter 3, this approach enhances the visual comfort evaluation, as this can now be assessed at a spatial level in terms of both daylight availability on the visual task (which was already possible through the available daylight simulation tools) and glare condition of the occupants. Such enhanced methodology could consistently support choices related to the design or operation of transparent adaptive façade components with a comprehensive and spatial evaluation of the effects of their operation (or intrinsic behaviour) on the visual comfort condition of a whole space. This was demonstrated by the operation of different active transparent adaptive components according to a control strategy aimed at the

optimisation of the glare condition for the whole space considered (see section 4.3).

Furthermore, the proposed simplified approach is not meant for the evaluation of the visual comfort performance of transparent adaptive technologies only, but could fruitfully be exploited to support decision-making relative also to static or more traditional glazing and shading system solutions. It could in fact provide a spatial information relative to the glare condition of the occupants which could be useful to support the daylighting design at early design stages.

Chapter 5

Conclusions

Transparent adaptive façades show high potentialities in improving the overall building performance, both in terms of energy use and visual comfort for the occupants. However, their successful building integration currently results as a challenging task. This is mainly due to: (i) a low awareness in the possibilities and drawbacks relative to the integration of transparent adaptive technologies in the building envelope; (ii) intrinsic difficulties of the currently available Building Performance Simulation tools to assess the performance of these components on the different domains they affect in a reliable way.

In this framework, the Ph.D. thesis proposed a novel integrated simulation methodology for a simultaneous and comprehensive evaluation, with a high degree of accuracy, of the effects of the modulation of the thermo-optical properties of transparent adaptive façade technologies on the energy performance of a building and on the visual comfort condition of its occupants. As for the latter, this is evaluated at a spatial level both as daylight availability on the visual task and as daylight glare condition of the occupants. This was enabled by the introduction of a simplified approach aimed at classifying a whole space according to daylight glare comfort classes, by means of solely the eye vertical illuminance.

The proposed integrated methodology proved to be suitable for the evaluation of the performance related both to passive (section 3.3) and active (sections 3.4 and 4.3) transparent adaptive façade components. Specifically, the application of such methodology enabled: (i) a simultaneous, accurate and comprehensive quantification of the effects of the behaviour of a transparent adaptive component over energy and visual comfort aspects; (ii) the simulation of complex phenomena relative to the behaviour typical of some transparent adaptive technologies (e.g. hysteretic behaviour of thermochromic and thermotropic glazing).

Such methodology could effectively support with reliable outcomes the decision-making relative to the design and the operation of transparent adaptive components. In more detail, its application could result useful to:

- support the possibility of material design to optimise different material optical and/or thermal properties;
- support the design of transparent adaptive components by evaluating the interdependency between the above thermo-optical properties and the component performance when building integrated;
- evaluate the interdependency of multiple performance aspects, such as heating and cooling energy uses, artificial lighting energy use and daylight visual comfort. This aspect could support both the design of transparent adaptive façades and the conception, development and implementation of advanced multi-domain and multi-objective control strategies for active transparent adaptive technologies.

This kind of information could increase the comprehension of possible risks and advantages related to the integration of transparent adaptive façades in the building envelope, helping thus exploiting their full technical potential. As a result, a higher awareness of all the stakeholder involved about the possibilities related to transparent adaptive façades could ultimately foster their adoption in the building industry, as well as support the development of innovative adaptive components.

As regard the simplified approach proposed for the evaluation of the glare condition of the occupants with a high spatial resolution, two main advantages were identified in its application: (i) it enables a spatial evaluation of the daylight glare comfort classes throughout a whole space; (ii) it consistently reduces the computational effort necessary for a spatial evaluation compared to the Daylight Glare Probability (currently the most widespread and accurate metric for the assessment of daylight glare). Other than its implementation within the proposed integrated simulation methodology, this simplified approach could effectively be exploited to support the decision-making at early design stages of the daylighting design relative to static or more traditional glazing and shading systems.

The main limitation relative to the proposed integrated simulation methodology regards the high level of expertise necessary for its correct application. It in fact requires a high-level knowledge relative to different fields, including building physics, building simulation, daylight and visual comfort and computer programming as well. For this reason, the application of this methodology is mainly suitable for qualified academic or professional figures, such as building envelope researchers and building and façade consultants. Although the proposed methodology shows a high flexibility, which allows modelling, simulating and evaluating the performance of available as well as innovative adaptive transparent technologies, this results in the need, for each of these technologies, to specifically create a numerical model describing their behaviour. The robustness of this numerical model in describing the actual system, as well as the uncertainty relative to the input data, can significantly affect the accuracy of the outcomes. Therefore, the numerical simulation should be coupled to experimental activities, as to increase the model robustness and ensure

the availability of accurate input data for the correct characterisation and the following modelling of the behaviour of the transparent adaptive façade technology.

In light of the research work presented in the framework of this Ph.D. thesis, the following research perspectives are suggested with the aim of further develop the integrated simulation methodology proposed and fill further gaps of knowledge not addressed in the present thesis:

- The novel simulation methodology proposed did not take into account the effects due to the interaction between the transparent adaptive façade components and the building occupants. This is mainly due to the fact that at present time no recognised model to precisely account for the occupant behaviour is available. Nonetheless the interaction *adaptive building envelope-occupants* may result in significant effects on the comfort condition and human performance of these ones, as well as on a lower overall building performance than that estimated. Future work should therefore address the interaction between transparent adaptive façades and occupants with the aim of providing a better understanding of how their operation or intrinsic behaviour may affect their comfort condition.
- The conception, testing and development of advanced multi-objective and multi-domain control strategies is allowed by the integrated simulation methodology proposed. However, when optimized at a simulative level, these mostly rely on variables difficult to measure in real spaces, especially in the case of spatial variables (e.g. horizonal or vertical illuminances for a grid of points). As a result, such control strategies are unlikely to be applied in real cases in this form. Future work should therefore focus on the reduction of the spatial variables to significant physical quantities measured in one or at most in few points in the room. In addition, the possibility of predicting the effects of the different thermo-optical states a transparent adaptive component can assume on the physical quantities measured (and their spatial distribution) should be deeply explored as well. A promising solution to perform this task is that of using the simulated case studies controlled according to an advanced control strategy to extract control rules mimicking optimal control based on more suitable physical quantities (rule extraction).
- The proposed simulation methodology comprehensively assesses the effects of the behavior of transparent adaptive components on energy and visual comfort aspects. However, recent studies have shown how the incoming solar radiation may as well significantly affect the thermal comfort condition of the occupants, when these are directly exposed direct sunlight [232,233]. Therefore, with the aim of providing a

comprehensive evaluation of the effects of transparent adaptive technologies both on the energy performance of a building and on the overall comfort condition of their occupants, this aspect should be carefully addressed. Specifically, similarly to the simplified approach for a spatial glare evaluation proposed in this study, the assessment of the thermal comfort condition should be carried out at a spatial level. In this sense a spatial evaluation of the overall comfort condition of the occupants, both in terms of visual and thermal comfort, would finally be possible.

References

[1] European Parliament - Council of the European Union, DIRECTIVE (EU) 2018/844 OF THE EUROPEAN PARLIAMENT AND OF THE COUNCIL of 30 May 2018 amending Directive 2010/31/EU on the energy performance of buildings and Directive 2012/27/EU on energy efficiency, Official Journal of the European Union - L 156. 61 (2018) 75–91.

[2] European Parliament - Council of the European Union, DIRECTIVE 2010/31/EU OF THE EUROPEAN PARLIAMENT AND OF THE COUNCIL of 19 May 2010 on the energy performance of buildings (recast), Official Journal of the European Union - L 153. 53 (2010) 13–35. doi:10.3000/17252555.L_2010.153.eng.

[3] European Parliament - Council of the European Union, DIRECTIVE 2012/27/EU OF THE EUROPEAN PARLIAMENT AND OF THE COUNCIL of 25 October 2012 on energy efficiency, amending Directives 2009/125/EC and 2010/30/EU and repealing Directives 2004/8/EC and 2006/32/EC, Official Journal of the European Union - L 315. 55 (2012) 1–56. doi:10.3000/19770677.L_2012.315.eng.

[4] R.C.G.M. Loonen, M. Trčka, D. Cóstola, J.L.M. Hensen, Climate adaptive building shells: State-of-the-art and future challenges, Renewable and Sustainable Energy Reviews. 25 (2013) 483–493. doi:https://doi.org/10.1016/j.rser.2013.04.016.

[5] D. Aelenei, L. Aelenei, C.P. Vieira, Adaptive Façade: Concept, Applications, Research Questions, Energy Procedia. 91 (2016) 269–275. doi:https://doi.org/10.1016/j.egypro.2016.06.218.

[6] P.R. Boyce, Human factors in lighting, 3rd editio, CRC Press, Taylor and Francis Group, Boca Raton, FL, USA, 2014. doi:10.1201/b16707.

[7] L. Giovannini, F. Favoino, A. Pellegrino, V.R.M. Lo Verso, V. Serra, M. Zinzi, Thermochromic glazing performance: From component experimental characterisation to whole building performance evaluation, Applied Energy. 251 (2019) 113335–113358. doi:https://doi.org/10.1016/j.apenergy.2019.113335.

[8] L. Giovannini, F. Favoino, V.R.M. Lo Verso, A. Pellegrino, V. Serra, A simplified approach for the annual and spatial evaluation of the comfort classes of daylight glare using vertical illuminances, Buildings. 8 (2018). doi:10.3390/buildings8120171.

[9] R.C.G.M. Loonen, J.M. Rico-Martinez, F. Favoino, M. Brzezicki, C. Menezo, G. La Ferla, L. Aelenei, Design for facade adaptability - Towards a unified and systematic characterization, in: 10th Energy Forum -

Advanced Building Skins, Bern, Switzerland, 3-4 November, 2015: pp. 1274–1284.

[10] L. Giovannini, V. Serra, V.R.M. Lo Verso, A. Pellegrino, M. Zinzi, F. Favoino, A Novel Methodology to Optimize Visual Comfort and Energy Performance for Transparent Adaptive Façades, in: 18 IEEE International Conference on Environment and Electrical Engineering and 2018 IEEE Industrial and Commercial Power Systems Europe, EEEIC/I and CPS Europe 2018, 2018. doi:10.1109/EEEIC.2018.8494565.

[11] C.G. Granqvist, Transparent conductors as solar energy materials: A panoramic review, Solar Energy Materials and Solar Cells. 91 (2007) 1529–1598. doi:https://doi.org/10.1016/j.solmat.2007.04.031.

[12] C.G. Granqvist, Electrochromics and Thermochromics: Towards a New Paradigm for Energy Efficient Buildings, in: 5th International Conference on Functional Materials and Devices (ICFMD 2015), Johor Bahru, Malaysia, 4-6 August 2015, 2015: pp. S2–S11. doi:https://doi.org/10.1016/j.matpr.2016.01.002.

[13] P. Nitz, H. Hartwig, Solar control with thermotropic layers, Solar Energy. 79 (2005) 573–582. doi:https://doi.org/10.1016/j.solener.2004.12.009.

[14] O. Muehling, A. Seeboth, T. Haeusler, R. Ruhmann, E. Potechius, R. Vetter, Variable solar control using thermotropic core/shell particles, Solar Energy Materials and Solar Cells. 93 (2009) 1510–1517. doi:https://doi.org/10.1016/j.solmat.2009.03.029.

[15] M. Casini, Smart windows for energy efficiency of buildings, International Journal of Civil and Structural Engineering. 2 (2015) 273–281.

[16] M. Kamalisarvestani, R. Saidur, S. Mekhilef, F.S. Javadi, Performance, materials and coating technologies of thermochromic thin films on smart windows, Renewable and Sustainable Energy Reviews. 26 (2013) 353–364. doi:https://doi.org/10.1016/j.rser.2013.05.038.

[17] I.P. Parkin, R. Binions, C. Piccirillo, C.S. Blackman, T.D. Manning, Thermochromic Coatings for Intelligent Architectural Glazing, Journal of Nano Research. 2 (2008) 1–20. doi:10.4028/www.scientific.net/JNanoR.2.1.

[18] R. Binions, G. Hyett, C. Piccirillo, I.P. Parkin, Doped and un-doped vanadium dioxide thin films prepared by atmospheric pressure chemical vapour deposition from vanadyl acetylacetonate and tungsten hexachloride: the effects of thickness and crystallographic orientation on thermochromic properties, Journal of Materials Chemistry. 17 (2007) 4652–4660. doi:10.1039/B708856F.

[19] N. Wang, S. Liu, X.T. Zeng, S. Magdassi, Y. Long, Mg/W-codoped vanadium dioxide thin films with enhanced visible transmittance and low phase transition temperature, Journal of Materials Chemistry C. 3 (2015) 6771–6777. doi:10.1039/C5TC01062D.

[20] T.-C. Chang, X. Cao, S.-H. Bao, S.-D. Ji, H.-J. Luo, P. Jin, Review on thermochromic vanadium dioxide based smart coatings: from lab to commercial application, Advances in Manufacturing. 6 (2018) 1–19. doi:10.1007/s40436-017-0209-2.

[21] H.J. Byker, P.H. Ogburn Jr., D.A. Vander Griend, B.S. Veldkamp, D.D. Winkle, Ligand exchange thermochromic, (letc), systems, US Patent US7542196B2, n.d.

[22] M.S. Queen, Development of the molecular level descripton for nickel(II)-

based ligand-exchange thermochromism, Montana State University, Bozeman, MT, USA, 2014. https://scholarworks.montana.edu/xmlui/handle/1/8702.

[23] K. Allen, K. Connelly, P. Rutherford, Y. Wu, Smart windows - dynamic control of building energy performance, Energy and Buildings. 139 (2017) 535–546. doi:10.1016/j.enbuild.2016.12.093.

[24] A. Seeboth, R. Ruhmann, O. Muehling, Thermotropic and Thermochromic Polymer Based Materials for Adaptive Solar Control., Materials. 3 (2010) 5143–5168. doi:10.3390/ma3125143.

[25] X.-H. Li, C. Liu, S.-P. Feng, N.X. Fang, Broadband Light Management with Thermochromic Hydrogel Microparticles for Smart Windows, Joule. 3 (2019) 290–302. doi:https://doi.org/10.1016/j.joule.2018.10.019.

[26] Y. Zhou, Y. Cai, X. Hu, Y. Long, Temperature-responsive hydrogel with ultra-large solar modulation and high luminous transmission for "smart window" applications, Journal of Materials Chemistry A. 2 (2014) 13550–13555. doi:10.1039/C4TA02287D.

[27] F. Xin, Q. Lu, B. Liu, S. Yuan, R. Zhang, Y. Wu, Y. Yu, Metal-ion-mediated hydrogels with thermo-responsiveness for smart windows, European Polymer Journal. 99 (2018) 65–71. doi:https://doi.org/10.1016/j.eurpolymj.2017.12.008.

[28] A. Farghaly Yasser, Using Smart Materials to Reduce Energy Consumption in Bui/dings, in: 3rd Ain Shams University International Conference on Environmental Engineering, Cairo, Egypt, 14-16 April, 2009.

[29] W.S.E. Bahlol, Smart Glazing Systems for Low Energy Architecture, in: Sustainable Architecture and Urban Development (SB10 Amman), Amman, Jordan, 12-14 July, 2010: pp. 149–165.

[30] A. V. Dotsenko, L.B. Glebov, V.A. Tsechomsky, Physics and Chemistry of Photochromic Glasses, CRC Press, Taylor and Francis Group, Boca Raton, FL, USA, 1997.

[31] Q. Meng, G. Wang, H. Jiang, Y. Wang, S. Xie, Preparation of a fast photochromic ormosil matrix coating for smart windows, Journal of Materials Science. 48 (2013) 5862–5870. doi:10.1007/s10853-013-7382-x.

[32] P.J. Coelho, C.J.R. Silva, C. Sousa, S.D.F.C. Moreira, Fast and fully reversible photochromic performance of hybrid sol–gel films doped with a fused-naphthopyran, Journal of Materials Chemistry C. 1 (2013) 5387–5394. doi:10.1039/C3TC31223B.

[33] L.Y.L. Wu, Q. Zhao, H. Huang, R.J. Lim, Sol-gel based photochromic coating for solar responsive smart window, Surface and Coatings Technology. 320 (2017) 601–607. doi:https://doi.org/10.1016/j.surfcoat.2016.10.074.

[34] F. Goia, L. Bianco, Y. Cascone, M. Perino, V. Serra, Experimental Analysis of an Advanced Dynamic Glazing Prototype Integrating PCM and Thermotropic Layers, Energy Procedia. 48 (2014) 1272–1281. doi:https://doi.org/10.1016/j.egypro.2014.02.144.

[35] P.A. Fokaides, A. Kylili, S.A. Kalogirou, Phase change materials (PCMs) integrated into transparent building elements: a review, Materials for Renewable and Sustainable Energy. 4 (2015) 6. doi:10.1007/s40243-015-0047-8.

[36] B. Nghana, F. Tariku, Phase change material's (PCM) impacts on the energy performance and thermal comfort of buildings in a mild climate,

Building and Environment. 99 (2016) 221–238. doi:https://doi.org/10.1016/j.buildenv.2016.01.023.

[37] V.V. Tyagi, D. Buddhi, PCM thermal storage in buildings: A state of art, Renewable and Sustainable Energy Reviews. 11 (2007) 1146–1166. doi:https://doi.org/10.1016/j.rser.2005.10.002.

[38] R. Baetens, B.P. Jelle, A. Gustavsen, Phase change materials for building applications: A state-of-the-art review, Energy and Buildings. 42 (2010) 1361–1368. doi:https://doi.org/10.1016/j.enbuild.2010.03.026.

[39] I. Vigna, L. Bianco, F. Goia, V. Serra, Phase Change Materials in Transparent Building Envelopes: A Strengths, Weakness, Opportunities and Threats (SWOT) Analysis, Energies . 11 (2018). doi:10.3390/en11010111.

[40] F. Goia, M. Perino, V. Serra, Experimental analysis of the energy performance of a full-scale PCM glazing prototype, Solar Energy. 100 (2014) 217–233. doi:https://doi.org/10.1016/j.solener.2013.12.002.

[41] F. Goia, M. Zinzi, E. Carnielo, V. Serra, Spectral and angular solar properties of a PCM-filled double glazing unit, Energy and Buildings. 87 (2015) 302–312. doi:https://doi.org/10.1016/j.enbuild.2014.11.019.

[42] L. Giovannini, F. Goia, V.R.M. Lo Verso, V. Serra, A comparative analysis of the visual comfort performance between a PCM glazing and a conventional selective double glazed unit, Sustainability (Switzerland). 10 (2018). doi:10.3390/su10103579.

[43] R. Baetens, B.P. Jelle, A. Gustavsen, Properties, requirements and possibilities of smart windows for dynamic daylight and solar energy control in buildings: A state-of-the-art review, Solar Energy Materials and Solar Cells. 94 (2010) 87–105. doi:https://doi.org/10.1016/j.solmat.2009.08.021.

[44] E. Pehlivan, F.Z. Tepehan, G.G. Tepehan, Comparison of optical, structural and electrochromic properties of undoped and WO3-doped Nb2O5 thin films, Solid State Ionics. 165 (2003) 105–110. doi:https://doi.org/10.1016/j.ssi.2003.08.021.

[45] C.G. Granqvist, Introduction, in: C.G.B.T.-H. of I.E.M. Granqvist (Ed.), Elsevier Science B.V., Amsterdam, 1995: pp. 1–15. doi:https://doi.org/10.1016/B978-044489930-9/50001-5.

[46] P. Schlotter, G.M. Baur, R. Schmidt, U. Weinberg, Laminated electrochromic device for smart windows, in: Proc.SPIE, 1994. https://doi.org/10.1117/12.185378.

[47] B.P. Jelle, T. Gao, The Utilization of Electrochromic Materials for Smart Window Applications in Energy-Efficient Buildings, in: TechConnect World Innovation Conference 2015, Washington, USA, 14-17 June, 2015: pp. 226–229.

[48] S. Papaefthimiou, Chromogenic technologies: Towards the realization of smart electrochromic glazing for energy-saving applications in buildings, Advances in Building Energy Research. 4 (2010) 77–126. doi:10.3763/aber.2009.0404.

[49] A. Cannavale, G.E. Eperon, P. Cossari, A. Abate, H.J. Snaith, G. Gigli, Perovskite photovoltachromic cells for building integration, Energy & Environmental Science. 8 (2015) 1578–1584. doi:10.1039/C5EE00896D.

[50] G. Garcia, R. Buonsanti, A. Llordes, E.L. Runnerstrom, A. Bergerud, D.J. Milliron, Near-Infrared Spectrally Selective Plasmonic Electrochromic

Thin Films, Advanced Optical Materials. 1 (2013) 215–220. doi:10.1002/adom.201200051.
[51] C.J. Dahlman, Y. Tan, M.A. Marcus, D.J. Milliron, Spectroelectrochemical Signatures of Capacitive Charging and Ion Insertion in Doped Anatase Titania Nanocrystals, Journal of the American Chemical Society. 137 (2015) 9160–9166. doi:10.1021/jacs.5b04933.
[52] H. Gu, C. Guo, S. Zhang, L. Bi, T. Li, T. Sun, S. Liu, Highly Efficient, Near-Infrared and Visible Light Modulated Electrochromic Devices Based on Polyoxometalates and W18O49 Nanowires, ACS Nano. 12 (2018) 559–567. doi:10.1021/acsnano.7b07360.
[53] A. Llordés, G. Garcia, J. Gazquez, D.J. Milliron, Tunable near-infrared and visible-light transmittance in nanocrystal-in-glass composites, Nature. 500 (2013) 323. https://doi.org/10.1038/nature12398.
[54] W. Feng, L. Zou, G. Gao, G. Wu, J. Shen, W. Li, Gasochromic smart window: optical and thermal properties, energy simulation and feasibility analysis, Solar Energy Materials and Solar Cells. 144 (2016) 316–323. doi:https://doi.org/10.1016/j.solmat.2015.09.029.
[55] M. Schwartz, Smart Materials, CRC Press, Taylor and Francis Group, Boca Raton, FL, USA, 2008.
[56] V. Wittwer, M. Datz, J. Ell, A. Georg, W. Graf, G. Walze, Gasochromic windows, Solar Energy Materials and Solar Cells. 84 (2004) 305–314. doi:https://doi.org/10.1016/j.solmat.2004.01.040.
[57] R. Ghosh, M.B. Baker, R. Lopez, Optical properties and aging of gasochromic WO3, Thin Solid Films. 518 (2010) 2247–2249. doi:https://doi.org/10.1016/j.tsf.2009.08.003.
[58] S. Chakrapani, S.M. Slovak, R.L. Saxe, B. Fanning, SPD films and light valves comprising same, 2002.
[59] A. Ghosh, B. Norton, A. Duffy, Measured overall heat transfer coefficient of a suspended particle device switchable glazing, Applied Energy. 159 (2015) 362–369. doi:https://doi.org/10.1016/j.apenergy.2015.09.019.
[60] D.J. Gardiner, S.M. Morris, H.J. Coles, High-efficiency multistable switchable glazing using smectic A liquid crystals, Solar Energy Materials and Solar Cells. 93 (2009) 301–306. doi:https://doi.org/10.1016/j.solmat.2008.10.023.
[61] Y. Kim, D. Jung, S. Jeong, K. Kim, W. Choi, Y. Seo, Optical properties and optimized conditions for polymer dispersed liquid crystal containing UV curable polymer and nematic liquid crystal, Current Applied Physics. 15 (2015) 292–297. doi:https://doi.org/10.1016/j.cap.2014.12.027.
[62] D. Barrios, R. Vergaz, J.M. Sanchez-Pena, B. Garcia-Camara, C.-G. Granqvist, G.A. Niklasson, Simulation of the thickness dependence of the optical properties of suspended particle devices, Solar Energy Materials and Solar Cells. 143 (2015) 613–622. doi:10.1016/j.solmat.2015.05.044i.
[63] S.D. Rezaei, S. Shannigrahi, S. Ramakrishna, A review of conventional, advanced, and smart glazing technologies and materials for improving indoor environment, Solar Energy Materials and Solar Cells. 159 (2017) 26–51. doi:https://doi.org/10.1016/j.solmat.2016.08.026.
[64] F. Favoino, M. Overend, Q. Jin, The optimal thermo-optical properties and energy saving potential of adaptive glazing technologies, Applied Energy. 156 (2015) 1–15. doi:https://doi.org/10.1016/j.apenergy.2015.05.065.
[65] F. Favoino, Simulation-Based Evaluation of Adaptive Materials for

Improved Building Performance, in: F. Pacheco Torgal, C. Buratti, S. Kalaiselvam, C.-G. Granqvist, V. Ivanov (Eds.), Nano and Biotech Based Materials for Energy Building Efficiency, Springer International Publishing, Cham, Switzerland, 2016: pp. 125–166. doi:10.1007/978-3-319-27505-5_6.

[66] Lawrence Berkeley National Laboratory, International Glazing Database (IGDB), (n.d.). https://windows.lbl.gov/software/igdb (accessed 9 April 2019).

[67] C.G. Granqvist, Recent progress in thermochromics and electrochromics: A brief survey, Thin Solid Films. 614 (2016) 90–96. doi:https://doi.org/10.1016/j.tsf.2016.02.029.

[68] B.P. Jelle, A. Hynd, A. Gustavsen, D. Arasteh, H. Goudey, R. Hart, Fenestration of today and tomorrow: A state-of-the-art review and future research opportunities, Solar Energy Materials and Solar Cells. 96 (2012) 1–28. doi:https://doi.org/10.1016/j.solmat.2011.08.010.

[69] F. Favoino, F. Fiorito, A. Cannavale, G. Ranzi, M. Overend, Optimal control and performance of photovoltachromic switchable glazing for building integration in temperate climates, Applied Energy. 178 (2016) 943–961. doi:10.1016/j.apenergy.2016.06.107.

[70] F. Gugliermetti, F. Bisegna, Visual and energy management of electrochromic windows in Mediterranean climate, Building and Environment. 38 (2003) 479–492. doi:10.1016/S0360-1323(02)00124-5.

[71] M. Zinzi, Office worker preferences of electrochromic windows: a pilot study, Building and Environment. 41 (2006) 1262–1273. doi:https://doi.org/10.1016/j.buildenv.2005.05.010.

[72] J.-M. Dussault, M. Sourbron, L. Gosselin, Reduced energy consumption and enhanced comfort with smart windows: Comparison between quasi-optimal, predictive and rule-based control strategies, Energy and Buildings. 127 (2016) 680–691. doi:https://doi.org/10.1016/j.enbuild.2016.06.024.

[73] G. Serale, M. Fiorentini, A. Capozzoli, D. Bernardini, A. Bemporad, Model Predictive Control (MPC) for Enhancing Building and HVAC System Energy Efficiency: Problem Formulation, Applications and Opportunities, Energies . 11 (2018). doi:10.3390/en11030631.

[74] A. Khakimova, A. Kusatayeva, A. Shamshimova, D. Sharipova, A. Bemporad, Y. Familiant, A. Shintemirov, V. Ten, M. Rubagotti, Optimal energy management of a small-size building via hybrid model predictive control, Energy and Buildings. 140 (2017) 1–8. doi:https://doi.org/10.1016/j.enbuild.2017.01.045.

[75] P.T. May-Ostendorp, G.P. Henze, B. Rajagopalan, D. Kalz, Experimental investigation of model predictive control-based rules for a radiantly cooled office, HVAC&R Research. 19 (2013) 602–615. doi:10.1080/10789669.2013.801303.

[76] Y. Ma, F. Borrelli, B. Hencey, B. Coffey, S. Bengea, P. Haves, Model Predictive Control for the Operation of Building Cooling Systems, IEEE Transactions on Control Systems Technology. 20 (2012) 796–803. doi:10.1109/TCST.2011.2124461.

[77] B.E. Coffey, Integrated control of operable fenestration systems and thermally massive HVAC systems: Methods and simulation studies of energy savings potential, 2012.

[78] A. Roos, J. Karlsson, B. Karlsson, Control strategies and energy saving

potentials for variable transmittance windows versus static windows, in: EuroSun 2000:ISES Europe Solar Congress, Copenhagen, Denmark, June, 2000.

[79] K. J, Control system and energy saving potential for switchable windows, in: 7th International IBPSA (International Building Performance Simulation Association) Conference—Building Simulation, Rio de Janeiro, Brazil; 13-15 August, 2001: pp. 199–206.

[80] M.N. Assimakopoulos, A. Tsangrassoulis, M. Santamouris, G. Guarracino, Comparing the energy performance of an electrochromic window under various control strategies, Building and Environment. 42 (2007) 2829–2834. doi:https://doi.org/10.1016/j.buildenv.2006.04.004.

[81] E.S. Lee, A. Tavil, Energy and visual comfort performance of electrochromic windows with overhangs, Building and Environment. 42 (2007) 2439–2449. doi:10.1016/j.buildenv.2006.04.016.

[82] N. DeForest, A. Shehabi, S. Selkowitz, D.J. Milliron, A comparative energy analysis of three electrochromic glazing technologies in commercial and residential buildings, Applied Energy. 192 (2017) 95–109. doi:https://doi.org/10.1016/j.apenergy.2017.02.007.

[83] C.-S. Park, G. Augenbroe, Local vs. integrated control strategies for double-skin systems, Automation in Construction. 30 (2013) 50–56. doi:https://doi.org/10.1016/j.autcon.2012.11.030.

[84] R. Sullivan, E.S. Lee, K. Papamichael, M. Rubin, S.E. Selkowitz, Effect of switching control strategies on the energy performance of electrochromic windows, in: V. Wittwer, C.G. Granqvist, C.M. Lampert (Eds.), Optical Materials Technology for Energy Efficiency and Solar Energy Conversion XIII, Society of Photo-Optical Instrumentation Engineers, Freiburg, Germany, 18-22 April, 1994: pp. 443–455. doi:10.1117/12.185387.

[85] Belzer, D. B., An Exploratory Energy Analysis of Electrochromic Windows in Small and Medium Office Buildings - Simulated Results Using EnergyPlus, United States, 2010. doi:10.2172/1025691.

[86] R.C.G.M. Loonen, J.L.M. Hensen, Smart windows with dynamic spectral selectivity - A scoping study, in: 14th International IBPSA (International Building Performance Simulation Association) Conference—Building Simulation, International Building Performance Simulation Association, Hyderabad, India; 7-9 December, 2015: pp. 2158–2165.

[87] A. Jonsson, A. Roos, Evaluation of control strategies for different smart window combinations using computer simulations, Solar Energy. 84 (2010) 1–9. doi:https://doi.org/10.1016/j.solener.2009.10.021.

[88] E.S. Lee, E.S. Claybaugh, M. LaFrance, End user impacts of automated electrochromic windows in a pilot retrofit application, Energy and Buildings. 47 (2012) 267–284. doi:10.1016/J.ENBUILD.2011.12.003.

[89] R.C.G.M. Loonen, S. Singaravel, M. Trčka, D. Cóstola, J.L.M. Hensen, Simulation-based support for product development of innovative building envelope components, Automation in Construction. 45 (2014) 86–95. doi:10.1016/j.autcon.2014.05.008.

[90] H. Khandelwal, R.C.G.M. Loonen, J.L.M. Hensen, M.G. Debije, A.P.H.J. Schenning, Electrically switchable polymer stabilised broadband infrared reflectors and their potential as smart windows for energy saving in buildings, Scientific Reports. 5 (2015). doi:10.1038/srep11773.

[91] Paladino & Company, Performance Assessment of SageGlass®

Electrochromic Coatings and Control Scenarios, (2010). https://www.sageglass.com/sites/default/files/whitepaper_final.pdf.
[92] P.C. da Silva, V. Leal, M. Andersen, Influence of shading control patterns on the energy assessment of office spaces, Energy and Buildings. 50 (2012) 35–48. doi:https://doi.org/10.1016/j.enbuild.2012.03.019.
[93] E.S. Lee, D.L. DiBartolomeo, Application issues for large-area electrochromic windows in commercial buildings, Solar Energy Materials and Solar Cells. 71 (2002) 465–491. doi:https://doi.org/10.1016/S0927-0248(01)00101-5.
[94] D.L. DiBartolomeo, J.H. Klems, E.S. Lee, S.E. Selkowitz, M. Yazdanian, Monitored energy performance of electrochromic windows controlled for daylight and visual comfort, in: ASHRAE Transactions, Amer. Soc. Heating, Ref. Air-Conditoning Eng. Inc., Quebec City, QC, Canada, 24-28 June, 2006: pp. 122–141. http://go.galegroup.com/ps/i.do?id=GALE%7CA156720150&v=2.1&u=capes58&it=r&p=AONE&sw=w&asid=397af26da49df926024fc3355e16856b.
[95] European Committee for Standardization (CEN), EN 12464-1, Light and Lighting. Lighting of Work Places. Part 1: Indoor Work Places, (2011).
[96] D. Jestico, Performance assessment of sageglass electronically tintable glazing, in: L. Rodrigues (Ed.), Sustainable Energy for a Resilient Future: Proceedings of the 14th International Conference on Sustainable Energy Technologies, Nottingham, UK; 25-27 August, 2015: pp. 256–265.
[97] S. Firląg, M. Yazdanian, C. Curcija, C. Kohler, S. Vidanovic, R. Hart, S. Czarnecki, Control algorithms for dynamic windows for residential buildings, Energy and Buildings. 109 (2015) 157–173. doi:https://doi.org/10.1016/j.enbuild.2015.09.069.
[98] M.N. Assimakopoulos, A. Tsangrassoulis, G. Guarracino, M. Santamouris, Integrated energetic approach for a controlable electrochromic device, Energy and Buildings. 36 (2004) 415–422. doi:10.1016/j.enbuild.2004.01.040.
[99] A. Tzempelikos, H. Shen, Comparative control strategies for roller shades with respect to daylighting and energy performance, Building and Environment. 67 (2013) 179–192. doi:https://doi.org/10.1016/j.buildenv.2013.05.016.
[100] R.G. Hopkinson, Glare from daylighting in buildings, Applied Ergonomics. 3 (1972) 206–215. doi:10.1016/0003-6870(72)90102-0.
[101] R.G. Hopkinson, J.B. Collins, The Ergonomics of Lighting, McDdonald & Company, Londo, UK, 1970.
[102] R.G. Hopkinson, Glare from windows, Journal of Construction Research and Development. 2 (1970) 98–105.
[103] P. Petherbridge, J. Longmore, Solid angles applied to visual comfort problems., Light and Lighting. 55 (1962) 146–158.
[104] J.-H. Kim, Y.-J. Park, M.-S. Yeo, K.-W. Kim, An experimental study on the environmental performance of the automated blind in summer, Building and Environment. 44 (2009) 1517–1527. doi:https://doi.org/10.1016/j.buildenv.2008.08.006.
[105] G. Yun, K.C. Yoon, K.S. Kim, The influence of shading control strategies on the visual comfort and energy demand of office buildings, Energy and Buildings. 84 (2014) 70–85.

doi:https://doi.org/10.1016/j.enbuild.2014.07.040.
[106] M. Husser, W. Haase, W. Sobek, Subdivided switchable sun protection glazing, Glass Structures & Engineering. (2018). doi:10.1007/s40940-018-0087-4.
[107] C.F. Reinhart, Lightswitch-2002: a model for manual and automated control of electric lighting and blinds, Solar Energy. 77 (2004) 15–28. doi:https://doi.org/10.1016/j.solener.2004.04.003.
[108] N. Aste, J. Compostella, M. Mazzon, Comparative energy and economic performance analysis of an electrochromic window and automated external venetian blind, Energy Procedia. 30 (2012) 404–413. doi:https://doi.org/10.1016/j.egypro.2012.11.048.
[109] C.E. Waters, R.G. Mistrick, C.A. Bernecker, Discomfort Glare from Sources of Nonuniform Luminance, Journal of the Illuminating Engineering Society. 24 (1995) 73–85. doi:10.1080/00994480.1995.10748120.
[110] EnergyPlus, (n.d.). https://energyplus.net/.
[111] J. Wienold, J. Christoffersen, Evaluation methods and development of a new glare prediction model for daylight environments with the use of CCD cameras, Energy and Buildings. 38 (2006) 743–757. doi:10.1016/J.ENBUILD.2006.03.017.
[112] C. Goovaerts, F. Descamps, V.A. Jacobs, Shading control strategy to avoid visual discomfort by using a low-cost camera: A field study of two cases, Building and Environment. 125 (2017) 26–38. doi:https://doi.org/10.1016/j.buildenv.2017.08.030.
[113] P. Tavares, H. Bernardo, A. Gaspar, A. Martins, Control criteria of electrochromic glasses for energy savings in mediterranean buildings refurbishment, Solar Energy. 134 (2016) 236–250. doi:https://doi.org/10.1016/j.solener.2016.04.022.
[114] P.F. Tavares, A.R. Gaspar, A.G. Martins, F. Frontini, Evaluation of electrochromic windows impact in the energy performance of buildings in Mediterranean climates, Energy Policy. 67 (2014) 68–81. doi:https://doi.org/10.1016/j.enpol.2013.07.038.
[115] L. Chiaraviglio, Assessment of Discomfort Glare in Daylit Rooms with Shading Devices: Results from a Field Study and Comparison with Software Simulation, Politecnico di Torino, Turin, Italy, 2009.
[116] P. Chauvel, J.B. Collins, R. Dogniaux, J. Longmore, Glare from windows: Current views of the problem, Lighting Research & Technology. 14 (1982) 31–46. doi:10.1177/096032718201400103.
[117] T. Iwata, M. Shukuja, N. Somekawa, K. Kimura, Experimental study on discomfort glare caused by windows—Part 1: Subjective response to glare from a simulated window, Journal of Architecture, Planning and Environmental Engineering (Transactions of AIJ). 432 (1992) 21–33. doi:10.3130/aijax.432.0_21.
[118] T. Iwata, M. Shukuja, N. Somekawa, K. Kimura, Experimental study on discomfort glare caused by windows—Part 2: Subjective response to glare from actual windows, Journal of Architecture, Planning and Environmental Engineering (Transactions of AIJ). 439 (1992) 19–31. doi:10.3130/aijax.439.0_19.
[119] M. Boubekri, L.L. Boyer, Optimization of window design for thermal, lighting and occupant appraisal considerations, in: ISES (International

Solar Energy Society) Solar World Congress (SWC1991), Denver, CO, USA, 19-23 August, 1991.
[120] W.K.E. Osterhaus, Discomfort glare assessment and prevention for daylight applications in office environments, Solar Energy. 79 (2005) 140–158. doi:10.1016/J.SOLENER.2004.11.011.
[121] M. Velds, Assessment of Lighting Quality in Office Rooms with Daylighting Systems, Delft University of Technology, Delft, The Netherlands, 1999.
[122] W.K.E. Osterhaus, Brightness as a simple indicator for discomfort glare from large area glare sources, in: First CIE Symposium on Lighting Quality, Ottawa, ON, Canada, 9-10 May, 1998: pp. 113–124.
[123] Radiance, (n.d.). https://www.radiance-online.org (accessed 3 December 2018).
[124] Evalglare, (n.d.). https://www.radiance-online.org/learning/documentation/manual-pages/pdfs/evalglare.pdf/view (accessed 3 December 2018).
[125] J. Suk, M. Schiler, Investigation of Evalglare software, daylight glare probability and high dynamic range imaging for daylight glare analysis, in: Lighting Research & Technology, SAGE Publications Ltd, 2013: pp. 450–463. doi:10.1177/1477153512458671.
[126] C. Pierson, J. Wienold, M. Bodart, Daylight discomfort glare evaluation with evalglare: Influence of parameters and methods on the accuracy of discomfort glare prediction, Buildings. 8 (2018) 94. doi:10.3390/buildings8080094.
[127] I. Konstantzos, A. Tzempelikos, Y.-C. Chan, Experimental and simulation analysis of daylight glare probability in offices with dynamic window shades, Building and Environment. 87 (2015) 244–254. doi:10.1016/J.BUILDENV.2015.02.007.
[128] B. Matusiak, K. Angelo, How to avoid glare from translucent façades?, in: 27th Session of CIE International Conference, Sun City, South Africa, 9-16 July, 2011.
[129] L. Brotas, J. Wienold, Solar reflected glare affecting visual performance, in: 8th Windsor Conference: Counting the Cost of Comfort in a Changing World, Windson, UK, 10-13 April, 2014.
[130] A. Borisuit, J.-L. Scartezzini, A. Thanachareonkit, Visual discomfort and glare rating assessment of integrated daylighting and electric lighting systems using HDR imaging techniques, Architectural Science Review. 53 (2010) 359–373.
[131] J. Mardaljevic, Climate-Based Daylight Analysis, (2008) 3–26.
[132] C.F. Reinhart, J. Mardaljevic, Z. Rogers, Dynamic daylight performance metrics for sustainable building design, Leukos. 3 (2006) 7–31.
[133] J. Wienold, Dynamic daylight glare evaluation, in: 11th International IBPSA (International Building Performance Simulation Association) Conference—Building Simulation, Glasgow, Scotland, 27-30 July, 2009: pp. 944–951.
[134] J. Wienold, Dynamic simulation of blind control strategies for visual comfort and energy balance analysis, in: 10th International IBPSA (International Building Performance Simulation Association) Conference—Building Simulation, Beijing, China, 3-6 September, 2007: pp. 1197–1204.
[135] S. Kleindienst, M. Andersen, The adaptation of daylight glare probability to

dynamic metrics in a computational setting, in: 1th European Lighting Conference (Lux Europa 2009), Istambul, Turkey, 9-11 September, 2009.
[136] J. M. L. Gagne, M. Andersen, Multi-Objective Façade Optimization for Daylighting Design Using a Genetic Algorithm, in: SimBuild 2010, Fourth National Conference of IBPSA-USA, New York, NY, USA, 11-13 August, 2010.
[137] S. Kleindienst, M. Andersen, Comprehensive annual daylight design through a goal-based approach, Building Research & Information. 40 (2012) 154–173.
[138] Lightsolve, (n.d.). http://lightsolve.epfl.ch/ (accessed 3 December 2018).
[139] L. Bellia, A. Cesarano, G.F. Iuliano, G. Spada, Daylight glare: A review of discomfort indexes., in: Visual Quality and Energy Efficiency in Indoor Lighting: Today for Tomorrow, Rome, Italy, 31 March - 2 April, 2008.
[140] A. Nabil, J. Mardaljevic, Useful daylight illuminance: A new paradigm for assessing daylight in buildings, Lighting Research & Technology. 37 (2005) 41–59. doi:10.1191/1365782805li128oa.
[141] A. Nabil, J. Mardaljevic, Useful daylight illuminances: A replacement for daylight factors, Energy and Buildings. 38 (2006) 905–913. doi:https://doi.org/10.1016/j.enbuild.2006.03.013.
[142] IES Daylight Metrics Committee, IES Lighting Measurements (LM) 83-12, Approved Method: IES Spatial Daylight Autonomy (sDA) and Annual Sunlight Exposure (ASE), (2012).
[143] S. Carlucci, F. Causone, F. De Rosa, L. Pagliano, A review of indices for assessing visual comfort with a view to their use in optimization processes to support building integrated design, Renewable and Sustainable Energy Reviews. 47 (2015) 1016–1033.
[144] S. Torres, V.R.M. Lo Verso, Comparative Analysis of Simplified Daylight Glare Methods and Proposal of a new Method Based on the Cylindrical Illuminance, Energy Procedia. 78 (2015) 699–704. doi:https://doi.org/10.1016/j.egypro.2015.11.074.
[145] J. Mardaljevic, M. Andersen, N. Roy, J. Christoffersen, Daylighting metrics: is there a relation between useful daylight illuminance and daylight glare probability?, in: First IBPSA-England Conference on "Building Simulation and Optimization", Loughborough, UK, 10–11 September, 2012.
[146] R.C.G.M. Loonen, F. Favoino, J.L.M. Hensen, M. Overend, Review of current status, requirements and opportunities for building performance simulation of adaptive facades †, Journal of Building Performance Simulation. 10 (2017) 205–223. doi:10.1080/19401493.2016.1152303.
[147] N. DeForest, A. Shehabi, G. Garcia, J. Greenblatt, E. Masanet, E.S. Lee, S. Selkowitz, D.J. Milliron, Regional performance targets for transparent near-infrared switching electrochromic window glazings, Building and Environment. 61 (2013) 160–168. doi:https://doi.org/10.1016/j.buildenv.2012.12.004.
[148] M.E.A. Warwick, I. Ridley, R. Binions, The effect of variation in the transition hysteresis width and gradient in thermochromic glazing systems, Solar Energy Materials and Solar Cells. 140 (2015) 253–265. doi:https://doi.org/10.1016/j.solmat.2015.04.022.
[149] IES Virtual Environment (IESVE), (n.d.). https://www.iesve.com/software.
[150] IDA Indoor Climate and Energy (IDA ICE), (n.d.).

https://www.equa.se/en/ida-ice.
[151] P.R. Tregenza, Daylighting computation: Radiosity method using triangular patches, Lighting Research & Technology. 26 (1994) 1–7. doi:doi.org/10.1177/096032719402600101.
[152] P.R. Tregenza, Mean daylight illuminance in rooms facing sunlit streets, Building and Environment. 30 (1995) 83–89. doi:https://doi.org/10.1016/0360-1323(94)E0006-D.
[153] B.Y. Yoon, R.W. Jeong, H.K. Lee, Window Material Daylighting Performance Assessment Algorithm: Comparing Radiosity and Split-Flux Methods, Energies . 7 (2014). doi:10.3390/en7042362.
[154] B.Y. Yoon, R. Manandhar, H.K. Lee, Comparative Study of Two Daylighting Analysis Methods with Regard to Window Orientation and Interior Wall Reflectance, Energies . 7 (2014). doi:10.3390/en7095825.
[155] DAYSIM, (n.d.). https://daysim.ning.com (accessed 25 January 2019).
[156] C.F. Reinhart, M. Andersen, Development and validation of a Radiance model for a translucent panel, Energy and Buildings. 38 (2006) 890–904. doi:https://doi.org/10.1016/j.enbuild.2006.03.006.
[157] C. Reinhart, P.-F. Breton, Experimental Validation of Autodesk® 3ds Max® Design 2009 and Daysim 3.0, LEUKOS. 6 (2009) 7–35. doi:10.1582/LEUKOS.2009.06.01001.
[158] G. Ramos, E. Ghisi, Analysis of daylight calculated using the EnergyPlus programme, Renewable and Sustainable Energy Reviews. 14 (2010) 1948–1958. doi:https://doi.org/10.1016/j.rser.2010.03.040.
[159] P.R. Tregenza, I.M. Waters, Daylight coefficients, Lighting Research & Technology. 15 (1983) 65–71. doi:10.1177/096032718301500201.
[160] D. Bourgeois, C.F. Reinhart, G. Ward, Standard daylight coefficient model for dynamic daylighting simulations, Building Research and Information. 36 (2008) 68–82. doi:10.1080/09613210701446325.
[161] M. Wetter, Co-simulation of building energy and control systems with the Building Controls Virtual Test Bed, Journal of Building Performance Simulation. 4 (2011) 185–203. doi:10.1080/19401493.2010.518631.
[162] W. Bustamante, D. Uribe, S. Vera, G. Molina, An integrated thermal and lighting simulation tool to support the design process of complex fenestration systems for office buildings, Applied Energy. 198 (2017) 36–48. doi:https://doi.org/10.1016/j.apenergy.2017.04.046.
[163] G. Molina, Integrated thermal and lighting analysis of spaces with controlled complex fenestration systems and artificial lighting during the design stage, Pontificia Universidad Católica de Chile, Santiago, Chile, 2014.
[164] S. Hoffmann, E.S. Lee, A. McNeil, L. Fernandes, D. Vidanovic, A. Thanachareonkit, Balancing daylight, glare, and energy-efficiency goals: An evaluation of exterior coplanar shading systems using complex fenestration modeling tools, Energy and Buildings. 112 (2016) 279–298. doi:https://doi.org/10.1016/j.enbuild.2015.12.009.
[165] G. De Michele, U.F. Oberegger, L. Baglivo, Building Simulation Applications, in: BSA 2015, the Second IBPSA-Italy Conference on “Building Simulation Applications", Bozen-Bolzano, Italy,4-6 February, 2015: pp. 289–296.
[166] M. Janak, Coupling building energy and lighting simulation, Prague, Czech Republic, 8-10 September, 1997.

[167] J. Wienold, F. Frontini, S. Herkel, S. Mende, Climate based simulation of different shading device systems for comfort and energy demand, Sydney, Australia, 14-16 November, 2011.
[168] A. Tzempelikos, A.K. Athienitis, The impact of shading design and control on building cooling and lighting demand, Solar Energy. 81 (2007) 369–382. doi:https://doi.org/10.1016/j.solener.2006.06.015.
[169] R.C.G.M. Loonen, Approaches for computational performance optimization of innovative adaptive façade concepts, Eindhoven University of Technology (TUe), Eindhoven, The Netherlands, 2018.
[170] BCVTB - Building Controls Virtual Test Bed, (n.d.). https://simulationresearch.lbl.gov/bcvtb.
[171] National Renewable Energy Laboratory (NREL), Energy plus, application guide for EMS. Energy Management System User Guide, (2013).
[172] MATLAB, (n.d.). https://mathworks.com/products/matlab.html.
[173] GenOpt, (n.d.). https://simulationresearch.lbl.gov/GO/.
[174] M. Baracani, L. Giovannini, V. Serra, F. Favoino, Control of dynamic glazing in heating dominated climate for office buildings: contrasting occupant visual comfort requirements with energy use, in: 51th AiCARR International Conference - The Human Dimension of Building Energy Performance, Associazione Italiana Condizionamento dell'Aria Riscaldamento e Refrigerazione (AiCARR), Venice, Italy, 20-22 February, 2019.
[175] Python, (n.d.). https://www.python.org/ (accessed 25 January 2019).
[176] Rhinoceros, (n.d.). https://www.rhino3d.com (accessed 25 January 2019).
[177] Grasshoper, (n.d.). https://www.grasshopper3d.com/ (accessed 25 January 2019).
[178] Ladybug Tools, (n.d.). https://www.ladybug.tools (accessed 25 January 2019).
[179] C. Tian, T. Chen, T. Chung, Experimental and simulating examination of computer tools, Radlink and DOE2, for daylighting and energy simulation with venetian blinds, Applied Energy. 124 (2014) 130–139. doi:10.1016/J.APENERGY.2014.03.002.
[180] F. Favoino, Y. Cascone, L. Bianco, F. Goia, M. Zinzi, M. Overend, Simulating switchable glazing with EnergyPlus: an empirical validation and calibration of a thermotropic glazing model, in: 14th International IBPSA (International Building Performance Simulation Association) Conference—Building Simulation, Hyderabad, India; 7-9 December, 2015: pp. 2833–2840.
[181] P.G. Loutzenhiser, H. Manz, S. Moosberger, G.M. Maxwell, An empirical validation of window solar gain models and the associated interactions, International Journal of Thermal Sciences. 48 (2009) 85–95. doi:10.1016/J.IJTHERMALSCI.2008.01.011.
[182] American Society for Heating Refrigerating Air-conditioning Engineers (ASHRAE), Standard 140 - Standard method of test for the evaluation of building energy analysis computer programs, (2011).
[183] J. Mardaljevic, Daylight simulation: validation, sky models and daylight coefficients, Loughborough University, Loughborough (UK), 2000.
[184] C.F. Reinhart, O. Walkenhorst, Validation of dynamic RADIANCE-based daylight simulations for a test office with external blinds, Energy and Buildings. 33 (2001) 683–697. doi:10.1016/S0378-7788(01)00058-5.

[185] Q. Jin, F. Favoino, M. Overend, Design and control optimisation of adaptive insulation systems for office buildings. Part 2: A parametric study for a temperate climate, Energy. 127 (2017) 634–649. doi:https://doi.org/10.1016/j.energy.2017.03.096.
[186] M.E.A. Warwick, I. Ridley, R. Binions, Variation of thermochromic glazing systems transition temperature, hysteresis gradient and width effect on energy efficiency, Buildings. 6 (2016). doi:10.3390/buildings6020022.
[187] V. Costanzo, G. Evola, L. Marletta, Thermal and visual performance of real and theoretical thermochromic glazing solutions for office buildings, Solar Energy Materials and Solar Cells. 149 (2016) 110–120. doi:https://doi.org/10.1016/j.solmat.2016.01.008.
[188] C. Sol, J. Schläfer, I.P. Parkin, I. Papakonstantinou, Mitigation of hysteresis due to a pseudo-photochromic effect in thermochromic smart window coatings, Scientific Reports. 8:13249 (2018). doi:10.1038/s41598-018-31519-x.
[189] J.L.M. Hensen, R.C.G.M. Loonen, M. Archontiki, M. Kanellis, Using building simulation for moving innovations across the 'Valley of Death', REHVA Journal. 52 (2015) 58–62.
[190] X. Cao, N. Wang, S. Magdassi, D. Mandler, Y. Long, Europium doped vanadium dioxide material: Reduced phase transition temperature, enhanced luminous transmittance and solar modulation, Science of Advanced Materials. 6 (2014) 558–561. doi:10.1166/sam.2014.1777.
[191] N.R. Mlyuka, G.A. Niklasson, C.G. Granqvist, Thermochromic multilayer films of VO2 and TiO2 with enhanced transmittance, Solar Energy Materials and Solar Cells. 93 (2009) 1685–1687. doi:https://doi.org/10.1016/j.solmat.2009.03.021.
[192] L. Zhao, L. Miao, C. Liu, C. Li, T. Asaka, Y. Kang, Y. Iwamoto, S. Tanemura, H. Gu, H. Su, Solution-processed VO2-SiO2 composite films with simultaneously enhanced luminous transmittance, solar modulation ability and anti-oxidation property, Scientific Reports. 4:7000 (2014). doi:10.1038/srep07000.
[193] Y. Cui, Y. Ke, C. Liu, Z. Chen, N. Wang, L. Zhang, Y. Zhou, S. Wang, Y. Gao, Y. Long, Thermochromic VO2 for Energy-Efficient Smart Windows, Joule. 2 (2018) 1707–1746. doi:10.1016/j.joule.2018.06.018.
[194] H. Tang, D.C. MacLaren, M.A. White, New insights concerning the mechanism of reversible thermochromic mixtures, Canadian Journal of Chemistry. 88 (2010) 1063–1070. doi:10.1139/V10-069.
[195] H.Y. Lee, Y. Cai, S. Velioglu, C. Mu, C.J. Chang, Y.L. Chen, Y. Song, J.W. Chew, X.M. Hu, Thermochromic Ionogel: A New Class of Stimuli Responsive Materials with Super Cyclic Stability for Solar Modulation, Chemistry of Materials. 29 (2017) 6947–6955. doi:10.1021/acs.chemmater.7b02402.
[196] Y. Zhou, Y. Cai, X. Hu, Y. Long, VO2/hydrogel hybrid nanothermochromic material with ultra-high solar modulation and luminous transmission, Journal of Materials Chemistry A. 3 (2015) 1121–1126. doi:10.1039/c4ta05035e.
[197] Y.-S. Yang, Y. Zhou, F.B.Y. Chiang, Y. Long, Tungsten doped VO2/microgels hybrid thermochromic material and its smart window application, RSC Advances. 7 (2017) 7758–7762. doi:10.1039/c6ra24686a.
[198] J. Zhu, A. Huang, H. Ma, Y. Ma, K. Tong, S. Ji, S. Bao, X. Cao, P. Jin,

Composite Film of Vanadium Dioxide Nanoparticles and Ionic Liquid-Nickel-Chlorine Complexes with Excellent Visible Thermochromic Performance, ACS Applied Materials and Interfaces. 8 (2016) 29742–29748. doi:10.1021/acsami.6b11202.

[199] J. Zhu, A. Huang, H. Ma, Y. Chen, S. Zhang, S. Ji, S. Bao, P. Jin, Hybrid films of VO2 nanoparticles and a nickel(ii)-based ligand exchange thermochromic system: excellent optical performance with a temperature responsive colour change, New Journal of Chemistry. 41 (2017) 830–835. doi:10.1039/C6NJ03369E.

[200] Y. Gao, H. Luo, Z. Zhang, L. Kang, Z. Chen, J. Du, M. Kanehira, C. Cao, Nanoceramic VO2 thermochromic smart glass: A review on progress in solution processing, Nano Energy. 1 (2012) 221–246. doi:https://doi.org/10.1016/j.nanoen.2011.12.002.

[201] J. Du, Y. Gao, H. Luo, L. Kang, Z. Zhang, Z. Chen, C. Cao, Significant changes in phase-transition hysteresis for Ti-doped VO2 films prepared by polymer-assisted deposition, Solar Energy Materials and Solar Cells. 95 (2011) 469–475. doi:https://doi.org/10.1016/j.solmat.2010.08.035.

[202] S. Ji, Y. Zhao, F. Zhang, P. Jin, Direct formation of single crystal VO2(R) nanorods by one-step hydrothermal treatment, Journal of Crystal Growth. 312 (2010) 282–286. doi:https://doi.org/10.1016/j.jcrysgro.2009.10.026.

[203] C.D. Anderson, M.D. Broekhuis, H.J. Byker, S.J. DeJong, Colour Neutral Thermochromic Layers and Laminates, US Patent 9465239B2, n.d.

[204] International Organization for Standardization (ISO), ISO 9050, Glass in building - determination of light transmittance, solar direct transmittance, total solar energy transmittance, ultraviolet transmittance and related glazing factors, (2003).

[205] A. Maccari, M. Montecchi, F. Treppo, M. Zinzi, CATRAM: An apparatus for the optical characterization of advanced transparent materials, Applied Optics. 37 (1998) 5156–5161. doi:10.1364/AO.37.005156.

[206] European Committee for Standardization (CEN), EN 410, Glass in building - Determination of luminous and solar characteristics of glazing, (2011).

[207] J. Mardaljevic, M. Andersen, N. Roy, J. Christoffersen, Daylighting Metrics for Residential Buildings, in: 27th Session of CIE International Conference, Sun City, South Africa, 11–15 July, 2011: pp. 93–111.

[208] International Organization for Standardization (ISO), ISO 10456, Building materials and products -- Hygrothermal properties -- Tabulated design values and procedures for determining declared and design thermal values, (2007).

[209] Ente Nazionale di Unificazione (UNI), UNI 10351, Building materials and products - Hygrothermal proprieties - Procedure for determining the design values, (2015).

[210] Ente Nazionale di Unificazione (UNI), UNI 10355, Walls and floors. Thermal resistance values and calculation method, (1994).

[211] American Society for Heating Refrigerating Air-conditioning Engineers (ASHRAE), ANSI/ASHRAE/IES Standard 90.1-2016 -- Energy Standard for Buildings Except Low-Rise Residential Buildings, (2016).

[212] European Committee for Standardization (CEN), EN 16798-2, Energy performance of buildings - Ventilation for buildings - Part 2: Interpretation of the requirements in EN 16798-1 - Indoor environmental input parameters for design and assessment of energy performance of buildings

addressing indoor air q, (2019).
[213] European Committee for Standardization (CEN), EN 673, Glass in building - Determination of thermal transmittance (U value) - Calculation method, (2011).
[214] American Society for Heating Refrigerating Air-conditioning Engineers (ASHRAE), 2009 ASHRAE Handbook - Fundamentals, (2009).
[215] International Energy Agency (IEA), No Title, (n.d.). https://www.iea.org/Sankey/#?c=United Arab Emirates&s=Balance (accessed 25 January 2019).
[216] Italian Republic, Inter-Ministerial Decree of 26 June 2015, Applicazione delle Metodologie di Calcolo delle Prestazioni Energetiche e Definizione delle Prescrizioni e dei Requisiti Minimi Degli Edifici, (2015).
[217] E. Molenbroek, E. Stricker, T. Boermans, Primary energy factors for electricity in buildings - Toward a flexible electricity supply, (2011). http://go.leonardo-energy.org/rs/europeancopper/images/PEF-finalreport.pdf.
[218] European Committee for Standardization (CEN), EN 16798-1, Energy performance of buildings - Part 1: Indoor environmental input parameters for design and assessment of energy performance of buildings addressing indoor air quality thermal environment lighting and acoustics - Module M1-6, (2016).
[219] A. Kraft, M. Rottmann, Electrochromic safety glass for smart-window applications, SPIE Newsroom: International Society for Optical Engineering. (2006) 1–2. doi:10.1117/2.1200603.0196.
[220] American Society for Heating Refrigerating Air-conditioning Engineers (ASHRAE), International Weather for Energy Calculations (IWEC Weather Files) Users Manual and CD-ROM, (2001).
[221] W.J.M. van Bommel, Non-visual biological effect of lighting and the practical meaning for lighting for work, Applied Ergonomics. 37 (2006) 461–466. doi:10.1016/J.APERGO.2006.04.009.
[222] M.S. Rea, M.G. Figueiro, Light as a circadian stimulus for architectural lighting, Lighting Research & Technology. 50 (2018) 497–510. doi:10.1177/1477153516682368.
[223] M.G. Figueiro, M. Kalsher, B.C. Steverson, J. Heerwagen, K. Kampschroer, M.S. Rea, Circadian-effective light and its impact on alertness in office workers, Lighting Research & Technology. 51 (2018) 171–183. doi:10.1177/1477153517750006.
[224] L. Bellia, A. Pedace, G. Barbato, Winter and summer analysis of daylight characteristics in offices, Building and Environment. 81 (2014) 150–161. doi:10.1016/J.BUILDENV.2014.06.015.
[225] V. De Giuli, Review on visual comfort in office buildings and influence of daylight in productivity, in: 11th International Conference on Indoor Air Quality and Climate, Copenhagen, Denmark, 17-22 August, 2008.
[226] Diva4Rhino, (n.d.). http://diva4rhino.com (accessed 3 December 2018).
[227] European Committee for Standardization (CEN), EN 15251, Indoor Environmental Input Parameters for Design and Assessment of Energy Performance of Buildings Addressing Indoor Air Quality, Thermal Environment, Lighting and Acoustics, (2007).
[228] S.K. Guth, A method for the evaluation of discomfort glare, Journal of the Illuminating Engineering Society. 58 (1963) 351–364.

[229] R.E. Levin, Position Index in VCP Calculations, Journal of the Illuminating Engineering Society. 4 (1975) 99–105. doi:10.1080/00994480.1975.10748496.
[230] U.S. Green Building Council, LEED v4 User Guide, (n.d.). http://www.usgbc.org/resources/leed-v4-user-guide.
[231] BRE Global, BREEAM, (n.d.). https://www.bregroup.com/.
[232] E. Arens, T. Hoyt, X. Zhou, L. Huang, H. Zhang, S. Schiavon, Modeling the comfort effects of short-wave solar radiation indoors, Building and Environment. 88 (2015) 3–9. doi:https://doi.org/10.1016/j.buildenv.2014.09.004.
[233] C. Marino, A. Nucara, M. Pietrafesa, Mapping of the indoor comfort conditions considering the effect of solar radiation, Solar Energy. 113 (2015) 63–77. doi:https://doi.org/10.1016/j.solener.2014.12.020.

List of publications

The Ph.D. research explores a multidisciplinary issue. As a consequence, the author's scientific production was published in international academic journals and presented in national and international conferences from different research fields, reflecting a roundtrip from energy consumption in buildings to human performance and comfort of their occupants.

Refereed journal papers:

- L. Giovannini, F. Favoino, A. Pellegrino, V.R.M. Lo Verso, V. Serra, M. Zinzi, Thermochromic glazing performance: From component experimental characterisation to whole building performance evaluation, Applied Energy. 251 (2019) 113335–113358.
  doi: 10.1016/j.apenergy.2019.113335.

- S.L. Pagliolico, V.R.M. Lo Verso, M. Zublena, L. Giovannini, Preliminary results on a novel photo-bio-screen as a shading system in a kindergarten: Visible transmittance, visual comfort and energy demand for lighting, Solar Energy. 185 (2019) 41–58.
  doi: 10.1016/j.solener.2019.03.095.

- L. Giovannini, F. Favoino, V.R.M. Lo Verso, A. Pellegrino, V. Serra, A simplified approach for the annual and spatial evaluation of the comfort classes of daylight glare using vertical illuminances, Buildings. 8 (2018) 171-191.
  doi: 10.3390/buildings8120171.

- L. Giovannini, F. Goia, V.R.M. Lo Verso, V. Serra, A comparative analysis of the visual comfort performance between a PCM glazing and a conventional selective double glazed unit, Sustainability. 10 (2018) 3579-3598.
  doi: 10.3390/su10103579.

Conference proceedings:

- L. Giovannini, F. Favoino, V.R.M. Lo Verso, A. Pellegrino, V. Serra, Annual Evaluation of Daylight Discomfort Glare: State of the Art and Description of a New Simplified Approach, presented at: 29th Quadriennial Session of the CIE (International Commission on Illumination) - CIE 2019, Connecting the World in Light, Washington DC, USA, 14-19 June 2019.

- L. Giovannini, F. Favoino, V. Serra, M. Zinzi, Thermo-chromic glazing in buildings: a novel methodological framework for a multi-objective performance evaluation, presented at: 10th International Conference on Applied Energy - ICAE2018, Hong Kong, China, 22-25 August 2018. In: Energy Procedia, 158 (2019) 4115–4122.
  doi: 10.1016/j.egypro.2019.01.822.

- M. Baracani, L. Giovannini, V. Serra, F. Favoino, Control of dynamic glazing in heating dominated climate for office buildings: contrasting occupant visual comfort requirements with energy use, in: 51th AiCARR International Conference - The Human Dimension of Building Energy Performance, Associazione Italiana Condizionamento dell'Aria Riscaldamento e Refrigerazione (AiCARR), Venice, Italy, 20-22 February 2019.

- L. Giovannini, V. Serra, V.R.M. Lo Verso, A. Pellegrino, M. Zinzi, F. Favoino, A Novel Methodology to Optimize Visual Comfort and Energy Performance for Transparent Adaptive Façades, in: 2018 IEEE International Conference on Environment and Electrical Engineering and 2018 IEEE Industrial and Commercial Power Systems Europe, EEEIC/I and CPS Europe 2018, Palermo, Italy, 12-15 June 2018.
  doi: 10.1109/EEEIC.2018.8494565.

- L. Giovannini, F. Goia, V.R.M. Lo Verso, V. Serra, Phase Change Materials in Glazing: Implications on Light Distribution and Visual Comfort. Preliminary Results, presented at: 8th International Conference on Sustainability in Energy and Buildings - SEB-16, Turin, Italy, 11-13 September 2016. In: Energy Procedia, 111 (2017) 357-366.
  doi: 10.1016/j.egypro.2017.03.197.

- Y. Cascone, M. Ferrara, L. Giovannini, G. Serale, Ethical issues of monitoring sensor networks for energy efficiency in smart buildings: A case study, presented at: 9th International Conference on Sustainability in Energy and Buildings - SEB-17, Chania, Crete, Greece, 5-7 July 2017. In: Energy Procedia, 134 (2017) 337-345.
  doi: 10.1016/j.egypro.2017.09.540.

- F. Favoino, L. Giovannini, R. Loonen, Smart glazing in Intelligent Buildings: what can we simulate?, in: Conference Proceedings of Glass Performance Days 2017 – GPD2017, Tampere, Finland, 28-30 June 2017, pp. 8–15.

- L. Giovannini, V.R.M. Lo Verso, B. Karamata, M. Andersen, Lighting and energy performance of an adaptive shading and daylighting system for arid climates, presented at: 6th International Building Physics Conference - IBPC 2015, Turin, Italy, 14-17 June 2016. In: Energy Procedia, 78 (2015) 370-375.
  doi: 10.1016/j.egypro.2015.11.675.

- V.R.M. Lo Verso, V. Serra, L. Giovannini, S. Iennarella, Light versus energy performance of office rooms with curtain walls: A parametric study, presented at: 6th International Conference on Sustainability in Energy and Buildings - SEB-14, Cardiff, Wales, UK, 25-27 June 2014. In: Energy Procedia, 62 (2014) 462-471.
  doi: 10.1016/j.egypro.2014.12.408.

- B. Karamata, L. Giovannini, V.R.M. Lo Verso, M. Andersen, Concept, Design and Performance of a Shape Variable Mashrabiya as a Shading and Daylighting System for Arid Climates, presented at: 30th International Passive and Low Energy Architecture conference (PLEA 2014), Ahmedabad, India, 16-18 December 2014. In: 30th PLEA Conference - Sustainable Habitat for Developing Societies, 2 (2014) 344-351.